A STUDY OF WATER WAVE REFLECTION USING CLOSE RANGE PHOTOGRAMMETRY

by

J. M. PETZER
BSc (Eng) in Civil Engineering,
University of Cape Town

A thesis submitted to the University of Cape Town in partial fulfilment of the requirements for the degree of Master of Science in Engineering

Department of Civil Engineering
University of Cape Town

October 1989

The University of Cape Town has been given the right to reproduce this thesis in whole or in part. Copyright is held by the author.

University of Cape Town

The copyright of this thesis vests in the author. No quotation from it or information derived from it is to be published without full acknowledgement of the source. The thesis is to be used for private study or non-commercial research purposes only.

Published by the University of Cape Town (UCT) in terms of the non-exclusive license granted to UCT by the author.

University of Cape Town

DECLARATION

I, John Martin Petzer, hereby declare that this dissertation is my own work and that it has not been submitted for a degree at any other university.

Signed by candidate Signature Removed

J.M. Petzer

October 1989.

University of Cape Town

to my parents

University of Cape Town

SYNOPSIS

The intention of this investigation is to investigate the various forms of water wave reflection to a high degree of accuracy. Close range photogrammetry is the technique that is used to measure the water surface profile, as it produces an accurate and comprehensive analysis of the water surface profiles.

Conventional photogrammetry techniques (photography) were used in preference to near real time photogrammetry (digital). Although near real time photogrammetry has the advantage of a far higher rate of data acquisition, it does not achieve the same degree of accuracy as can be achieved by conventional photogrammetry, the technique finally used for this investigation.

For the generation of the desired wave patterns, certain equipment was developed and modified. To test the various angles of incidence a moveable reflecting wall was built. Due to the small size of the wave basin, an efficient wave absorber was required to absorb the reflected wave generated when oblique wave reflection was investigated. It was observed that a very poor quality wave was being generated by the wave generator, as a result of its flexibility. Consequently the wave generator was stiffened considerably which improved the wave generated.

Interesting information was obtained from the analysis of the standing wave. A coefficient of reflection of 1,6 at the reflecting wall was obtained, this places new emphasis on the relationship between the standing wave and overtopping. The oblique wave reflection results corresponded well with theoretical predictions, while no well defined trends were established for the mach wave. The data for the mach wave did however suggest that previously established trends for the mach wave may not be correct.

Close range photogrammetry produced accurate results, and is an excellent method for water surface profile measurement. The results obtained showed that the wave generator was not generating a pure wave, which lead to unknown errors in the results of spot heights. Conventional photogrammetry is a slow process, so not enough data was acquired to adequately analyse the

University of Cape Town

reflection trends. This suggests that in order for the trends to be well established, near real time photogrammetry should be used once these systems have developed sufficient accuracy.

University of Cape Town

ACKNOWLEDGEMENTS

I would like to thank my thesis supervisors Professor F A Kilner of the Department of Civil Engineering, and Professor H Ruther of the Department of Surveying, University of Cape Town, for their help and guidance during the two years of this investigation. Their encouragement, constant enthusiasm and interest were much appreciated.

A particular word of thanks to Professor L P Adams and particularly Miss Ann Tregidga of the Department of Surveying for their help, experience and assistance regarding the stereo comparator and computer analysis for the photogrammetric analysis of the wave data.

I extend my thanks to the technical staff, Messrs I von Guerard, D Botha, G Bertuzzi and R Edge, who helped me in the construction and modification of the experimental apparatus. I would also like to thank Messrs J George, S Smity and J Williams for their practical aid and assistance throughout the construction and experimentation stages.

My thanks are also due to the staff of the Department of Civil Engineering for general assistance throughout the two years of the study.

University of Cape Town

TABLE OF CONTENTS

		Page
	Title page	
	Declaration	i
	Dedication	ii
	Synopsis	iii
	Acknowledgements	v
	Table of contents	vi
	List of illustrations	xi
	List of tables	xiii
	Nomenclature	xiv
1.	Introduction	1.1
2.	Photogrammetrical technique	2.1
2.1	Theory of photogrammetry	2.1
2.1.1	Basic requirements	2.2
2.1.2	The normal photogrammatric case	2.4
2.1.2.1	The image	2.4
2.1.2.2	The stereo pair	2.5
2.1.3	The general solution	2.7
2.2	Near real time photogrammetry	2.7
2.3	PHOENICS : PHOtogrammetric ENgineering and Industrial digital Camera System	2.9
2.3.1	Phoenics hardware	2.9
2.3.2	Thresholding	2.10
2.3.3	Phoenics software	2.10
2.3.4	Proposed implementation of Phoenics for wave reflection analysis	2.10
2.3.5	Alternative solutions	2.11
2.3.5.1	Transportation of the signal over a distance	2.12
2.3.5.2	The use of a mixer and video recorder	2.12
2.3.5.3	The use of two separate video recorders	2.14
2.3.6	Quantitative determination of the fastest dynamic motion allowable	2.14
2.3.7	Conclusions	2.15

University of Cape Town

3.	The application of conventional stereo photogrammetry to wave measurement		3.1
	3.1	Photographing a defined water surface	3.2
	3.2	Photographing dynamic surfaces	3.2
	3.3	Anticipated accuracy of stereo photogrammetry	3.3
4.	Wave theory as applied to wave reflection		4.1
	4.1	Progressive wave theory	4.1
	4.1.1	Progressive wave linear theory (Airy theory)	4.1
	4.1.2	Progressive finite amplitude wave theory	4.2
	4.1.2	Stokes second order wave theory	4.2
	4.2	The standing wave	4.3
	4.2.1	Partial clapotis	4.5
	4.2.2	Standing wave, linear theory	4.6
	4.2.3	Standing wave, second order Stokes theory	4.6
	4.2.4	Anomalies in the standing wave theory	4.7
	4.3	Clapotis gaufre	4.7
	4.4	Mach wave reflection	4.10
	4.4.1	Review of previous investigations	4.12
	4.4.2	Theoretical explanation of the Mach wave	4.13
5.	Equipment used for the investigation		5.1
	5.1	Equipment used for photogrammetry	5.1
	5.1.1	Zeiss Jena UMK 10/1318 universal measuring cameras	5.1
	5.1.1.1	Photographic plates	5.2
	5.1.2	Carl Zeiss Jena Steko 1818 Stereo comparator	5.2
	5.1.3	HP 9816 microcomputer	5.3
	5.1.4	The DEC/UMS 6230	5.4
	5.2	Equipment required to generate the required wave patterns	5.5
	5.2.1	Wave basin floor	5.5
	5.2.2	Wave generator	5.5
	5.2.3	Moveable reflecting wall	5.10
	5.2.4	Side walls	5.12
	5.3	The design of the wave absorbers	5.13

University of Cape Town

5.3.1	A review of pertinent papers	5.13
5.3.1.1	A perforated vertical wall breakwater, by G.E. Jordan	5.13
5.3.1.2	Experimental development of a perforated wave absorber of minimum length, by P.A. Hamill	5.14
5.3.2	Initial choice of wave absorber	5.16
5.3.3	Testing of the wave absorber	5.17
5.3.3.1	Design of the test absorber	5.17
5.3.3.2	Method for measurement of relative wave absorption	5.18
5.3.3.3	Selection of the design wave	5.19
5.3.4	Mechanism of wave absorption	5.19
5.3.5	Relationship of the various parameters	5.21
5.3.5.1	The optimum slope of the wave absorber	5.21
5.3.5.2	The importance of the chamber	5.23
5.3.5.3	Optimum number of holes	5.24
5.3.5.4	Size of the chamber	5.26
5.3.5.5	Other factors affecting the efficiency of the wave absorber	5.26
5.3.6	Design for the prototype wave absorber	5.27
5.4	Techniques for the implementation of photogrammetry	5.27
5.4.1	Camera positioning	5.27
5.4.2	Control point network	5.29
5.4.3	Water surface identification	5.30
5.4.4	The wave trigger mechanism	5.32
6.	Acquisition of experimental data	6.1
6.1	Selection of parameters for the waves generated	6.1
6.1.1	Water depth	6.1
6.1.2	Wave period selected	6.1
6.1.3	Wave height	6.2
6.2	Considerations for the experimental procedure	6.3
6.2.1	The occurrence of the repeatable wave	6.3
6.2.2	Photographing the incident wave	6.3
6.2.3	Photographing the standing wave	6.4
6.2.3.1	The standing wave	6.4

University of Cape Town

	6.2.3.2	The oblique standing wave	6.4
	6.2.4	Obtaining standing wave 180° out of phase	6.5
	6.2.5	Positioning the wave paddle	6.5
	6.2.6	Determining the SWL for a stereopair	6.6
	6.3	The display of results obtained	6.9
	6.3.1	List of stereopairs obtained	6.9
	6.3.2	Acquisition of data from the stereopairs	6.9
	6.4	Procedure for analysis of the contour plots	6.11
	6.4.1	Incident waves	6.11
	6.4.2	Standing waves	6.11
	6.4.3	Oblique wave reflection	6.12
7.	Results and analysis		7.1
	7.1	Incident waves	7.1
	7.2	The standing wave	7.2
	7.3	Oblique wave reflection	7.6
	7.3.1	Diffraction effects	7.9
	7.3.2	Degree of reflection	7.11
	7.4	Mach wave reflection	7.11
	7.4.1	Definition of Mach wave	7.13
	7.4.2	Relationships investigated for Mach wave reflection	7.14
	7.4.2.1	Effect of angle of incidence	7.14
	7.4.2.2	Effect of varying wave height and changes in period	7.18
	7.4.2.3	Coefficient of reflection plots	7.19
	7.4.3	Trends in Mach wave development	7.20
	7.4.3.1	Limiting angle for the Mach wave	7.20
	7.4.3.2	Growth of Mach wave as a function of incident energy	7.20
	7.4.3.3	Second Mach stem	7.21
8.	Conclusions and recommendations		8.1
	8.1	Accuracy of analysis	8.1
	8.2	Standing wave data	8.1

University of Cape Town

8.4 Mach wave reflection 8.2
8.5 Future investigation 8.2

Bibliography

Appendix A - Contour plots

Appendix B - Coeficient of reflection contour plots

Appendix C - Wave Data

Appendix D - Examinations written by the author to complete the requirements for the degree

University of Cape Town

LIST OF ILLUSTRATIONS

Figures		Page
Fig 2.1	The image created on a negative	2.4
Fig 2.2	The stereopair	2.5
Fig 2.3	Parallax of a pair of negatives	2.6
Fig 2.4	Alternative implementations of Phoenics	2.13
Fig 4.1	The formation of a standing wave (linear theory)	4.4
Fig 4.2	Extreme amplitude envelope	4.5
Fig 4.3	Comparison of measured and theoretical standing wave lengths	4.8
Fig 4.4	Clapotis gaufre	4.8
Fig 4.5	Mach wave reflection	4.10
Fig 4.6	Development of second mach stem (Berger, Kohlhase 1976)	4.13
Fig 4.7	Stem height along a vertical wall (Berger, Kohlhase 1976)	4.14
Fig 5.1	Cross section of the reflecting wall	5.10
Fig 5.2	Model A (Hamill 1963)	5.15
Fig 5.3	Model B (Hamill 1963)	5.15
Fig 5.4	Reflection coefficients for perforated wave absorber (Hamill 1963)	5.16
Fig 5.5	Model wave absorber	5.18
Fig 5.6	Optimum wave absorber: optimum slope	5.22
Fig 5.7	Optimum wave absorber: importance of the chamber	5.23
Fig 5.8	Optimum wave absorber: optimum number of holes	5.25
Fig 5.9	Wave basin configuration	5.28
Fig 5.10	Flow chart of camera firing procedure	5.34
Fig 6.1	Contour plot - Clapotis gaufre	6.10
Fig 6.2	Incident wave	6.13
Fig 6.3	Oblique wave reflection	6.14
Fig 6.4	Coeficient of reflection contour plot	6.15
Fig 7.1	Summary of reflection data	7.5
Fig 7.2	Standing wave comparison	7.6
Fig 7.3	Diffraction effect of the reflected wave	7.8
Fig 7.4	Coefficient of reflection plot $T = 0{,}765$; $\theta_o = 69^o$	7.9
Fig 7.5	Wave diffraction diagram - 75^o wave angle (From Coastal Engineering Research Centre, 1984)	7.11
Fig 7.6	Contour plot of Mach wave reflection	7.11
Fig 7.7	Mach stem width	7.15

University of Cape Town

Fig 7.6	Contour plot of Mach wave reflection	7.11
Fig 7.7	Mach stem width	7.15
Fig 7.8	Growth of Mach stem	7.16
Fig 7.9	Relative height of Mach stem	7.17
Fig 7.10	Mach stem width	7.19

Plates

Plate 5.1	Steko 1818 Stereo componeter and peripherals	5.3
Plate 5.2	An IBM compatible PC acting as a Vax terminal	5.4
Plate 5.3	Wave generator	5.6
Plate 5.4	Impure wave generated by the wave generator	5.7
Plate 5.5	Modifications to the wave paddle	5.8
Plate 5.6	Wave generated after modification	5.9
Plate 5.7	The moveable reflecting wall	5.11
Plate 5.8	Side wall "hiding" the tins	5.12
Plate 5.9	The flume used for testing the wave absorber	5.17
Plate 5.10	Wave absorption process	5.20
Plate 5.11	A control point	5.29
Plate 5.12	Overhead projectors mounted on the ceiling	5.31
Plate 5.13	The wave trigger	5.33
Plate 6.1	The water surface as last wave generated reaches the wave absorber	6.4
Plate 6.2	Typical stereopair	6.7
Plate 7.1	Oblique wave reflection	7.7
Plate 7.2	Mach wave $\theta_o = 20^o$	7.21

University of Cape Town

LIST OF TABLES

		Page
Table 4.1	Previous experimental and theoretical examinations of the mach reflection at straight vertical walls	4.11
Table 5.1	Comparison of Hamill's wave data to UCT wave data	5.16
Table 6.1	Resonant periods for the width of the wave basin	6.2
Table 6.2	List of stereopairs	6.8
Table 7.1	Average incident wave data	7.1
Table 7.2	Standing wave data from stereopairs 10/12 for T = 1,5	7.2
Table 7.3	Standing wave data from stereopairs 13/16 for T = 1,01	7.2
Table 7.4	Summary of reflection data	7.4
Table 7.5	Data for T = 0,765; H_i = 24,8mm	7.14
Table 7.6	Data for $\theta_o = 34^o$	7.18

University of Cape Town

NOMENCLATURE

a	-	wave amplitude
a_{ci}	-	incident wave crest amplitude from SWL
a_{cs}	-	standing wave crest amplitude from SWL
a_{ti}	-	incident wave trough amplitude from SWL
a_{ts}	-	standing wave trough amplitude from SWL
B	-	Mach stem width
d	-	water depth
g	-	acceleration due to gravity; 9.82 m/s^2
H	-	wave height
H_i	-	incident wave height
H_r	-	reflected wave height
H_s	-	standing wave height
H_{ms}	-	Mach stem height
k	-	$2\pi/L$
K_r	-	coefficient of reflection
L_i		incident wave length
L_s	-	standing wave length
MWL	-	mean water level
SWL	-	stationary water level
T	-	period of wave
Y_s	-	water surface displacement from SWL
Y_{si}	-	incident wave surface displacement from SWL
Y_{sr}	-	reflected wave surface displacement from SWL
α	-	angle of growth of mach stem
θ_o	-	angle of incident wave orthogonal to reflecting wall
θ_r	-	angle of reflected wave orthogonal to reflecting wall
σ	-	$2\pi/T$

University of Cape Town

1. INTRODUCTION

In this investigation close range photogrammetry is used to investigate three cases of water wave reflection,

i) standing wave reflection.

ii) clapotis gaufre or oblique reflection.

iii) Mach wave reflection.

Close range photogrammetry is used to investigate the water wave patterns as it is an ideal technique for measuring water surface profiles. Close range photogrammetry offers important advantages over conventional wave profile measurements, forthe following reasons:-

i) an almost infinite amount of accurate information is available.

ii) it does not disturb nor interfere with the water surface in any way.

iii) a permanent record of the water surface is available, should any feature warrant further investigation, without further testing.

Before any experimental work was performed, it was necessary to establish whether conventional close range photogrammetry (photography) or near real time photogrammetry (digital) should be used. The use of near real time photogrammetry would have resulted in far more data being acquired than could be obtained using conventional photogrammetry. It was finally established that it would not be possible to implement near real time photogrammetry with sufficient accuracy, so conventional photogrammetry was used for this investigation.

Close range photogrammetry has the potential to describe a water surface far more comprehensively than any other measuring technique. As a result various reflection scenarios were investigated with the aim of verifying present knowledge of wave reflection, and possibly to identify new phenomena. Mach wave reflection has not been

University of Cape Town

extensively investigated, and it is possible that an accurate, comprehensive description of the various Mach wave scenarios will reveal presently unknown phenomena.

To establish images of the desired wave reflection pattern it was necessary to identify and accommodate the physical limitations of the equipment used. The major limitation in this investigation was the small size of the wave basin. Consequently the reflected waves were soon reflected from the sides of the waves basin and this disturbed the desired wave pattern. Special modifications to the experimental procedure and equipment were required, amongst these was the design of a suitably efficient wave absorber.

Great care was taken with both the wave reflection generating equipment and the photogrammetry requirements, to optimise all factors affecting the accuracy of the results. It is hoped that this investigation will lead to a valuable contribution to the existing knowledge of water wave reflection.

University of Cape Town

2. PHOTOGRAMMETRICAL TECHNIQUE

2.1 Theory of photogrammetry

Remote sensing is the science of identifying or measuring an object, potentially very accurately, without physically touching that object. The two applicable branches of remote sensing that can be identified are:-

i) metric photogrammetry, which involves the precise measurement and calculation of points which then describe a particular object.

ii) photographic interpretation, which involves analysis of remotely sensed objects, and is used for the recognition and identification of features.

In this investigation, metric photogrammetry is of particular interest, with special consideration given to close range photogrammetry. Close range photogrammetry is generally considered to be the measurement of an object in the range of 300 m down to fractions of a millimetre (Atkinson, 1980). Any object can be measured using close range photogrammetry, as long as it is possible to obtain images of the area of interest.

Close range photogrammetry derives the object space three dimensional coordinates of a body from the images of the body. The image coordinates of the object are measured from two or more negatives using a comparator. The three dimensional coordinates of the object are then calculated from the image coordinates using photogrammetric algorithms.

Close range photogrammetry has distinct advantages over conventional measurement techniques (Atkinson, 1980):-

i) the object is not touched during measurement.

ii) data capture (acquisition) is rapid.

iii) the photographs store both semantic and metric data with very high density.

University of Cape Town

iv) the photographs are documents related to the time when they were taken and they can be used as legal evidence.

v) not only rigid and fixed objects but also deformation and movement can be measures.

iv) time dependent parameters such as velocity, acceleration and frequency can be determine.

vii) evaluation of the metric photographs can be done at any time in the office and repetition and amendment are always possible.

viii) photography and evaluation are flexible and can easily be optimised to the project requirements as, for example, in accuracy.

ix) the invisible part of the spectrum can be used for creating images.

x) complicated shapes and movements are easily measured.

xi) stereoscopy is the basis for continuous contouring of irregular objects.

xii) analytical methods provide a means of integration with succeeding calculations and data handling.

University of Cape Town

2.1.1 Basic requirements

The use of photography in photogrammetry entails the projection of a three dimensional body onto a plane. It is required that the lens must not significantly distort the rays (i.e. there must be straight lines from the object points through the perspective centre to the corresponding points on the plane). As the image is recorded on photographic emulsion, the emulsion must lie in a plane.

To simulate these conditions, the interior orientations of the camera to be used must be evaluated. The interior orientations of a camera are the relative position of the principal point (x,y coordinates) and the size of the principal distance (see Section 2.1.2.1). Factors affecting the interior orientations of the camera are :-

i) lens distortion.

ii) film flatness.

iii) film stretch.

To account for for these factors mathematical models are used to correct the image coordinates distorted by these phenomona.

Two types of cameras are availavle, non-metric cameras and metric cameras. Non-metric cameras have unknown and unstable interior orientations, the film is not well supported, and their lenses lead to significant distortion. Metric cameras are superior to non-metric cameras as they have fixed and constant interior orientations, and their lenses produce little distortion. A far higher degree of accuracy is obtainable from metric cameras than from non-metric cameras. For this investigation two metric cameras were be used for the close range photogrammetry.

A stereo comparator is used to measure the image coordinates of the object on two stereoscopic negatives, which are then used in the calculation for the projective transformations, or similar mathematical model. The calculation of the object space coordinates assumes that the object points, the principal point and the corresponding image points are collinear. Knowing the camera positions the coordinates of the object points can then be calculated.

University of Cape Town

Two possible possible situations can exist for the cameras to obtain a stereo pair:-

i) firstly where the positions and attitudes of the cameras are known to a high degree of accuracy.

ii) secondly where the positions of the cameras are not available, for which a number of points of known position must be known in object space such that the relative positions of the cameras can be determined. For this purpose a network of control points (points of known position) is normally used.

It is the second situation that is used in this investigation, so an accurately known control point network was established for this purpose.

2.1.2 The Normal photogrammetric case

The Normal case in photogrammetry is simple but would very seldom be used. However it serves to explain the basic concept of photogrammetry.

2.1.2.1 The image

Fig 2.1 The image created on a negative

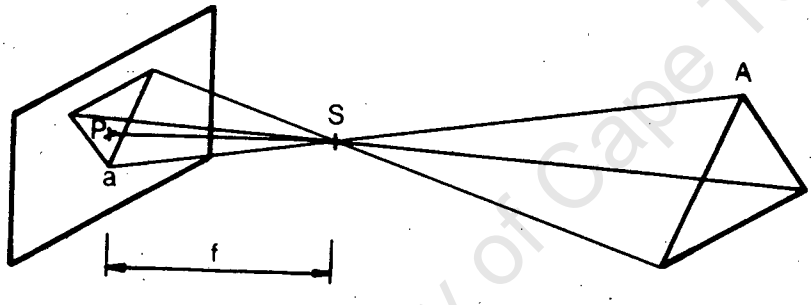

In fig 2.1 the following can be defined

i) "S" the perspective centre of the camera, the point through which all rays pass.

ii) "P" the principal point is the point where the optical axis of the lens intersects the plane of the negative.

iii) "f" the focal length (in photogrammetry known as the principal distance) is the distance from the perspective centre to the principal point.

University of Cape Town

2.1.2.2 The stereo pair

Fig 2.2 The stereopair

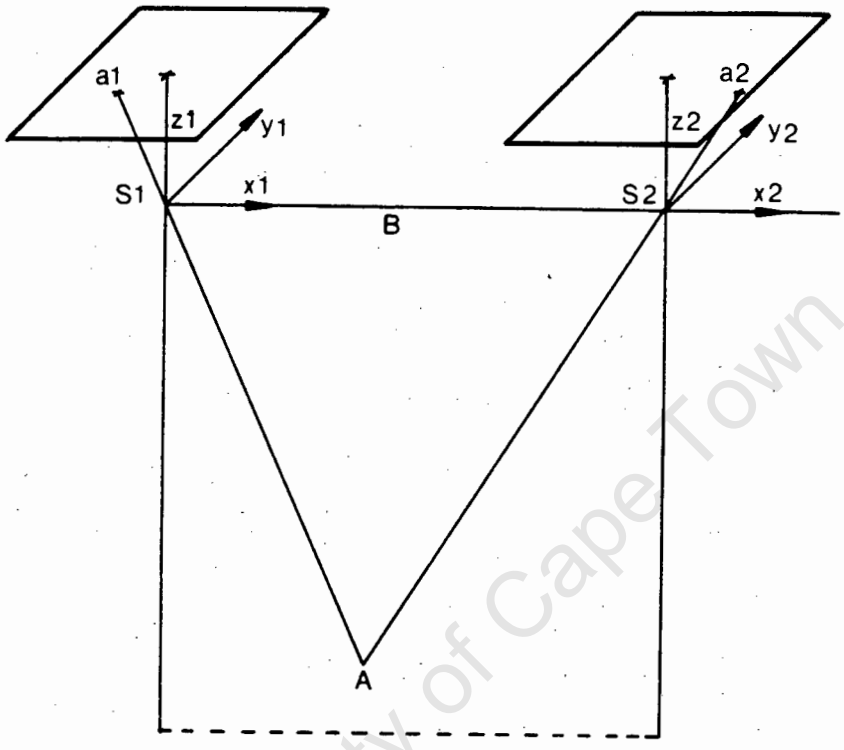

University of Cape Town

Fig. 2.2 shows the two images orientated in real space. Each image has a perspective centre S_1 and S_2 respectively separated by a horizontal base width B. Each image has its own coordinate system (x_1, y_1, z_1) and (x_2, y_2, z_2) with their origins at S_1 and S_2 respectively. For this ideal case, the Normal case, the two images are considered to be coplanar, and the x axes collinear. Relative to point A, the origins of the two images (S_1 , S_2) have the coordinates (X_{A1}, Y_{A1}, Z_{A1}) and (Z_{A2}, Y_{A2}, Z_{A2}) respectively. The images points (a_1) and (a_2) have the coordinates (x_{a1}, y_{a1}, z_{a1}) and (x_{a2}, y_{a2}, z_{a2}) respectively. As the x axes are collinear the xz plane can be viewed independently as in fig.2.3.

Fig. 2.3 Parallax of a pair of negatives

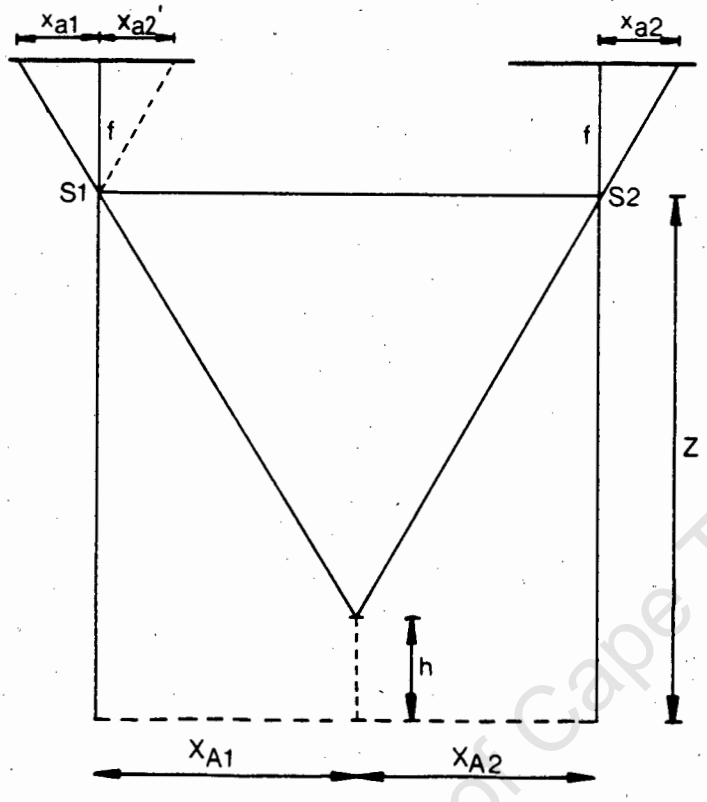

The two plates are coplanar so

$$Z_{A1} = Z_{A2} = Z$$
$$z_{a1} = z_{a2} = f$$

Construct a line parallel to the line $(S_2;\ (x_{a2},\ f))$ from S_1 to $(x_{a2}',\ f)$. By similar triangles

$$(x_{a1} - x_{a2})/f = (X_{A1} - X_{A2}) / (Z - h)$$

But $(X_{A1} - X_{A2}) = B$

So $(x_{a1} - x_{a2}) = Bf/(Z - h)$.

The term $(x_{a1} - x_{a2})$ is known as the linear parallax (P)

thus $P = Bf(H - h)$

Thus by the use of the difference in linear parallax the height of A is

$$h = H - Bf/P$$

University of Cape Town

This height "h" is called a crude height, as it is only an approximation. The above parallax equations are based on the assumption that

i) the cameras are truly vertical and have no tilt.

ii) the x axes are collinear and the planes are situated at the same level.

iii) all rays pass through the perspective centre.

This is a very special case, which seldom occurs in practice.

2.1.3 The general solution

The general solution requires

i) a knowledge of the interior orientation elements of the photographic negatives.

ii) a mathematical model of any lens distortion.

iii) precise knowledge of the orientations and positions of the cameras, or control points on or surrounding the object.

The images are analysed on a stereo comparator to obtain the image coordinates. This information may be used to accurately obtain the z coordinates of points on the object using one of the four basic general solutions:-

i) relative/absolute orientation.

ii) direct linear transformation (DLT).

iii) bundle solution

iv) 11 parameter solution

The solution used for all the calculations in this document is the modified 11 parameter solution (Adams 1978).

2.2 Near real time photogrammetry

Due to the relatively recent advancements made in computer and sensor technology, and the related decline in costs, a photogrammetric system based totally on electronic devices is now possible. These

University of Cape Town

new systems have the capability to capture images and automatically measure the image coordinates, creating what is called Near Real Time Photogrammetry (NRTP).

Conventional photogrammetry is an extremely powerful tool, but it does have the following drawbacks:-

1) the results of the photography are not immediately available, as time is needed for development (of negatives) and analysis.
2) specialised and expensive equipment is required, as well as the trained personnel to operate the equipment.
3) if any errors occur during photography and development they will not be immediately identified.

The use of NRTP would solve these problems very successfully while simultaneously creating further advantages. Using conventional photogrammetry it could easily take 24 hours before the finished product of a contour map is obtained of the object photographed. It took Thinking Machines Corporation, Massachusetts with its 16 000 to 64 000 processors working in parallel just two seconds to transform the stereoscopic images from two television cameras into a detailed contour map (Gruen, 1989). Such equipment is obviously not affordable by research institutions but demonstrates the future potential of real time photogrammetry (RTP) for rapidly processing vast quantities of detailed information.

The equipment required for conventional photogrammetry is extremely expensive and specialised. This can be compared to the NRTP system developed by Prof Ruther (Ruther & Parkyn, 1988) at the University of Cape Town. This system uses equipment which is easily available (even in South Africa) and costs 5 to 10% of conventional photogrammetry equipment. This equipment is easily operated by a person unskilled in the techniques of photogrammetry.

In conventional photogrammetry numerous errors can occur in the photographic process. These errors may only be discovered hours later with valuable information being permanently lost. With a NRTP

University of Cape Town

system it would be possible to tell within 15 minutes the quality of data. The speed of the system would also significantly increase the speed of data acquisition, with a similar saving in manpower.

It appears that if NRTP could be implemented in an experimental situation it would be far superior to conventional photogrammetry. Consequently NRTP was investigated to see whether it was viable to use NRTP instead of the conventional photographic techniques.

2.3 PHOENICS : PHOtogrammetric ENgineering and Industrial digital Camera System

Phoenics is the Near Real Time Photogrammetry (NRTP) system that has been developed by Prof Ruther at the University of Cape Town. Initial NRTP systems have operated using expensive, powerful computers, either mainframes or minis. Phoenics has been designed as a low cost system; the hardware used has been specially selected to ensure that the quality or accuracy of the system would not be significantly impaired when compared with more expensive systems.

2.3.1 Phoenics' Hardware

The hardware Phoenics presently operates on is :-

i) a personal computer (IBM Personal system/2 Model 30).
ii) a parallel processor.
iii) two video frame grabbers (MATROX PIP 512/PIP 1024 boards).
iv) two CCD cameras (Siemens-ok 211).
v) two external monitors (Phillips RGB monitors CM 8833).

The two stereoscopic images are obtained from the CCD cameras (Charge Coupled Device). These images, which are in analogue form, are sent to the video frame grabbers, which have an analogue to digital converter. The analogue signal is then processed into digital form and stored in the video frame grabbers buffer (either on the PIP512 or PIP1024 card).

University of Cape Town

2.3.2 Thresholding

When the frame grabber digitises the analogue signal it receives from the CCD camera, it gives each pixel a grey value between 0 to 255, 0 being black and 255 being white (or vice versa). When the image is thresholded for a particular grey value of say 100, a binary image is formed. In this binary image all pixels with grey values less than 100 become black and all other pixels become white. The object of thresholding is to ensure that the only black images left are those of the points whose positions you wish to determine.

2.3.3 Phoenics software

Software has been written for Phoenics for the identification of points occurring in both images, and obtaining their respective xy coordinates in both images. The identification of points in the images can be done using one of two available methods, namely

i) point mode (Ruther, Parkyn 1988).

ii) Grid mode (Ruther 89).

Before either of these methods can be used the images need to be thresholded. Point mode requires user interaction for the determination of corresponding points while grid mode is essentially automatic. The accuracy of the system is good. Control points imaged at 1,7 m from the cameras produced standard deviations of ±0,4 mm in x and y and ±0,8 mm in z.

2.3.4 Proposed implementation of Phoenics for wave reflection analysis.

The implementation of NRTP to obtain experimental data on wave reflection requires special consideration. The experimental application varies considerably from the applications Phoenics has been considered for up to now. New conditions now exist

i) it is now required that images of a dynamic surface be obtained.

ii) although Phoenics is a portable system it is not practical to move such sensitive equipment between the experimental site and the photogrammetry lab on a regular basis. Hence

University of Cape Town

alternatives are required that allow Phoenics to be used some distance from the experimental site.

Two alternative implementations of Phoenics have been identified:-

i) a system be arranged that allows the signal to pass from the cameras to Phoenix, separated by a couple of hundred metres, instantaneously.

ii) a method be used where the images of the waves be stored at the experimental site, then transported and downloaded onto Phoenics.

In both these implementations certain criteria must be met:-

i) the two stereoscopic images must be obtained simultaneously so synchronised cameras are required.

ii) a sequence of images is required so that extreme events, which only occur for a short period of time, can be recorded.

iii) the facility must then exist to select from the recorded images which are to be analysed.

iv) in order for meaningful wave information to be obtained accurate results are required, so the resolution of the system must be optimised.

v) the dynamic event being recorded should not move significantly during the time it takes a CCD camera to obtain an image.

2.3.5 Alternative Solutions

Within the criteria that have been established three possible solutions can be identified (fig 2.4)

i) the connection of synchronised cameras to Phoenics over a distance of 200m by coaxial cable with an amplifier to increase the signal.

ii) images from two synchronised cameras are joined by a mixer to form one image (i.e. the right half of the left image and the left half of the right image are added). The mixed image is then recorded on a video recorder. The video tape is then played with the video recorder connected to the frame buffer.

University of Cape Town

The signal from the video recorder is the same as that from a CCD camera.

iii) the images from the two synchronised cameras are recorded on separate video recorders. The video recorders are then played as input for Phoenics, but the input of images must in some way be synchronised so that matching stereoscopic images are obtained.

2.3.5.1 Transportation of the signal over a distance

Option (i) requires the images to be transported over a long distance (200 m) by coaxial cable. Due to the distance an amplifier is required to boost the signal. The signal from the CCD camera is analogue, so distortions are likely to occur during amplification. It is also anticipated that the images will pick up further distortions as the cable passes other electrical circuits, even though co-axial cable is being used. The standard deviation of the Z coordinate is not expected to be better than $\pm$ 5 to 6 mm.

2.3.5.2 The use of a mixer and video recorder

For option (ii) three mappings of the original image obtained from the CCD camera occur before Phoenics obtains the image. As a result two major problems are envisaged:-

i) distortions of the signal.

ii) a loss in accuracy, as a result of a loss in the effective number of pixels.

iii) a reduction in image size.

The CCD cameras observe with 500 x 468 pixels (500 across and 468 down), but after mixing the single half image of the total image is represented by 250 x 468 pixels. A VHS video recorder only records 240 x 280 pixels. So 500 x 468 pixels are mapped to 240 x 280 pixels, halving the accuracy to which the image coordinates can be determined. A further loss in resolution occurs from the video recorder to the frame grabber. The image or frame on a video tape

University of Cape Town

Fig 2.4 Alternative implementations of Phoenics

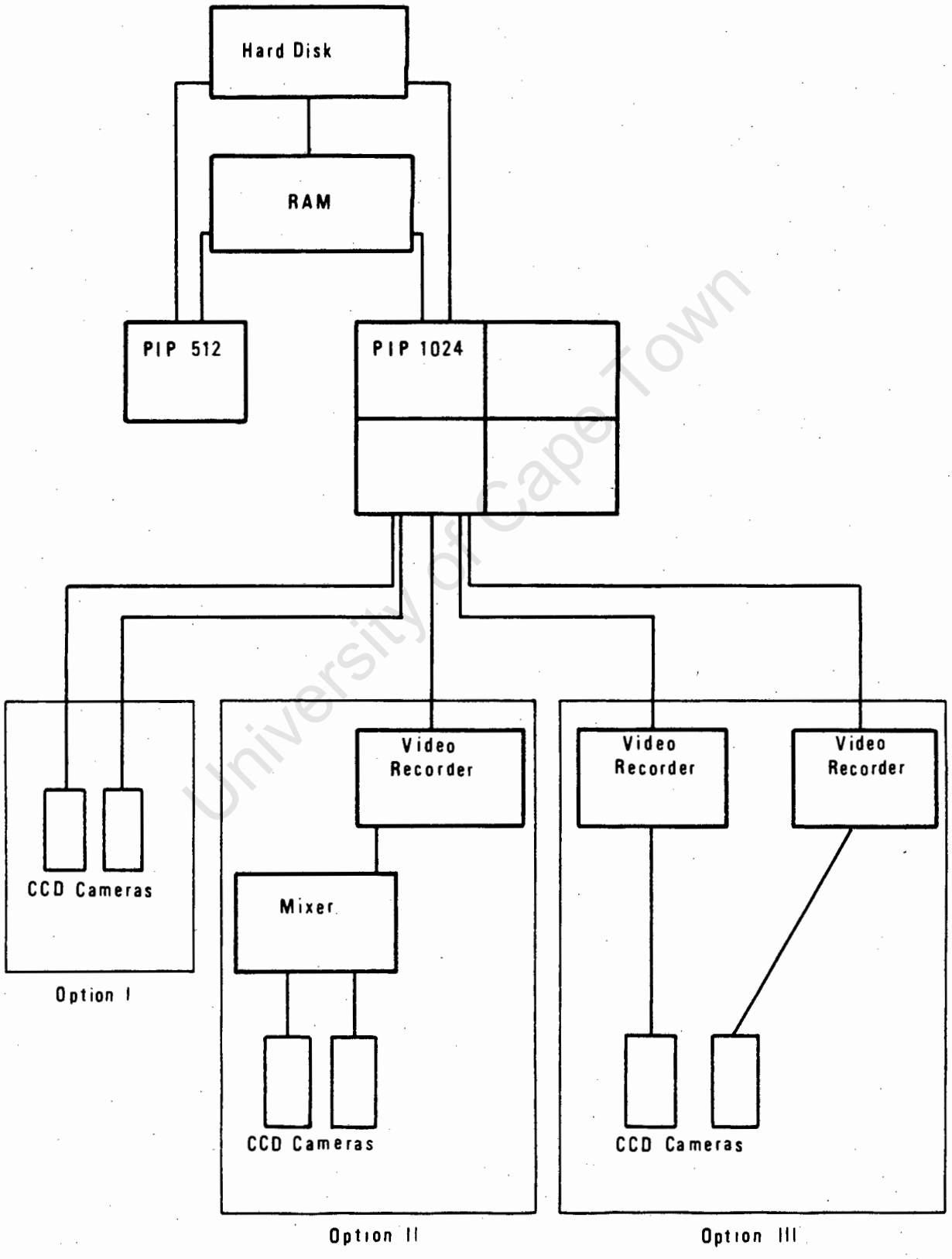

University of Cape Town

is stored in two files, each file containing alternate lines of the frame. When viewing the video tape in slow motion, or viewing a still image only one of the two files can be sent to the frame grabber. Resolution now decreases further to 240 x 140 pixels mapped to 516 x 516 pixels on the frame grabber. This process again halves the accuracy of the image coordinate in the vertical plane, reducing the accuracy to a quarter of what it was.

It is unknown how these mappings actually occur electronically, as this information is not freely available. This could lead to unquantifiable distortions which may be critical. Further distortions could also occur if the video tape stretches which would affect the analogue signal the frame buffers receive. This process, apart from radically reducing the accuracy, also halves the single image, reducing the effective size of the object that can be analysed. It is estimated that the standard deviation of the system could be approximately 10 to 15 mm for the Z coordinate.

2.3.5.3 The use of two separate video recorders

Option (iii) would have the same resolution as option (ii). Each video recorder would record an image of 248 x 280 pixels, one file would then contain 240 x 140 pixels which would then be mapped to 510 x 510 pixels on the frame grabbers buffer. There would be further problems in trying to synchronise the replay of the two video recorders. Although it is possible to do so, it would be very expensive. The advantage of option (iii) over option (ii) is that a larger object could be investigated because the single image is twice the horizontal coordinate. A standard deviation of $\pm$ 10 mm could be expected for this system.

2.3.6 Quantitative determination of the fastest dynamic motion allowable:

An experiment was performed to check the maximum velocity a moving body could travel before its shape would become deformed within the imaging period of a CCD camera. The experiment consisted of a pendulum oscillating in a control field. The period of the system was determined by the length of cord of the pendulum, while the

University of Cape Town

velocity of the pendulum was determined as the pendulum passed its vertical axis. Various periods and amplitudes were then recorded on video tape. These sequences were then observed in slow motion to determine under which conditions the pendulum blurred as it passed its vertical axis. From this experiment it was determined that the maximum velocity of a body that a CCD camera can observe, without blurring is 0,45 m/s. The celerity of the waves to be investigated is 1 to 2 m/s. This experiment shows that th present CCD cameras can not be used, without some modification to this system. However there do exist cameras with a much faster imaging rate (1/2000 second), but these cameras are still in their development stage.

2.3.7 Conclusions

Conventional photogrammetric techniques which can give an accuracy of ± 1 mm over the distance of the cameras will be utilised for this investigation. This is superior to the accuracy available from the present NRTP systems. Equipment, such as high resolution cameras, does exist which could increase the accuracy of NRTP systems to approximate that of conventional techniques but it is very expensive. The problem of the CCD camera viewing for too long could be solved either by using a flash system or by using a camera with a faster imaging rate. Presently Phoenics does not possess the accuracy required for accurate experimental work, but with the rate of increase in technology such a system could be viable in the near future. However for the purpose of experimental work in this thesis conventional photogrammetric techniques will be used.

University of Cape Town

3. THE APPLICATION OF CONVENTIONAL STEREO PHOTOGRAMMETRY TO WAVE MEASUREMENT

Stereo photogrammetry was initially applied to the measurement of prototype waveheights and wave patterns. The waves were photographed at oblique angles either from bridges of ships or sea cliffs (Maresca, Seibel 1976); (Adams 1978). Later developments were to use stereo photogrammetry from aeroplanes flying in pairs to obtain wave information. This technique has been used to investigate two dimensional wave energy spectra (Marks, Ronne 1955).

Subsequently it was realised that stereo photogrammetry could have great potential in hydraulic research. When complex wave phenomena are to be investigated, stereo photogrammetry has obvious advantages over traditional wave measurement techniques, for example.

i) there can be no doubt, if sufficient care is taken, that the results obtained are in fact a true interpretation of the waves photographed. For complex wave patterns 100 points/m^2 can easily be obtained using stereo photogrammetry, which should adequately describe most water surfaces.

ii) it is quite possible that the initial analysis would identify a special feature that requires further investigation. This information is easily accessible, without needing to retest, as the stereo pairs provide a permanent record.

iii) it is seldom that more than a few waves can be generated before random wave reflections disturb the desired wave profiles. Using stereo photogrammetry, information may be obtained in a short period before random reflections disturb the surface. This is in contrast with the use of wave probes on a moveable platform, where it is required that waves be generated continuously for a long period of time (½ hr) to obtain the relevant data (Berger, Kohlhase 1976).

University of Cape Town

3.1 Photographing a defined water surface

A liquid surface can not reflect light, and this has been a major limitation in using stereo photogrammetry. In the process of trying to overcome this problem, researchers have experimented with many methods. There are two basic approaches:-

i) to spread particles on the surface to form random observation points.

ii) to colour the water such that the surface can be identified on the stereographic images.

Many types of particles can be floated on the water surface to define it, an example is IBM computer punch card confetti (Sorensen 1968). This method has the disadvantage that the confetti clusters together, and has the tendency to drift out of the area being photographed. This requires that the area being photographed be seeded before each test. Good results have been achieved by spraying the water surface with aluminium powder just before testing (Szczechowski and Mucha 1980). However this method is not popular as it is a very tedious task to clean the basin after each test.

The use of dyes has not been successful, even though it does reduce light penetration. The dyed water creates a monotonous image which is almost impossible to view stereoscopically. Ballistic Research Laboratories, Aberdeen (Faig 1972) are reported to have used cutting oil added to the water to create a white opaque surface on to which a point pattern was projected. Such a surface is relatively easy to analyse stereoscopically. At the University of Cape Town (Adams, Pos 1981) cutting oil was also used, with a random letraset pattern projected onto the surface. Very good results were obtained using this method. Fluorescein, a fluorescent chemical mixed into the water (Faig 1972) in very low concentrations has also been used to identify the water surface. When fluorescein is illuminated with ultra violet radiation it emits a green fluoresecent light. The

University of Cape Town

ultra violet illumination is passed through a grid so that a monotonous image is not created, but the resulting image is still very difficult to analyse.

3.2 Photographing dynamic surfaces:

The celerity of the waves used in hydraulic research is normally in the order of 1 to 2 m/s. Consequently it is important to ensure that the exposure time of the negatives is short enough to ensure there is no significant movement of the wave front. It is also very important to ensure that the two cameras are synchronised so that the same wave state is photographed.

In order for the two photographs to accurately correlate the wave pattern, Individual waves must not be allowed to move more than 1 to 2 mm from when the shutter of the faster camera opens to when the shutter of the slower camera closes. At a celerity of 1 to 2 m/s the minimum time is 1/1000 to 1/2000 of a second. Methods that have been used to synchronise the cameras are,as follows:-

i) to connect the camera shutter assemblies with pneumatic air releases, joined by equal lengths of air hose to a common air bulb. A single squeeze of the bulb would then ideally produce synchronised exposures (Sorensen 1986). However the camera speed will often not be fast enough to reduce movement to within the 1 to 2 mm limit.

ii) to synchronise the shutters by building in electronic delays so that both shutters operate almost simultaneously. Usir this method it is difficult to synchronise the cameras to a difference better than 5 ms (Marks, Ronne 1955). This difference is too large for the accuracy desired.

iii) to use a flash, a method which has produced very successful results. The advantages of this approach is that no attempt need be made to synchronise the shutters of the two cameras. The flashes used generally produce a pulse of light which

University of Cape Town

lasts 1/2000 of a second, freezing the water surface to within 1 to 2 mm limit. Generally the flashes are used at night (Szczechowski, Mucha 1980), with the camera shutters held open until after the flash. This is also the approach used at the University of Cape Town (Adams, Pos 1981).

3.3 Anticipated accuracy of stereo photogrammetry

In previous experimental work (Szczechowski and Mucha 1980) Carl Zeiss UMK 10/1318 photogrammetric cameras were used 10 to 12 m above the water surface to investigate wave patterns around coastal structures. The stereo pairs were taken at night, using flash illumination. A standard deviation in the Z coordinate (height) obtained was $\pm$ 4 mm, which from ten metres height is good. This is equivalent to the accuracy that has been obtained at the University of Cape Town using similar cameras, where a standard deviation of $\pm$ 2 mm was obtained in the Z coordinate when the wave surface was photographed from a height of five metres. It is anticipated that the standard deviations in the z coordinate for experiments to be performed in this investigation will be $\pm$ 2 mm.

University of Cape Town

4. WAVE THEORY AS APPLIED TO WAVE REFLECTION

4.1 Progressive wave theory

A progressive wave is the term used to descibe a wave in which shape visibly moves forward with elapsed time, by contrast with a standing (stationary) wave, where there is no sense of movement in a particular direction. Wave theories are developed to describe such motion by expanding the velocity potential about the still water level to obtain a nonlinear surface condition consisting of an infinite series of partial derivatives.

The most common wave theory is attributed to Stokes. If the first term in the series is used and the rest of the terms ignored then linear wave theory results. Most engineering problems can be calculated to sufficient accuracy using linear wave theory. In deep water it has been shown experimentally and for certain theoretical criteria that the other common higher order theories, 2nd, 3rd and 5th order Stokes theories are less accurate than linear wave theory.

4.1.1 Progressive wave linear theory (Airy theory)

Linear Stokes wave theory was developed by Airy, and is also called small amplitude wave theory as the theory is only valid when vertical displacements are relatively small. This boundary condition implies that the H/d and H/L parameters are small, so the higher order terms in these terms may be considered to have a negligible effect and can be ignored. The resulting free surface displacement as proposed by linear wave theory is sinusoidal and can be expressed as

$$Y_s = \frac{H}{2} \sin (kx - \sigma t)$$

where $k = 2\pi/L$ and $\sigma = 2\pi/T$

The wavelength for linear theory is

$$L = gT^2/2\pi \tanh kd$$

University of Cape Town

4.1.2 Progressive finite amplitude waves

As the wave amplitude becomes "large", the small amplitude assumptions are no longer valid. It is then necessary to include the higher order terms to obtain a more accurate indication of the wave characteristics. Typically, as the waves enter shallower water steepening occurs of the wave crest, and the wave shape, from being sinusoidal tends to become peakier at the crests and flatter in the troughs as predicted by higher order theory.

4.1.3 Stokes 2nd order wave theory

Stokes 2nd order wave theory contains the first and second terms of the Stokes theory expansion. The first term is sinusoidal and the second term represents an elevation (Δh) of mean water level (MWL) above stationary water level (SWL). This theory describes a wave that has steeper crests and flatter troughs than first order wave theory. The free surface displacement is expressed by

$$Y_s = \frac{H}{2}\cos(kx - \sigma t) + \frac{\pi H^2}{4L}\left(1 + \frac{3}{2\sinh^2 kd}\right)\coth kd \cos 2(kx - \sigma t)$$

The equation for the wavelength is the same as that for linear wave theory

$$L = gT^2/2\pi \tanh kd$$

From the second term a number of effects can be identified

i) There is an increase in the mean water level (Δh) of

$$\Delta h = \frac{\pi H^2}{4L}\left(1 + \frac{3}{2\sinh^2 kd}\right)\coth kd$$

ii) There is an increase in the crest amplitude to above the linear wave amplitude of

$$\frac{a_c}{H} = \frac{1}{2} + \frac{\pi H}{4L}\left(1 + \frac{3}{2\sinh^2 kd}\right)\coth kd$$

University of Cape Town

iii) There is a decrease in the trough wave amplitude to less than the linear wave amplitude

$$\frac{at}{H} = \frac{1}{2} - \frac{\pi H}{4L}\left(1 + \frac{3}{2\sinh^2 kd}\right) \coth kd$$

The effects of the second order Stokes wave equation are to describe a wave for which

i) the crest is shorter and more peaked than the trough.

ii) the mean water level is above stationary water level.

iii) the crest amplitude is greater than the trough amplitude.

iv) a_c/H is much greater in shallow water than in deep water.

4.2 The Standing Wave

Clapotis is the term used to describe the standing wave where the crests of the waves are parallel to the reflecting wall. Clapotis exists in effect when two progressive waves are travelling in opposite directions, and the characteristics of the two systems are simultaneously super-imposed. The surface pattern that results has alternating crests and troughs half a wavelength apart. A zone that is a crest one instant becomes a trough half a period later and then a crest again after a further half a period.

For a true standing wave to exist the two opposing progressive waves should be equal in height and period. If these conditions do not exist a partial standing wave results. The standing wave is formed with the incident wave travelling towards a solid vertical barrier, (the wave orthogonal being normal to the barrier) with the reflected wave train travelling away from the vertical wall, having its source at the vertical wall. The reflected wave appears to be a mirror image of the continuation of the incident wave (fig. 4.1). The period of the two waves are the same, and for perfect reflection the wave heights of the two wave trains are also the same.

University of Cape Town

Fig. 4.1 The formation of a standing wave (Linear theory)

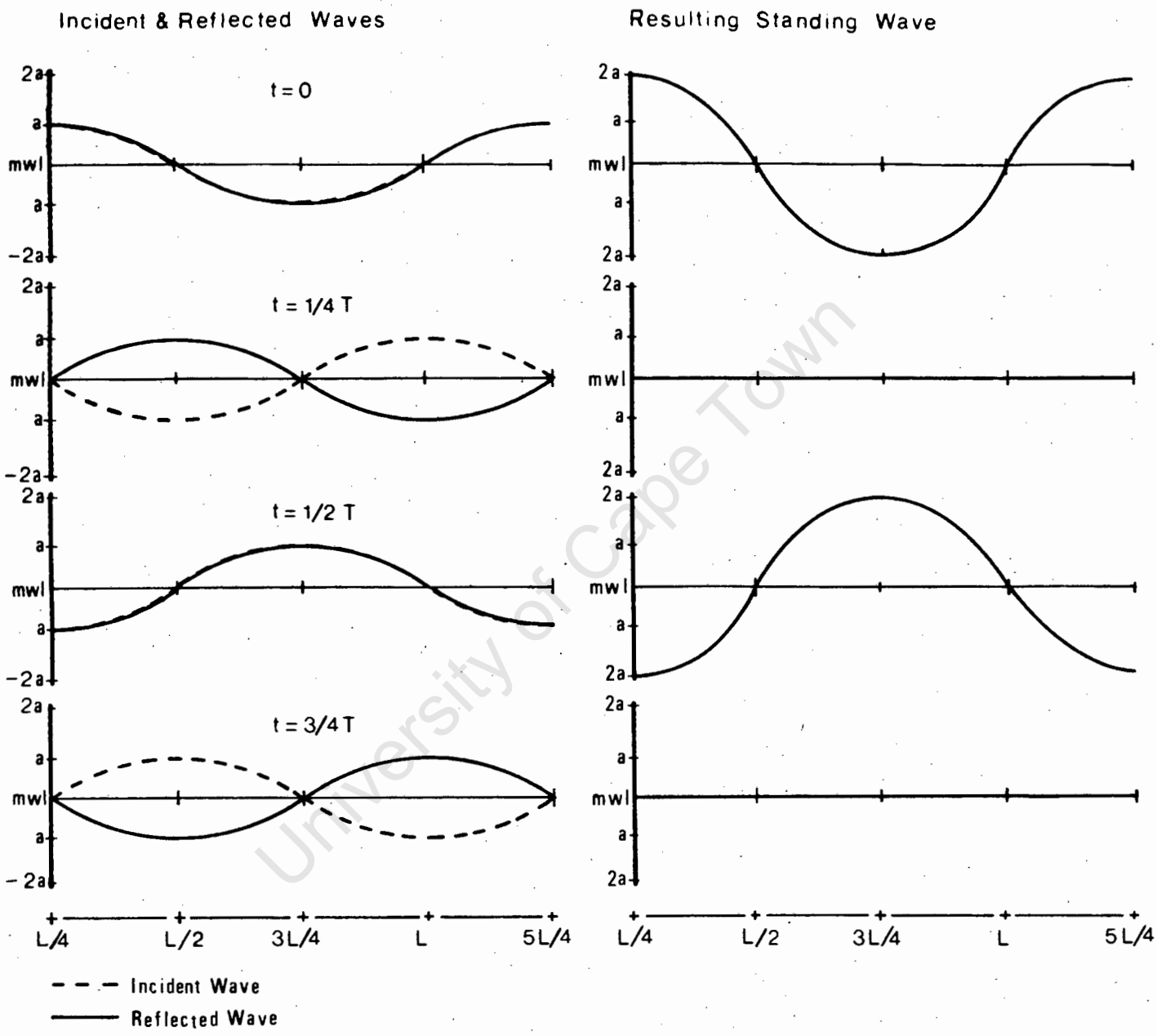

University of Cape Town

The water surface (for linear wave theory) has the appearance of oscillating vertically with maximum deflections of 2 H/2 at points called antinodes, with points of zero deflections called nodes. Antinodes are formed by the superposition of two crests or two troughs, while at nodes the interference of a crest and trough causes

zero surface displacement. For higher order wave theory fig. 4.1 is not correct as a_c is greater than a_t, so stationary nodes do not exist.

4.2.1 Partial clapotis

For partial clapotis two progressive waves must be travelling in opposite directions with the same wavelength and period, but with different waveheights. This is what occurs when a wave is reflected, with some loss in wave energy at the reflecting surface, and the reflected wave height is less than the incident wave height. This might also be accompanied by a slight change in period (Silvester 1974). There are no longer stationary nodes or antinodes. Generally an extreme envelope can be identified which is stationary. It is formed with extreme differences H_{max} and H_{min} (see fig. 4.2) where

$$H_{max} = H_i + H_r$$
$$H_{min} = H_i - H_r$$

so $H_i = (H_{max} + H_{min})/2$

$H_r = (H_{max} - H_{min})/2$

Fig. 4.2 Extreme amplitude envelope

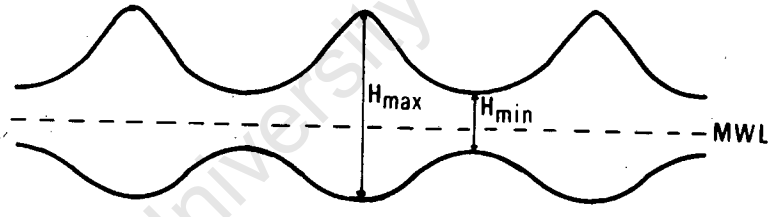

The degree of reflection is measured by the coefficient of reflection (K_r) and is the ratio of the reflected wave height to the incident wave height. K_r is obtained from the standing wave height, less the incident wave height

$$\text{thus } K_r = \frac{H_r}{H_i} = \frac{H_s - H_i}{H_i} = \frac{H_s}{H_i} - 1$$

University of Cape Town

4.2.2 Standing wave, linear wave theory

The reflecting wall is considered to be situated at x = L/4, with the approaching wave normal to it. The equation expressing the incident wave is

$$Y_{si} = \frac{H_i}{2} \sin (kx - \sigma t)$$

The standing wave is defined by $(Y_{si} + Y_{sr})$ where

$$Y_s = Y_{si} + Y_{sr} = (\frac{H_i}{2} + \frac{H_r}{2}) \sin kx \cos \sigma t - (\frac{H_i}{2} - \frac{H_r}{2}) \cos kx \sin \sigma t$$

For partial clapotis or $K_r < 1$, $H_i > H_r$

For perfect reflection or $K_r = 1$, $H_i = H_r$ so

$$Y_s = H_i \sin kx \cos \sigma t$$

The position of nodes, points of zero displacement for all t, will form where

$$\sin kx = 0$$

So $x = nL/2$, where $n = 1,2,3,.....$

Antinodes, positions of maximum displacement, occur where

$$\sin kx = \pm 1$$

so $x = (2n + 1) L/4$, where $n = 0,1,2,3,....$

An antinode will form at time t when

$$\cos \sigma t = \pm 1$$

so $t = nT/2$, where $n = 0,1,2,3,...$

4.2.3 Standing wave 2nd order Stokes

Stokes wave theory is only valid for depths approximately greater than d/L = 0,1. This value changes as shallowing occurs and the wave gets steeper. The waves that will be investigated have d/L values ranging from 0,2 - 0,027, creating a band about d/L = 0,1. This suggests that for extreme events (d/L > 0,01) cnoidal theory should be used in calculations of the theoretical standing wave conditions. However wave theories other than Stokes first or second order are not amenable to standing waves (Silvester 1974).

University of Cape Town

The second order Stokes equation describing the water surface profile is

$$Y_s = H/2 \sin kx \sin \sigma t - \frac{\pi H^2}{4L} \coth kd \cos 2kx \left[\sin^2 \sigma t - \frac{3\cos 2\sigma t + \tanh^2 kd}{4\sinh^2 kd}\right]$$

This assumes $H_i = H_r = H$

The first term of the expression is the same as the linear derivation (but in a different form). The second term represents an incremental increase (Δh) in water level above SWL, which only occurs under the crests L/2 apart. This increase in water level is unlike that of the progressive wave as it is not a global increase in water level. This increase (Δh) under the crests is caused by the $\cos 2kx$ term. The magnitude of Δh is

$$\Delta h = \frac{\pi H^2}{4L} \coth kd \left[1 + \frac{3}{4 \sinh^2 kd} - \frac{1}{4 \cosh^2 kd}\right]$$

4.2.4 Anomalies in the standing wave theory

A major anomaly in the wave theory has been observed experimentaly by Wiegel (1964a). It can be seen in fig. 4.3 that the standing wave wave length appears shorter than the wave length predicted by first or second order Stokes theory. This is contrary to experimental results obtained at the University of Cape Town (Petzer 1987), (Jamie 1988). This is an area that requires further investigation.

Another anomaly that has been shown by Wiegel (1964b) is that the height of the reflected wave at the reflecting wall is 20% greater than twice the incident wave height. This is also something that is requires verification.

4.3 Clapotis gaufre

Clapotis gaufre or oblique wave reflection is the standing wave that results when two waves meet with an angular intersection. Clapotis gaufre occurs when the incident wave orthogonal is not normal to the reflecting wall, but approaches the wall at an angle (fig. 4.3).

University of Cape Town

Fig. 4.3 Comparison of measured and theoretical standing wave lengths

Wiegel (1964a)

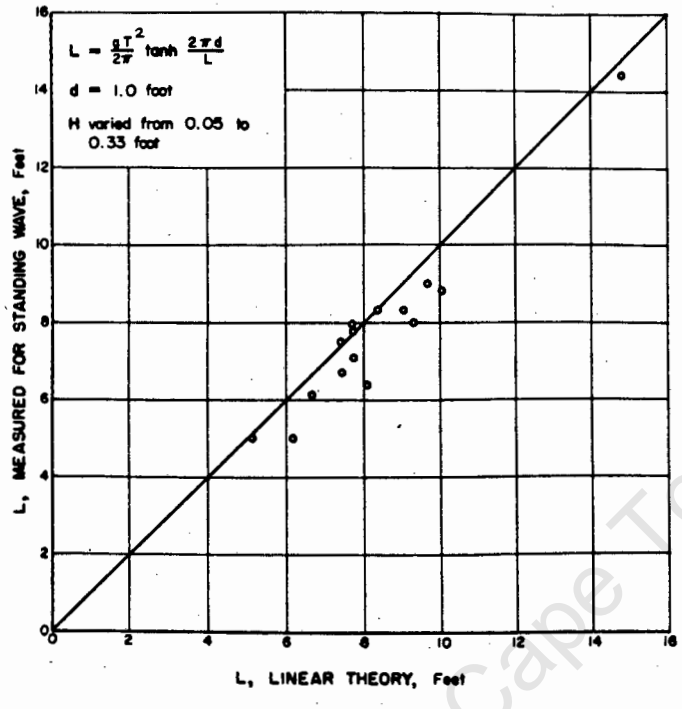

Fig 4.4 Clapotis gaufre

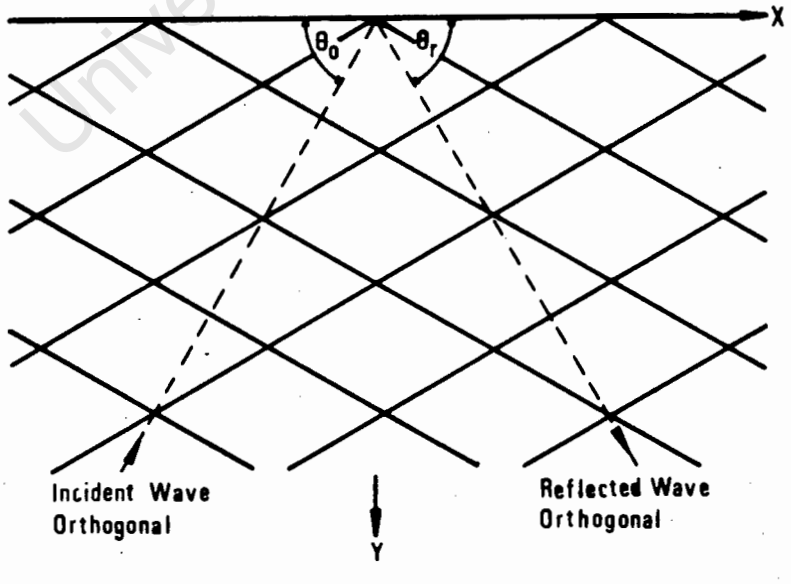

University of Cape Town

In fig 4.4 the x-axis is assumed parallel to the vertical reflecting wall. The angle of approach for the incident wave orthogonal is $(\pi - \theta_o)$, measured from the positive x axis. The angle of reflection for the reflected wave orthoganal is "θ_r" where $\theta_r = \theta_o$.

The wave profile for the incident wave perpendicular to the x axis can be described by (linear theory).

$$Y_{si} = \frac{H}{2} \sin (\sigma t - kx \cos\theta_o + ky \sin\theta_o)$$

The wave profile for the reflected wave assuming $H_i = H_r$ is

$$Y_{sr} = \frac{H}{2} \sin (\sigma t - kx\cos\theta_o - ky\sin\theta_o)$$

The resulting water surface profile is

$$Y_s = H \sin (\sigma t - kx \cos\theta_o) \cos (ky \sin\theta_o)$$

The nodal lines, which are the lines along which no displacement occurs, occur for

$$\cos (ky \sin\theta_o) = 0$$

where $y = \left(\frac{2n + 1}{4\sin\theta_o} \right) L \qquad n = 0, 1, 2, 3 .....$

The antinodal lines are lines along which both maxima and minima occur simultaneously. Antinodal lines occur when

$$\cos (ky \sin\theta_o) = \pm 1$$

where $y = \frac{n}{2\sin\theta_o} L \qquad n = 0, 1, 2, 3 .....$

These quasiantinodal lines move in the positive x direction at a velocity = $L/(T \cos\theta_o)$ with wavelength = $L/\cos\theta_o$.

The resulting surface will appear to be a grid of alternating high and low displacements spaced $L/\cos\theta_o$ apart parallel to the x axis, and $L/\sin\theta_o$ apart along the y axis. These maxima and minima occur in a stationary pattern separated by a stationary pattern of no displacement, the nodal lines.

University of Cape Town

4.4 Mach wave reflection

The Mach wave phenomena is of particular interest to the coastal engineer for two reasons.

i) It appears possible for the Mach wave to attain a wave height of more than twice the incident wave height, so traditional overtopping concepts may be superseded.

ii) Once the Mach stem has formed it will continue to follow the wall, even through changes in direction of the wall of up to 90^{o} (Wiegel 1964b). This could introduce a wave in a coastal structure of more than twice the incident wave height, which conventional diffraction and refraction techniques would not predict.

There exist certain conditions for which the conventional laws of oblique reflection do not apply. When θ_o is less than 35^{o} to 45^{o} (the angle between the incident wave orthogonal and the reflecting wall) the reflected wave does not leave the wall but forms a wave stem perpendicular to the reflecting wall (fig 4.5a). It has been suggested (Berger, Kohlhase, 1976) that the stem height (fig. 4.5b) which increases progressively along the wall can reach a height of more than twice the incident wave height.

Fig 4.5 Mach wave reflection

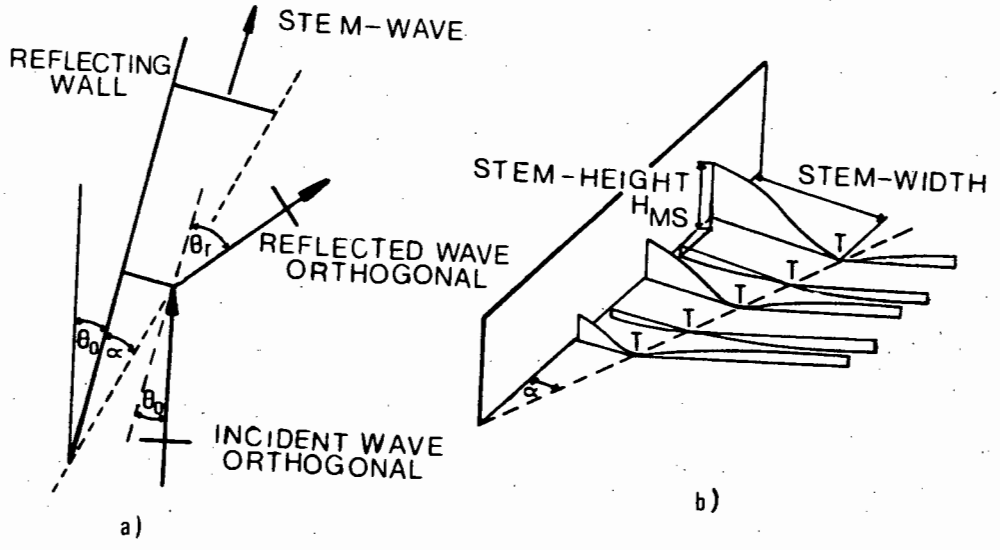

University of Cape Town

PREVIOUS EXPERIMENTAL AND THEORETICAL EXAMINATIONS OF THE MACH-REFLECTION AT STRAIGHT VERTICAL WALLS

author	MACH-stem-parameter				remarks concerning the experiments	remarks on theory
	stem-height	stem-width	stem-angle	behaviour of the reflecting wave		
NIELSEN dimensions of the test basin a = 609,6 cm b = 111.7 cm h = 12,7 cm monochromatic waves H (cm) L (cm) H/d [θ_8] 1.07 45.72 0.22 5 10 0.49 14.65 0.07 15 20	increase of the stem-height with increasing angle of incidence θ_o the stem height is independent of the wave length Remarks: The second MACH-stem effect is not observed in shoaling water In deep water the 2. MACH-stem increases with an increasing angle of incidence θ_o	decrease of the stem-width with increasing angle θ_o increase of the stem-width with increasing wave-height independent of the wave-height decrease of the stem-width with increasing water level supposition: the stem-width increases linearly progressively along the length of the wall	the stem-angle decreases with an increasing angle θ_o	NIELSEN shows that there is a reflecting wave with an angle $\theta_o < 20°$ as opposed to PERROUD	NIELSEN mentions that the stem-width at the end of the wall can be wrong because the model is too small the first part of the reflecting wall touches the wall of the test basin the experiments of the 2.MACH-stem have only been done qualitatively	there is no theoretical explanation
PERROUD The same basin as NIELSEN solitary wave H (cm) L (cm) H/d [θ_8] 1.52 0.38 5 22,5 45	the stem-height is a function of the angle of incidence and has two maxima $\theta_o = 22,5°$ $\theta_o = 45,0°$	the stem-width increases linearly along the length of the wall the stem width of the solitary wave is smaller than that of the periodic waves	the stem-angle decreases	no reflecting wave for an angle of incidence $\theta_o < 20°$ the wave height of the reflecting wave is smaller than that of the incoming wave		PERROUD describes the MACH-stem-effect for a solitary-wave with simple geometric connection
HAGER Eckernforde harbour wind wave H (cm) L (cm) H/d [θ_8] 165 3800 0.05 5.30 10.35 15.45 20.50	the stem-height is a function of the angle of incidence and increases progressively along the length of the wall				the dependance of the stem height of the incoming wave on angle of incidence changes	HAGER computes the stem-height along the reflecting wall. The equation system is similar to PERROUD's

TABLE 4.1 : (Berger, Kohlhase, 1976)

University of Cape Town

In fig. 4.5a the incident wave orthogonal approaches the reflecting wall at an angle θ_o. The Mach stem width (Wiegel 1964b), (Berger Kohlhase, 1976), is thought to grow linearly at an angle α from its point of origin and is the distance from the reflecting wall to the point "T". The point T is the intersection of the incident wave and the mach stem. The reflected wave is reflected at angle θ_r, where $\theta_r = \theta_o + \alpha$. These conditions exist for $d/L < 0.5$ and where $45^o > \theta_o > 20^o$. For $\theta o < 20^o$ the wave crest and mach wave are continuous possibly without a reflected wave being formed (Wiegel 1964b).

4.4.1 Review of previous investigations

Mach reflection has been investigated under various conditions in the sea and in hydraulic models. Major contributions to Mach reflection have been made by P.H. Perroud, A.H. Nielsen and M. Hager as reported by Berger and Kohlhase (1976). A pertinent summary of this data is presented in table 4.1.

Wiegel (1964b) and Perroud both investigated the Mach effect related to solitary waves, with particular emphasis on explaining the unexpected effects that occurred for tsunamis entering the Bay of Hilo, Hawaii. Prototype data was obtained by Hager at the jetty of the Echernforde Harbour, Germany, but unfortunately a limited amount of measurements and the scatter of the data only allow qualitative conclusions to be drawn.

Nielssen and Berger, Kohlhase (1976) both investigated Mach reflection for periodic waves. Nielsen showed there was an increase in stem height along the wall, and that the stem width was a function

University of Cape Town

of the angle of incidence and wavelength. Unfortunately too little data on too small a scale did not allow any definite trends to be established.

Berger and Kohlhase (1976) attained further experimental results in a much larger wave basin, to compare their results to the diffraction theory they propose. These investigators report the development of a second stem wave for θ_o = 20°, 25° and 30°, five wavelengths from the origin of the wall (fig. 4.6).

Fig. 4.6 Development of second mach stem. (Berger Kohlhase, 1976)

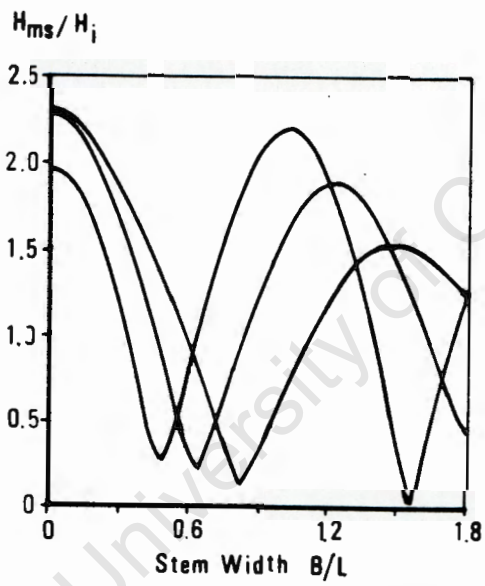

University of Cape Town

4.4.2 Theoretical explanation of the Mach wave

Originally Wiegel (1964b) proposed that the Mach reflection phenomenon might be analogous to the Mach reflection occurring in acoustics, hence the name Mach reflection. This theory though has not been satisfactorily applied to gravity waves. A theory has been proposed since, by Berger and Kohlhase (1976). They propose that Mach reflection should be interpreted as a diffraction problem in the area of reflection. From linear wave theory and the diffraction

solution for a half-infinite breakwater a Fourier series expansion was proposed. The solution to this expansion can only be solved numerically on a computer. Fig. 4.7 is a comparison between the theory and the results obtained by Berger and Kohlhase (1976). It is evident that the theory proposes that the mach stem height should increase, then decrease with increased distance from the origin of the breakwater.

Fig 4.7 Stem height along a vertical wall (Berger, Kohlhase 1976)

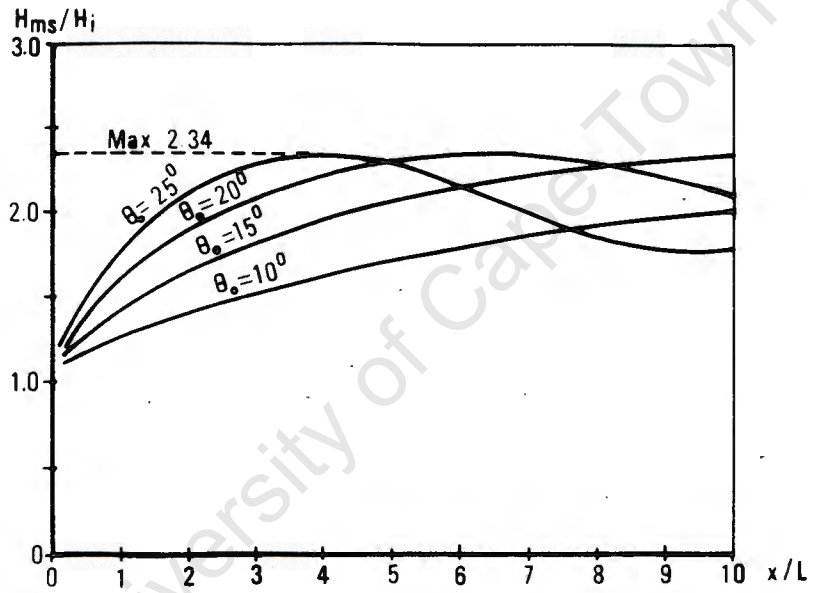

University of Cape Town

5. EQUIPMENT USED FOR THE INVESTIGATION

5.1 Equipment used for the photogrammetry

5.1.1 Zeiss Jena UMK 10/1318 universal measuring cameras

Two Zeiss Jena UMK 10/1318 metric cameras were used for the photogrammetry. These cameras have a near distortion free Lamegon 8/100 lens system. Another feature of these cameras is that the principal distance of the cameras can be changed to allow focusing for distances from 3,6m to infinity. This is a particularly important feature as the cameras are mounted 5 m above the wave basin, and numerous other metric cameras can only focus on infinity, so any images obtained from fixed focus cameras would not be useable.

The important specifications for these cameras are:

Focal distance at infinity	99 mm (approximately)
Distortion (focusing to infinity)	max 5 µm
Average resolution	55 lines/mm
Shutter speed	1 sec - 1/400 sec
Stop settings	8 to 32
Focus settings for distances	∞; 25 m; 12 m; 8 m; 6 m; 5 m; 4,2 m; 3,6 m
Format size	120 mm x 166 mm
Field of view - long format	78^{o}
- short format	58^{o}

These specifications show that these cameras are ideal for the purposes of close range photogrammetry as

i) the cameras are metric cameras, so the interior orientation elements are known (See Section 2.1.1).

ii) the lens is near distortion free (see Section 2.1.1).

iii) the negative has a large format and the wide angle lens allow the entire area of the wave basin to be photographed.

University of Cape Town

5.1.1.1 Photographic plates

Photogrammetry requires that the photographic emulsion be in a single plane (see Section 2.1.1). To ensure this, photographic plates are available, which consist of a ground glass surface with the photographic emulsion fixed to the ground surface. These photographic plates are extremely expensive, so an alternative, sheet film was glued onto the ground glass plates. This process does not appear to reduce the resultant accuracy of the photogrammetry (Ruther 1982).

For the lighting condition available, with the cameras set to the largest F-stop (F8), a film with a speed rating of ± 320 ASA is required. Normally Ilford HP5 film is used, unfortunately the incorrect film (Ilford FP4) was supplied, with a speed rating of 125 ASA. Due to time constraints (it takes 3 months to import film) the HP4 film was used for the investigations and was push processed using Microphen, a special push processing developer. Adequate results were finally obtained using this process.

5.1.2 Carl Zeiss Jena Steko 1818 Stereo Comparator

The Steko 1818 Stereo Comparator (plate 5.1) is used to obtain the (x, y) and (Px, Py) cooordinates from the negatives (See Section 2.1.1). The Steko 1818 has a reading accuracy of better than 10 μm for the (x, y) coordinates and 2 μm for the (Px, Py) coordinates. A Motronic electronic analogue to digital converter (plate 5.1) is used to convert the analogue signal from the Steko 1818 into digital coordinate values for the two plates. The values of the (x, y, Px, Py) coordinates now in digital form are sent to the HP 9816 micro computer.

University of Cape Town

Plate 5.1 Steko 1818 Stereo comparator and peripherals.

5.1.3 HP 9816 microcomputer

The HP 9816 microcomputer (plate 5.1) is used

i) to accept and store the control point coordinates, and the image coordinates obtained from the Motronic A-D converter,

ii) to produce the projective transformation parameters of the wave basin for the pair of negatives being observed, using the (x, y, Px, Py) coordinates of the control points (see Section 5.4.2),

iii) to calculate the global coordinates (relative to the axes of the wave basin) of the object points observed on the wave surfaces using these projective transformation parameters previously calculated on the HP 9816. The coordinates of the object points are then down loaded onto the VAX computer descibed below.

5.1.4 The DEC VAX/VMS 6230

The Vax 6230 mainframe is operated from various terminals, for which IBM compatible PCs may be used (plate 5.2). All analysis of the data (object points) is performed on the VAX. The data is processed using a contour package "SACLANT" which is available on the VAX. Saclant can be used to obtain contour plots and three dimensional plots. The data can be manipulated, such that different wave patterns may be subtracted or added to each other, perhaps to show the differences between two wave patterns.

Plate 5.2 An IBM compatible PC acting as a Vax terminal

University of Cape Town

5.2 Equipment required to generate the required wave patterns

5.2.1 Wave Basin floor

In order to investigate the desired wave phenomenon the incident wave must be as uniform as possible. The incident wave must stay parallel to the wave generator along its entire length. The waves that will be investigated are shallow to intermediate waves (d/L values < 0,5), so the celerity of these waves will be a function of depth. Consequently changes in the floor basin level will cause the wave to refract, and disturb the pure incident wave desired. To minimise this effect the wave basin floor was levelled to within as small tolerance as possible. Pos (1984) managed to level the wave basin floor to within $\pm$ 1 mm. This represents a variation in water depth of less than 1% for a 150 mm water depth.

The dampness had caused the epoxy which had been used to level the basin, to lift in places. The epoxy which had lifted was removed, and the gaps were then filled and leveled to the surrounding basin floor. Polyfilla and a strong mortar mix was used to repair the gaps. These repairs were carefully cured to avoid shrinkage and were very successful.

5.2.2 Wave Generator

The wave paddle is driven by an electric motor at a constant speed, through a gearbox. The first drive arm (Plate 5.3) is connected eccentrically to the driveshaft from the gear box by an offset cam. The period of this shaft is the same as that of the wave paddle. The wave height is varied mechanically by moving the position of the first drive arm up or down on the wave height rocking arm. This changes the amplitude of the wave height rocking arm oscillations and so changes the wave height. The second drive arm is attached to the wave height rocking arm and to a single bar which is cantilevered from the shaft about which the wave paddle is oscillated. The oscillation of the wave paddle should ideally be simple harmonic motion.

University of Cape Town

Plate 5.3 Wave generator

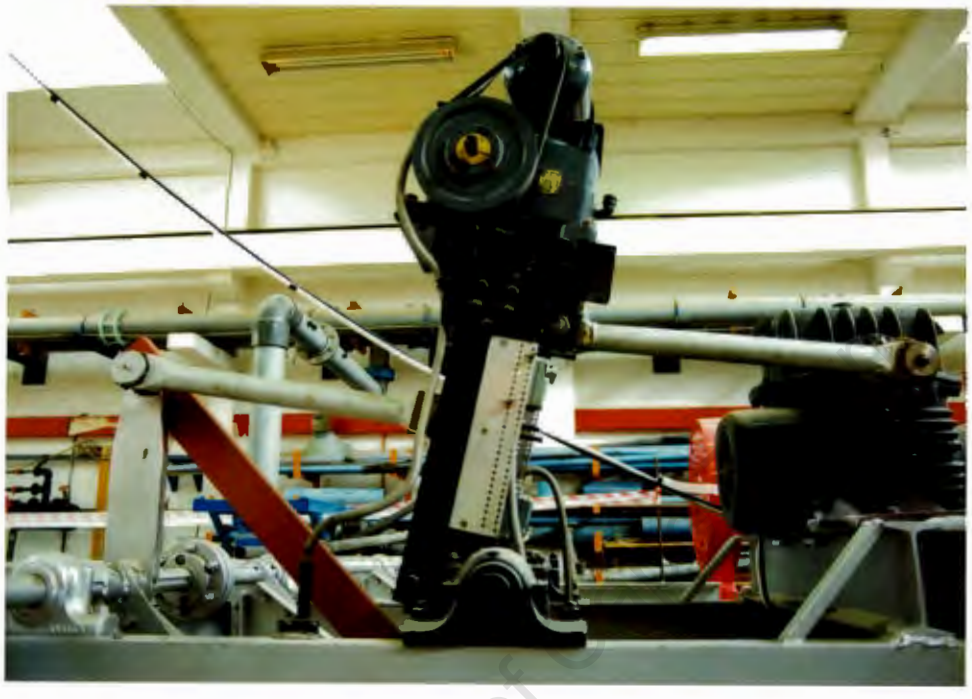

It was observed that the wave generator was not generating a pure sine wave, but a wave with a small crest in the trough and a double crest. Further aberations to the ideal wave can be identified in plate 5.3.

i) The paddle generated crests curved in plan, as the crest near the walls lags behind the central crest.

ii) The wave paddle is made from five box sections, each with a strut running down the centre (as seen in plate 5.4). These box sections are not connected and appear to be moving relative to each other, producing small concentric wave patterns from the middle of each section at its supporting strut.

Furthermore, when the wave generator was switched off the previously generated waves trapped in the basin, reflected off the wave paddle and moved it by 50 mm.

University of

Plate 5.4 Impure wave generated by wave generator

These problems appear to occur because of the general flexibility of the paddle. The entire wave paddle is moved by the torsional transfer of moments from the single cantilever attached to the 50 mm diameter shaft. This shaft does not have the torsional stiffness to move the wave paddle without undergoing significant torsional strain. From this it was deduced that

i) the far edges of the wave paddle would lag behind the centre of the wave paddle, creating a curved crest (Plate 5.4),

ii) as the wave paddle moves either forward or backward, torsional strain is induced in the shaft. When the shaft slows down and stops at the extreme point of its oscillation the strain energy is released. The paddle then jerks in the original direction of travel inducing a crest, either next to an old crest or in the middle of a trough.

iii) the strain energy when released, is released at the point of connection of the supports of each of the boxes making up the paddle. These boxes are able to move relative to each other, and so create high points along the crest.

Plate 5.5 Modifications to the wave paddle

To reduce these torsional effects it was required that the driving force be supplied in some alternate manner. The solution adopted was two fold.

i) The vertical plane in which the load is applied to the cantilever was significantly stiffened so that the load would not be torsionally transferred along the shaft. A strut (plate 5.5) was installed from the top of the cantilever to the rear of the wave paddle. This creates a strong stiff section that can not easily deflect.

ii) The horizontal plane of the wave paddle was significantly stiffened to transmit the load. The box sections are welded

together along their top plane (see plate 5.5). This creates a plate which is well supported against buckling and is very stiff.

Plate 5.6 Wave generated after modification

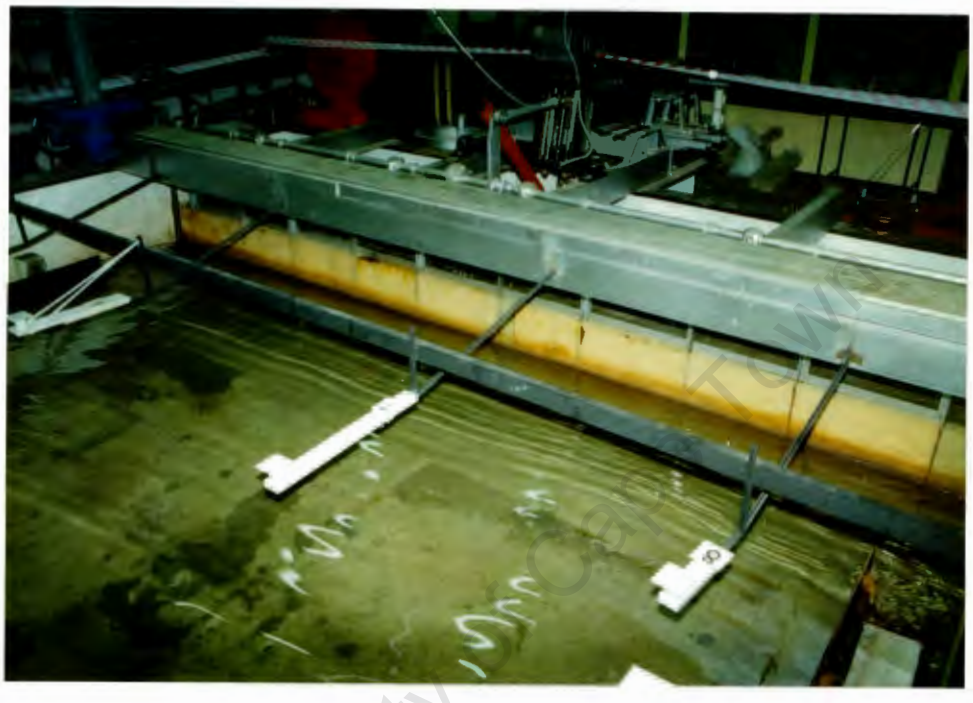

University of Cape Town

The modifications made the wave paddle significantly stiffer, but displacement still occurred when a load was applied. Using dial gauges the displacement of the entire wave generator was measured. It was found that small deflections (0,1 mm) occurred in the bearings joining the various shafts. These displacements were, because of the relative lengths of the lever arms, being amplified to create deflections in the order of 1,5 mm. These deflections cannot be reduced as even if the bushes were replaced, it is expected that the displacements in the bearings would still be of a similar magnitude. A further measure to reduce any unevenness in the generated wave was to place a layer of expanded foam on the front face of the wave paddle. Plate 5.6 shows the wave generated after modification. This wave is not ideal but has been significantly improved.

5.2.3 Moveable reflecting wall

Fig. 5.1 Cross section of the reflecting wall

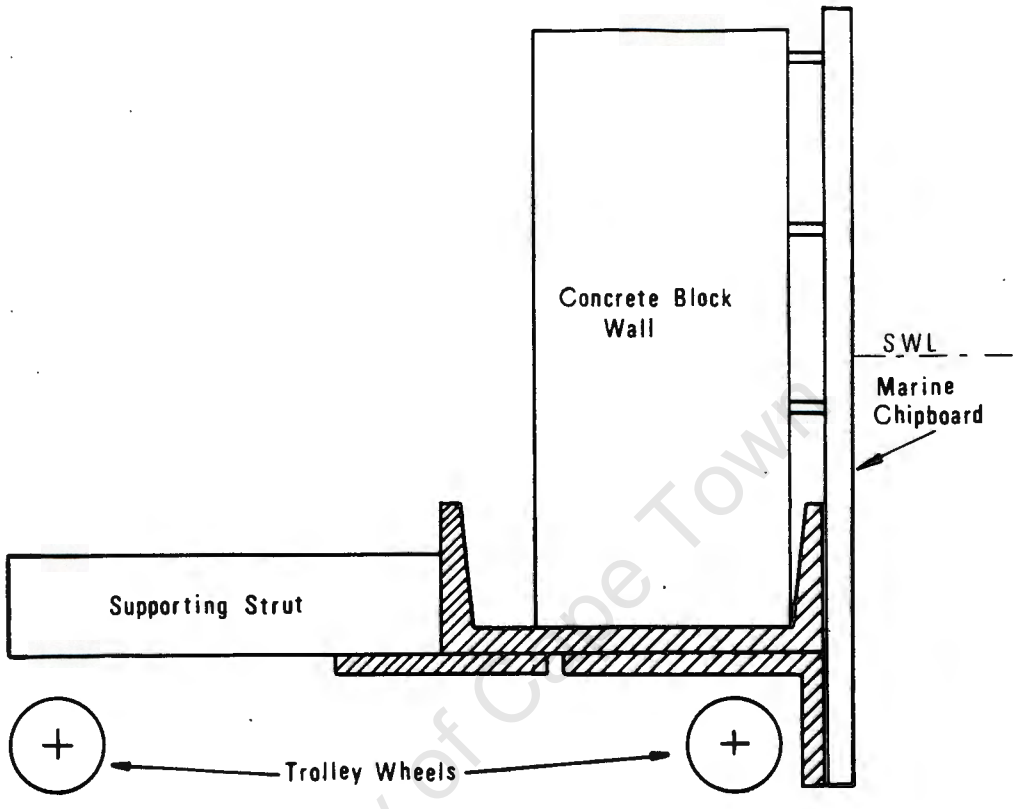

A vertical reflecting wall is required which can be moved and so positioned to obtain optimum usage of the wave basin. It is particularly important for oblique reflection that the reflecting wall be moved as far to the edge of the wave basin, to create the maximum area of clapotis gaufre. In addition to the wall being mobile it is required that

i) the wall be rigid, so no deflections or vibrations occur under wave loading, inducing an impure reflected wave,

ii) the wall be vertical once positioned in its new position,

iii) water cannot eddy under the wall, absorbing some of the incident wave energy.

University of Cape Town

Plate 5.7 The Moveable reflecting wall.

It was decided to build a wall (fig. 5.1) consisting of an inverted steel channel mounted on trolley wheels, with an angle welded onto the base of the channel to make the front wall face continuous. Four legs were welded onto the back of the channel to which trolley wheels were also attached for stability. Rods were welded vertically on the inside of the channel. Concrete blocks were then laid on the inside of the channel. A sheet of marine chipboard was then attached at an angle, racked backwards with its lower edge just above the wave basin floor. The board was used to ensure the wall had a perfectly flat front face. The board was attached at numerous points along the concrete and steel substructure and could not deflect or vibrate.

University of Cape Town

Nuts were welded to the four stability legs, threaded studs with points could then be screwed down locking the wall in its desired position and pushing it into a vertical plane. In doing this the marine chipboard came into contact with the wave basin floor, effectively sealing the wall so no water could flow under it. The completed wall can be seen in plate 5.7.

5.2.4 Side walls

Plate 5.8 Side walls "hiding" the tins

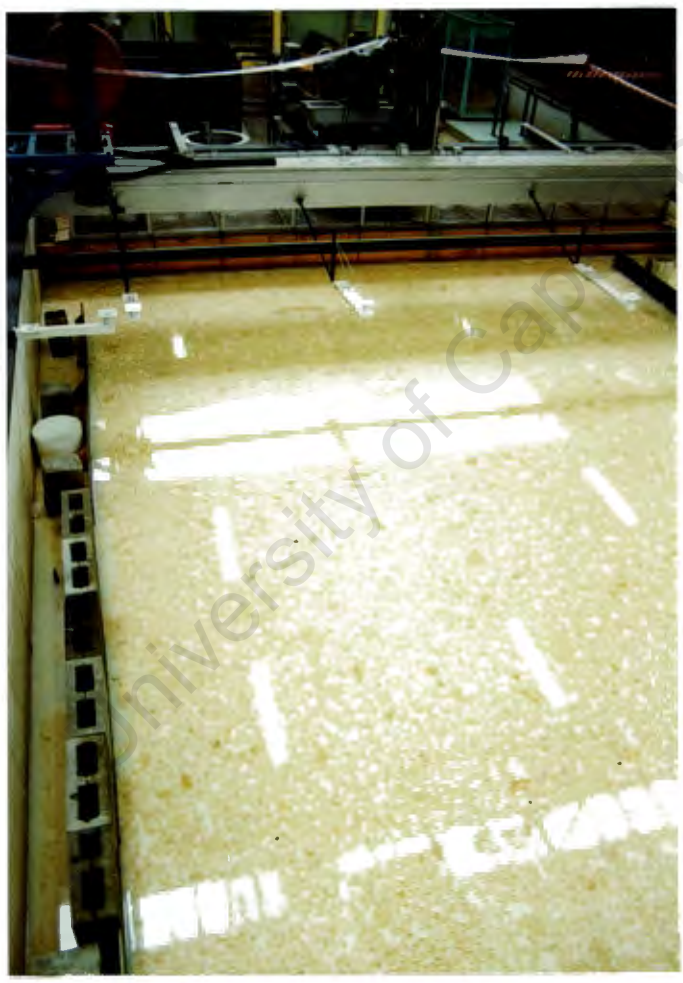

University of Cape Town

Four control points are positioned below the water surface in tins (see Section 5.4.2). These tins create a confused water surface when waves are generated because of their diffraction effects. To stop these effects the tins must be "hidden", and this was done by

building false walls (plate 5.8). It is required that the false walls be designed to absorb the wave energy generated across the width of the false walls. This also means that the section of the side wall that meets the wave front must be sharp to act as a wave splitter or another set of diffraction patterns could occur.

The false walls consist of concrete blocks packed on top of each other between the tins. Then for the wave splitters and the sections of the wall covering the tins marine plywood cantilevered retaining walls were built. The wooden supports for the marine ply wall next to the section acting as the wave splitter, were sawn flush with the water surface. This arrangement worked well in absorbing the wave energy behind the wave splitter.

5.3 The design of the wave absorbers

When oblique wave reflection patterns are investigated, the reflected wave will soon reach the side of the wave basin. The wave will then reflect again, advancing into the area of photography creating a confused wave pattern. If any meaningful results for oblique reflection are to be obtained, an efficient wave absorber is required to absorb this reflected wave.

Traditionally the most effective wave absorber is a gradual spending beach. Unfortunately such a beach would occupy most of the wave basin, significantly reducing the area of the wave basin in which an undisturbed wave pattern could be photographed. As a gradual spending beach is not practical, an efficient narrow wave absorber had to be found.

5.3.1 A review of pertinent papers

5.3.1.1 A perforated vertical wall breakwater, by G E Jarlan

(The Dock and Harbour Authority, April 1961, p.394)

In this paper a perforated vertical wall is proposed as a method of designing a caison structure for wave energy absorption. The structure consists of a double walled structure separated by a chamber. The wall facing the incoming wave train is perforated.

University of Cape Town

This perforated vertical wall breakwater achieves a coefficient of reflection of 0,1 to 0,2.

The perforated breakwater was designed for a regular wave train. The waves cause a filling and emptying of the enclosed chamber by resultant horizontal water jets in both directions. The impedance of the perforated wall causes a phase difference and a decrease in motion between the outer wave and the water level in the chamber. As the water spills into the chamber there is a significant energy loss, and as the chamber empties into the wave trough it creates a surface current opposing the incoming wave, acting as a hydraulic breakwater. These two processes create an efficient system for wave absorption.

5.3.1.2 Experimental development of a perforated wave absorber of simple construction and minimum length, by P A Hamill

(Mechanical Engineering report, M3-252, National Research Council of Canada, May 1963.)

This paper tries to develop an efficient wave absorber of minimum length. It is assumed that a beach that gives a coefficient of reflection (K_r) of less than 0,1 is very efficient. This assumption is made as wave energy is proportional to wave height squared, so if a beach absorbs 99% of the wave energy, the coefficient of reflection is 0,1. Hamill decided that an optimum beach would have a coefficient of reflection of less than 0,08. The range of waves investigated were deep to intermediate depth waves.

Two break waters were investigated, which were found to be particularly effective.

i) Model A (fig. 5.2) a 0,9 long section of 12 mm plywood with 25,4 mm holes at 51 mm centres projecting from a perforated breakwater.

ii) Model B (fig 5.3) was similar to Model A but without the perforated breakwater, with an angled perforated support.

University of Cape Town

Hamill states 'the choice of perforation was arbitrary'. Fig 5.4 is a graph of the wavelength against average reflection coefficients for various H/L values.

Fig 5.2 Model A (Hamill 1963)

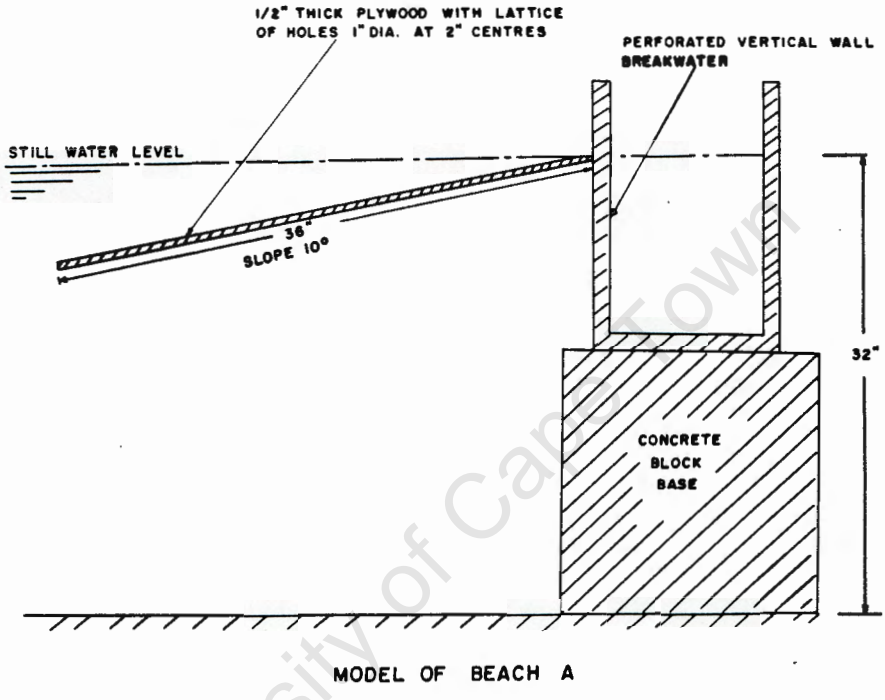

Fig. 5.3 Model B (Hamill 1963)

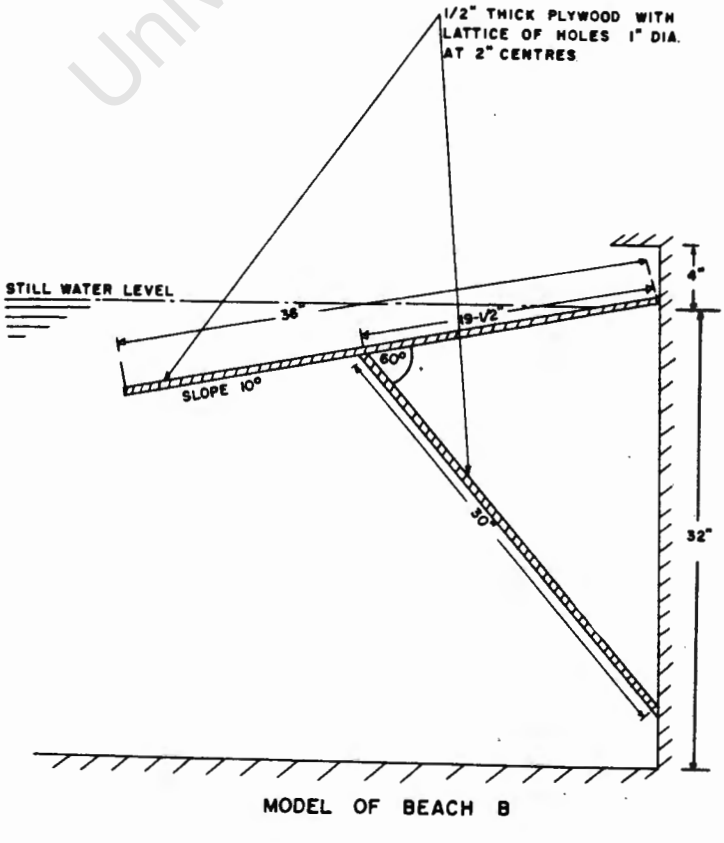

University of Cape Town

Fig. 5.4 Reflection coeficients for perforated wave absorber (Hamill 1963)

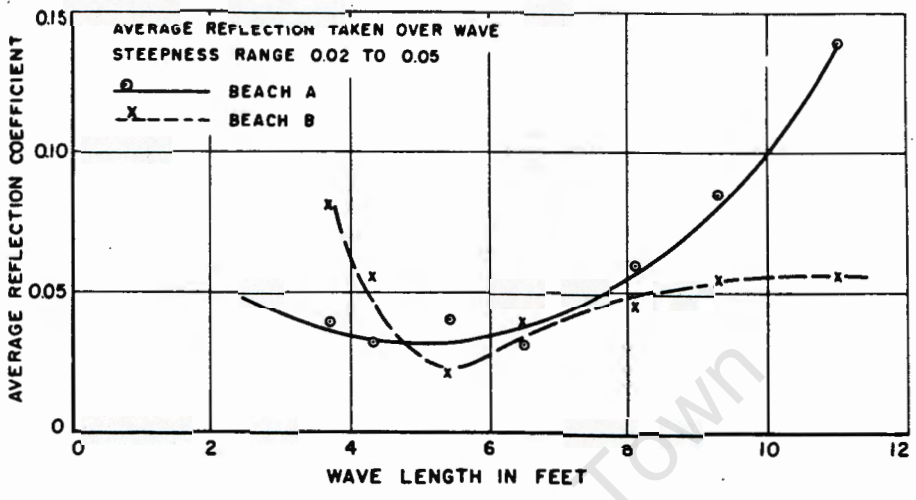

AVERAGE REFLECTION COEFFICIENT AS A FUNCTION OF WAVE LENGTH

5.3.2 Initial choice of wave absorber

It was on the basis of Hamill's design that the initial design for the wave absorber was selected for this investigation. Hamill achieved a very small coefficient of reflection for his perforated wave absorber of 0,04 to 0,06. It is hoped that similar coefficients of reflection will be obtained for the wave absorber to be implemented in this investigation.

It was difficult to decide on the choice of scale factor to be used. Table 5.1 summarises the pertinent wave data for comparison.

Table 5.1 Comparison of Hamill's wave data with UCT wave data

	Hamill's wave data	UCT wave data
depth (d)	813 mm	150 mm
waveheight (H)	22,6 - 167 mm	20 - 35 mm
wavelength (L)	1130 - 3350 mm	750 - 1750 mm
wave steepness (H/L)	1/20 - 1/50	≈ 1/30
wave type (d/L)	0,24 - 0,72	0,088 - 0,2

University of Cape Town

The data cannot be compared in a dimensionless form by dividing by the depth (d) as the ratio of the depths of UCT : Hamill is 1 : 5. Hamill uses a wave absorber that is 910 mm long and a wave absorber a fifth of that length is not realistic. Froude scaling was investigated on the basis of determining the relative celerities of the waves, but then the length ratio for UCT : Hamill is 1 : 3,5. This does not appear correct either.

The essential difference between the data presented, is that Hamill investigates deep water waves while at UCT intermediate water waves will be investigated. As the type of wave is not comparable, scaling must occur based on wave height and wave length. The average of Hamill's data for both wave height and wave length is higher than the data for UCT, so the initial approximation for the length of the absorber to be tested was 0,9 x (Hamill's wave absorber length) = 820 mm. From fig 5.5 it can be seen that in shallower water Hamill's "Beach B" was most effective. The design for the wave absorber to be tested was based on "Beach B".

5.3.3 Testing of the wave absorber

5.3.3.1 Design of the test absorber

Plate 5.9 The flume used for testing the wave absorber.

University of Cape Town

The wave absorber was tested in the small flume (plate 5.9), which has a maximum operating depth of 100 mm, two thirds the depth of the prototype. The model was then built on a two thirds scaling of the prototype. The wavelengths tested were scaled down by keeping the d/L ratios constant. The scaled down wave absorber was 545 mm long. The first design for the wave absorber used an absorber of 590 mm long.

The model wave absorber (fig 5.5) was designed with a heavy hinged support, about which the entire wave absorber could be rotated. In this way numerous different slopes of the wave absorber could be investigated. The chamber wall was attached by soft steel plates to the main wave absorber and could be bent to fit any slope of the wave absorber. Both the wave absorber and the chamber wall were perforated. The length of the chamber (L_c) is the distance from the end wall of the flume to the chamber wall.

Fig 5.5 Model wave absorber

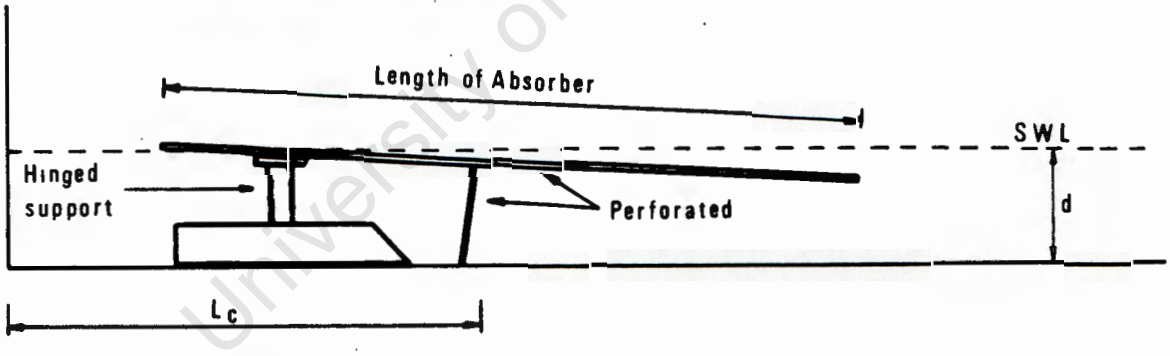

University of Cape Town

5.3.3.2 Method for measurement of relative wave absorption

The efficiency of the alternative arrangements of the wave absorber were examined qualitatively. The wave generator was run for 20 wave periods and then stopped, such that the wave paddle always stopped in its highest position, displacing the least amount of water. A probe was then placed 1,5 mm above this SWL. The time was then recorded on

a stop watch from when the wave generator stopped till the last wave to touch the probe. This time period is known as the time till minimal displacement (ttmd).

This method worked well, and it was easy to distinguish when a wave touched the probe. The repeatability of experiments was good with average differences in the ttmd of 0,1 seconds. It must be recognised though that the results cannot be interpreted linearly. Situations were observed where the probe was touched at 6 seconds and then again at 11 seconds, so the ttmd is 11 seconds. Then in a following experiment with only a slight change in the apparatus, the ttmd was 6 seconds but it was observed that the water just missed touching the probe after 11 seconds. This observation shows that the results obtained are not linear, so ttmd = 11 does not have a reflection coefficient twice that for ttmd = 6, the difference could actually only be 10%.

5.3.3.3 Selection of the design wave

It was observed that for the longer wavelengths the ttmd was longer than for the shorter wavelengths. On this basis it was decided to use the longest wavelength for the experimental testing. A wave with a 1,2 second period for the model corresponds to the longest wave that could be expected for the prototype. In order to ensure the worst case conditions a wave height of 40 mm was used. This wave height is larger than any wave expected in the prototype.

5.3.4 Mechanism of wave absorption

There are two noticeable effects which appear to affect the energy absorption process.

i) The first and most important effect is shown in plate 5.10. It appears that it is the orbital wave motion that actually destroys the wave energy. When the wave meets the wave absorber the crest slows down as it is entering a semi-shallow water wave condition. The rest of the wave, below the wave absorber, does not realise there is an obstruction and tries to continue its orbital motion to raise water particles to

University of Cape Town

create the continuation of the crest. This upward motion of the water particles creates jets of water, ahead of the crest, as the water particles force through the holes in the wave absorber. In this way, as the crest travels along the wave absorber, strong hydraulic jets are breaking up the crest dissipating its energy. This process appears to be the major factor in the effectiveness of the wave absorber.

Plate 5.10 Wave absorption process

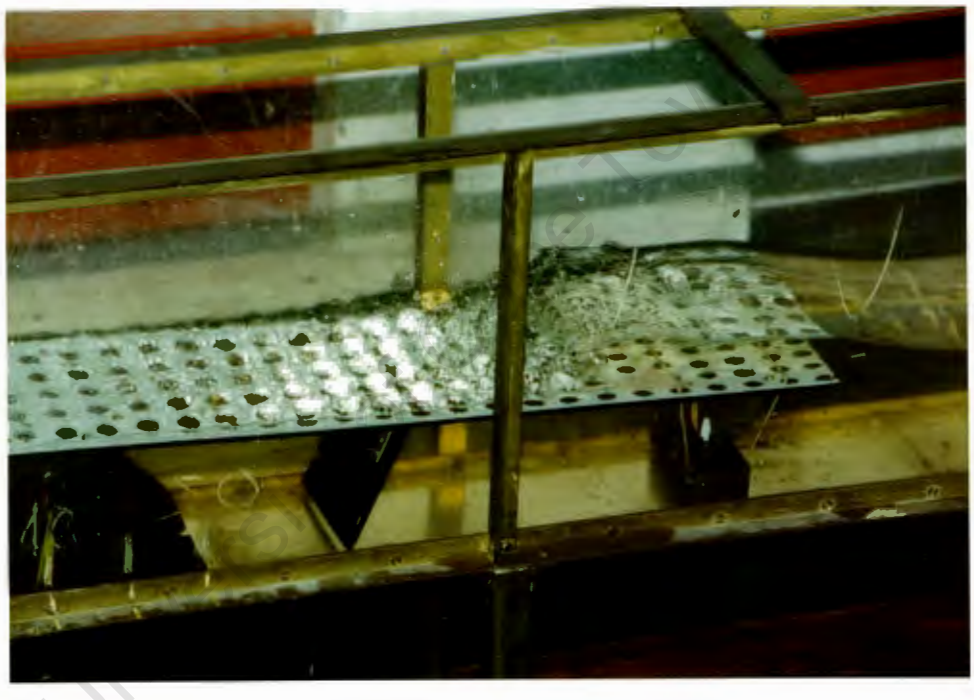

ii) Another effect, similar to the impedance of the vertical breakwater (Jarlan 1961), was observed. The water from the waves runs into the chamber behind the wave absorber, creating a standing wave which empties after a certain phase difference, depending on the length of the chamber. For small chamber lengths the chamber empties before the arrival of the following wave, this is an effective combination. For intermediate chamber lengths the chamber empties just before the wave arrives, interfering with the hydraulic jets and creating a bed of water for the wave to run up without being

dissipated. Finally the chamber can empty just as the wave crest reaches the chamber, creating further hydraulic jets, which is also effective; this case can be identified in plate 5.10.

5.3.5 Relationship of the various parameters

Two wave absorbers were tested:

i) Design 1 - with a length of 590 mm and initially 120 12 mm diameter holes.

ii) Design 2 - with a length of 680 mm and initially 182 10 mm diameter holes.

The parameters investigated for the two designs were all based on the selected wave (see Section 5.3.3.3) which is a wave with a period of 1,2 seconds and a wave height of 40 mm. The parameters investigated were the slope of the wave absorber, the necessity for a chamber, and the optimum number of holes in the wave absorber and their size. The optimum chamber length was also identified. This investigation was limited for time and the effects of all possible parameters could not be investigated in as much detail as may have been desired. It required 600 independent tests to produce the data presented, and was very time consuming.

5.3.5.1 The optimum slope of the wave absorber

Four different chamber sizes were compared for various wave absorber slopes, the slope of the wave absorber being measured from the horizontal. For Design 1 (Fig 5.6a) $2,2^{o}$ appears to be the optimum slope. The optimum slope for Design 2 (Fig 5.6b) is $2,7^{o}$. These two results produce an average optimum angle of $2,5^{o}$.

University of Cape Town

Fig 5.6 Optimim wave absorber

a)

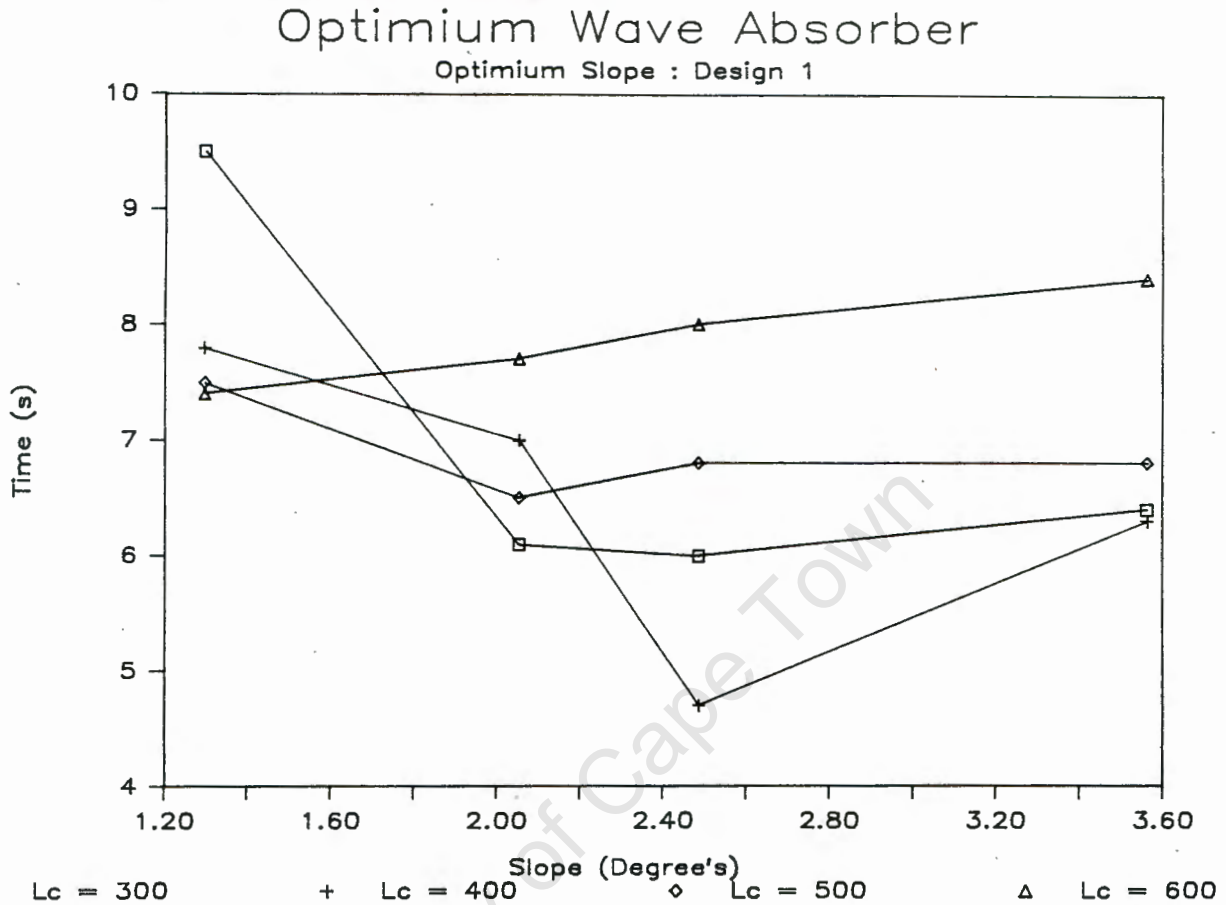

b)

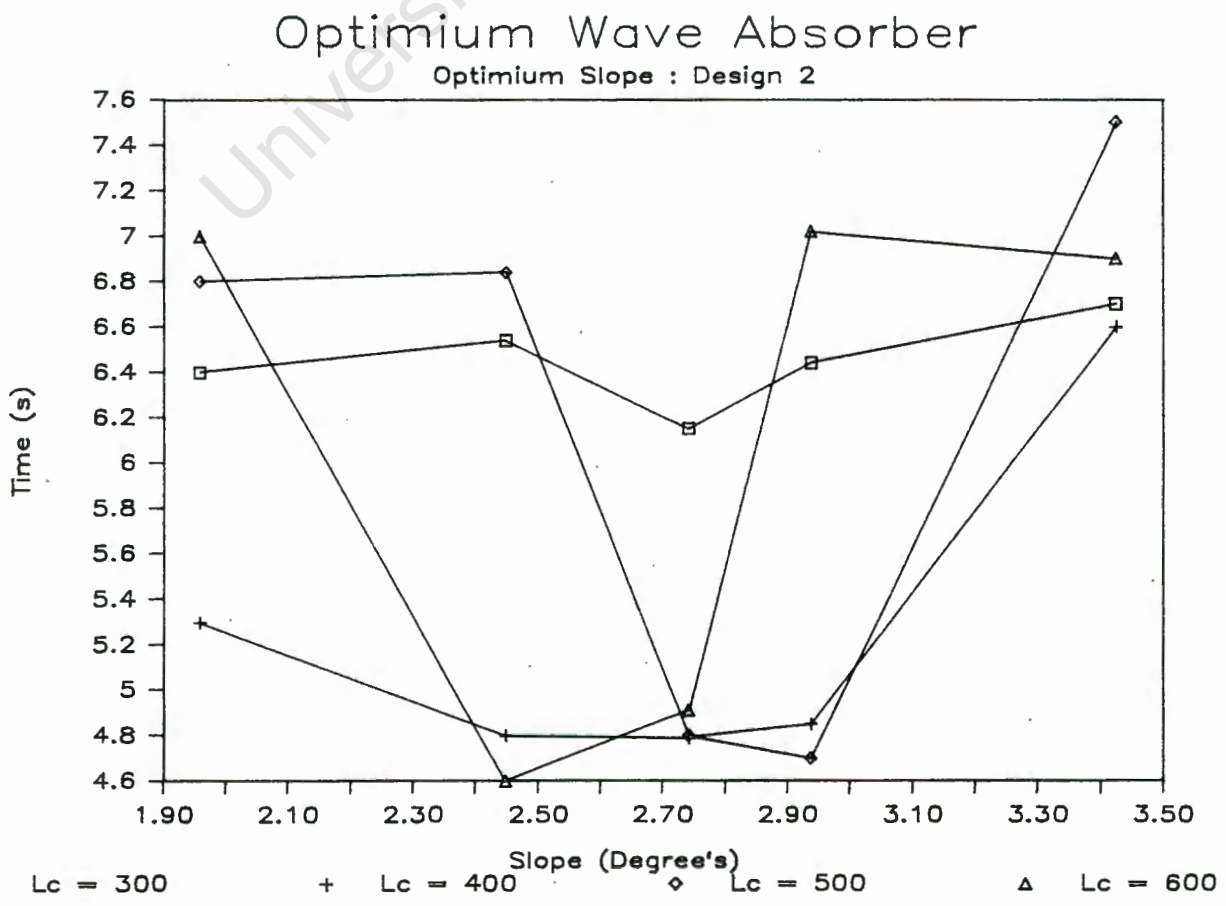

University of Cape Town

5.3.5.2 The importance of the chamber

Fig 5.7 Optimim wave absorber

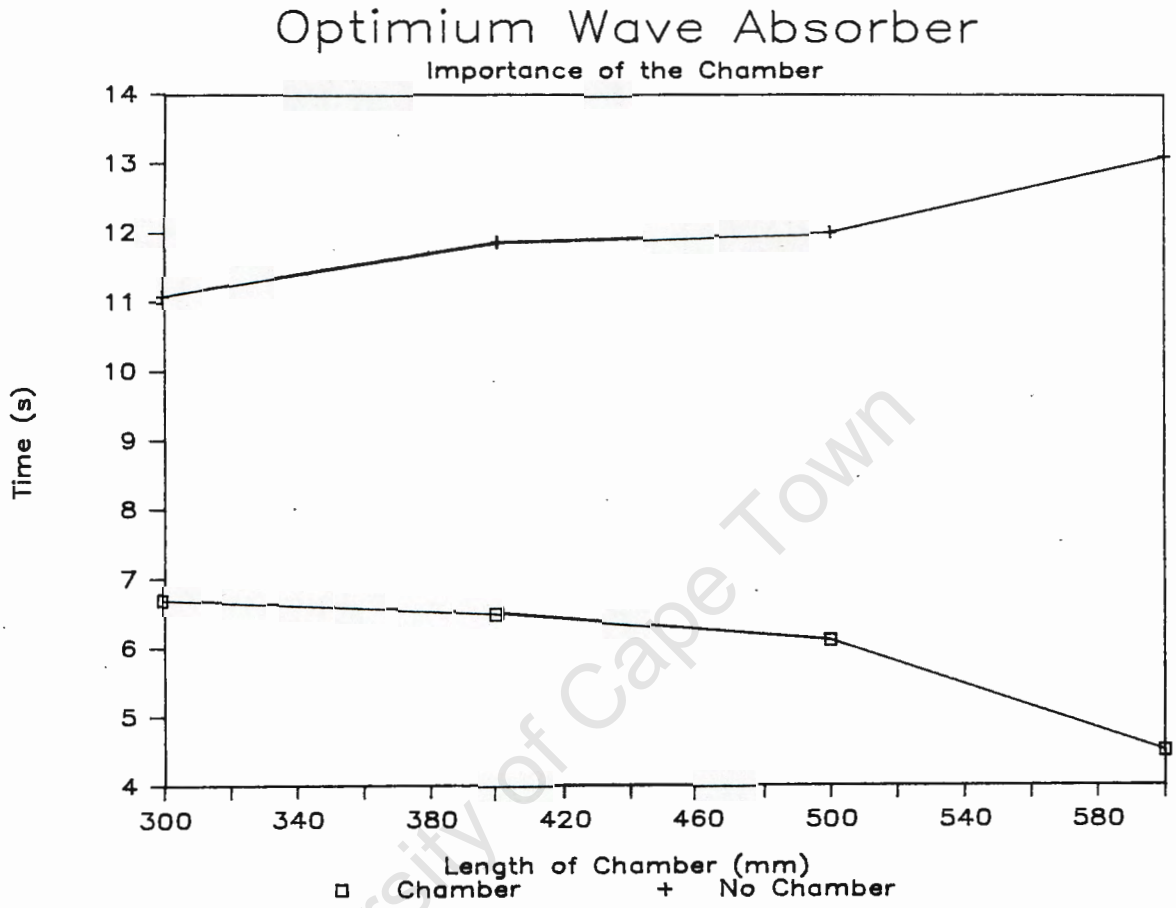

University of Cape Town

In this experiment the chamber was removed and compared to results with the chamber wall included (see fig. 5.7). In fig. 5.7 the length of the chamber for the wave absorber without a chamber wall, is the distance from the end wall of the flume to the position normally occupied by the chamber wall. There is a large difference between the two curves showing that a chamber is required. The author feels that the relative positioning of the chamber wall with respect to the wave absorber could also have been investigated.

5.3.5.3 Optimum number of holes

For Design 1 two sets of holes were tested

i) 120 12 mm diameter holes in 145 x 590 mm^2

ii) 120 12 mm diameter and 108 5 mm diameter holes in 145 x 590 mm^2

The first case (Fig. 5.8a) gives superior results.

For Design 2 two sets of holes were also tested

i) 182 10 mm diameter holes in 145 x 680 mm^2

ii) 182 10 mm diameter and 150 5,5 mm diameter holes in 145 x 680mm^2

Again the first case (Fig 5.8b) gives superior results.

From these results a relationship was required to relate the data obtained from each of the two designs. It was also necessary to account for the effectiveness of the different hole sizes used in the two designs. The two designs can be related by the sum of the hydraulic radii of the holes in the wave absorber. The hydraulic radius (R) is the area of the hole divided by its perimeter. The summed hydraulic radius per unit area simplifies to

$$\sum_{1}^{n} R = \frac{1}{2} nr/A$$

where n = number of holes per unit area

r = radius of the holes (mm)

A = unit area encompassing the holes (mm^2)

Using this relationship, the data for Design 1 converts to

i) 120 12 mm diameter holes : $\frac{1}{2} nr/A = 4160/1000 \times 1000$

ii) 120 12mm diameter and 108 5mm diameter holes;

$\frac{1}{2} nr/A = 5720/1000 \times 1000$

University of Cape Town

Fig 5.8 Optimum wave absorber

a)

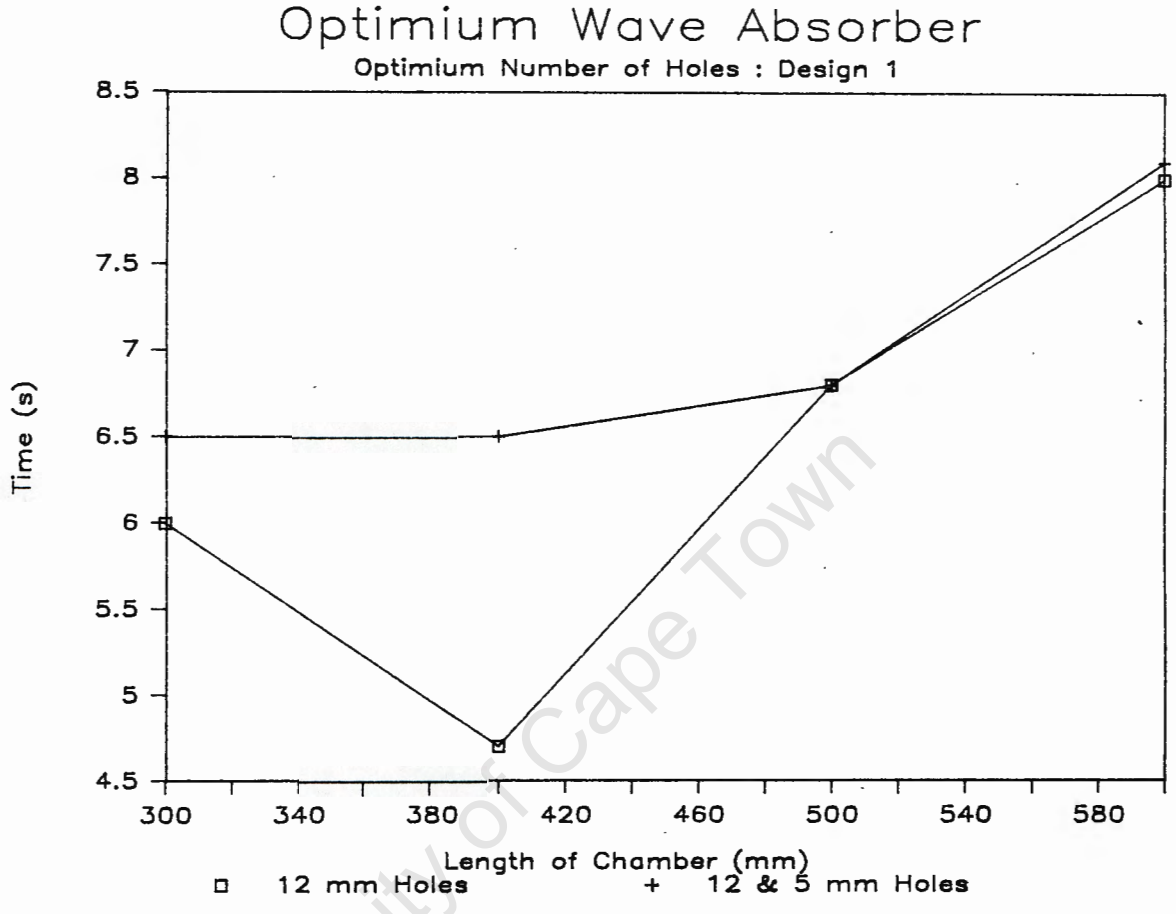

b)

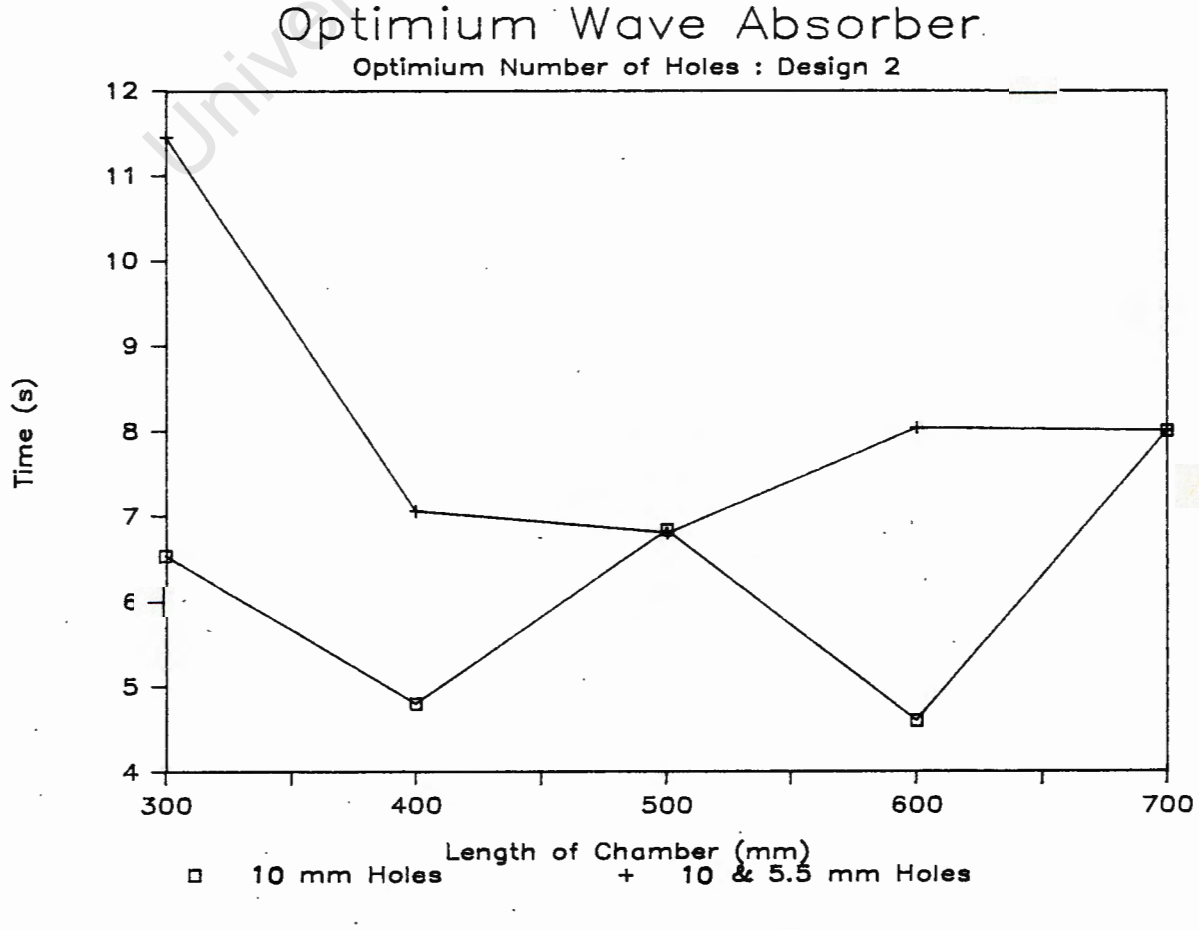

University of Cape Town

and the data for Design 2 converts to

i) 182 10mm diameter holes : $\frac{1}{2}$ nr/A = 4615/1000 x 1000

ii) 182 10mm diameter and 150 5,5mm diameter holes;

$\frac{1}{2}$ nr/A = 7636/1000 x 1000

The best results were obtained from the first case for both designs (Fig 5.8 a,b). On these results it was concluded that

i) The diameter of the hole is not critical, though it may still be influential (Design 1's 12 mm holes and Design 2's 10 mm holes both produced good results.)

ii) The ideal hydraulic radius relationship is

$\frac{1}{2}$ nr/A = 4500/1000 x 1000.

To scale the hydraulic radius relationship, the relationship can be considered to be

$\frac{1}{2}$ nr/L for a unit width

So $\frac{1}{2}$ nr/L is dimensionless and can therefore be applied to any change in scale of the model without change.

So $\frac{1}{2}$ nr/L = 4,5 per unit width.

5.3.5.4 Size of the chamber

Fig 5.8 shows that for the optimum arrangement of the holes, Design 1 with 12 mm diameter holes and Design 2 with 10 mm diameter holes, a chamber length of 400mm is optimum. The reason for this relationship is identified in Section 5.3.4 (i).

5.3.5.5 Other factors affecting the efficiency of the wave absorber

Two factors were identified that could improve the efficiency of the wave absorber.

i) If the front of the wave absorber is allowed to oscillate with the wave, then a shorter ttmd results.

University of Cape Town

ii) A particularly important feature identified was to place an object of height H, where H/d = 0,2, 30 to 60 mm in front of the leading edge of the wave absorber. This object should have holes through it. This obstruction halves the average ttmd, which would appear to be a 20 to 30% decrease in the coefficient of reflection. It is believed that the water oscillating past this obstruction absorbs wave energy that would not normally be affected by the wave absorber.

5.3.6 Design for the prototype wave absorber

To obtain the maximum number of wave absorbers from a sheet of plywood, an absorber length of 810 mm was selected. This is also the length initially obtained from scaling Hamill's data. If the absorber length had been scaled according to Design 1 or 2, the prototype absorber length would have been 885 mm or 1020 mm respectively. It is felt that this change would not create a large increase in the coefficient of reflection as the increase in length of Design 2 over Design 1 did not produce significant differences in the ttmd's.

The slope for the prototype wave absorber should be $2,5^{o}$. The number of holes and their size were obtained from the relationship $\frac{1}{2}$ nr/L = 4,5 per unit width. Each absorber which is 810 by 1220mm has $\frac{1}{2}$ nr/880 x 1220 = 4445. So 1334 13 mm diameter holes were drilled in each of the four wave absorbers. The chamber length should be 3/2 x 400 = 600 mm. A suitable obstruction of height h/d = 0,2 should be used 60 mm in front of the wave absorber.

5.4 Techniques for the implementation of photogrammetry

5.4.1 Camera Positioning

The Zeiss Jena UMK cameras are positioned approximately 5 metres above the water surface, 1,9 metres apart and are aligned parallel to the wave generator. The effective format size is 120 mm x 160 mm (see Section 5.1.1), this gives each camera an effective field of view of 6 x 8 m. The cameras are positioned with their long axes

University of Cape Town

Fig. 5.9 Wave Basin configuration

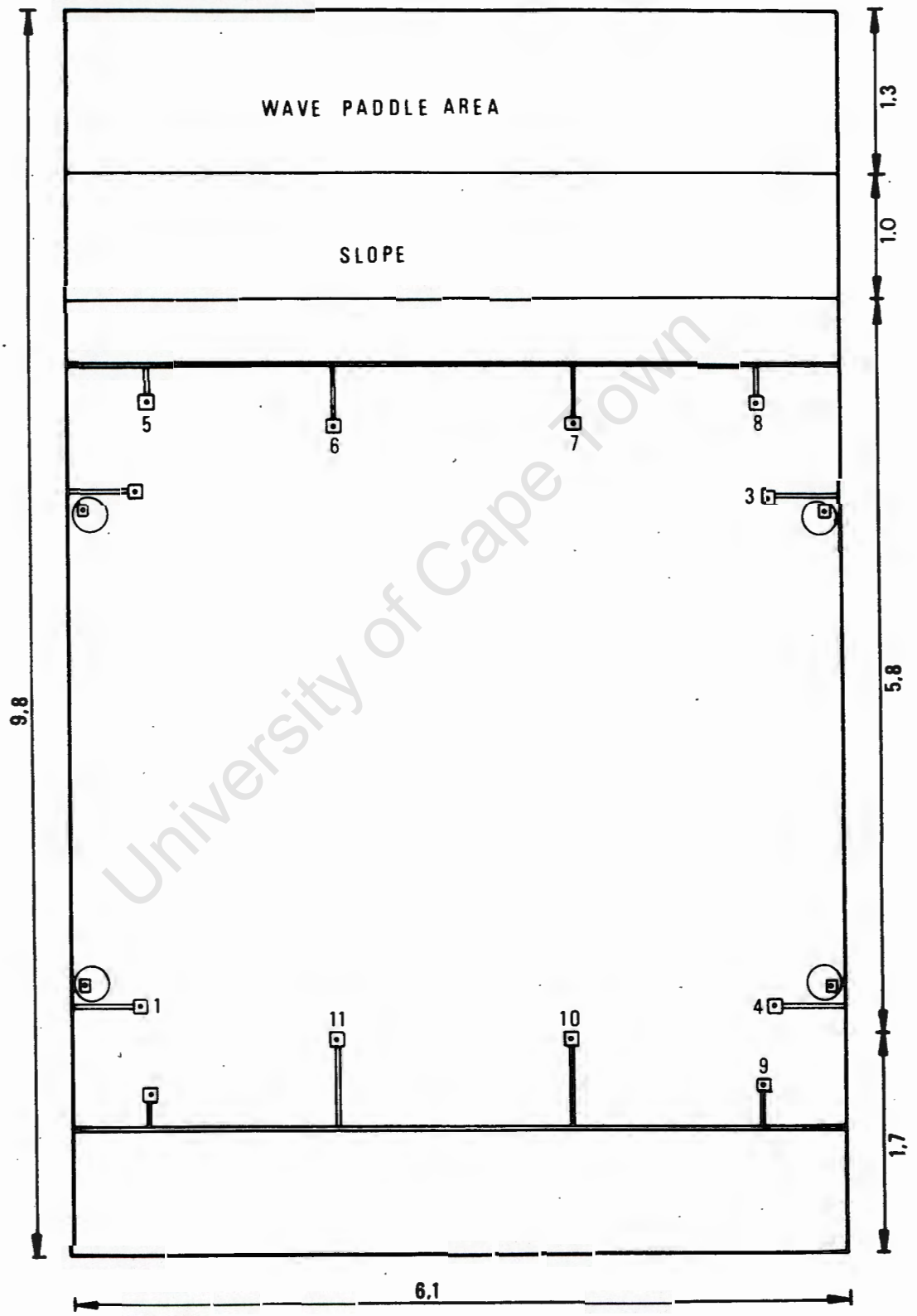

University of Cape Town

parallel to the wave paddle, this produces an overlap area of 6,1 m, so each camera covers the entire width of the wave basin.

5.4.2 Control point network

A control point network is required so the cameras can be positioned in the global axes of the wave basin using the theory of projective transformations (see Section 2.1.1(ii)). Welham (1982) investigated the relationship between measurement accuracy and the control point configuration. Welham showed that accuracy improved significantly when up to 16 to 20 control points were used. The accuracy then improved very little for further increase in the number of control points. As a result a network of sixteen control points has been adopted for use in the wave basin (fig. 5.9).

The control points were arranged in three layers. Control points (1-4)(from fig 5.9) were 950 mm from the base of the wave basin, control point (5-12) were 750 mm from the base of the basin and control points (13-16) were 80 mm from the base of the basin. These four control points were placed in tins so that they could be placed below the water surface. It was required that the range of levels of the control points straddle the water surface so heights on the water surface can be interpolated with respect the control points and not extrapolated, when calculating their heights from the theory of projective transformations.

Plate 5.11 A control point

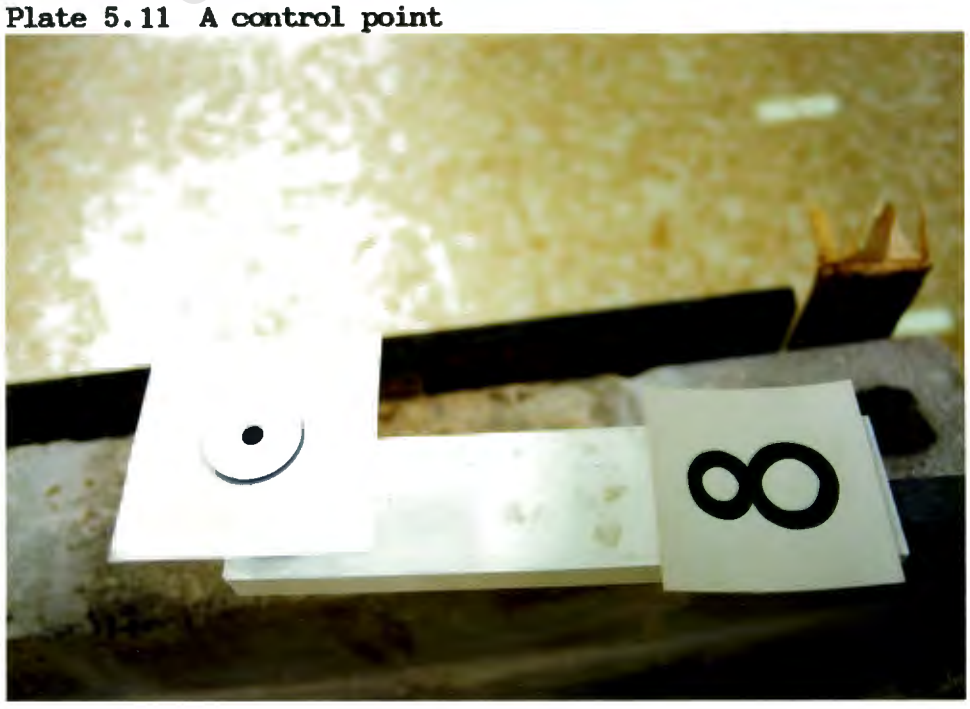

University of Cape Town

The design of the control points are based on the black hole theory. The control points (plate 5.11) consist of a hollow structure (pvc pipe) painted matt black on the inside with a plate on top. The plate is matt black on the bottom and gloss white on top, with a hole (8 mm diameter) in the centre of the plate. This hole now acts as the most black object possible, as no light can be reflected from it. In this way any shadows from the overhead projectors (see Section 5.4.3) which fall on the control point, can easily be identified from the actual black hole.

It is required that the positions of the control points be known to a high degree of accuracy (≈ 1 mm in xyz). To do this brass cones were turned that fitted into the control point. The brass cones were exactly 10 mm from the surface of the black hole to their apex. The control point coordinates (x_i, y_i, z_i) were then calculated relative to these points. The real coordinates of the centres of the control points were then (x_i, y_i, z_i - 10). The height of the apex of the cones was obtained using a metre rule and a level. The distances between the control points was then measured with a tape. This data was then used in a least squares adjustment program to obtain the coordinates of the control points. The coordinates of the points were finally established to within a standard deviation of 1,15 mm.

5.4.3 Water surface identification

It is essential that the images obtained by the two cameras, when photographing a wave pattern, be synchronised and of short duration (see Section 3.2). To do this a flash of short duration is very effective. Conventional flashes can not be used as they would produce a monotonous image (see Section 3.1). To overcome the lack of contrast in the images, four overhead projectors mounted on the ceiling are used (plate 5.12). Flash bulbs of short duration 1/2000 seconds are used instead of the normal light bulbs in the projectors. Any desired pattern can now be projected onto the water surface during the flash.

University of Cape Town

Plate 5.12 Overhead projectors mounted on the ceiling.

Each overhead projector illuminates a 3 x 3 m^2 area of the wave basin. To cover the entire area of the wave basin four overhead projectors are required. The slower camera fires 8 milli-seconds after the faster camera, when both cameras are simultaneously triggered. To obtain an image from both cameras, the flash is connected to the slower camera and the shutter speeds are set to 1/30 second. In this way the shutter of the faster camera is still open when the flash is set off by the slower camera.

The original pattern projected onto the water surface was a random letraset pattern. This pattern is good for identifying position when viewing the images stereoscopically, but the author found it difficult to accurately obtain the position of points with this pattern. Small black paint dots were placed on the overhead projector screens in conjunction with the letraset pattern. This pattern was much easier to view accurately stereoscopically.

The overhead projectors needed to be focused to the 150 mm water depth. To do this a normal light bulb was positioned just in front of the flash bulb in the overhead projector. A white object 150 mm high was then placed below the overhead projector. The overhead projector was then focused for the best clarity of the letraset pattern.

5.4.4 The wave trigger mechanism

Previous experiments (Petzer 1987) to photograph the superimposed wave for normal clapotis (section 4.2) were not successful, as it was difficult to synchronise the instant the photographs were taken with the instant the super-imposed wave occurred. Petzer (1987) tried to visually calibrate the instant the waves were super-imposed with the position of the wave generator to trigger the cameras. The inaccuracies in this method were large as shown by the poor coefficients of reflection obtained (K_r = 0,4 to 0,5)

To obtain optimum results, a trigger mechanism was required at the reflecting wall which would trigger the cameras when the maximum wave height was reached. The trigger mechanism selected was based on an integrated circuit (LM 1830) designed for detecting the presence, absence, or level of polar fluids (National Semiconductors 1978). The LM-1830 is a monolithic bipolar integrated circuit that determines the presence or absence of the fluid by comparing the resistance of the fluid between the probes with the resistance internal to the integrated circuit. When the probe resistance increases above a preset valve the low current relay connected to the integrated circuit closes, and the circuit to trigger the cameras is closed (plate 5.13).

University of Cape Town

Plate 5.12 The wave trigger

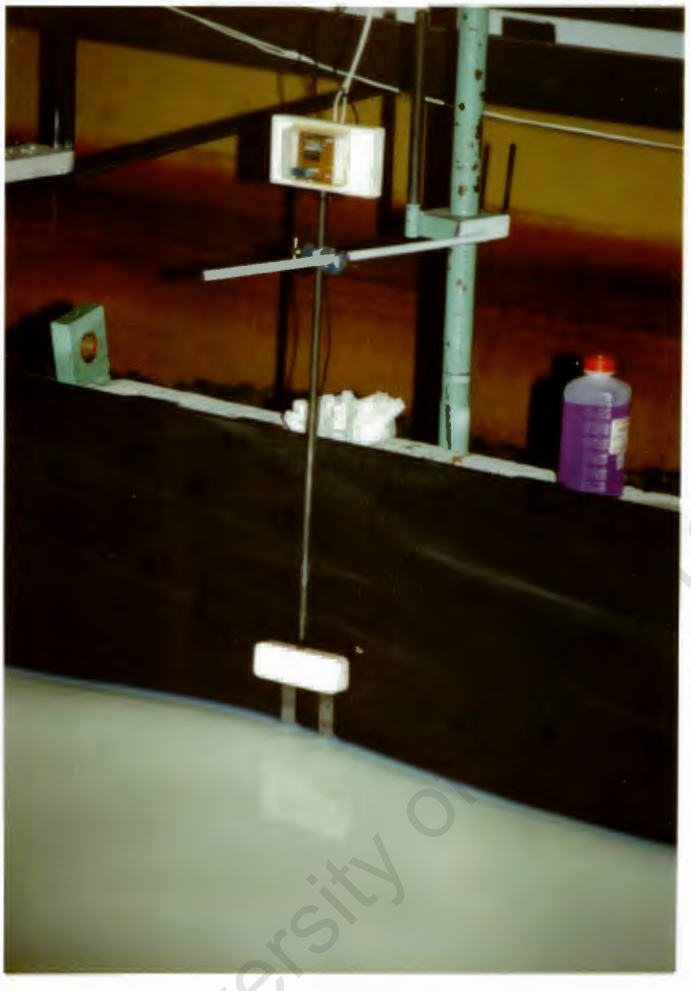

The cameras are triggered from the synchronisation box built by Pos (1984) and were triggered from one of two micro switches connected to the wave generator. The synchronisation box was modified by replacing the micro switches with the low current relay in the water detection circuit. In this way when the low current relay circuit was closed the cameras would be triggered. The water detection circuit was mounted above the wave wall on a variable position stand (Plate 5.12). The flow chart (fig.5.10) shows the interaction of the various components required to obtain the stereo pair of a standing wave.

Fig 5.10 Flow chart of camera firing procedure

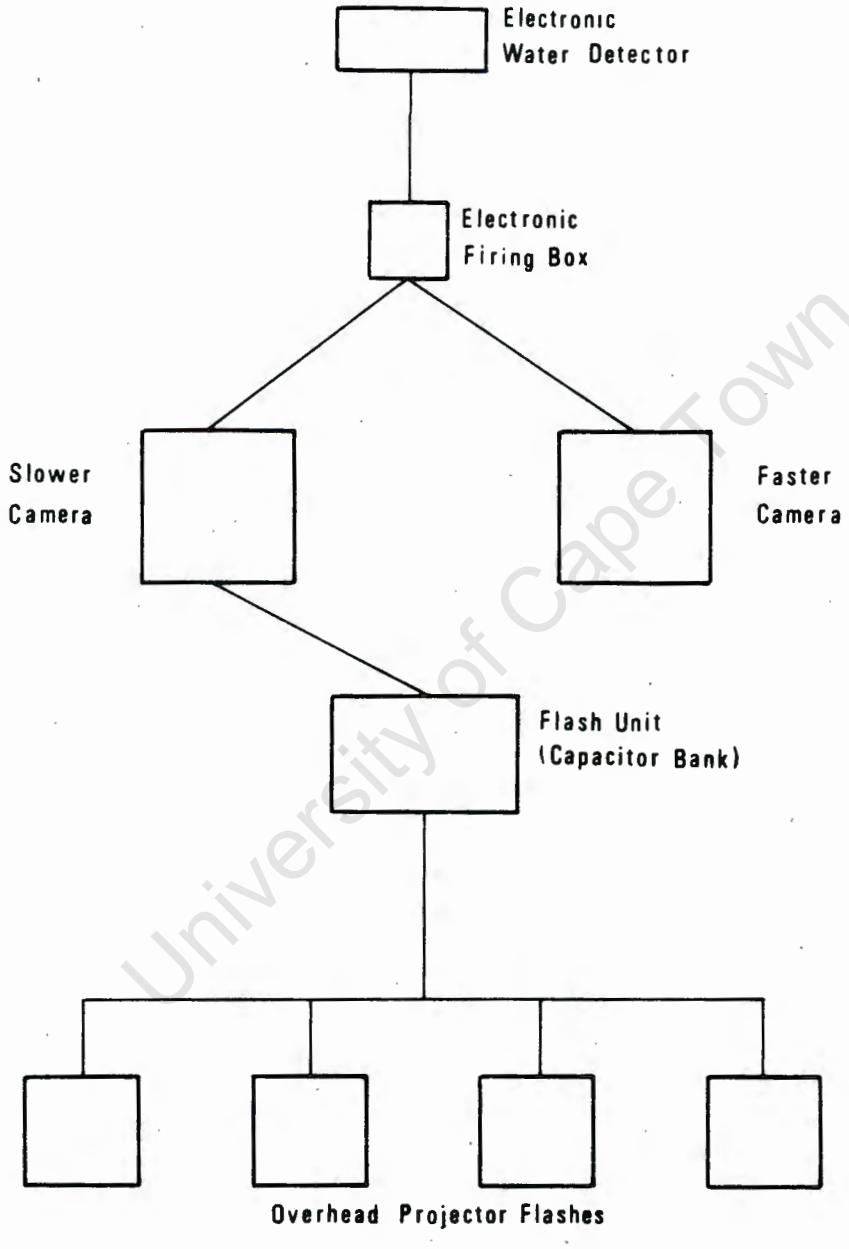

University of Cape Town

6. ACQUISITION OF EXPERIMENTAL DATA

6.1 Selection of parameters for the waves generated

6.1.1 Water depth

For all experiments a water depth of 150 millimetres was used. This water depth was selected as

i) for this water depth, the deviations in water depth due to unevenness of the wave basin floor are less than 1% (see Section 5.2.1),

ii) a vertical wall is seldom built in shallow water ($d/L < 0,04$), as intense scouring would occur at the base of the structure (Jarlan 1961). A limit for the shallowest water wave to be tested of $d/L = 0,09$ was selected, as the horizontal velocity (U_H) is small enough ($U_H < 1,5$ m/s) to produce minimal scouring at a 1 : 100 scale. The investigation also requires sufficient waves be present in the photograph to allow a good analysis of the wave pattern, a minimum of two full waves was required to be visible. From this requirement for the maximum wavelength, and the requirment for the minimium d/L ratio a water depth of 150 millimetres was used.

6.1.2 Wave periods selected

The initial wave period (T) selected was T = 1,5 seconds, based on the wavelength obtained from section 6.1.1. The analysis of the stereopairs for T = 1,5 showed a series of high and low points occurring across the wave crests and troughs. The paddle was considered to be very stiff, and it was unlikely that these high and low points were being caused by the wave paddle (see Section 5.2.2).

Resonance in an enclosed basin was investigated as a possible explanation (Coastal Engineering Reseach Centre 1984). Resonance in an enclosed wave basin requires the formation of a standing wave with anti-nodes at the two boundaries, usually vertical walls. Resonance will occur when the forcing wave has a wavelength (L) that is some multiple of a horizontal dimension of the wave basin (L_B - length or width). So the dimension L_B must be a multiple of L/2.

University of Cape Town

$$\text{So } T_n = \left[\frac{4\pi L_B}{n g \tanh (\pi nd/L_B)} \right]^{\frac{1}{2}} \quad \text{for } n = 1,2,3,\ldots$$

For waves entering the basin with a period close to one calculated from the above equation, resonance will occur. For smaller values of n, the amplitude of the resonance can be significant. Using this equation, where L_B is the width of the wave basin, the following values were calculated (table 6.1).

Table 6.1 Resonant periods for the width of the wave basin

n	1	2	3	4	5	6	7	8	9	10
T_n	8,66	4,35	2,92	2,31	1,79	1,51	1,31	1,17	1,06	0,97

Table 6.1 shows that T = 1,5 seconds is one of the natural periods for resonance. No further experiments were done for T = 1,5 seconds. The further experiments for the standing wave with the crest parallel to the wall, were done for T = 1,01 seconds, which is between the two natural periods of the wave basin.

For oblique reflection, T = 0,765 seconds was also investigated, as it increased the number of repetitions of the standing wave pattern. T = 0,765 is not a natural period, but as the wave absorbers are used for oblique reflection it was not serious if T = 0,765 was a critical period.

6.1.3 Wave height

The maximum wave heights that could be created, without the waves being close to breaking, were investigated. Photogrammetry determines the heights of points on the waves with a standard deviation of 2 mm. By maximising the waveheight, the percentage error occurring in the photogrammetry would be minimised. For the individual wave periods tested for different wave scenarios, the wave height was always kept

University of Cape Town

constant to ensure that the results from different wave scenarios could be compared. Breaking waves were however investigated for Mach wave reflection.

6.2 Considerations for the experimental procedure

6.2.1 The occurrence of the repeatable wave

The wave generator takes 4,5 seconds to start up, and then the starter switches over to run. In the first 4,5 seconds the waves developed are smaller than average wave generated later. At the point when the motor switches over, a single large wave is generated. All waves generated after this appear to be regular. It is important that the discrepancies in the generated wave be allowed for in determining when the photograph of the wave pattern should be taken. It was noticed that the size of the wave generated is dependent on how long the wave generator had been run before the test. As a result the wave generator was always run before a test, but discrepancies still occurred.

6.2.2 Photographing the incident wave

Initial attempts to photograph the incident wave were not successful. For these tests the wave wall was situated at the end of the wave basin, parallel to the generated crest. The wave trigger was then positioned at the wave wall just above the water surface, so the first wave crest generated would set the cameras off. When the problem with the initial waves generated was realised, an alternative approach was required.

The wave absorbers that were developed (see Section 5.3) were extremely efficient, so the wave absorbers were used to absorb the initial waves generated. The wave absorbers were placed at the far end of the wave basin, with the wave wall pushed against the side of the wave basin. The time for the large wave generated to reach the wave absorber from starting was taken. For the tests the cameras were set off after this time. The stereo pairs taken then recorded an entire regular wave train.

University of Cape Town

6.2.3 Photographing the standing wave

6.2.3.1 The standing wave

The standing wave, with the crest parallel to the reflecting wall, has a definite maximum time before which the stereopair must be taken. This is the time from when the first wave is generated, which is then reflected from the reflecting wall, reflected from the wave paddle and then until just before the wave enters the area of photography. Unfortunately for large period waves this time is not long enough for the waves generated in the first 4,5 seconds to have travelled out of the area of photography. This factor needs to be considered during analysis.

Plate 6.1 The water surface as last wave generated reaches the wave absorber

University of Cape Town

6.2.3.2 The oblique standing wave

The oblique standing wave with the crest oblique to the reflecting wall, does not have a definite maximum time in which the stereopairs must be taken. The wave absorbers are very effective in absorbving the reflected wave, and lead to a steady state situation where very little interference

exists. In plate 6.1 the wave generator has been switched off and the last wave generated is breaking on the wave absorber. There is very little disturbance on the remaining water surface except for two reflected Mach stems which were abnormally large waves. Although the wave absorbers are very effective, to minimise the interference created, the stereopairs were taken just after the large wave generated after 4,5 seconds had reached the wave absorber.

6.2.4 Obtaining standing waves 180^{o} out of phase

The stereo pair with the crest parallel to the reflecting wall requires two stereo pairs to be fully described. The stereopairs are required when crest is at the wall, and then 180^{o} later when the trough is at the wall. These two stereo pairs allow the maxima for each antinode to be described.

These maxima at the antinodes are obtained using the wave trigger (see Section 5.4.5). To obtain the maxima for the crest at the wall (an antinode) the wave trigger is placed at the reflecting wall and adjusted so that when the maximum wave height is reached at the antinodes, the wave just touches the wave trigger and the cameras are set off. To obtain the maxima for the trough at the wall, the wave trigger was placed L/2 away from the wall, and positioned above the antinode where the crests would be superimposed. The wave trigger was then adjusted to set the cameras off when the maximum wave height was reached. There is a known delay of 8 milliseconds before the cameras are fired after being triggered. To compensate for this delay the wave trigger was placed a couple of millimetres below the height that just triggered the wave trigger.

6.2.5 Positioning the wave paddle

To ensure repeatability of the generated wave, so the wave data could be compared, the wave paddle was always started from the same position in each test. The starting of the wave paddle from the same position for each experiment ensures that

University of Cape Town

i) the stationary water level (SWL) is kept constant. The wave paddle is a displacement wave paddle, and the difference in SWL between the two extreme positions of the wave paddle is 2 mm. SWL can only be accurately known if the wave paddle is started from the same position

ii) the wave train is as similar as possible for successive tests.

The wave paddle was started from its furthest forward position. This position was selected as

i) the wave paddle is linked eccentrically to a rotating cam, so the wave paddle moves in an approximately sinusoidal motion (see Section 5.2.4). When the wave paddle is furthest forward, its position is defined by sin ϕ where $\phi = \pi/2$, for the cam. In this position, because of the sine function, slight inaccuracies in the desired angle ϕ of the cam do not change the position of the paddle significantly. This may be compared to the much larger displacements of the wave paddle that would occur for the same inaccuracies in ϕ where the desired ϕ was $\phi = \pi, 2\pi$. By selecting the position of the wave paddle to be furthest forward, errors in the static positioning of the rotating cam are minimised and there is more chance for repeatability.

ii) by starting the wave paddle in its most forward position, when the wave paddle starts, its moves backwards accelerating and then forwards, ensuring that the largest possible first crest is developed in case it is ever recorded in a photograph.

6.2.6 Determining the SWL for a stereopair

The SWL changes by 2 mm depending on the wave paddle position. For any stereopair the initial SWL will always be the maximum, but the SWL for the stereopair needs to be determined, as the wave paddle is not necessarily in its maximum position when the stereo pair is photographed. In this investigation the SWL for the stereopair was considered to be the SWL for the position of the wave paddle when the stereopair was photographed. To record the position of the wave paddle when the stereopair was photographed, a strut was pinned to the wave paddle, with the other end supported on a calibrated white board in the field of view

University of Cape Town

Plate 6.2 Typical stereopair

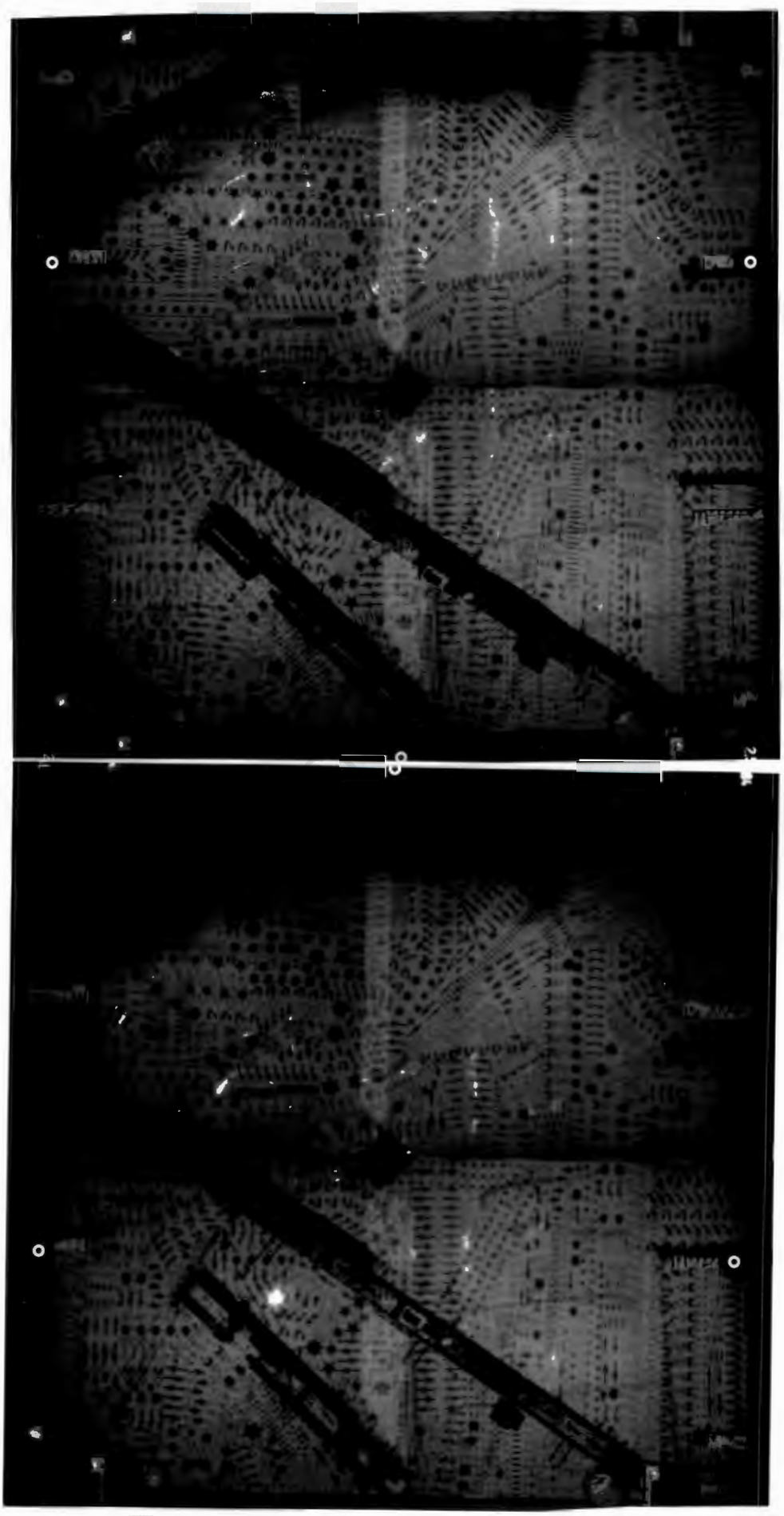

Table 6.2 List of stereopairs

Stereopair Number	Angle of crest(θ_o)	Periods (s)	Wave Height Setting	Comment
3	90^o	1,5	75	Standing wave - crest at wall
10	90^o	1,5	75	Standing wave - crest at wall
12	90^o	1,5	75	Standing wave - trough at wall
13	90^o	1,01	138	Standing wave - trough at wall
16	90^o	1,01	138	Standing wave - crest at wall
17	69^o	1,01	138	Oblique reflection
18	69^o	0,765	182	Oblique reflection
19	47^o	0,765	182	Mach reflection
20	34^o	0,765	182	Mach reflection - wave breaking
21	34^o	0,765	224	Mach reflection
22	34^o	1,01	156	Mach reflection
23	34^o	1,01	138	Mach reflection - crest breaking
24	56^o	1,01	120	Mach reflection - wave breaking
25	25^o	0,765	224	Mach reflection
26	20^o	0,765	224	Mach reflection
27	11^o	0,765	224	Mach reflection
28	-	0,765	224	Incident wave
29	-	0,765	182	Incident wave
30	-	1,01	156	Incident wave
31	-	1,01	138	Incident wave
32	-	1,01	120	Incident wave
33	-	1,5	75	Incident wave
34	-	-	-	Flat water surface d = 150mm

University of Cape Town

of the cameras. So when the stereopair is taken, the position of the wave paddle is recorded by the relative position of the end of the strut to the calibration markers. The calibration marks represent the maximum position of the wave paddles oscillation. The height by which the SWL should be decreased could then be determined to an accuracy of 0,25 mm.

6.3 The display of the results obtained by stereo analysis

6.3.1 List of the stereopairs obtained

The typical stereopair consists of a pair of negatives, the contact print of two such negatives can be seen in plate 6.2. If these points are viewed stereoscopically clapotis gaufre is visible. All the useful stereopairs obtained are listed in table 6.2.

6.3.2 Acquisition of data from the stereopairs

From the pairs of negatives forming a stereopair the height coordinates of the point on the wave surface are observed on the stereo comparator (Section 5.1.2) and then calculated by the HP9816 microcomputer (Section 5.1.3). These values are down-loaded onto the VAX mainframe (Section 5.1.4). Using a software package "SACLANT" available on the VAX the data can be manipulated to produce contour plots.

The contour plots were the primary source of information for the analysis of the wave reflection patterns. A stereopair (34) was taken of the stationary water surface to obtain the SWL in terms of the z coordinates for the wave basin. This water depth, less the correction for the wave paddle position (see Section 6.2.6), was subtracted from all the wave height values. The contour plots would then show the troughs with negative contour values and the crests with positive contour values. The contour plots were produced with 5 millimetre contours to a 1 : 25 scale. Fig. 6.1 is a typical contour plot, all the contour plots of the stereopairs appear in Appendix A.

University of Cape Town

Fig 6.1 Contour plot - Clapotis gaufre

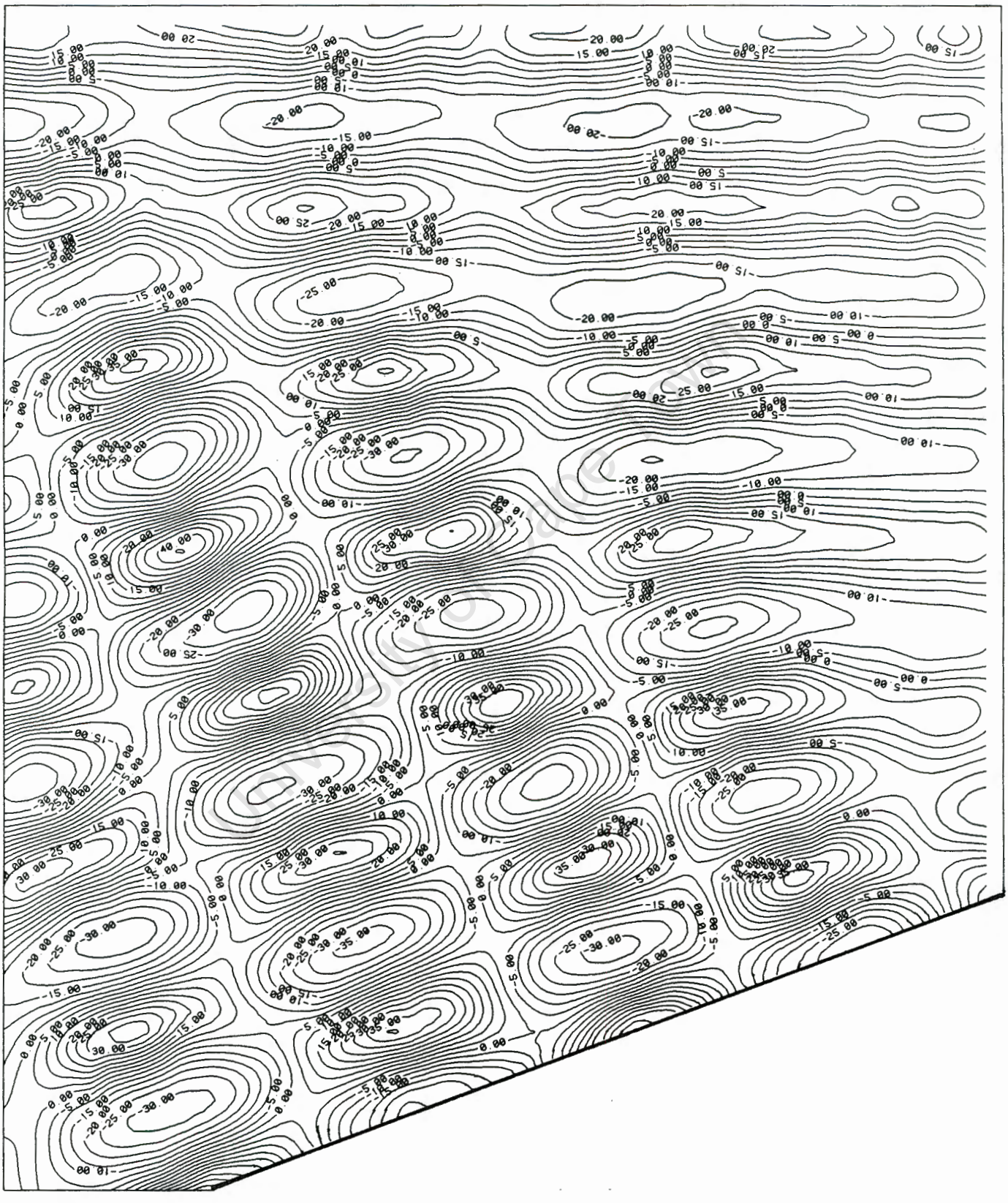

6.4 Procedure for the analysis of the contour plots

6.4.1 Incident waves

The determination of the most probable incident wave characteristics is important as all future analysis is based on the comparison between the incident wave and the various standing waves. The lines marking the crests and troughs are drawn on the contour plot (fig 6.2), then lines were drawn across the waves, parallel to the wave orthogonal. This was done to obtain an average height across the wave as the waves varied by up to 10 mm in height across the length of a crest or trough. For a particular wave crest or trough, the heights at the intersections of the crest of trough line and the wave orthogonals were interpolated from the contours. The average crest (a_{ci}) or trough (a_{ti}) amplitude is then calculated together with its standard deviation. From the crest and trough amplitudes the wave height between the crests and troughs was obtained. These wave heights were averaged, recognising that the initial waves generated must be omitted if they were recorded in the stereopair. The wave height (H) was then used for calculating the coefficients of reflection, rather than the wave amplitudes, as the wave height is independent of mean water level (MWL) fluctuations, like setup. The lengths between consecutive crests and troughs were measured and then the average wave length was obtained with its standard deviation.

4.2 Standing waves

The average standing wave crest amplitudes (a_{cs}), trough amplitudes (a_{ts}), and standing wave heights (H_s) were obtained in the same manner as for the incident waves. These values are then compared to the corresponding incident wave data to obtain the coefficients of reflection (K_r). The coefficients of reflection can be determined from

$$K_r = \frac{H_s - H_i}{H_i}$$

From the data presented it would also be possible to determine whether any setup has occurred, even though the wave generator had only run for a short time. The wavelengths for the standing wave can also be compared to the wavelengths of the incident wave.

University of Cape Town

6.4.3 Oblique wave reflection

On the contour plots the lines for the crests and troughs of the incident and reflected waves are drawn (fig 6.3). From these lines the positions and angles of the phenomenon occurring can easily be measured. The line representing the reflected wave orthogonal from the initial point of the reflecting wall is drawn as a dotted line. This dotted line represents the theoretical edge of the reflected wave with out diffraction effects occuring. The trough and crest amplitudes for point values can easily be determined. This data is then compared to the incident wave, and the coefficients of reflection can be determined.

In determining the coefficients of reflection for the oblique wave it is necessary to show the change in the coefficients of reflection within the spatial area of the wave basin. To do this contour plots of the coefficient of reflection were computed for the two dimensional area of the wave basin (see Fig. 6.4). A set of axes was used similar to the one used in Section 4.3, with the x axis assumed parallel to the reflecting wall. Then the amplitudes for the crests and troughs, together with their coordinates on the defined axes were obtained. The coefficient of reflection for a particular antinode is then determined by adding that amplitude to the average amplitude of the two opposite adjacent antinodes that are parallel to the reflecting wall and comparing this height to the incident wave height. This data is presented in Appendix B.

University of Cape Town

Fig. 6.2 Contour plot - Incident wave

Stereopair 29, Incident wave, T = 0,765, H_i = 38,4mm

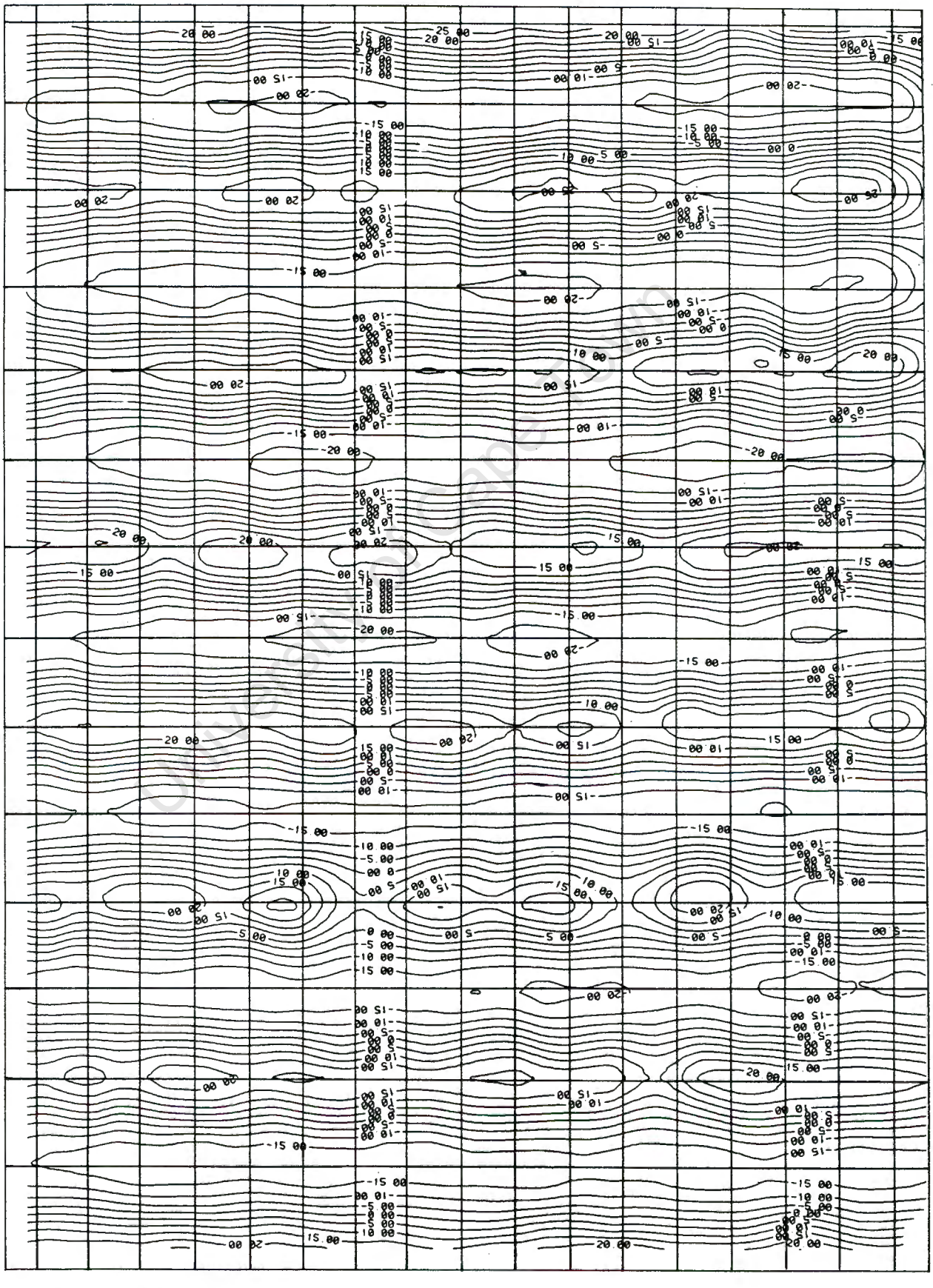

Scale 1 : 25

Fig. 6.3 Contour plot - Oblique wave reflection

Stereopair 18, $\theta_o = 69^o$, oblique wave reflection, T = 0.765, H_i = 38,4mm

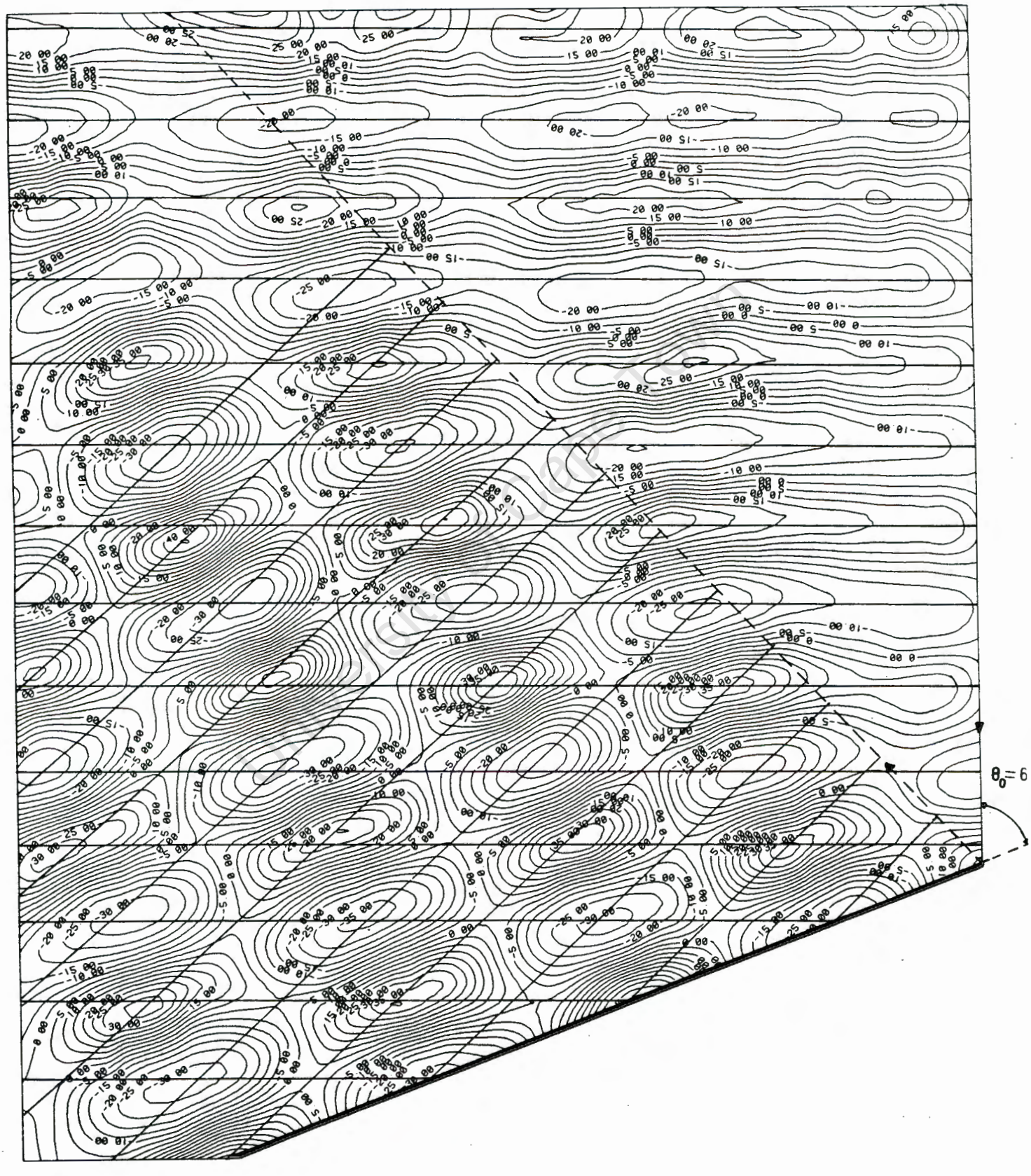

Scale 1 : 25

Fig 6.4 Contour plot - Coefficients of reflection

Stereopair 18, $\theta_o = 69^o$, oblique wave reflection, T = 0.765, H_i = 38,4mm

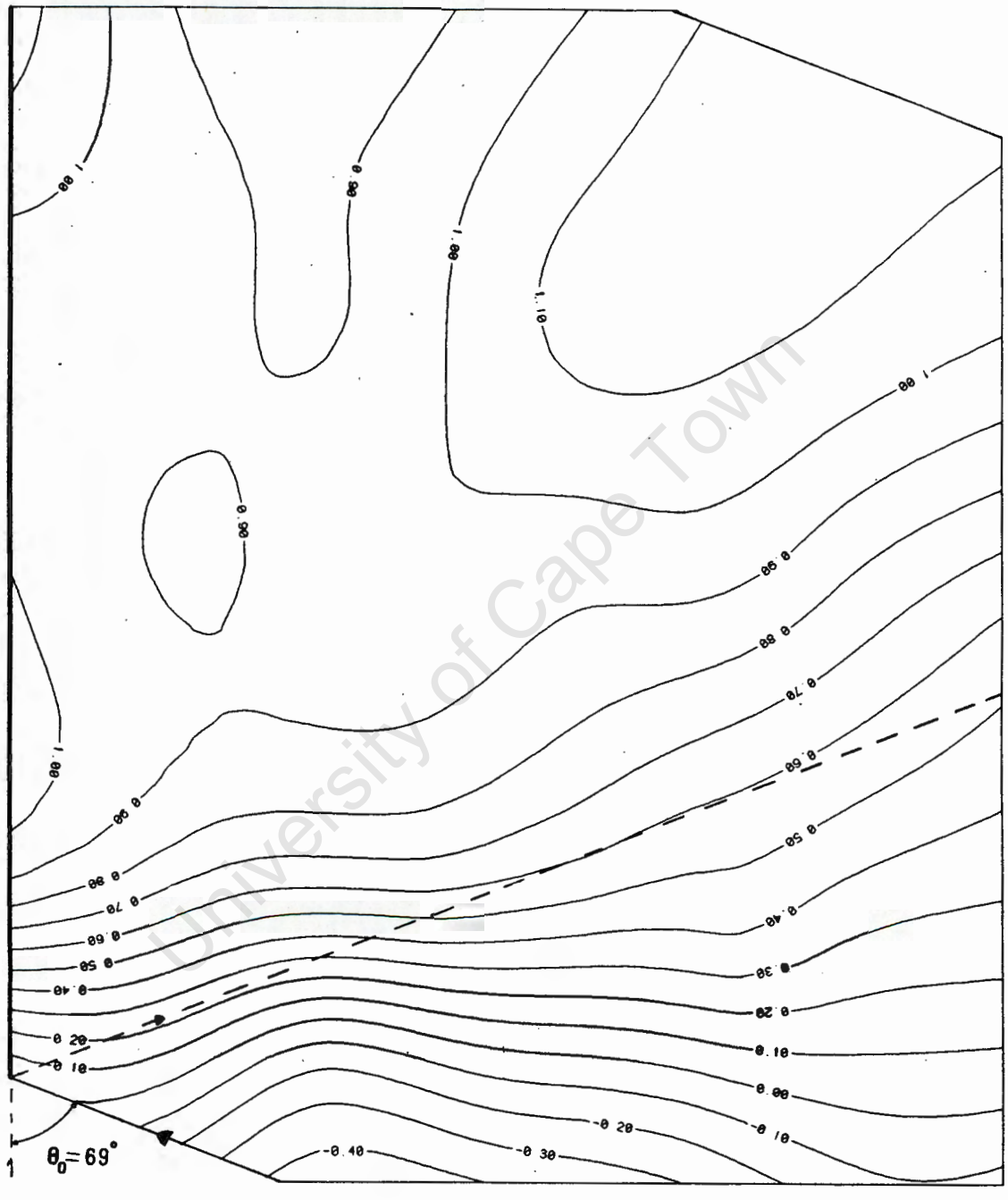

University of Cape Town

Scale 1 : 25

7. RESULTS AND ANALYSIS

7.1 Incident waves

The crest and trough amplitudes and the corresponding wave height for the various wave periods and wave generator settings is presented in Appendix C. The values with an asterix (*) represent waves generated within the first 4,5 seconds (see Section 6.2.1), and were not included in the calculations of the average incident wave height (H_i). There are deviations in the incident wave heights but no pattern appears to be evident. The incident wave data for T=1,5 seconds is poor, and the incident wave height could only be approximately determined. The average wave heights and the average wave periods are presented in table 7.1.

Table 7.1 Average incident wave data

	Coord 28	Coord 29	Coord 30	Coord 31	Coord 32	Coord 33
Wave period (s)	0,765	0.765	1,01	1,01	1,01	1,5
Wave generator setting	224	182	156	138	120	78
Average wave height (mm)	24,8	38,1	32,7	34,0	39,9	37,0
Standard deviation	1,3	1,3	1,4	0,65	1,4	1,7
Average wave length (m)	0,762	0,771	1,122	1,122	1,122	1,850
Standard deviation	0,013	0,010	0,016	0,025	0,031	0,126

7.2 The Standing Wave

The wave data for the corresponding stereopairs (10/12 and 13/16) is compiled in tables 7.2 and 7.3 respectively. The amplitudes from each stereopair occur at corresponding antinodes, 180° out of phase, so both maxima at each antinode are described, and the standing wave height (H_s) is easily determined. The values with an asterix (*), representing waves generated in the first 4,5 seconds, were easily

University of Cape Town

identifiable and were not used for comparison. The data is compared to the corresponding incident wave height, and the coefficients of reflection are calculated for the different antinodes.

Table 7.2 Standing wave data from stereopairs 10/12 for T=1,5

A_{cs} (mm)	62,3	36,3	31,7	40,2*	38,9*	33,4*
Standard deviation	6,5	2,6	1,6	2,6	6,1	1,9
A_{ts} (mm)	20,9	23,7	25,4	25,5	23,6	22,1
Standard deviation	2,2	1,8	1,8	1,6	1,3	2,2
H_s (mm)	83,1	60	57,1	65,5*	52,5*	55*
K_r (H_i=37)	1,25	0,62	0,54	0,77*	0,42*	0,49*

Table 7.3 Standing wave data from stereopairs 13/16 for T=1,01

a_{cs} (mm)	54,5	36,1	37,6	34,8	34,5	36,8	42,8*	30,1	24,6*	42,1*
Standard deviation	4,0	3,2	2,9	3,1	1,8	2,4	2,9	3,1	9,9	6,5
a_{ts} (mm)	34,2	28,0	26,4	31,8	27,4	27,6	27,2	32,0*	22,5	29,8
Standard deviation	2,6	2,7	3,7	2,2	2,4	0,8	1,9	2,6	2,8	2,9
H_s (mm)	88,7	64,0	64,0	66,6	61,9	64,4	70*	62,1*	47.1*	71,9*
K_r (H_i=34,0)	1,61	0.88	0,88	0,96	0,82	0,89	1,06*	0,83*	0,39*	1,12*

University of Cape Town

The coefficients of reflection for T = 1,01 are higher and more regular than those for T = 1,5. The data for T = 1,5 is poor as there are too few waves to analyse, and the incident wave (stereopair 33) seems to show that the wave train created for T = 1,5 seconds is not regular. This makes it difficult to obtain accurate data for the standing wave for T = 1,5.

The data obtained for T = 1,01 appear more realistic, and produced interesting results. For T = 1,01 an average coefficient of reflection of 0,89 was obtained, with an exception of the antinode at the wall, where a coefficient of reflection of 1,6 was obtained. Wiegel 1964(b) (see Section 4.2.4) suggests the coefficient of reflection could reach a magnitude of 1,4 at the reflecting wall. Even for T = 1,5 the coefficient of reflection, based on the largest incident wave, was 1,25 at the wall. This phenomenon occurring at the reflecting wall is very interesting and could be very important in future harbour design. For T = 1,01 the depth of the trough at the reflecting wall is 22% deeper than the average antinode trough depth away from the wall, while the crest is 51% higher than the average antinode crest height away from the wall. The extreme height that can be reached by the standing wave crest at the reflecting wall is very important for overtopping as it does not appear to have been previously identified in the literature. The reason for these extremely large wave heights being developed at the reflecting wall could be as a result of the waves being generated in relatively shallow water. When the water particles strike the wall, across the entire water depth, the water particles are forced upwards, as this is the only unrestrained direction for the water particles to move in.

University of Cape Town

Table 7.4 Summary of reflection data

Investigator	d/L_i	H_i/L_i	K_r ave	K_r wall	L_i/L_s
Moraes (1970)	0,05	0,008	0,72	-	-
	0,09	0,012	0,84	-	-
	0,22	0,025	0,87	-	-
Schoemaker	0,25	0,06	0,92	-	-
Thijsse (1949)	0,135	0,025	0,90		
Wiegel (1964a,b)	-	-	-	1,4	1,05
UCT	0,081	0,020	0,58	1,25	1,07
	0,133	0,031	0,89	1,61	0,99

In table 7.4 all pertinent data from previous investigators, together with data obtained in this investigation (UCT) is summarised. From the data presented by Moraes, Schoemaker and Thijsse, and the data obtained at UCT a trend appears to exist (see fig. 7.1). It appears that the degree of reflection is dependent on the type of wave being reflected, namely the more shallow the wave the less the coefficient of reflection. A possible explanation for this trend is that for standing waves the resulting orbital motion is mainly in the vertical plane at the antinodes. For shallow waves orbital motion occurs throughout the water depth, so the creation the crest or trough requires a large scale movement of water between the antinodal troughs and crests, relative to deeper waves. Possibly this large scale movement in water results in an inertial lag, and the physical model does not behave as predicted by the theory.

University of Cape Town

Fig. 7.1 Summary of reflection data

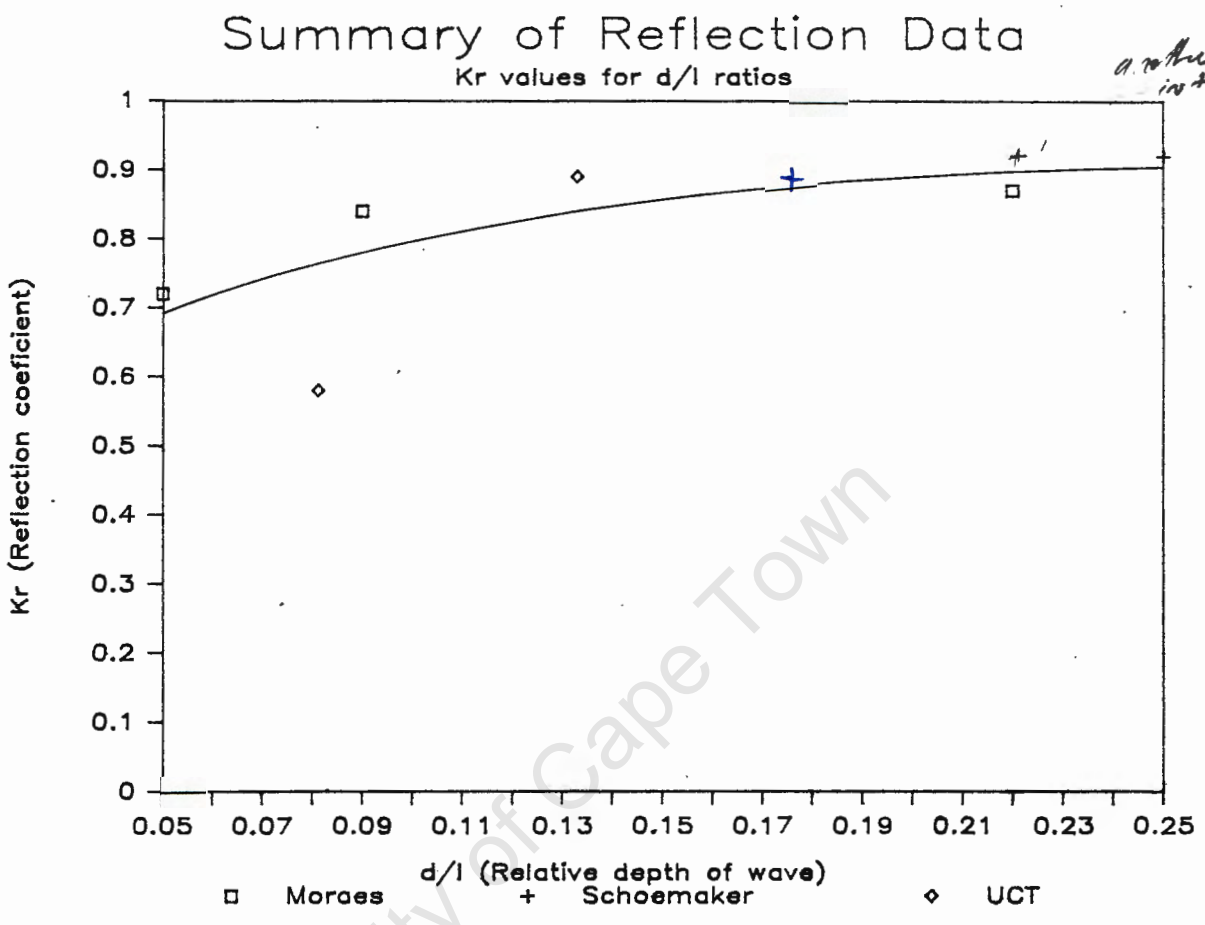

University of Cape Town

It is interesting to note the decrease in the standing wave length compared to the incident wave length for T = 1,5 (L_i/L_s = 1,07). This phenomenon was also identified by Wiegel (1964b) (see Section 4.2.4) where the data presented gave an average ratio of L_i/L_s = 1,05. It is possible that due to the large difference in water particle orbital velocities throughout the entire depth of the two opposing shallow waves creates a hysteresis effect. This results in the water particles not moving as far as they should before the next section in the cycle of the orbital motion. This effect was only noticed for the shallowest water wave (T = 1,5), where the lower coefficient of reflection occurs, so perhaps the two phenomena are related by the interactions of the orbital motions of the two opposing wave trains.

In fig 7.2 the actual standing wave data is compared to the two wave theories presented in Section 4.2. A typical standing wave occuring for T = 1.01 is compared against the first and second order wave theories. This comparison shows that the standing wave occuring appears to be between the first and second order. This result could be expected as the wave is generated by the simple harmonic motion of the wave paddle.

Fig. 7.2 Standing wave comparison

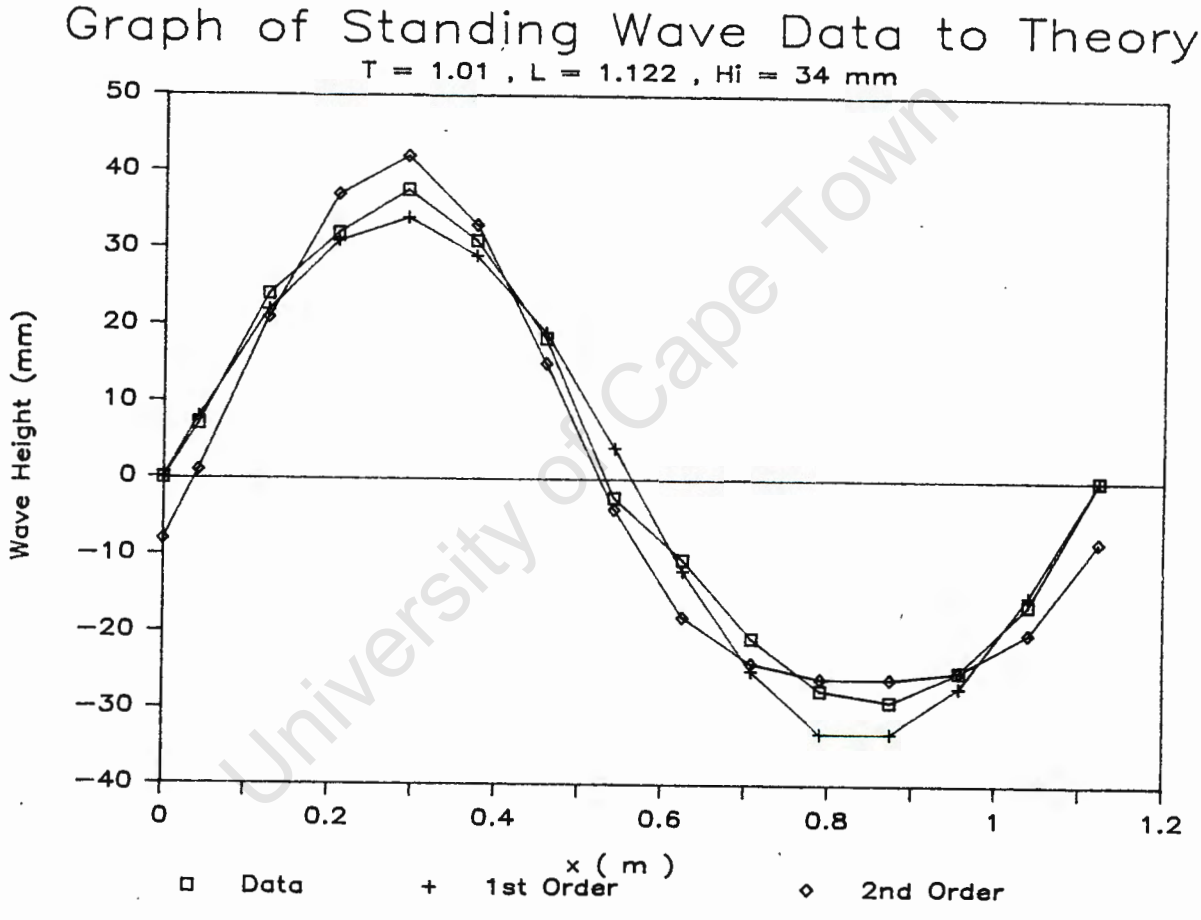

University of Cape Town

7.3 Oblique wave reflection

Oblique reflection was investigated for one angle, $\theta_o = 69^o$; where "θ_o" is the angle between the wall and the wave orthoganal (see plate 7.1). For $\theta_o = 69^o$ two wave periods, T = 1,01 and T = 0,765

(stereopairs 17, 18), were investigated. The data obtained for T = 1,01 is poor because there are too few repetitions of the clapotis gaufre pattern. It was suggested by previous investigators (see Section 4.4) that the border between clapotis gaufre and Mach reflection was θ_o = 35 to 45°, while the present series of investigations suggest that the Mach wave is developed for $\theta_o \leq 47°$ (Stereopair 19), where d/L_i = 0,098

Plate 7.1 Oblique wave reflection

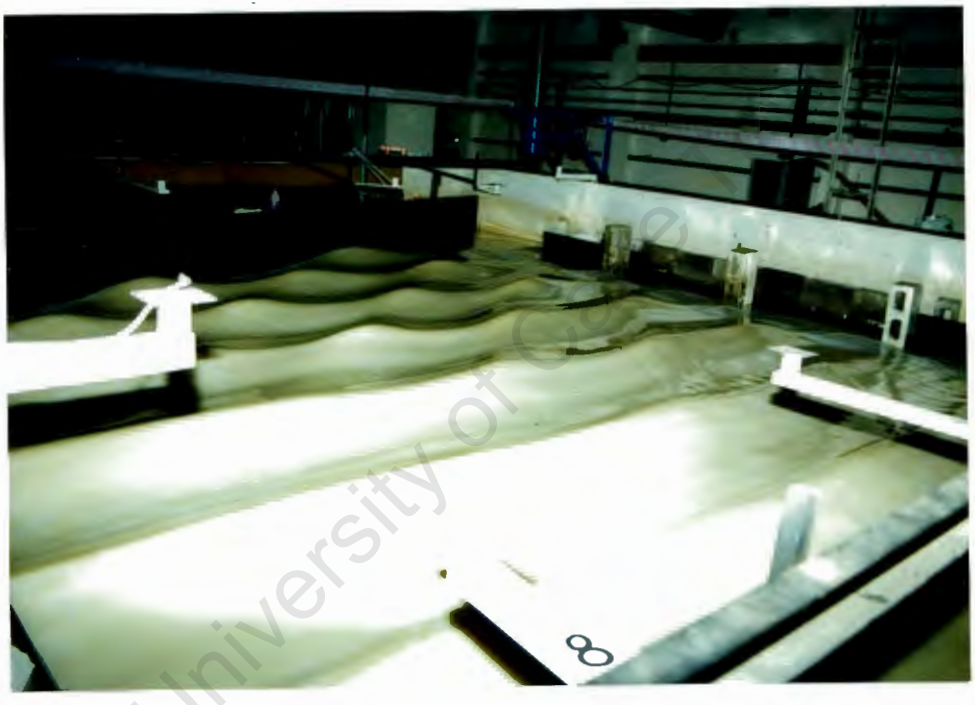

University of Cape

The lines drawn on the contour plots (Stereopairs 17, 18), are drawn as best fit lines through the antinodes, corresponding to the incident and reflected troughs and crests. The angles of incidence and reflection differ by 1°, this is considered an acceptable experimental error. The differences between the intersections of these lines and the actual centres of the quasiantinodes can be accounted for by the diffraction effects (see Section 7.3.1), as well as by the unevenness of the actual waves which could offset the

Fig. 7.3 Diffraction effect of the reflected wave

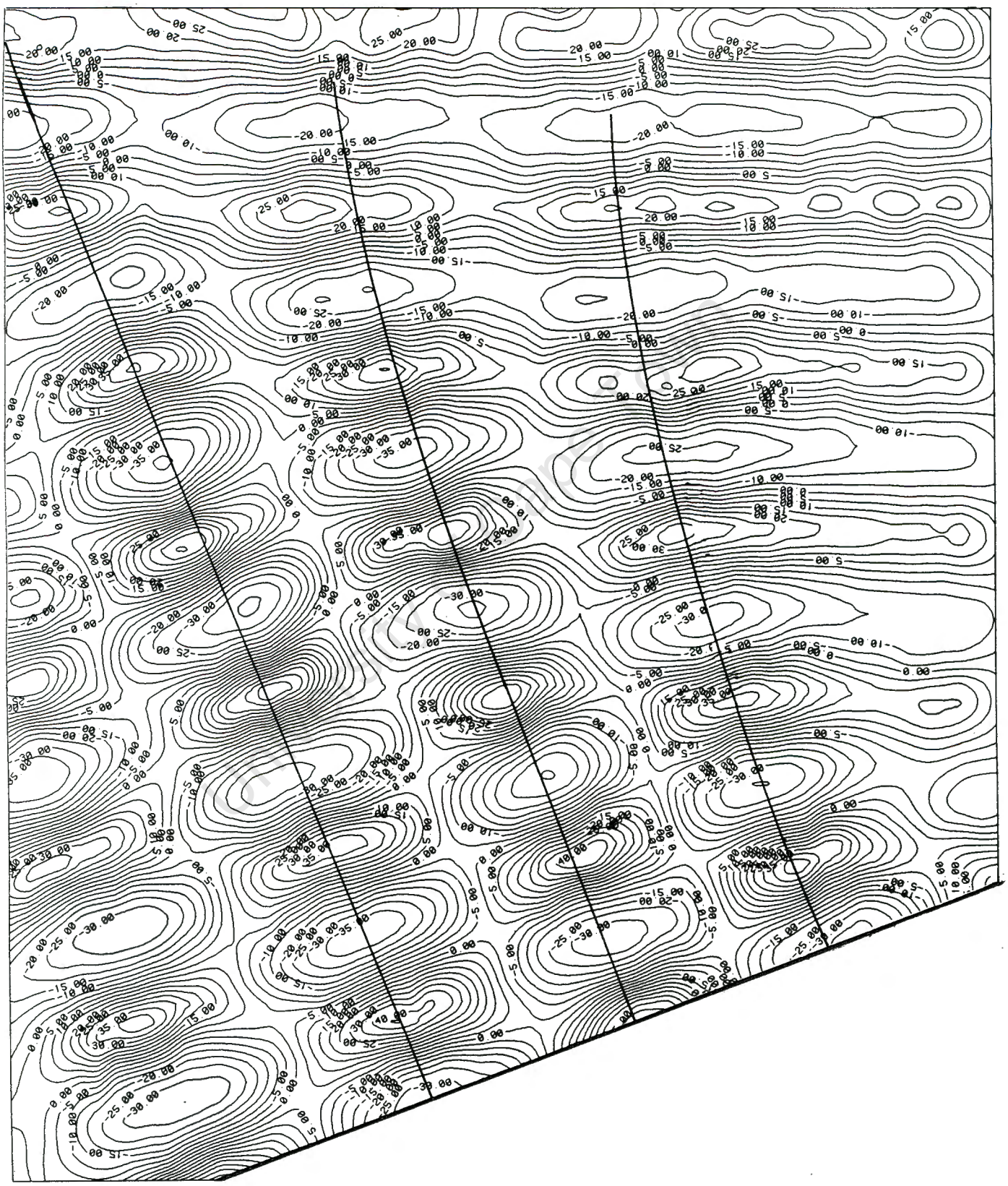

centres of the antinodes. The incident and reflected wave lengths do not differ, and the wavelength of the quasiantinodes is $L/\cos\theta_o$ as predicted.

7.3.1 Diffraction effects

Fig 7.4 Coefficient of Reflection (K_r) plot T = 0,765; $\theta_o = 69^o$

Stereopair 18, $\theta_o = 69^o$, oblique wave reflection, T = 0.765, H_i = 38,4mm

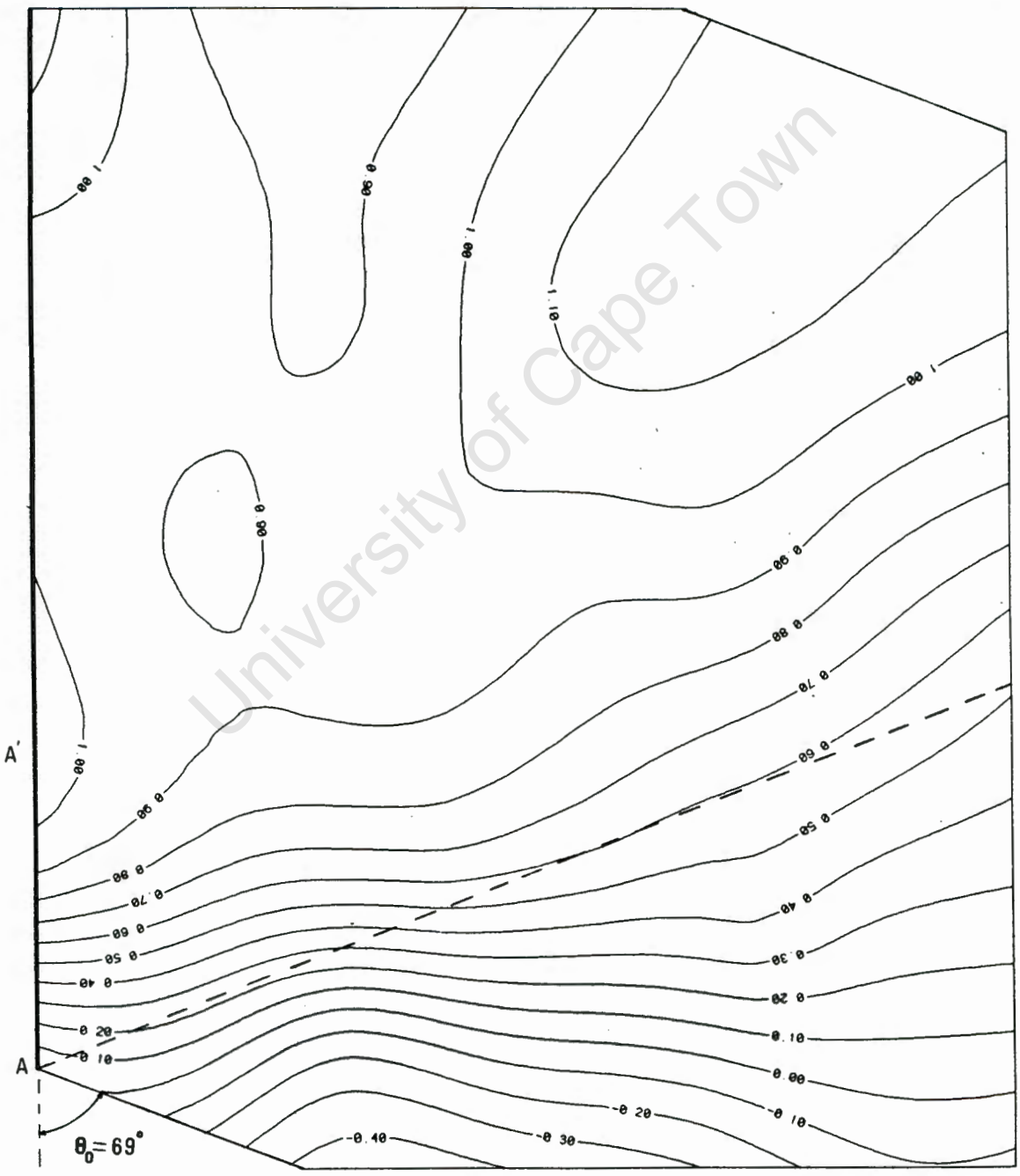

Scale 1 : 25

University of Cape Town

When comparing the reflection pattern developed to the theory, it can be seen that the lines representing the quasiantinodal lines rake backwards slightly (see fig. 7.3). It appears that the edge of the reflected wave, the section of the wave first reflected by the wall, acts as a wave that has just passed a single breakwater creating a diffraction pattern. This results in the bending of the edge of the reflected wave, which changes the positions of the antinodes so that they rake backwards in a curve.

The coefficient of reflection (K_r) plots (see Section 6.4 3) are only presented for T = 0,765 and $\theta_o = 69^o$, (see fig. 7.4). For the T = 1,01 center plots only 1,5 wave lengths are visible, so no meaningful trends could be established on the K_r plot.

In fig 7.4 the incident wave orthogonal is drawn showing the edge of the wave basin, joined to the initial point on the reflecting wall "A". The dotted line represents a reflected wave orthogonal, drawn from point A. This dotted line represents the line along which the reflected wave would travel without diffraction. The contours for the K_r contour plot are similar to those for the conventional diffraction pattern obtained for a single breakwater (see fig. 7.5)

In the Kr plot the reflected orthogonal passes between the contours K_r = 0,5 to 0,6; while for the diffraction diagram, which is for a similar wave angle, the wave orthogonal also passes between the lines of equal diffraction K' = 0,5 to 0,6. In both cases , the edge wave orthogonals have a wave height of 0,5 H_i to 0,6 H_i. This appears to confirm that the edge of the reflected wave does behave as a diffracted wave as expected. Between A and A' there is a gradual increase in K_r. This is not realistic as the contourer interpolated the contours between A and the first antinode at the wall. If more information from further experiments was available, the contours would most probably increase more rapidly, and look more like the initial section of the diffraction diagram.

University of Cape Town

Fig 7.5 Wave diffraction diagram - 75° wave angle (From Coastal Engineering Research Centre, 1984).

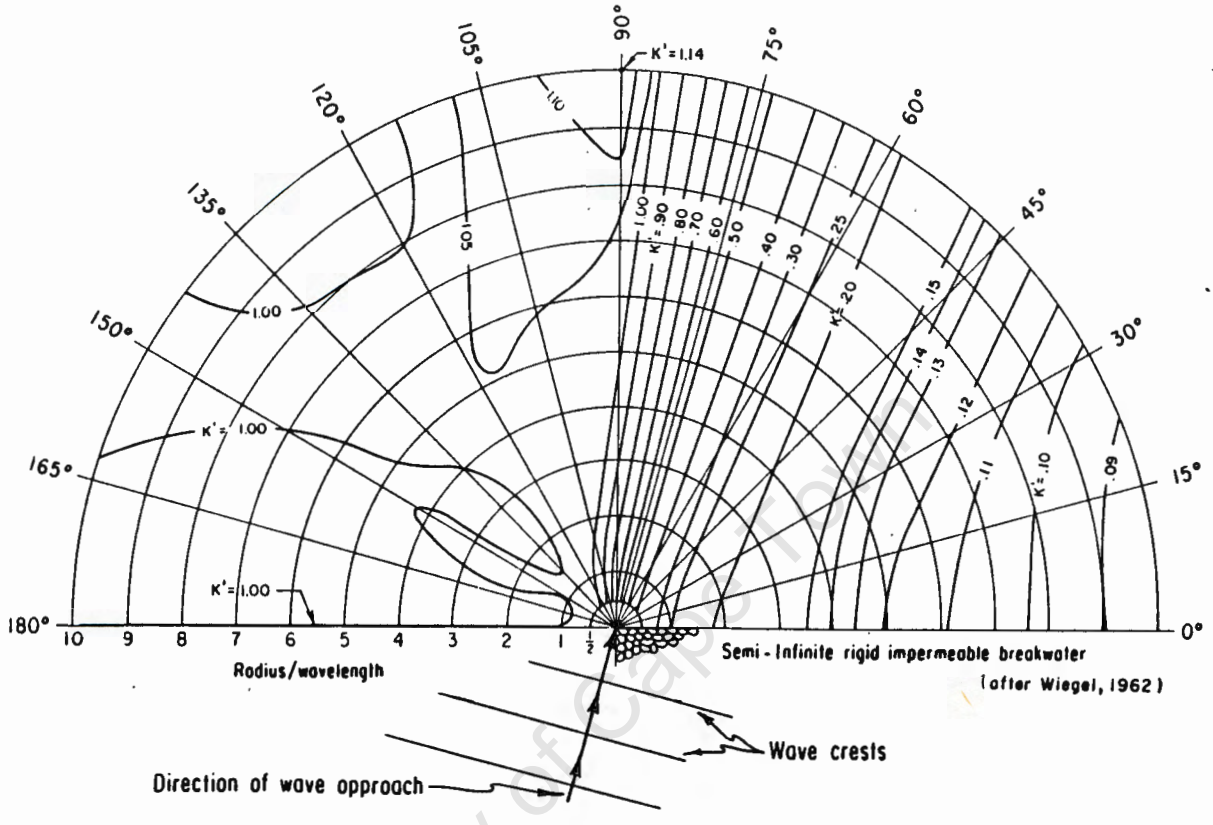

7.3.2 Degree of reflection

It would be realistic to assume that diffraction does occur for the edge of the reflected wave, so as both the diffraction diagrams suggest similar values along the wave orthogonal it would appear that the coefficient of reflection is ≈ 1, The K_r contour plot shows that for where diffraction effects do not occur, $K_r \approx 1$. The negative contour values in the K_r contour plot are attributed to the variation in the incident wave heights.

7.4 Mach wave reflection

Mach wave reflection was investigated for two wave periods T = 0,765 and T = 1,01. The majority of tests were done using T = 0,765 where the effect of change in incidence was investigated. Tests were

Fig 7.6 Contour plot of Mach wave reflection

Stereopair 20, $\theta_o = 34^o$, Mach wave reflection, T = 0,765, H_i = 38,4mm

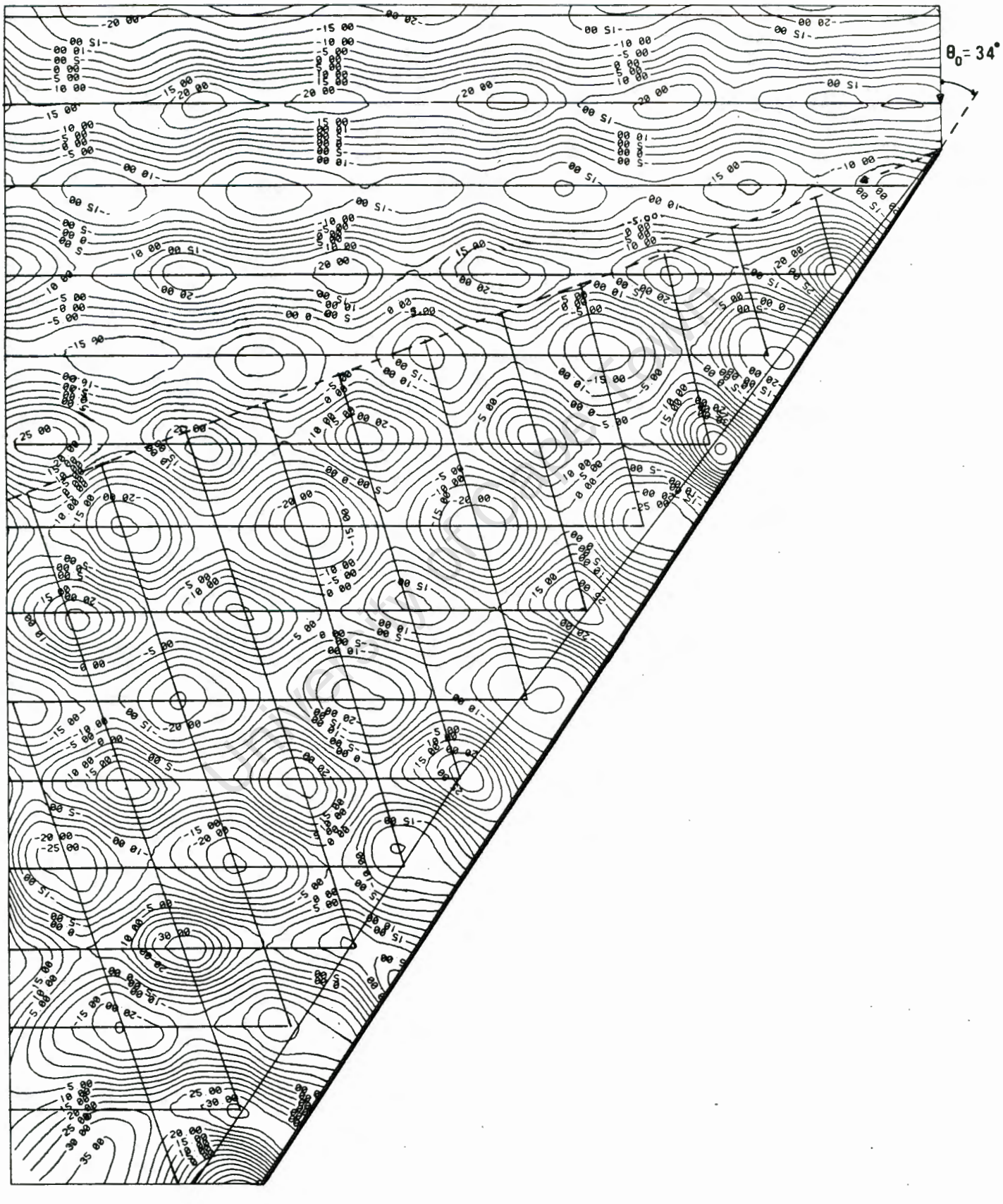

Scale 1 : 25

performed for T = 1,01 with $\theta_o = 34^o$, to investgate the effect of the incident wave height on Mach reflection.

The Mach stem width appears to grow linearly from the start of the wall (see Fig. 7.6), which is consistent with the observations of previous investigators. The angle the Mach stem grows at is α. The Mach stem width is made dimensionless by dividing by the incident wave length. On this basis comparisons could be made between different wave periods.

From the data available it appears that the starting angle for identifiable Mach wave reflection is $\theta_o = 47^o$ (Stereopair 19). In Fig 7.6 it can be seen that the effect of the Mach wave is that the normal oblique reflection pattern starts a finite distance away from the wall. This distance, as defined in Section 7.4.1, is the width of the Mach stem (B). For the section of linear growth of the Mach wave, the incident wave is reflected as if an imaginary reflecting wall was positioned at $(\theta_o + \alpha)^o$. Once the Mach stem has achieved maturity the incident wave reflects from an imaginary wall, parallel to the actual wall, but positioned B away from the actual wall. The incident and reflected wavelengths are similar, and the Mach waves have a wavelength of $L_i/\cos\theta_o$. The angles of incidence and reflection are similar, about the corresponding imaginary walls.

7.4.1 Definition of the Mach wave

The Mach stem width (B) has been previously defined by Berger and Kohlhase (1976) as the distance from the reflecting wall to the trough adjacent to the Mach wave (see Section 4.4). From the contour plots of the Mach waves (see fig 7.6) obtained, it was realised that the Mach stem width needed to be redefined. In fig 7.6 the incident and reflected waves have been identified with best fit lines placed through the relevant antinodes. The initial intersection of the incident and reflected lines occurs either at a crest or a trough, and would normally represent the antinode adjacent to the reflecting

University of Cape Town

wall, intersecting on the boundary of the wall for conventional oblique reflection. It is proposed that the Mach stem width be defined as the distance from the wall to the intersection representing the final antinode before the wall. It is according to this definition that the Mach stem width will be compared in this investigation.

7.4.2 Relationships investigated for Mach wave reflection

There appear to be three factors which affect the resulting Mach wave. The factors identified are

i) angle of incidence

ii) period of the incident wave, or its wavelength

iii) incident wave height.

7.4.2.1 Effect of angle of incidence

To investigate the effects of the angle of incidence, only one set of data is available, stereopairs 21, 25, 26, 27. For these stereopairs the wave period was constant (T = 0,765) and the incident wave height was also kept constant (H_i = 24,8 mm). The data for these stereopairs is presented in table 7.5.

Table 7.5 Data for T = 0,765; H_i = 24,8mm

Stereopair	θ_o	Tan θ_o	α	B	Maximum H_s/H_i
21	34^o	0,675	3^o	0,13 L_i	2,581
25	25^o	0,466	6^o	0,308 L_i	2,419
26	20^o	0,364	$8,5^o$	0,422 L_i	1,774
27	10^o	0,176	$9,5^o$	0,649 L_i	1,472

The only trend that definitely appeared to exist for the data is the linear relationship between the angle of incidence and the Mach stem width. This relationship is described in fig. 7.7, and the line fitted to the data by linear regression obtained a correlation

University of Cape Town

coefficient of -0,999. This function is empirical as the effects occurring due to the incident waveheight and period are unknown. The possibility of the angle of incidence being a tan relationship was investigated, but it does not fit the available data better than the linear relationship. It is possible however that a tan θ_o relationship could be applicable.

Fig 7.7 Mach stem width

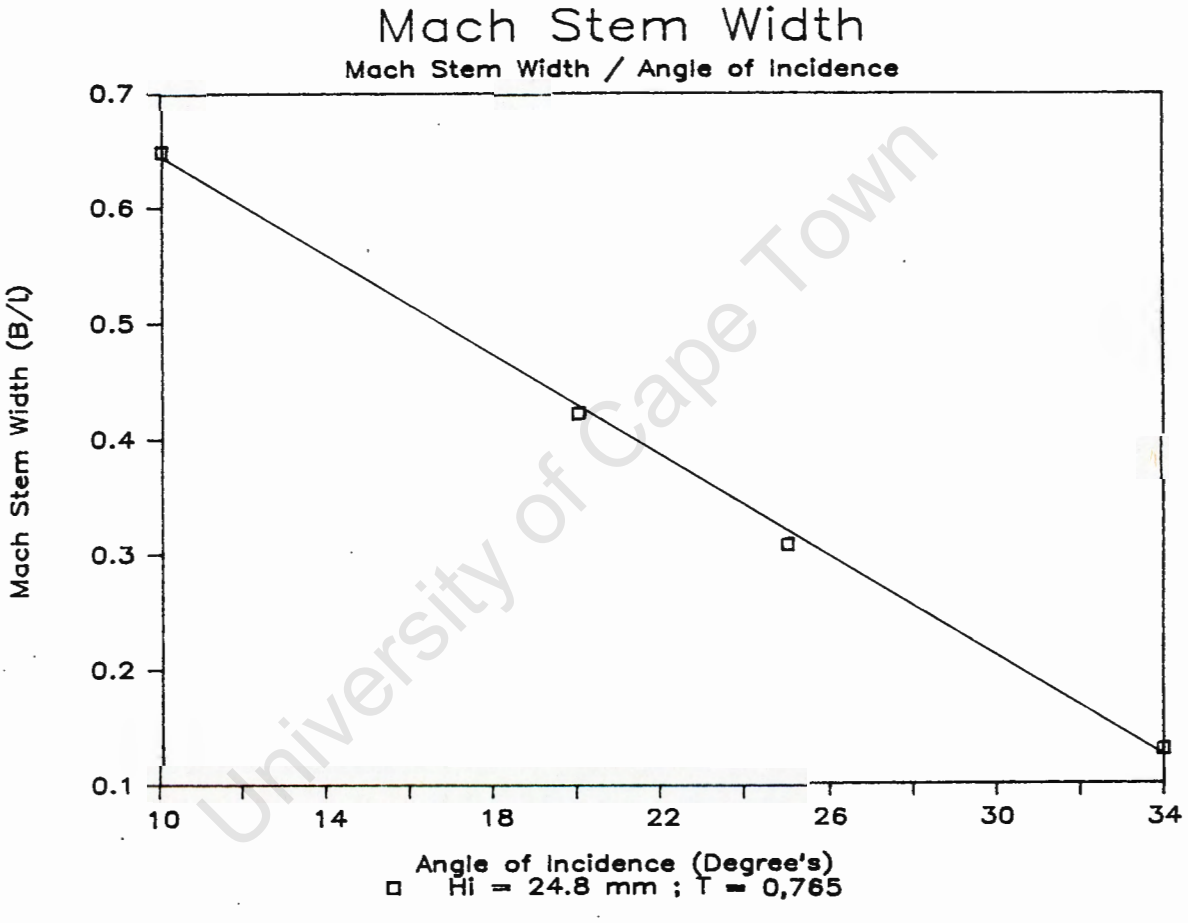

University of Cape Town

The Mach stem grows linearly from the start of the reflecting wall with angle α. The relationship between θ_o and α can be seen in fig 7.8. It appears that a linear relationship could exist for this data, as the line fitted through the data produced a correlation coefficient of -0,961. The stem angle was also plotted against

tan θ_o and a similar coefficient of reflection was obtained as tan is almost linear in this range. More data is required before a decision can be made as to what the exact relationship is.

Fig 7.8 Growth of Mach stem

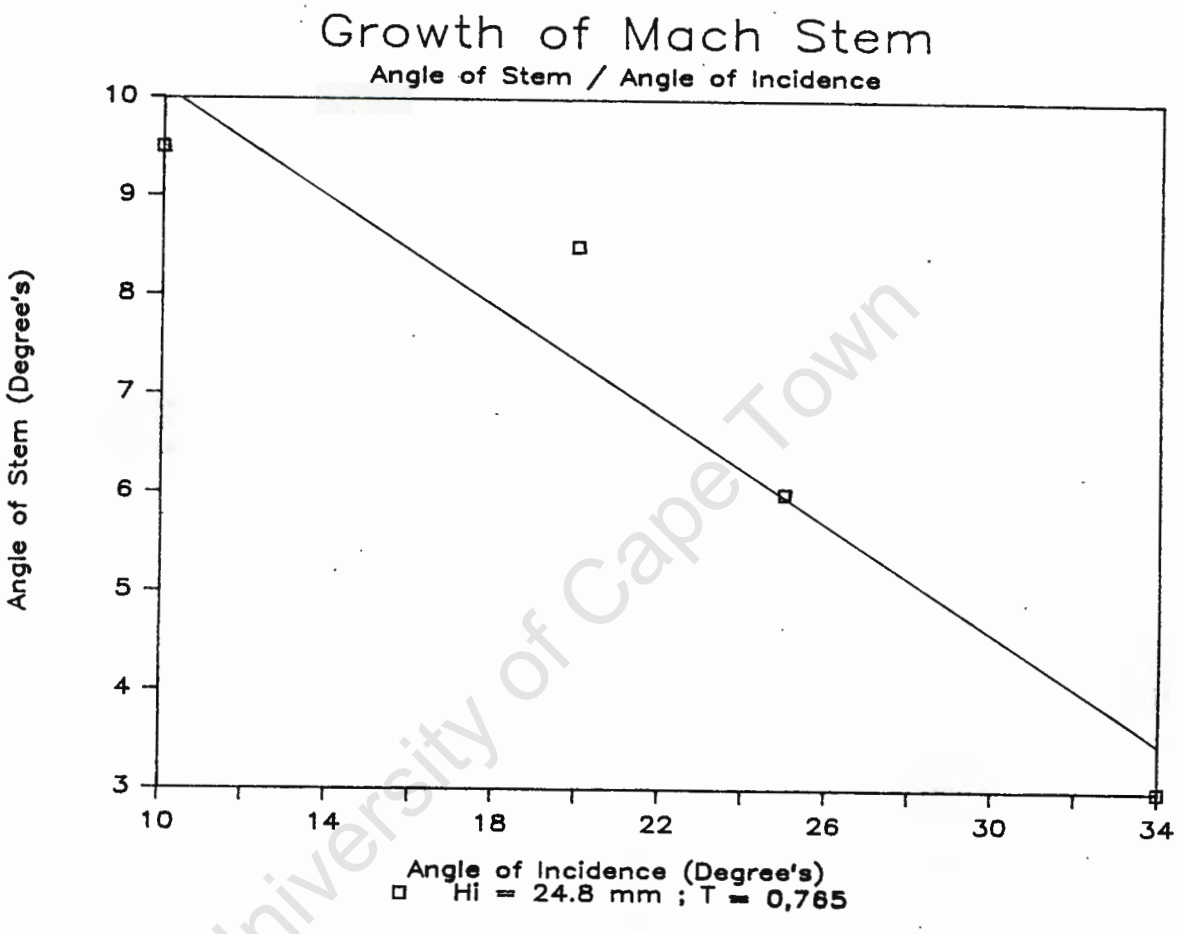

University of Cape Town

Wiegel (1964b) presents data for the α/θ_o relationship for solitary waves for an average of wave heights H_i/d = 0,05 to 0,43. Wiegel obtained a linear relationship for α/θ_o with a gradient that was almost identical to the gradient obtained in this investigation, except that the α intercept was 2^o below the α intercept for this investigation. Wiegel used solitary waves for his investigation and it would appear that Wiegel used the same definition for the edge of the Mach wave as is used in this investigation. The discrepancy in the size of α could be due to the solitary waves, as Wiegel did

observe that solitary waves produce a smaller stem width than periodic waves.

There is a relationship between the maximum H_{ms}/H_i ratio that occurs and its respective angle of incidence. Fig 7.9 shows the increase in H_{ms}/H_i for increasing θ_o, Although the coefficients of reflection for $\theta_o = 10^o$, 20^o may not have reached their maximum values as the length of the reflecting wall may have been too short for the waves to reach maturity. The relationship for this data is not well defined. A linear relationship, which although it fits the available data well, does not predict the probable decrease in the H_{ms}/H_i ratio for increasing angles of incidence as shown by data for different incident waveheights.

Fig. 7.9 Relative height of Mach stem.

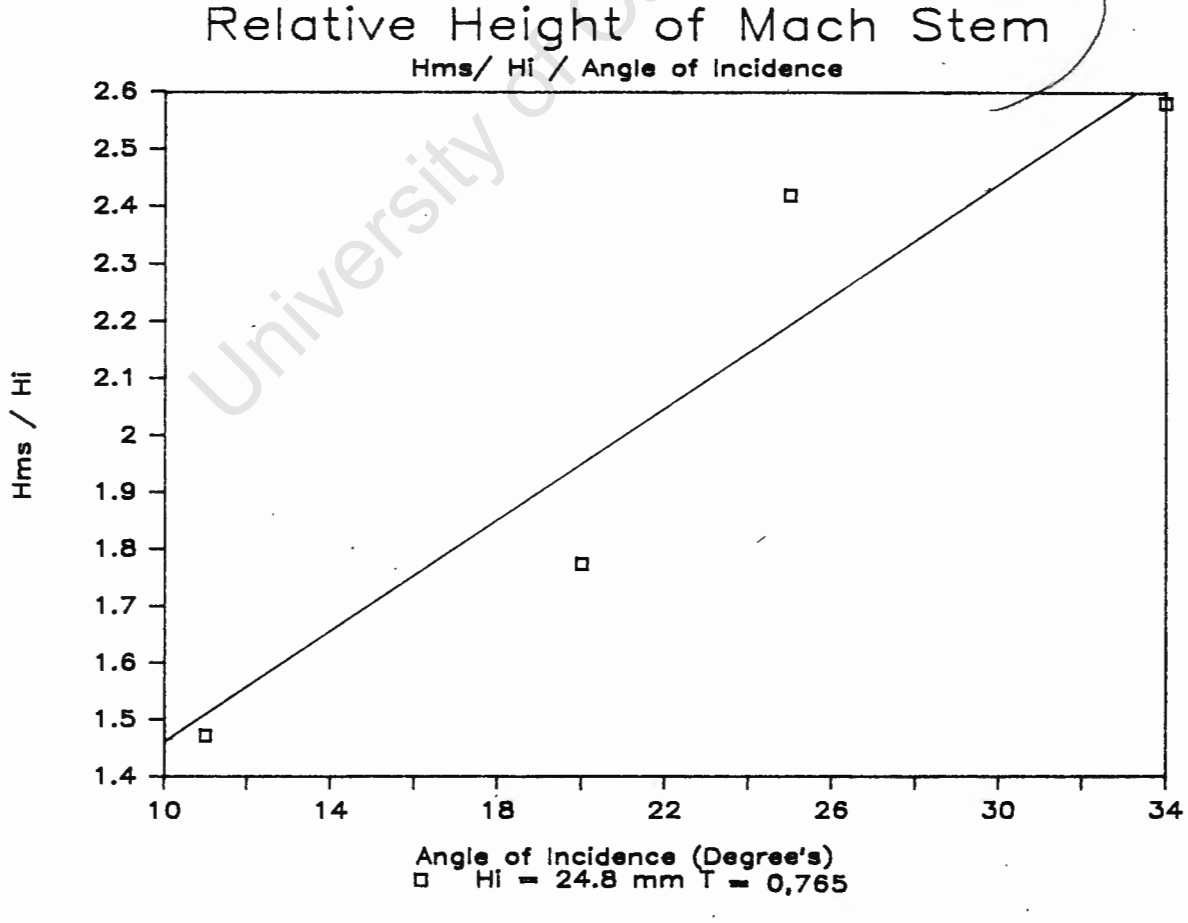

University of Cape Town

7.4.2.2 Effect of varing incident wave height and changes in period

The Mach stem width is affected by the incident wave height, as for as increasing incident wave height the Mach stem becomes wider. An attempt was made to try to establish the relationship between the Mach stem width and the incident wave height for T = 0,765 and T = 1,01 for constant angle of incidence, $\theta_o = 34^o$. The data is summarised in Table 7.6

Table 7.6 Data for $\theta_o = 34^o$

Stereopair	T	H_i	H_i/L	H_s/H_i	B	Comment
20	0,765	38,2	0,050	2,044	$0,325L_i$	Mach wave breaking
21	0,765	24,8	0,032	2,581	$0,130L_i$	
22	1,01	32,7	0,029	2,339	$0,156L_i$	
23	1,01	34,0	0,030	2,882	$0,178L_i$	Mach wave on verge of breaking
24	1,01	39,9	0,036	2,105	$0,183L_i$	Mach wave breaking

The above data is plotted in fig. 7.10, and there does not appear to be any definite relationship. It would appear that the amount of energy available from the incident wave determines the Mach stem width. The effect of the Mach wave breaking on the Mach stem width does not appear to be related for different periods. When the wave starts to break for T = 1,01 there is not a significant increase in the Mach stem width for increase in incident wave height. The opposite relationship exists for T = 0,765. A lot more data is required to define this effect. However for both cases of the Mach stem breaking the incident wave heights are similar (≈ 39 mm) and the H_s/H_i values are similar. This suggests that the wave heights are unstable because of the shallow water relationship. For T = 1,01 the Mach stem would break for a smaller H_i/L ratio than for T = 0,765. If the growth of the Mach stem width is dependent on the incident energy, then when the wave starts to break, any increase in incident

University of Cape Town

energy is dissipated in breaking, so the Mach stem grows very little once breaking starts. In this way the size of the Mach stem for T = 0,765 could have grown somewhat bigger before breaking started than for T = 1,01 before it started to break. This is a possible explanation for the discrepancy in the Mach stem width data.

Fig. 7.10 Mach stem width

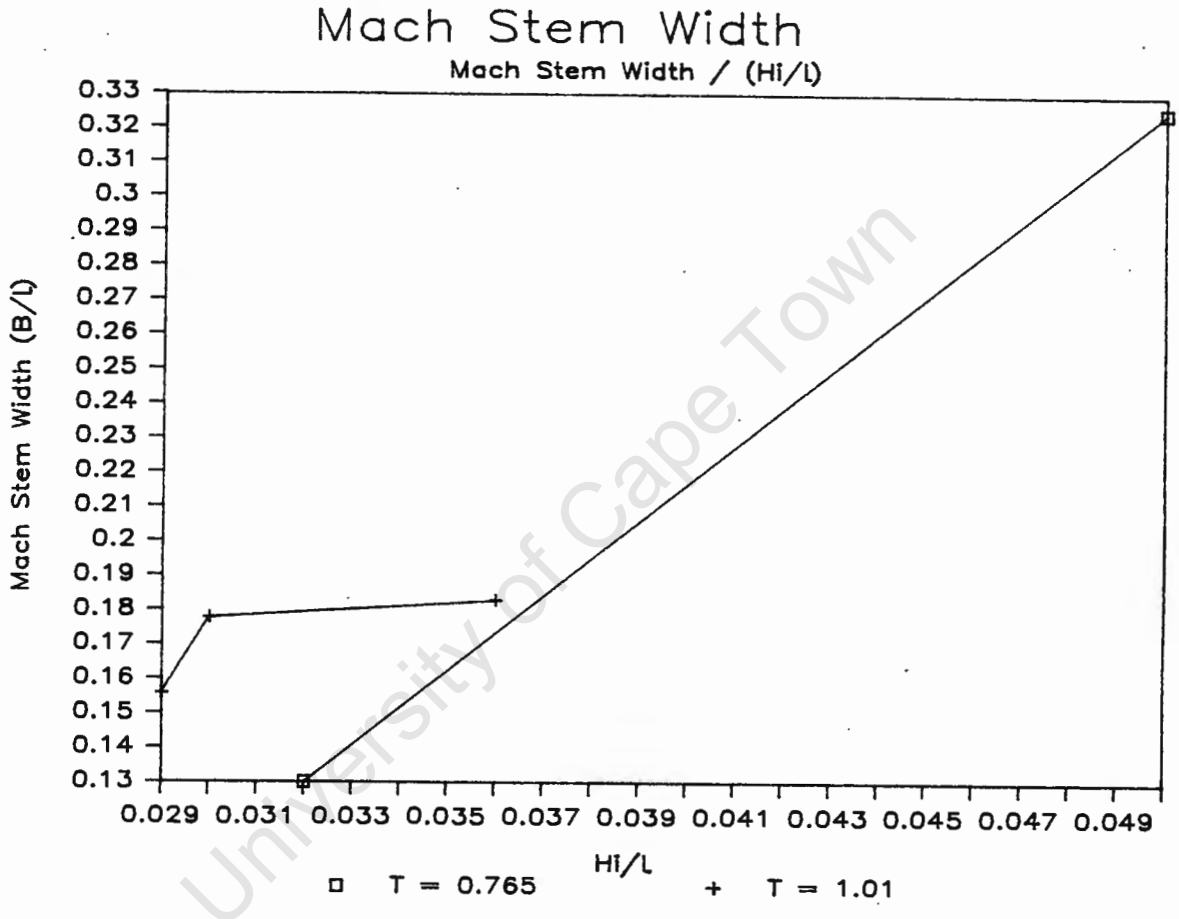

University of Cape Town

7.4.2.3 Coefficient of reflection plots

To investigate any noticeable effects in the reflected wave, coefficient of reflection (K_r) plots were generated (See Appendix B). In the K_r plots the relative height of the Mach wave is also described by K_r values rather than H_{ms}/H_i, so the wave heights can be compared, and contours plotted for the data.

For stereopairs 19,21 where T = 0,765, θ_o = 47, 34° and H_i = 34 mm; 24,8 mm respectively, the Mach stem reaches a peak and then drops off to a trough with an increase in the K_r values next to the trough in the Mach stem. The peak in the Mach stem heights corresponds in both scenarios to the Mach stem reaching its maximum width (B).

7.4.3 Trends in Mach wave development

7.4.3.1 Limiting angle for the mach wave

Previous investigations (Berger, Kohlhase, 1976) suggest that Mach reflection occurs for θ_o less than 45°. In stereopair 19, where T = 0,765 and H_i = 38,4mm, the Mach wave first occurs for θ_o = 47° which is outside the previously established limit. The identification of the Mach wave was only made possible by the technique described in section 7.3, as this wave pattern could very easily be considered to be ordinary oblique reflection by casual inspection. The occurrence of the Mach wave for θ_o = 47° suggests that there does not exist a finite point where the Mach wave does not exist, but that as θ_o tends to 90° the Mach wave tends to zero.

7.4.3.2 Growth of the Mach wave as a function of incident energy

There appears to be a definite relationship between the amount of energy input and the height, the width and the rate of growth of the Mach wave. This incident energy input is affected by the incident waveheight, the incident wave wavelength, and the angle of incidence. From the data presented it is possible that the Mach wave exists for all reflection situations, and could be defined by a relationship which tends to zero for the Mach stem width and angle of growth of the Mach stem, and which tends to 2 for H_{ms}/H_i as θ_o tends to 90°. This relationship could tend to infinity for the Mach stem width and angle of growth and to 1 for H_{ms}/H_i as θ_o tends to 0°.

University of Cape Town

7.4.3.3 Second Mach stem

Berger and Kohlhase (1976) suggest that a second Mach stem exists adjacent to the main Mach wave for $\theta_o < 30^o$. Plate 7.2 shows the phenomenon that was observed during this investigation for $\theta_o = 20^o$. This plate, together with the contour plot (Appendix A; stereopair 26) appear to show that this second Mach wave is actually the resulting reflecting pattern. The angle between the wall and reflected wave orthogonal is small, so the reflected wave which is also small is diffracted and attenuated such that within the limits of the wave basin only one set of defined antinodes is developed next to the Mach stem. Beyond this the reflected wave is so small that it cannot be distinguished from the other imperfections in the incident wave.

Plate 7.2 Mach wave, $\theta_o = 20^o$

University of Cape Town

8. CONCLUSIONS AND RECOMMENDATIONS

8.1 Accuracy of analysis

Photogrammetry is an extremely accurate tool, with a standard deviation for the analysed data of ± 2 mm. The standard deviation for the average heights of the incident waves generated by the wave generator were ± 1 to 3 mm. The standard deviations calculated for the average height of the standing waves were 1 to 5 mm. Unfortunately the error for the oblique wave reflection antinodes is unquantifiable, but could be as large as 15 mm.

It would have been desirable to photograph each wave scenario at least twice, so some idea of the actual magnitude of the deviation of the generated wave could be established. Due to the long period of time required to obtain and analyse a stereopair, it would have been very difficult for any more stereopairs to be taken than were actually taken. The solution to this problem could be to use near real time photogrammetry, once adequately developed, to obtain many sets of data for each wave scenario.

8.2 Standing wave data

The investigation of the standing wave revealed interesting information. The extreme coefficients of reflection (K_r = 1,6) at the reflecting wall was unexpected. Previous investigators had suggested that a K_r = 1,4 could occur at the reflecting wall, but the extreme value of K_r = 1,6 places new emphasis on the importance of the standing wave and the effect it would have for overtopping.

The reduction in the standing wave length compared to the incident wave length for the shallower wave tested was surprising, although it had been suggested by previous investigators. A likely explanation is that there is energy interference between the opposing wave trains, as it would not appear likely that there is a reduction in the wave periods of the two wave trains.

University of Cape Town

8.3 Oblique wave reflection

The oblique wave reflection scenarios behaved as predicted by the wave theory. The angles of incidence and reflection were equal and a reflection coefficient of ≈ 1 was obtained. It was interesting to note that the diffraction pattern occuring for the edge of the reflected wave was similar to that predicted by previously established diffraction diagrams.

8.4 Mach wave reflection

The Mach wave is a complicated relationship, and a lot more data will be required before an adequate knowledge of its characteristics can be established. Two proposed concepts for possible relationships existing for Mach waves are proposed :

i) The Mach wave may exist for all θ_o, but be of negligible stem width for $\theta_o > 50^o$.

ii) The development of the Mach wave is a function of the incident wave energy which depends on the wave height and the period of the incident wave. It is felt that the Mach wave is not a diffraction problem, but an energy problem developing as a function of the non linear properties of the wave.

8.5 Future investigation

This investigation has shown that close range photogrammetry is an excellent technique for investigating water wave surfaces to a high degree of accuracy, and obtaining accurate, comprehensive representations of the water surface. Unfortunately it does not appear possible to use conventional photogrammetrical techniques to perform a comprehensive investigation into wave reflection as an enormous number of man hours would be required.

The author is of the opinion that when near real time photogrammetry systems have developed to sufficient accuracy, the potential exists to complete this wave reflection investigation. It is felt that a large wave basin equipped with a good quality wave generator should be adapted for permanent photogrammetric use. The area of the basin

University of Cape Town

could be covered with pairs of digital cameras synchronised from a single host computer. In this way not only wave reflection, but alternative harbour designs and other wave phenomenon could be investigated to a degree of accuracy and comprehensiveness never before realised. Such a system, although expensive, with adequate software, could revolutionise hydraulic model investigations.

University of Cape Town

BIBLIOGRAPHY

ADAMS, L.P.	1978	The use of Photogrammetry in the Study of the Sea and the Coasts. Proceedings of the 6th Conference of South African Surveyors, Part 1, 1978.
ADAMS, L.P.	1981	X-Ray Stereo Photogrammetry, Locating the Precise Three-Dimensional Position of Image Points. Medical and Biological Engineering Completing, September 1981, pg. 569.
ADAMS, L.P.; POS, J.D.	1981	Model Harbour Waveform Studies by Short Range Photogrammetry. Photogrammetric Record, October 1981, pg. 457.
ATKINSON, K.B.	1980	Developments in Close Range Photogrammetry. Applied Science Publishers 1980.
BERGER, U.; KOHLHASE, S.	1976	Mach Reflection as a Diffraction Problem. Coastal Engineering 1976 Proceedings, Vol. 1, pg. 796.
THE CANADIAN INSTITUTE OF SURVEYING	1986	Proceedings of Symposium "Real Time Photogrammetry - A New Challenge". International Archives of Photogrammetry and Remote Sensing.
COASTAL ENGINEERING RESEARCH CENTRE	1984	Shore Protection Manual, U.S. Government Printing Office, 1984.
FAIG, W.	1972	Photogrammetry and Hydraulic Surfaces. Journal of the Surveying and Mapping Division, Proceedings of the American Society of Civil Engineers, November 1972, pg. 145.
GRUEN, A.W.	1989	Digital Photogrammetric Processing Systems: Current Status and Prospects. Photogrammetric Engineering and Remote Sensing, Vol. 55, No. 5, May 1989, pg. 581.

University of Cape Town

HAMILL, P.A.	1963	Experimental Development of a Perforated Wave Absorber of Simple Construction and Minimum Length. National Research Laboratories, Ottowa Canada, Report No MB-252, May 1963.
HART, C.A.	1943	Air Photography Applied to Surveying. Longmans, Green and Co. Ltd, 1943.
IPPEN, A.T.	1966	Estuary and Coastline Hydrodynamics. McGraw-Hill Book Company, 1966.
JAMIE, A.	1988	Analysis of Wave Reflection at a Vertical Wall Using Close Range Photogrammetry. BSc Thesis, University of Cape Town.
JARLAN, G.E.	1961	A Perforated Vertical Wall Breakwater. The Dock and Harbour Authority, April 1961, pg. 394.
MARESCA, J.W.; SEIBEL, E.	1976	Terrestrial Photogrammetric Measurements of Breaking Waves and Long Shore Currents in the Near Shore Zone. Coastal Engineering 1976 Proceedings, Vol. 1, pg. 681.
MARKS, W.; RONNE, F.C.	1955	Aerial Stereophotography and Ocean Waves. Photogrammetric Engineering 2(1), pg. 107.
NATIONAL SEMI CONDUCTORS	1978	Linear Data Book, pg. 62.
MOFFIT, F.H.	1968	Wave Surface Configuration. Photogrammetric Engineering, Vol. 34, 1968, pg. 179.
moves 1970		
PATERSON, A.J.C.	1986	A Study of Ship Wave Resistance from an Analysis of the Wave Pattern using Close Range Photogrammetry. MSc Thesis, University of Cape Town.
PETZER, J.M.	1987	Analysis of Water Wave Reflection using Photogrammetry, BSc Thesis, University of Cape Town.

University of Cape Town

POS, J.D.; ADAMS, L.P.; KILNER, F.A.	1988	Synoptic Wave Height and Pattern Measurements in Laboratory Wave Basins using Close-Range Photogrammetry. Photogrammetric Engineering and Remote Sensing, Vol. 54, No. 12, December 1988, pg. 1749.
POS, J.D.	1984	A study of breakwater gap diffraction using close range photogrammetry and finite and infinite elements. PhD, University of Cape Town.
RUTHER, H.	1982	Relative Orientation with Limited Control in Close Range Photogrammetry. PhD, University of Cape Town.
RUTHER, H.	1989	Near-Real-Time Photogrammetry on a Personal Computer - PHOENICS. Conference of Southern African Surveyors 1989, Paper No. 3-2.
RUTHER, H.; PARKYN, N.	1988	The Development of a PC-based Near-Real-Time Photogrammetry System - PHOENICS. International Archives for Photogrammetry and Remote Sensing, Vol. 45, Sept. 1988, pg. 1231.
SCHOEMAKER, H.J.; THIJSSE, J.T.H.	1949	Investigations of the Reflections of Waves. International Association for Hydraulic Structures Research, Third Meeting Grenoble, 1949, pg. I-2.
SORENSEN, R.M.	1968	Stereo Photogrammetric Analysis of Waves Surfaces. Journal of the Hydraulics Division, Proceedings of the American Society of Civil Engineers, January 1968, pg. 181.
SILVESTER, R.	1974	Developments in Geotechnical Engineering 4A, Coastal Engineering 1. Elsevier Scientific Publishing Company, 1974.
SZCZECHOWSKI, B.; MUCHA, A.	1980	The Photogrammetric Measurements of Water Ripples on Hydrotechnic Models. International Archives of Photogrammetry, Vol. 23, No. B5, 1980, pg. 764.

University of Cape Town

UNIVERSITY OF CAPE TOWN 1987 Hydraulic Engineering CIV403F.

WELHAM, L.G. 1982 Underwater Stereometrology for Scientists and Engineers using non-Metric Cameras. MSc, University of Cape Town.

WIEGEL, R.L. 1964(a) Oceanographical Engineering. Prentice-Hall, Inc/Engle Wood Cliffs, N.J.

WIEGEL, R.L. 1964(b) Water Wave Equivalent of Mach Reflection. Coastal Engineering, 1964 Proceedings, pg. 82.

University of Cape Town

CONTOUR PLOT

Stereopair 10, $\theta_o = 90^o$. standing wave - crest at the wall T = 1,5, H_i = 37,0mm

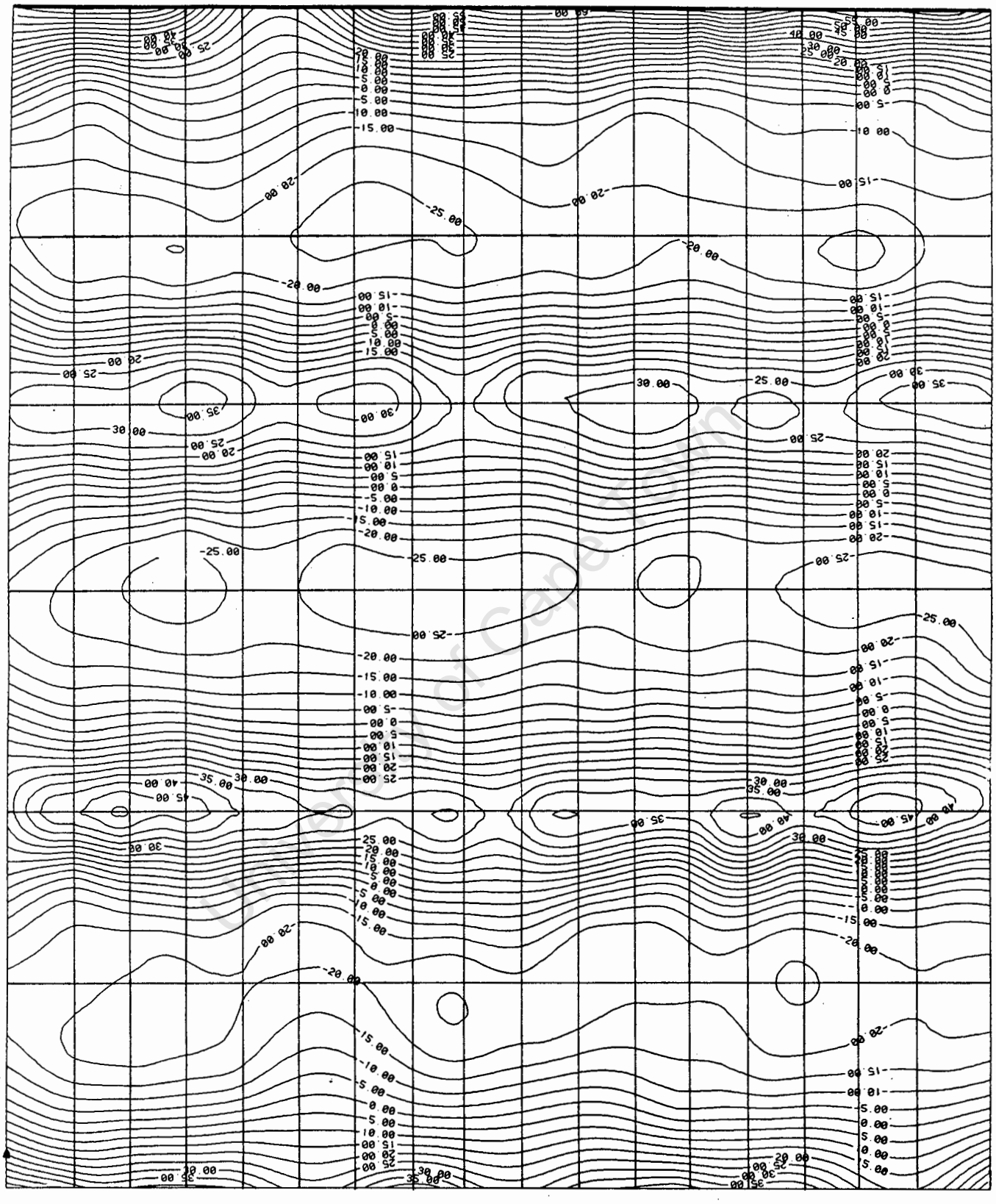

Scale 1 : 25

CONTOUR PLOT

Stereopair 12, $\theta_o = 90^o$, standing wave - Trough at the wall T = 1,5, H_i = 37,0mm

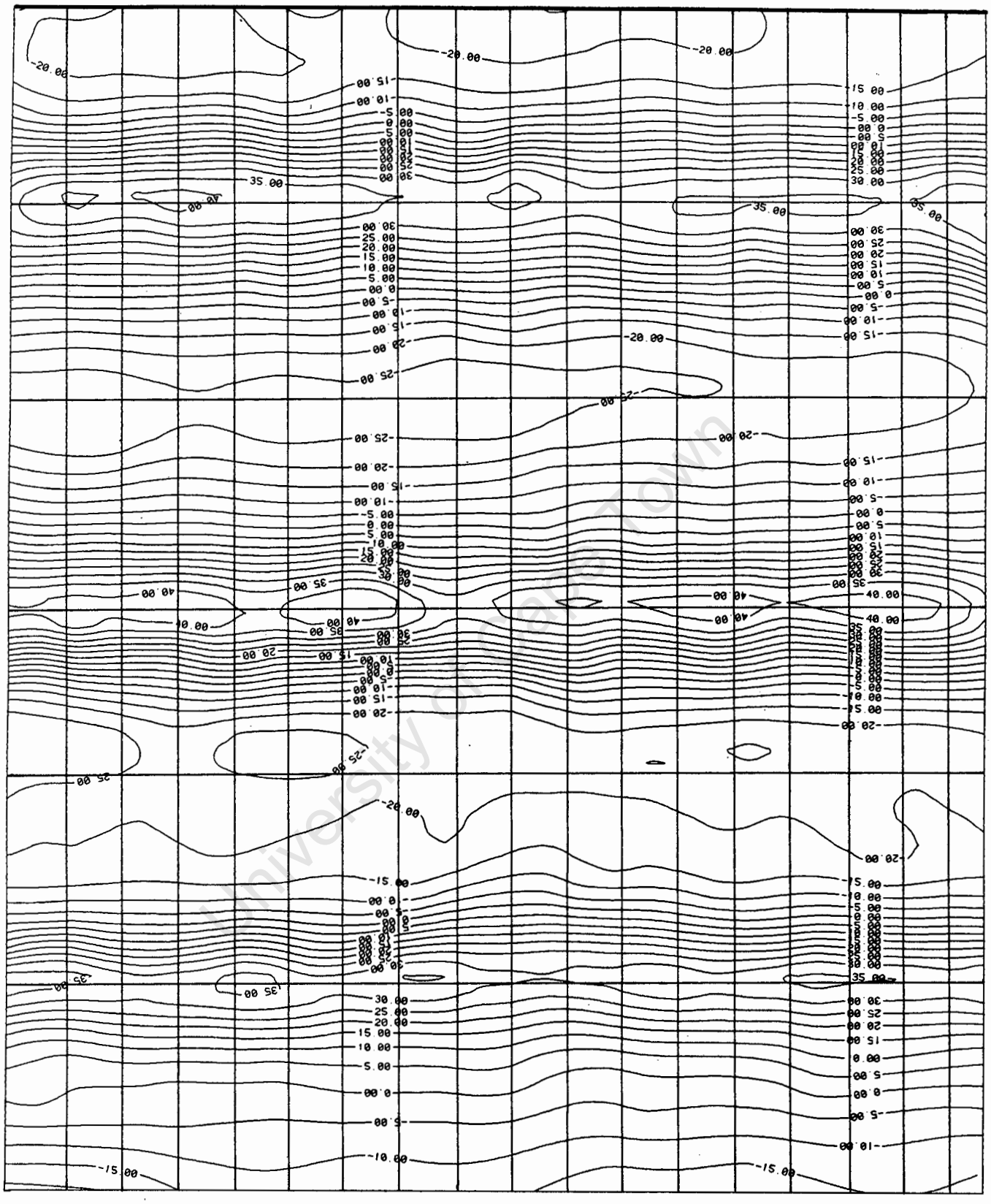

Scale 1 : 25

University of Cape Town

CONTOUR PLOT

Stereopair 13, $\theta_o = 90^o$, standing wave - Trough at the wall T = 1,01, H_i = 34,0mm

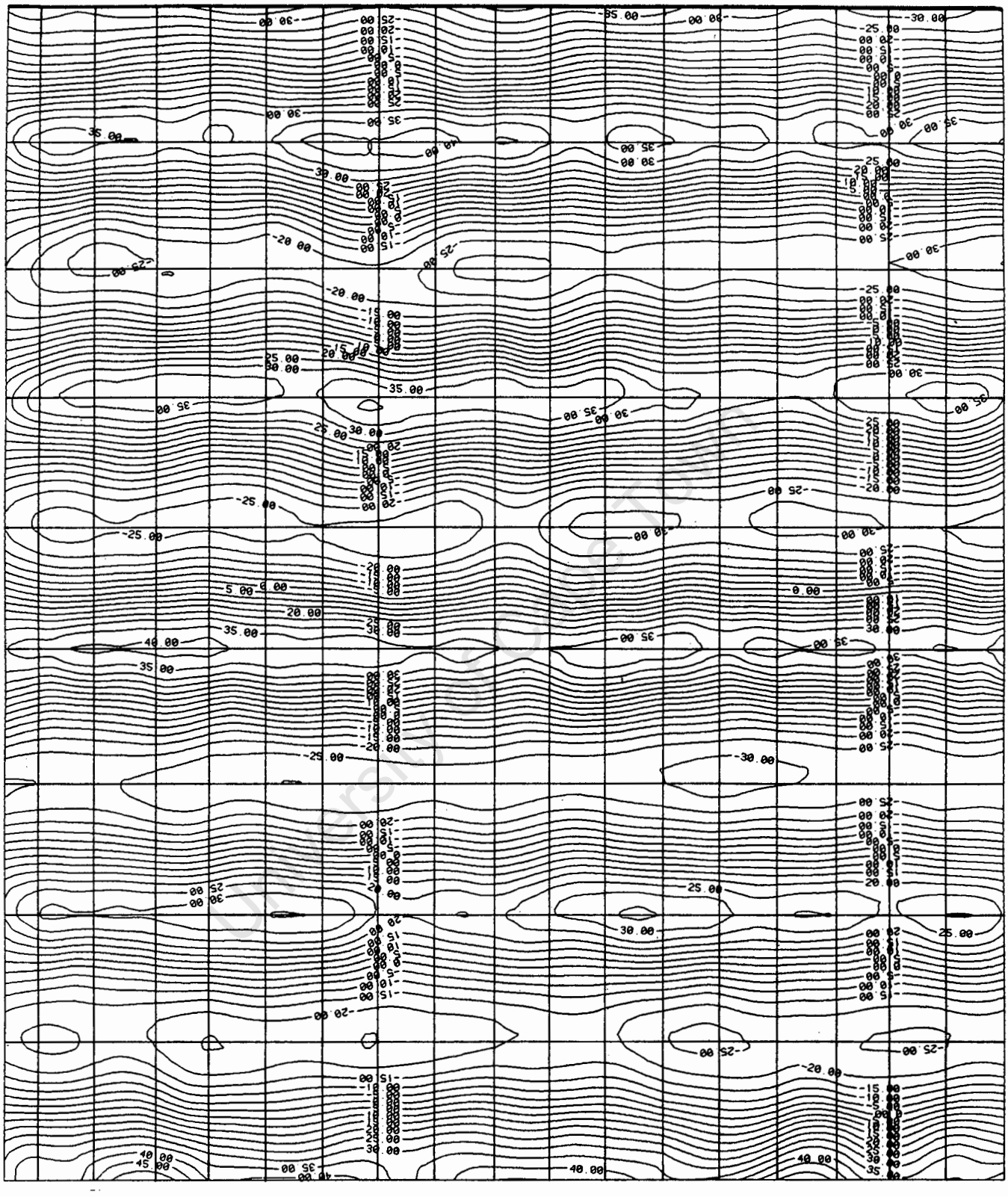

Scale 1 : 25

CONTOUR PLOT

Stereopair 16, $\theta_o = 90^o$, standing wave - Crest at the wall T = 1,01, H_i = 34,0mm

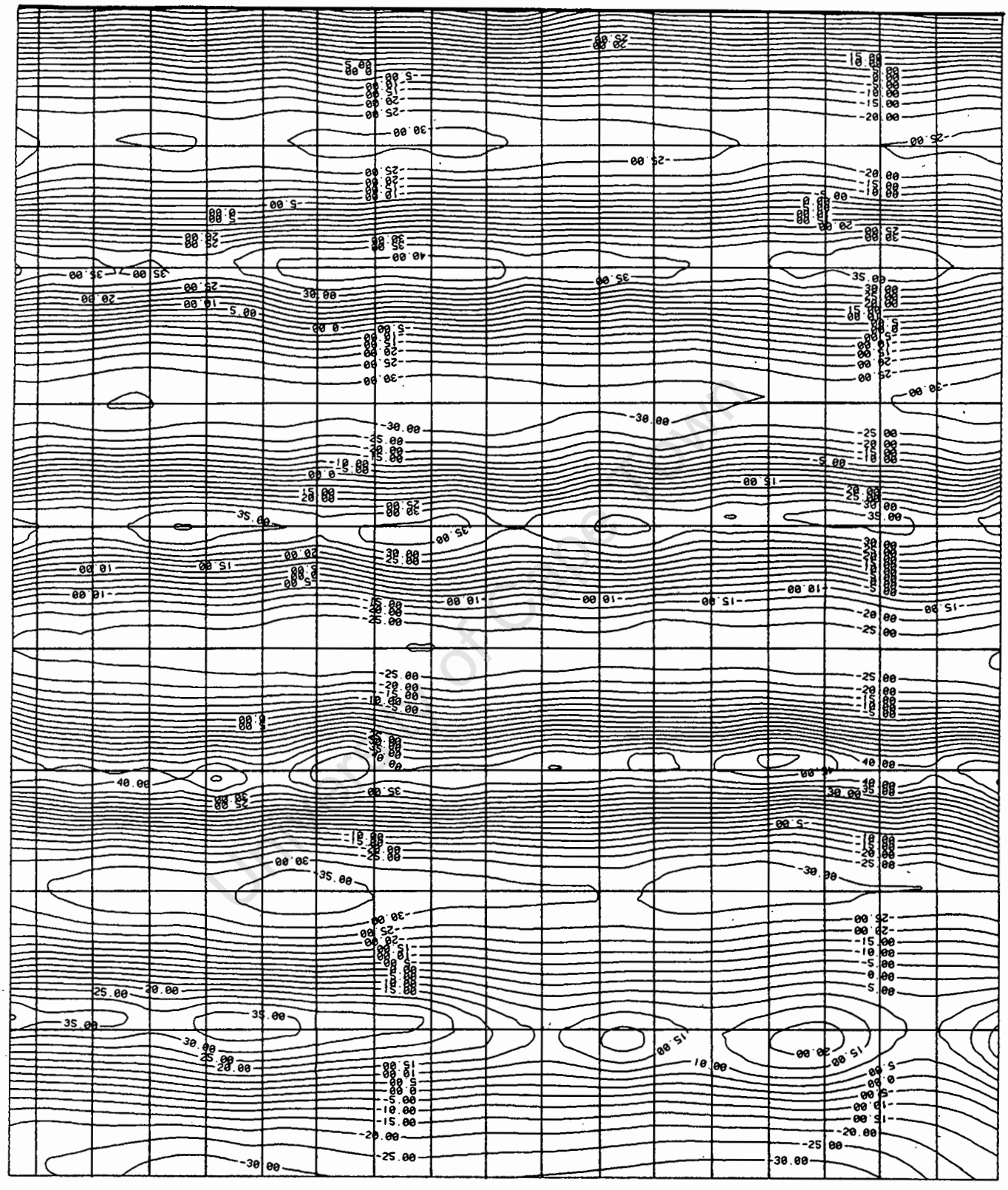

Scale 1 : 25

CONTOUR PLOT

Stereopair 17, $\theta_o = 69^o$, oblique wave reflection, T = 1,01, H_i = 34,0mm

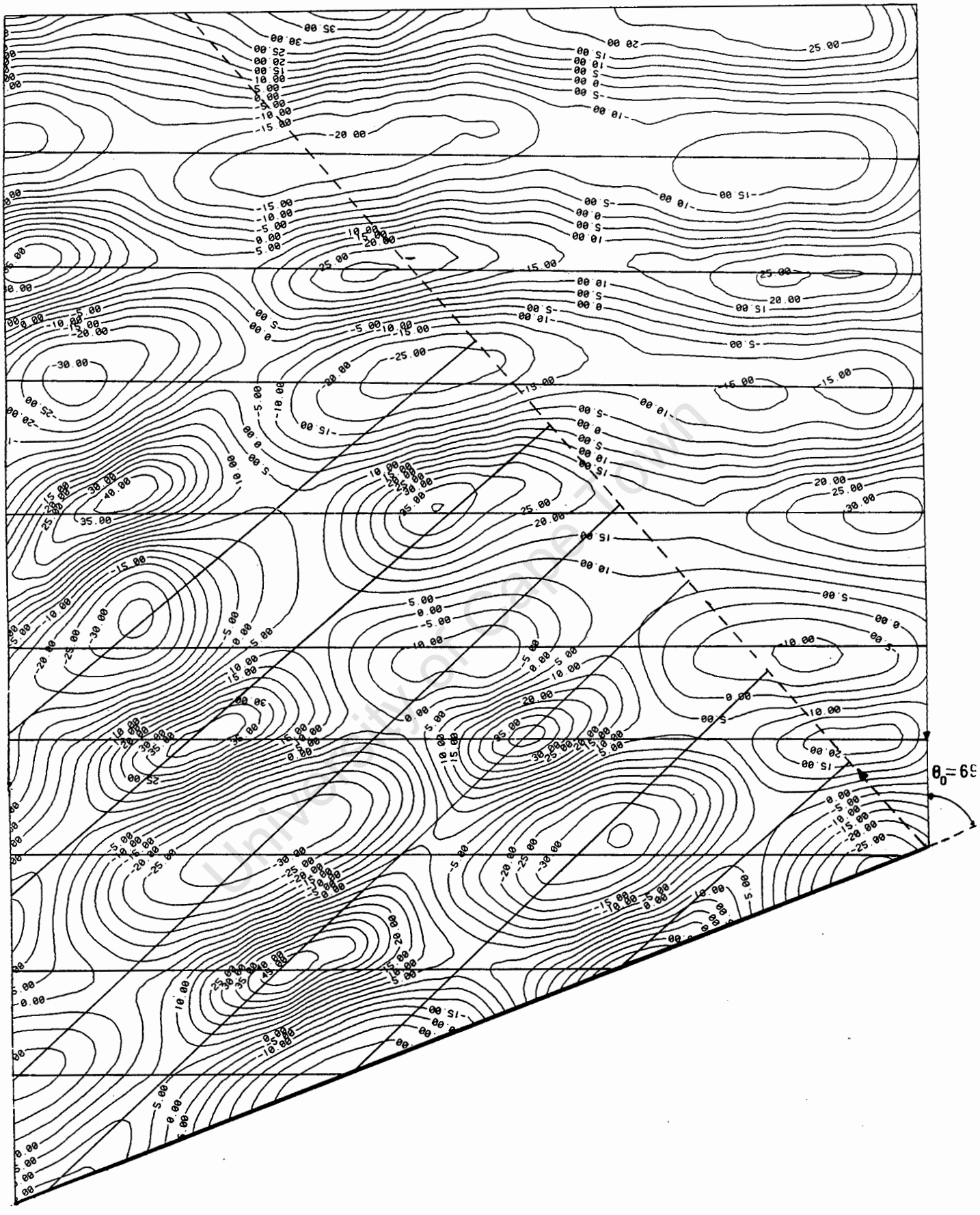

Scale 1 : 25

University of Cape Town

CONTOUR PLOT

Stereopair 18, $\theta_o = 69^o$, oblique wave reflection, T = 0.765, H_i = 38,4mm

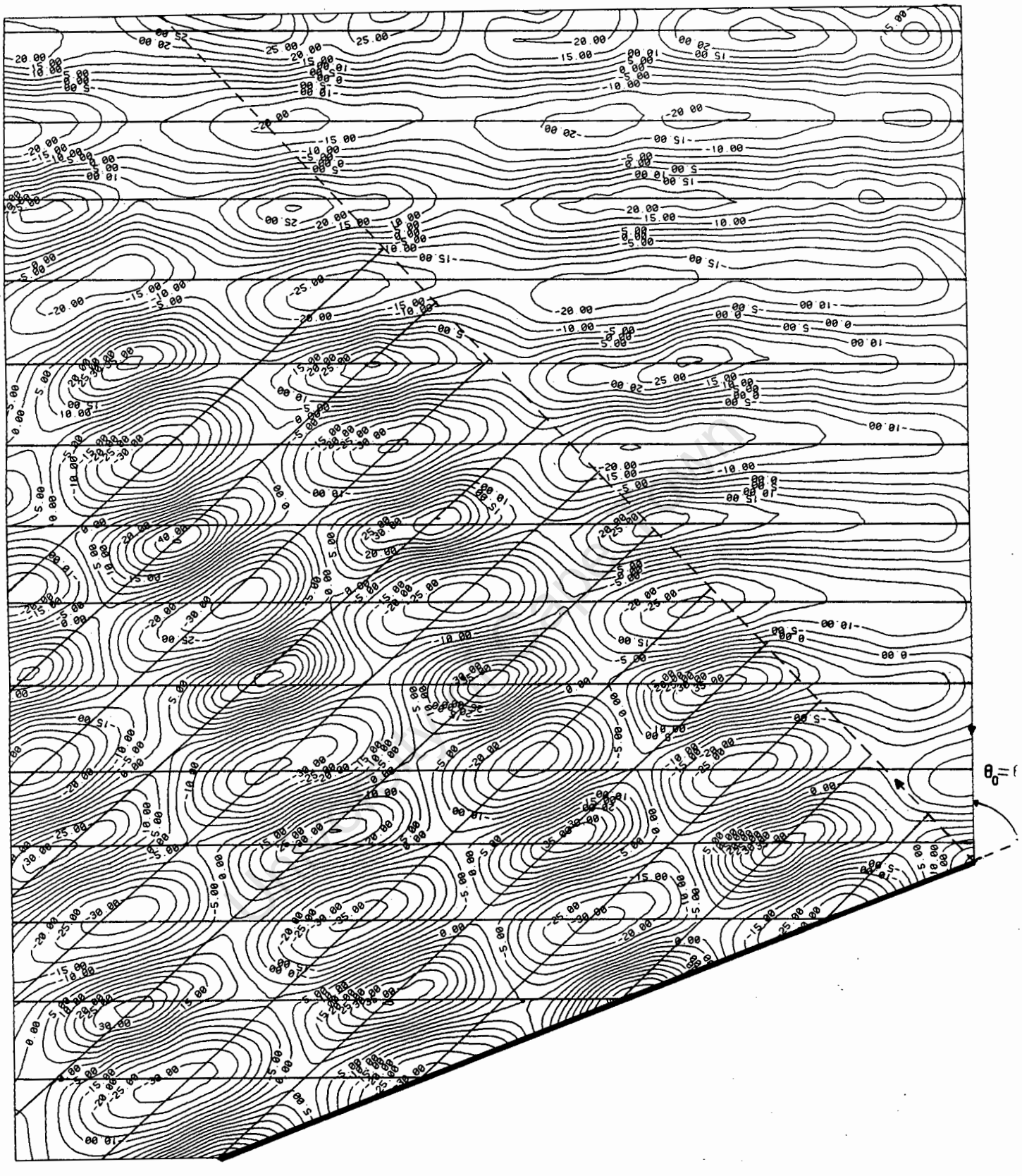

Scale 1 : 25

Stereopair 19, $\theta_o = 47^o$, Mach wave reflection, T = 0,765, H_i = 38,4mm

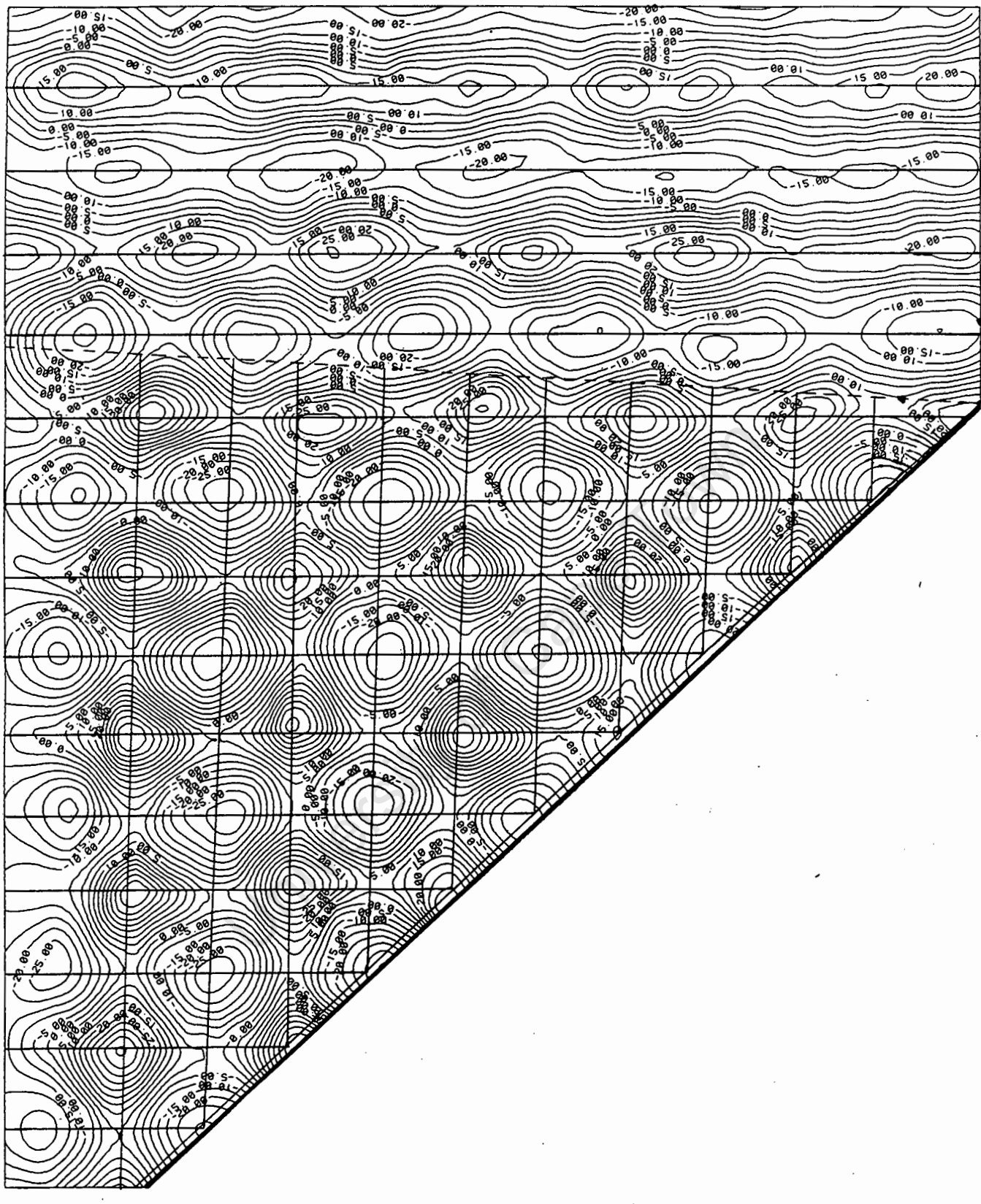

Scale 1 : 25

Stereopair 20, $\theta_o = 34^o$, Mach wave reflection, T = 0,765, H_i = 38,4mm

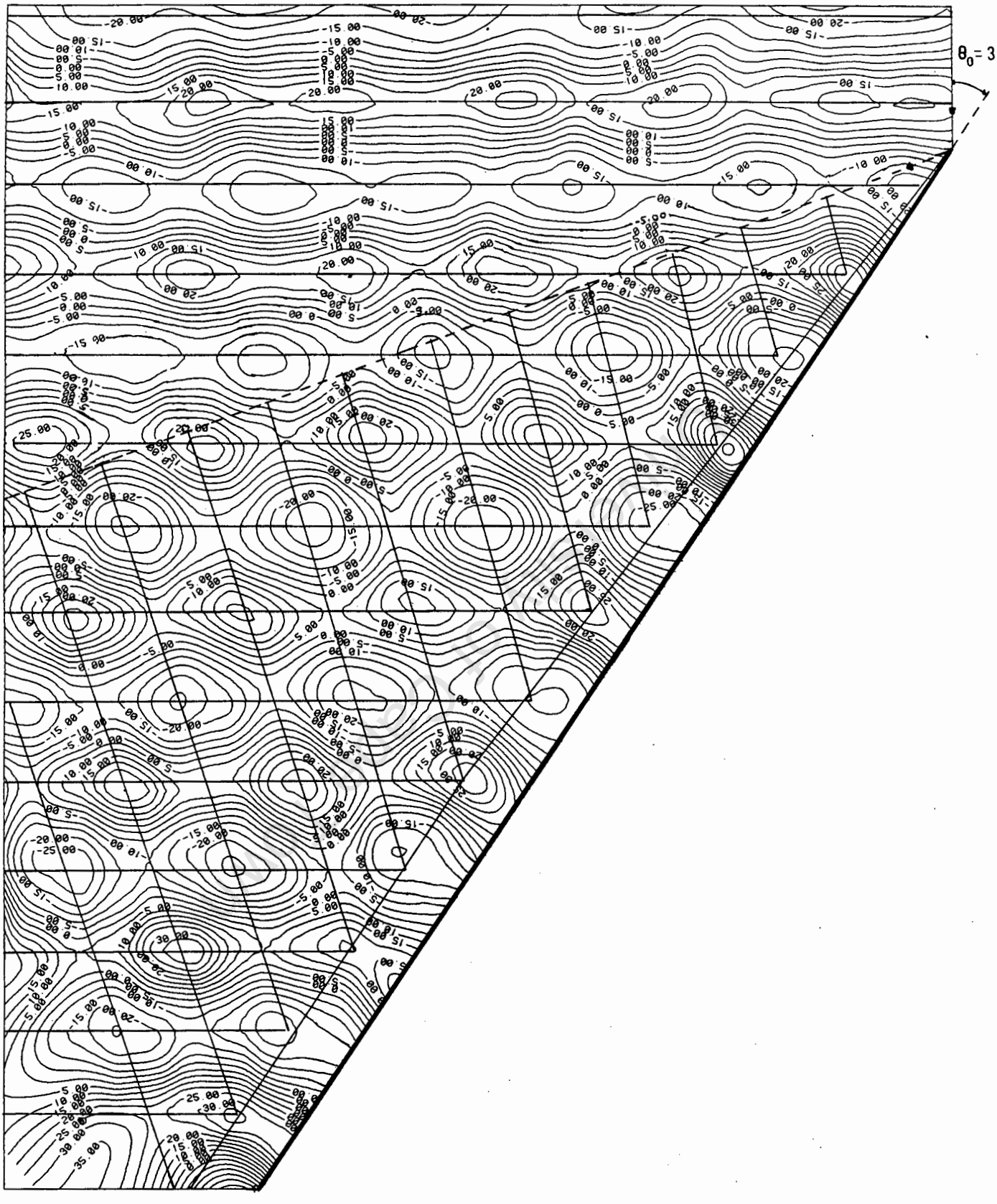

Scale 1 : 25

Stereopair 21, $\theta_o = 34^o$, Mach wave reflection, T = 0,765, H_i = 24,8mm

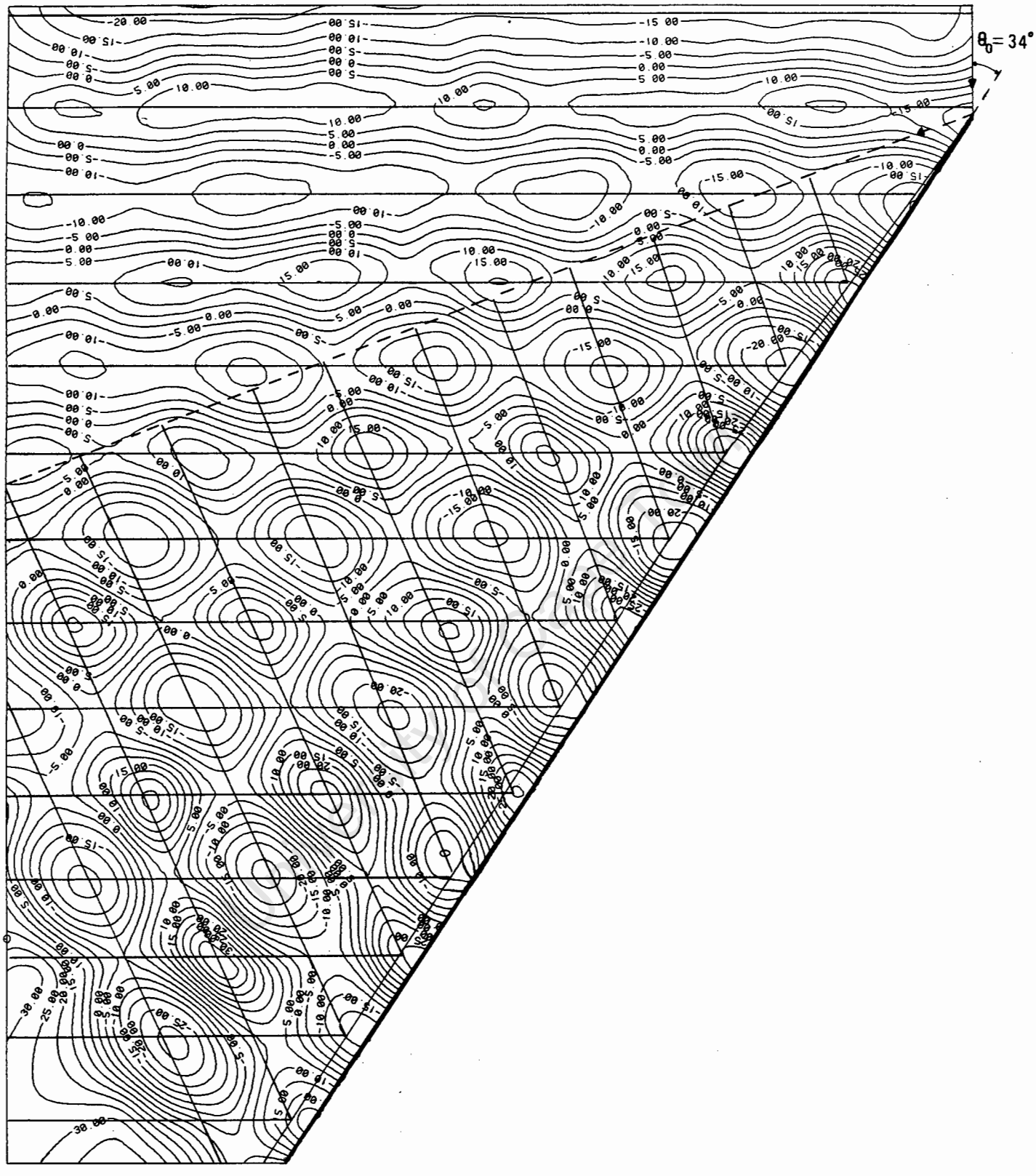

Scale 1 : 25

CONTOUR PLOT

Stereopair 22, $\theta_o = 34^o$, Mach wave reflection, T = 1,01, H_i = 32,7mm

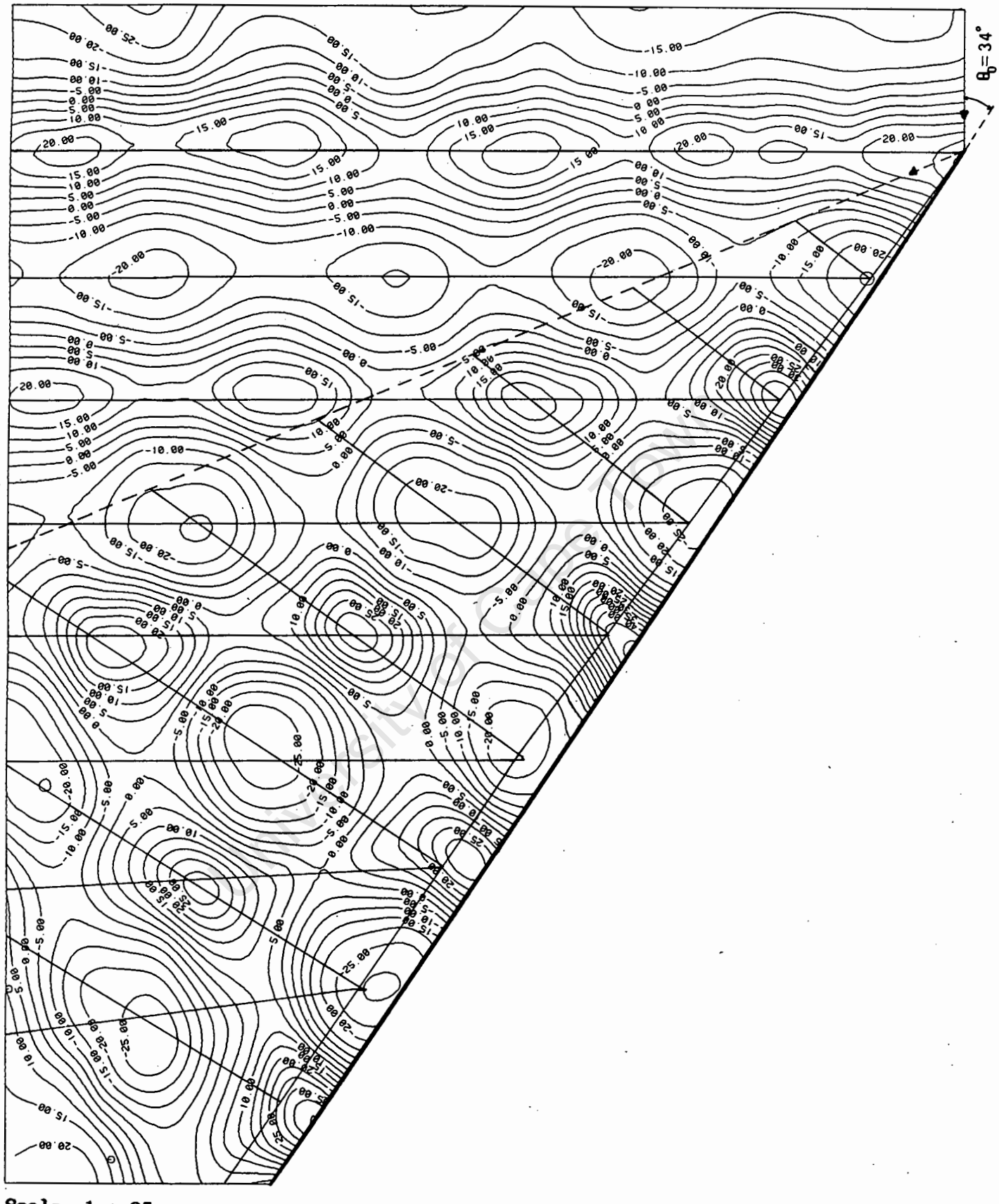

Scale 1 : 25

CONTOUR PLOT

Stereopair 23, $\theta_o = 34^o$, Mach wave reflection, T = 1,01, H_i = 34,0mm

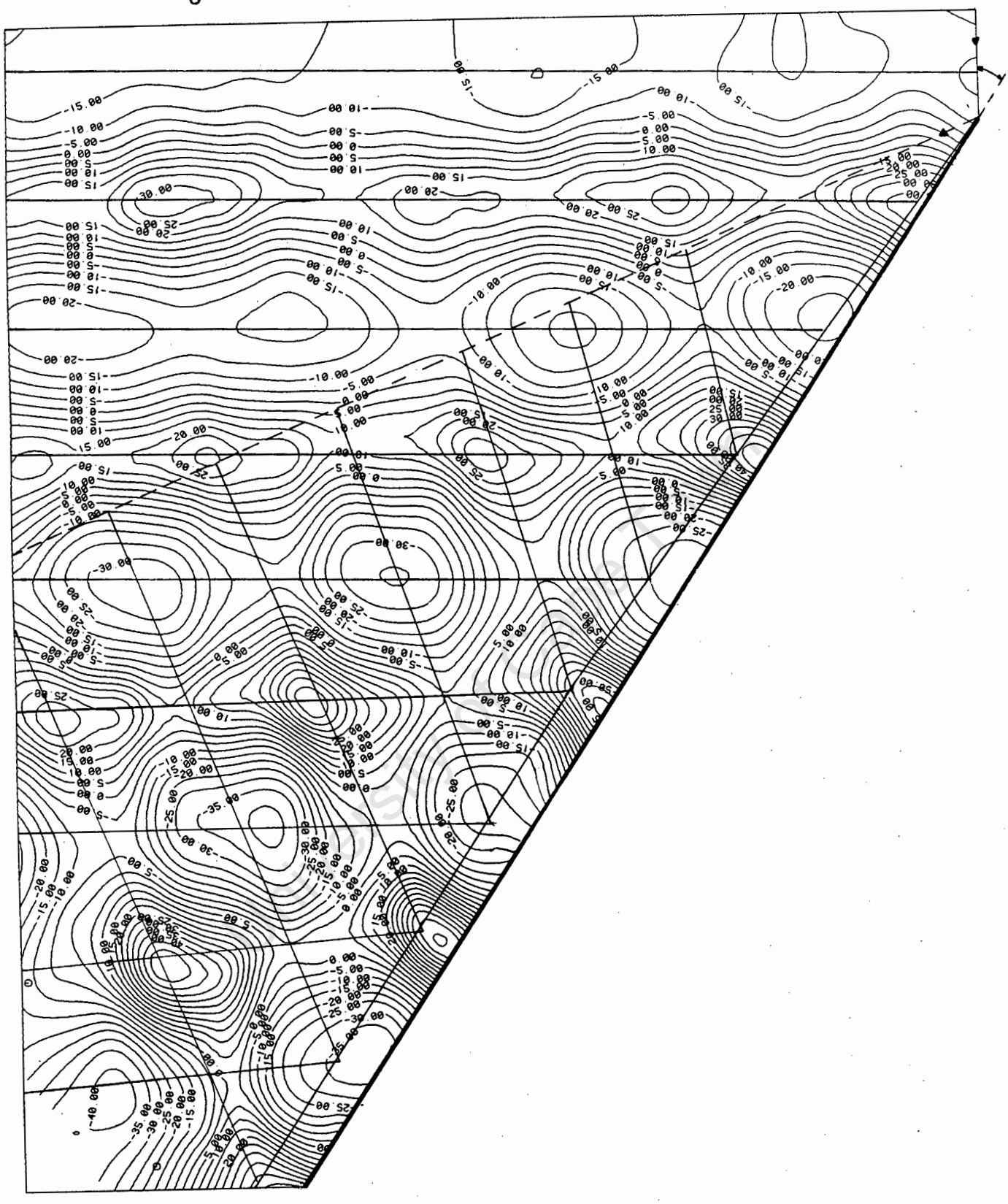

Scale 1 : 25

Stereopair 24, $\theta_o = 34^o$, Mach wave reflection, T = 1,01, H_i = 39,9mm

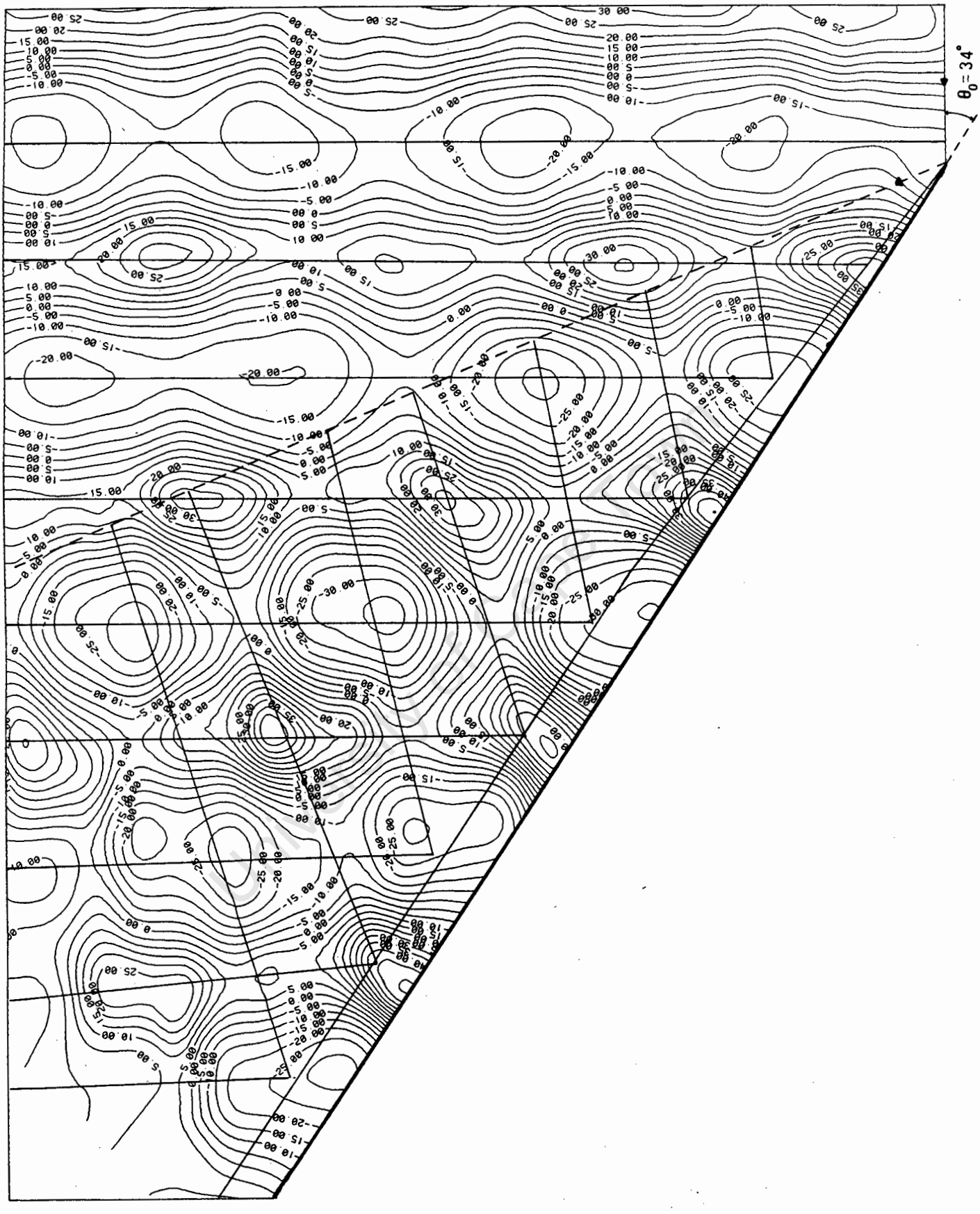

Scale 1 : 25

CONTOUR PLOT

Stereopair 25, $\theta_o = 25^o$, Mach wave reflection, T = 0,765, H_i = 24,8mm

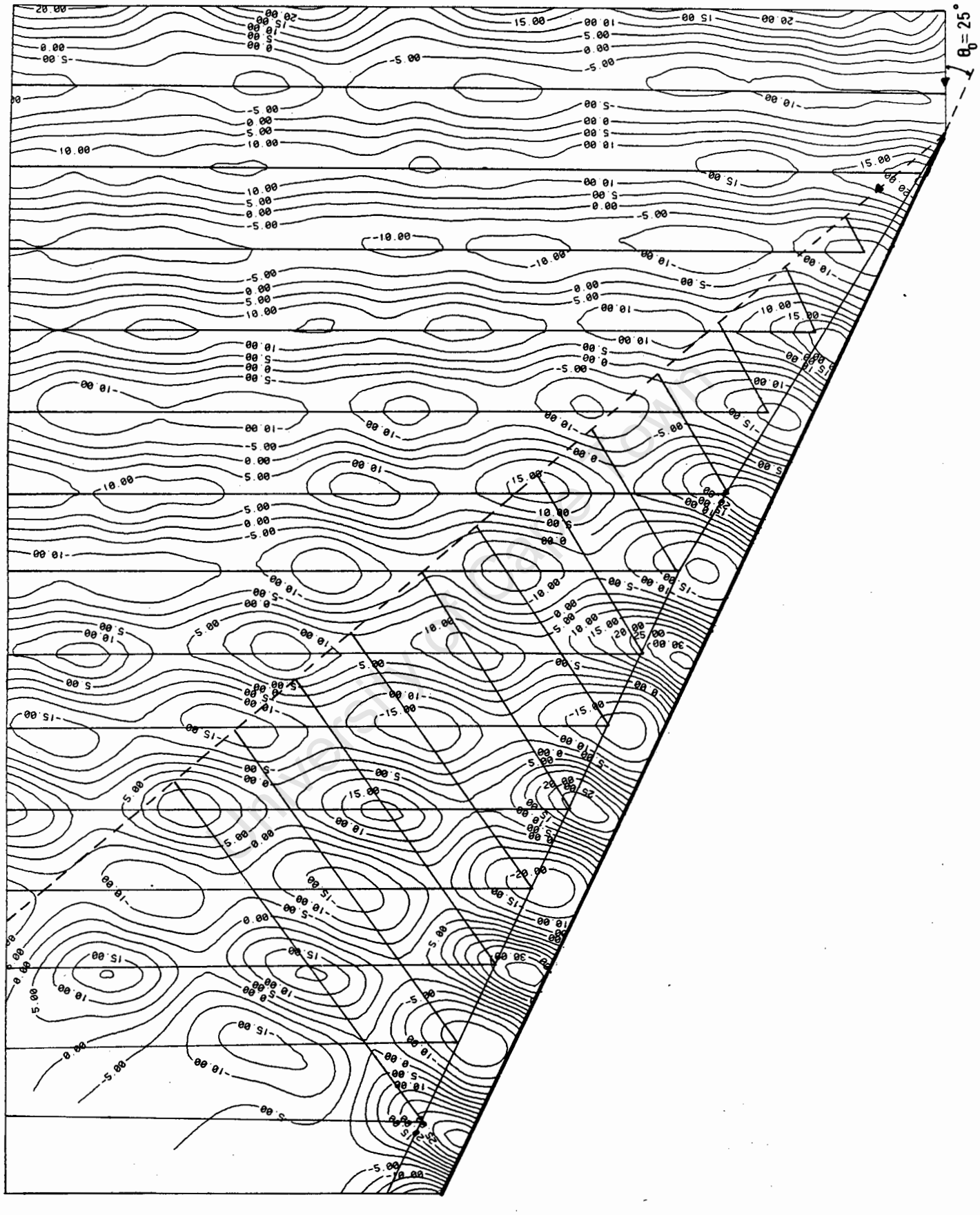

Scale 1 : 25

CONTOUR PLOT

Stereopair 26, $\theta_o = 20^o$, Mach wave reflection, T = 0,765, H_i = 24,8mm

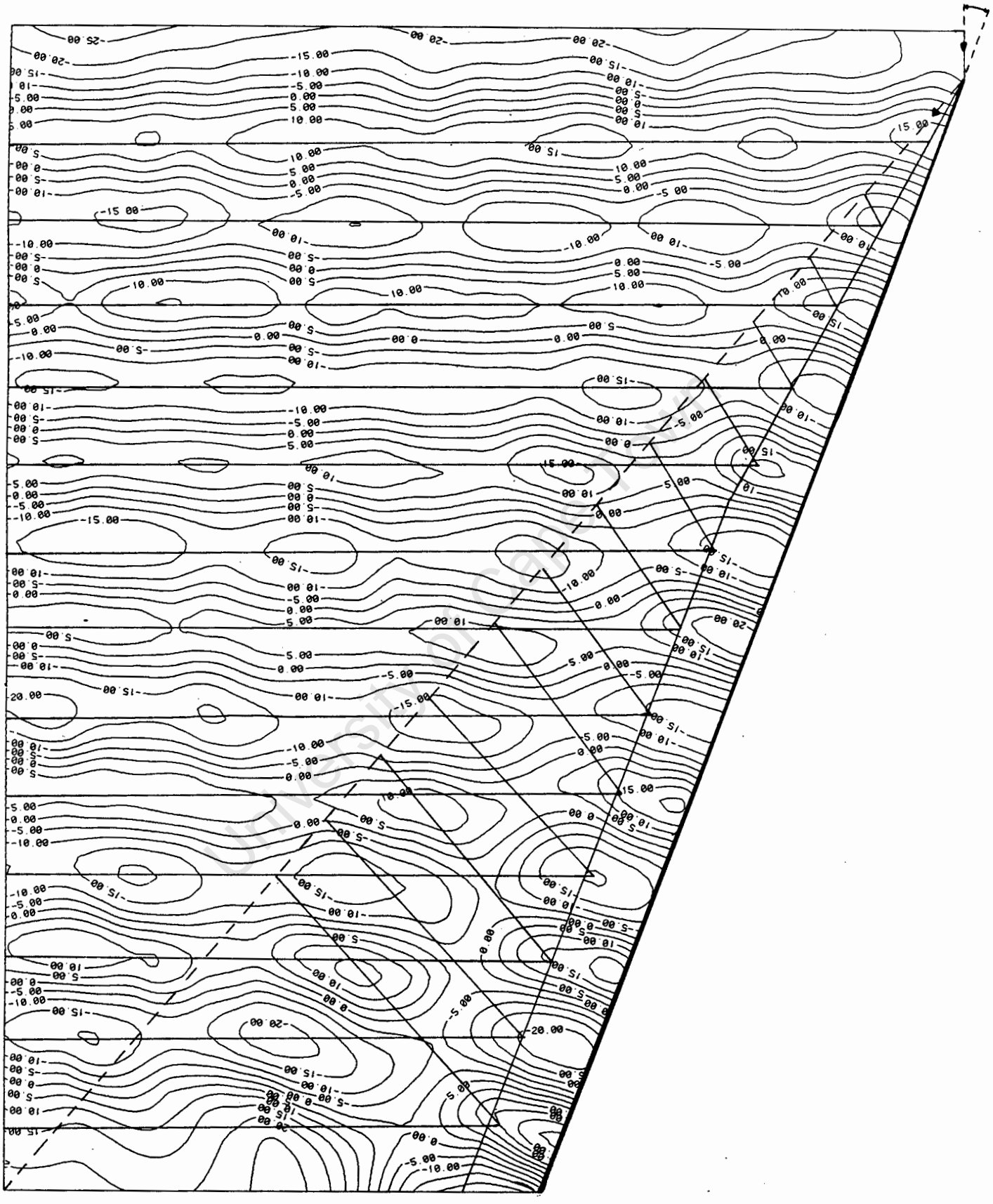

Scale 1 : 25

CONTOUR PLOT

Stereopair 27, $\theta_o = 11^o$, Mach wave reflection, T = 0,765, H_i = 24,8mm

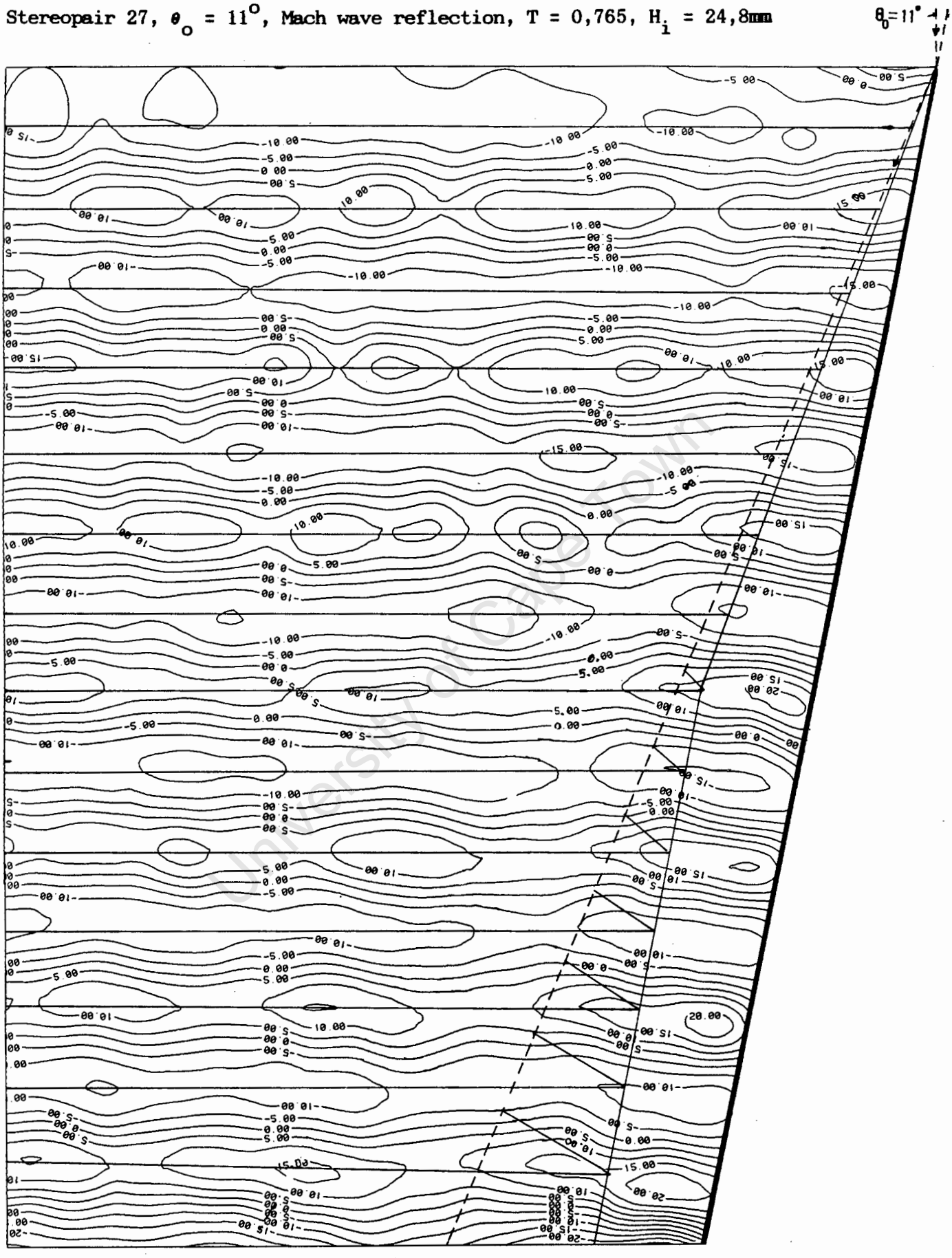

Scale 1 : 25

University of Cape Town

CONTOUR PLOT

Stereopair 28, Incident wave, T = 0,765, H_i = 24,8mm

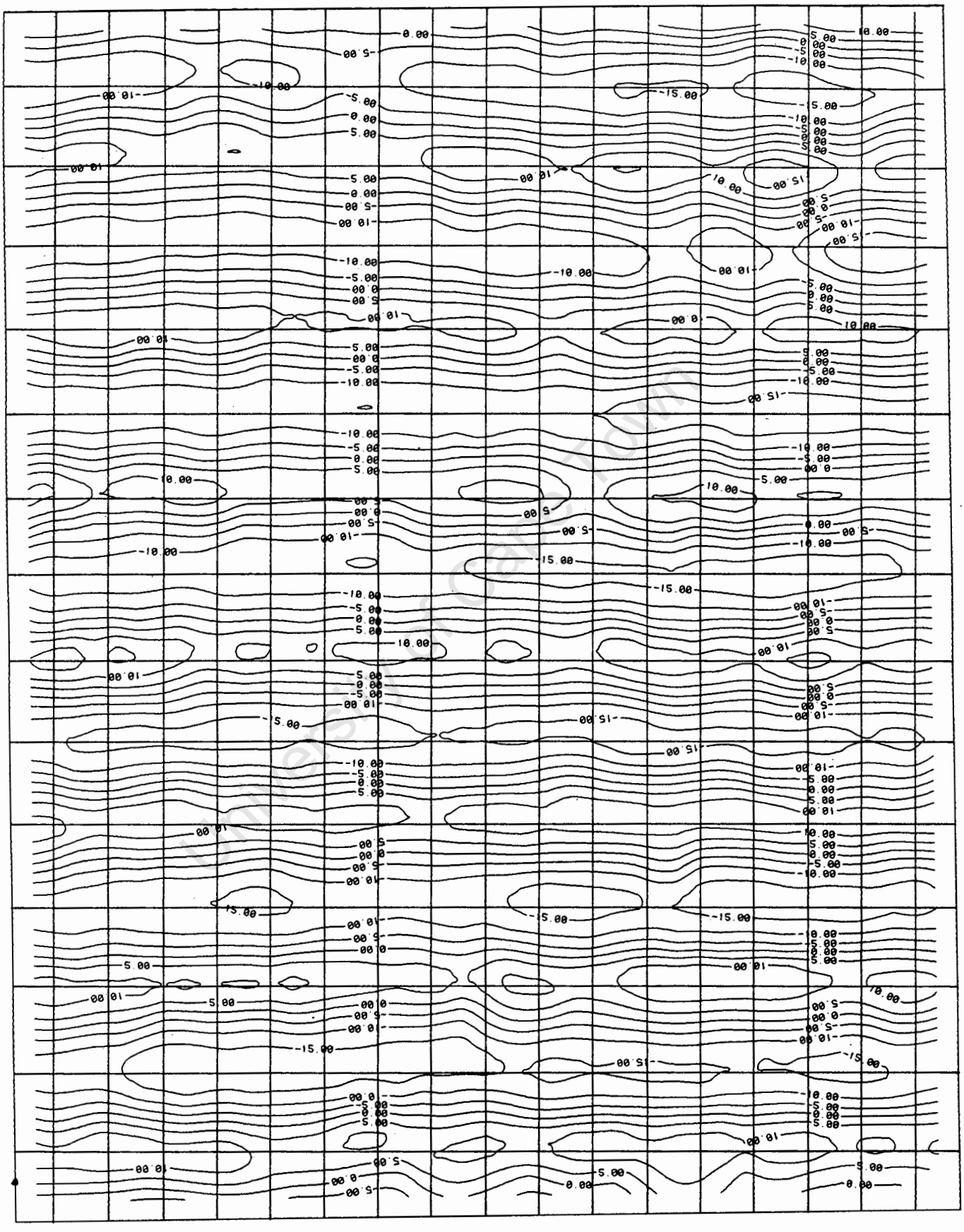

Scale 1 : 25

CONTOUR PLOT

Stereopair 29, Incident wave, T = 0,765, H_i = 38,4mm

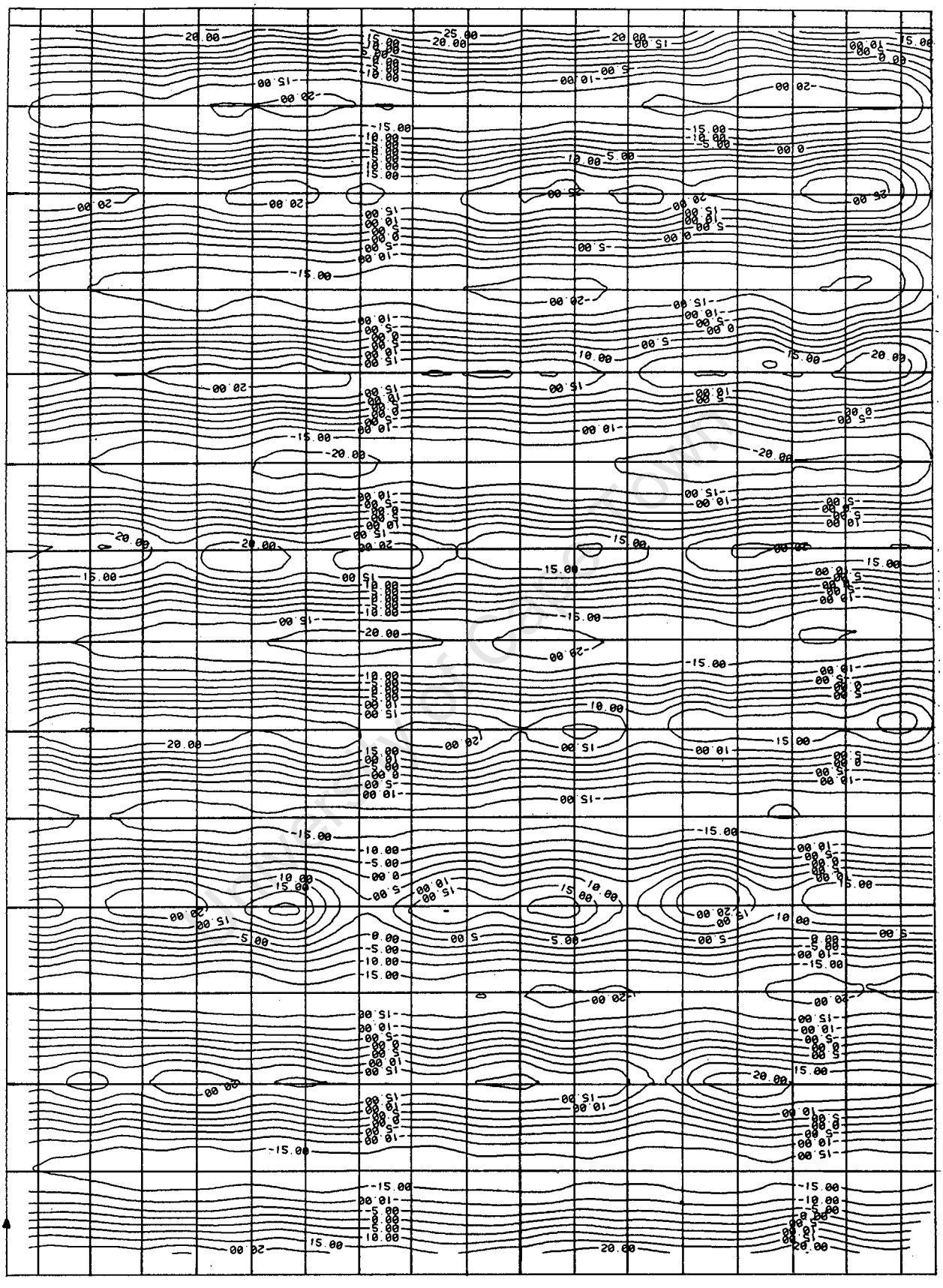

Scale 1 : 25

Stereopair 30, Incident wave, T = 1,01, H_i = 32,7mm

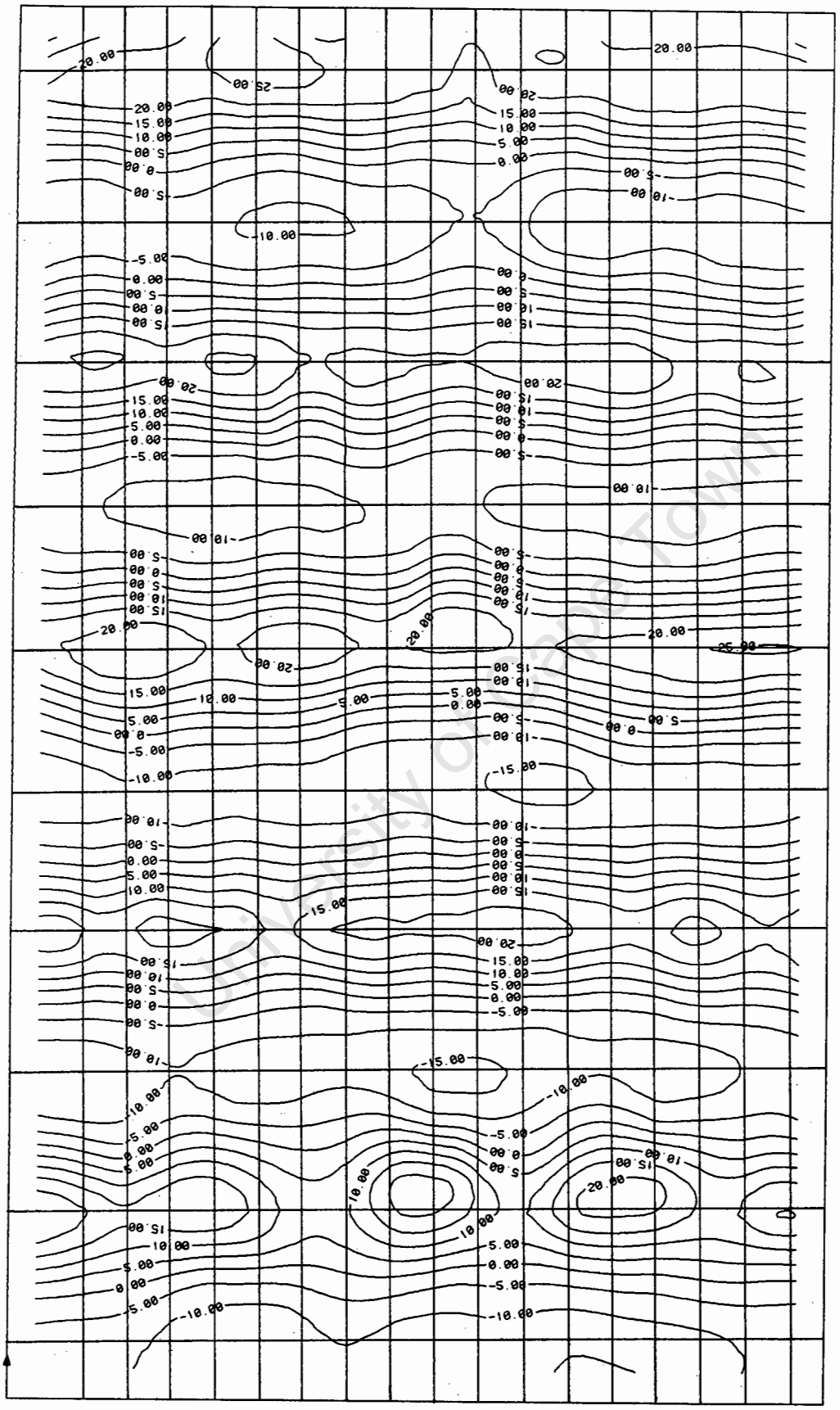

Scale 1 : 25

University of Cape Town

CONTOUR PLOT

Stereopair 31, Incident wave, T = 1,01, H_i = 34,0mm

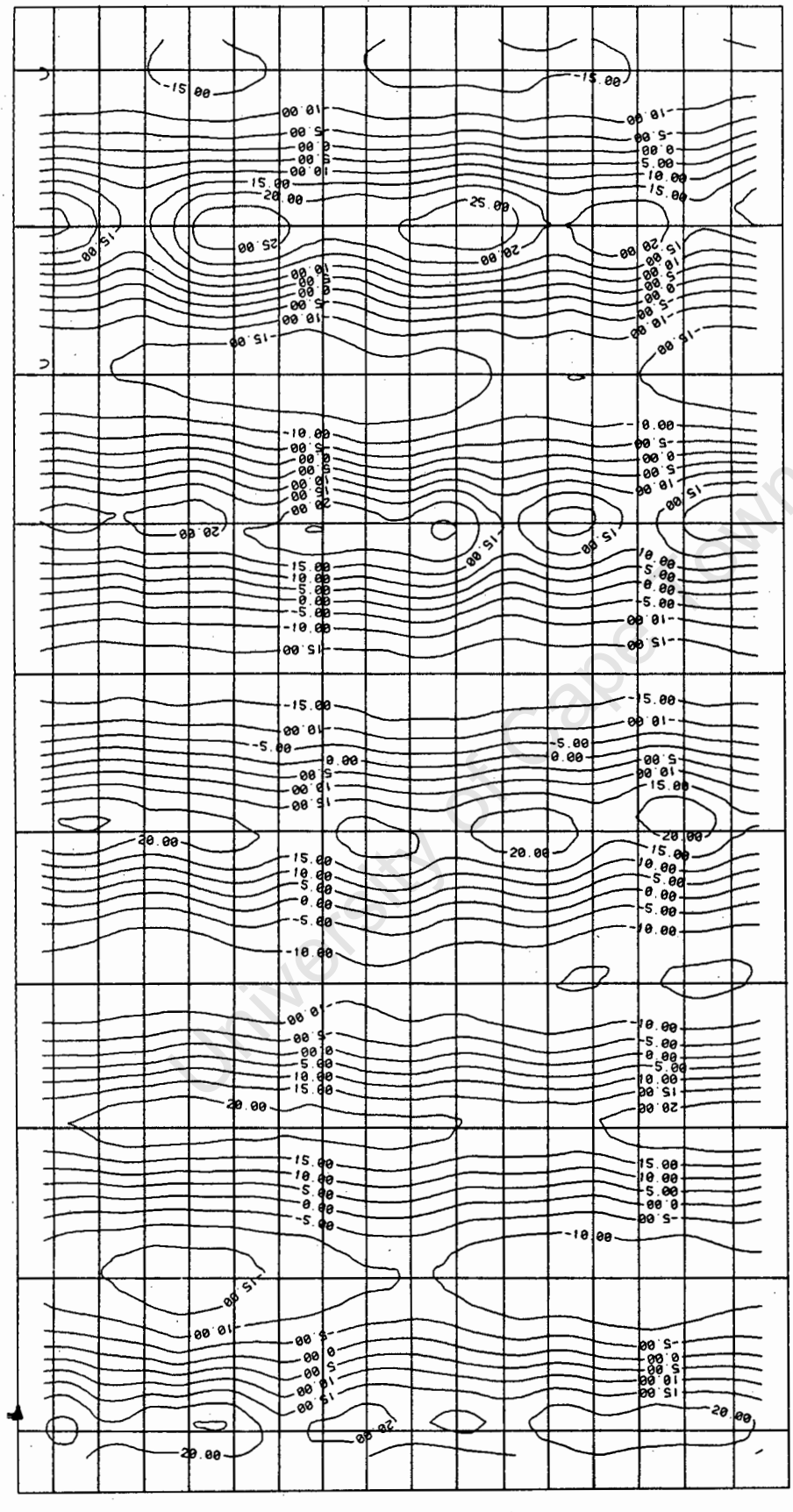

Scale 1 : 25

CONTOUR PLOT

Stereopair 32, Incident wave, T = 1,01, H_i = 39,9mm

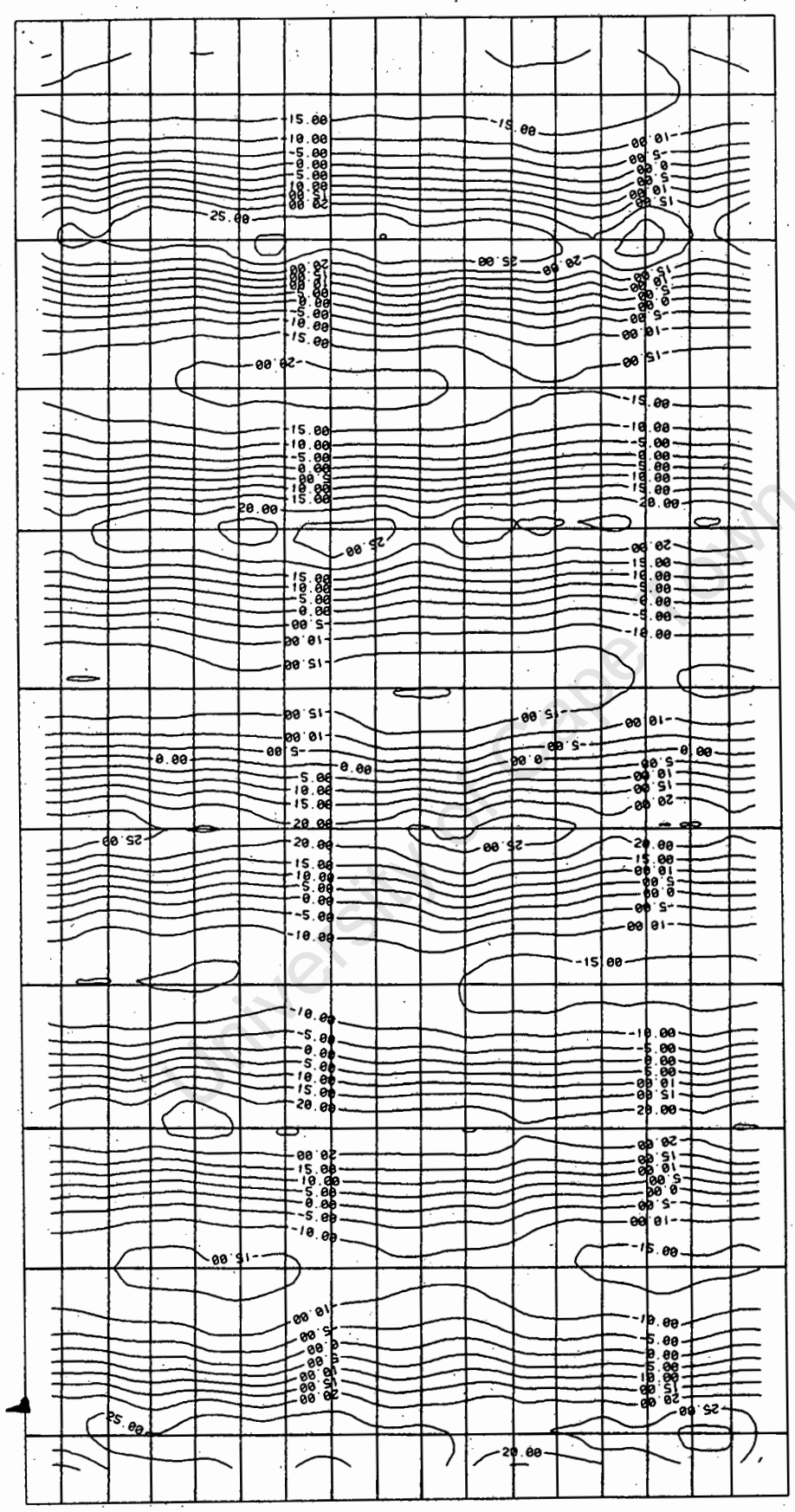

Scale 1 : 25

COEFFICIENT OF REFLECTION CONTOUR PLOT

Stereopair 18, $\theta_o = 69^o$, oblique wave reflection, T = 0.765, H_i = 38,4mm

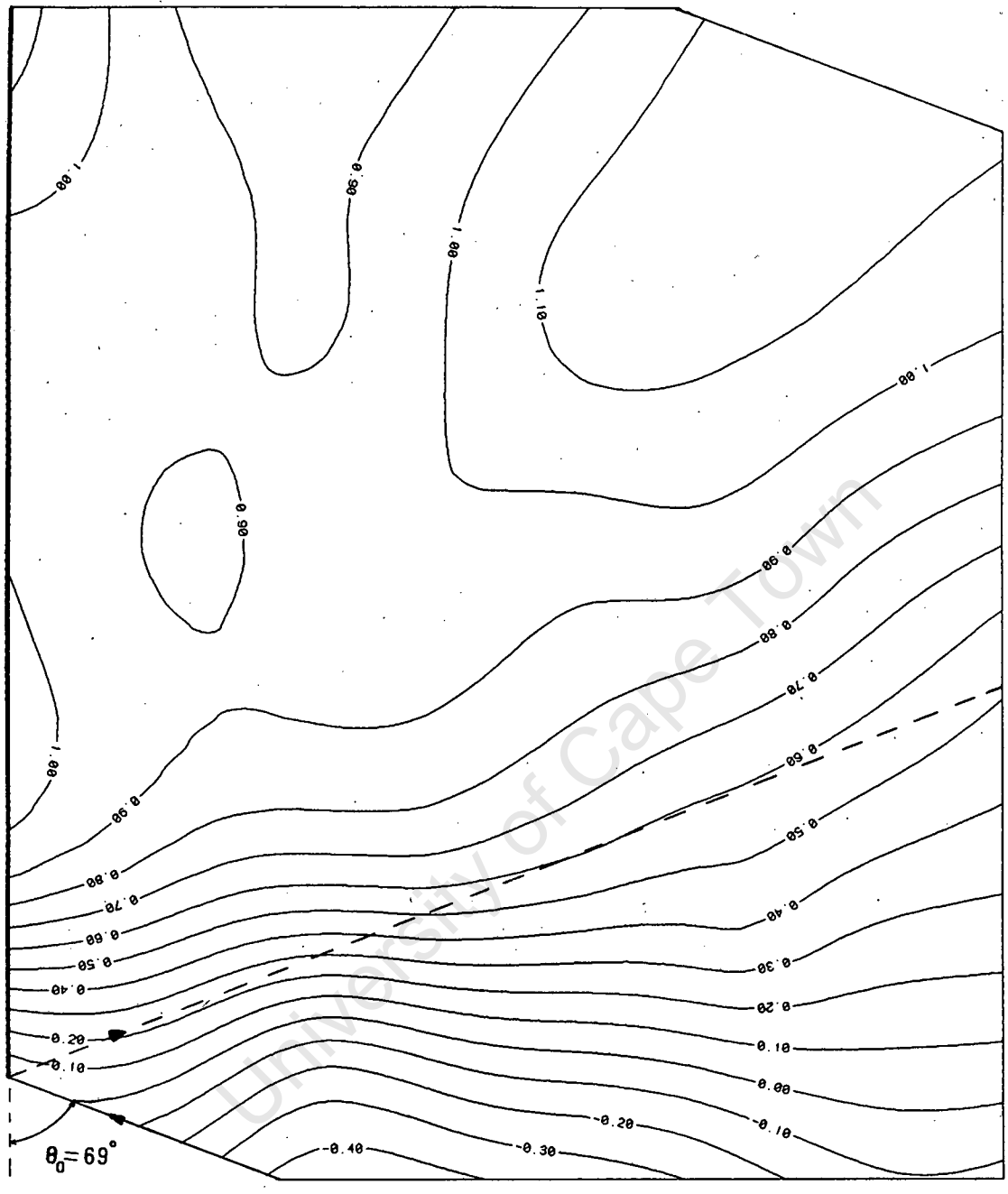

University of Cape Town

Scale 1 : 25

COEFFICIENT OF REFLECTION CONTOUR PLOT

Stereopair 19, $\theta_o = 47^o$, Mach wave reflection, T = 0,765, H_i = 38,4mm

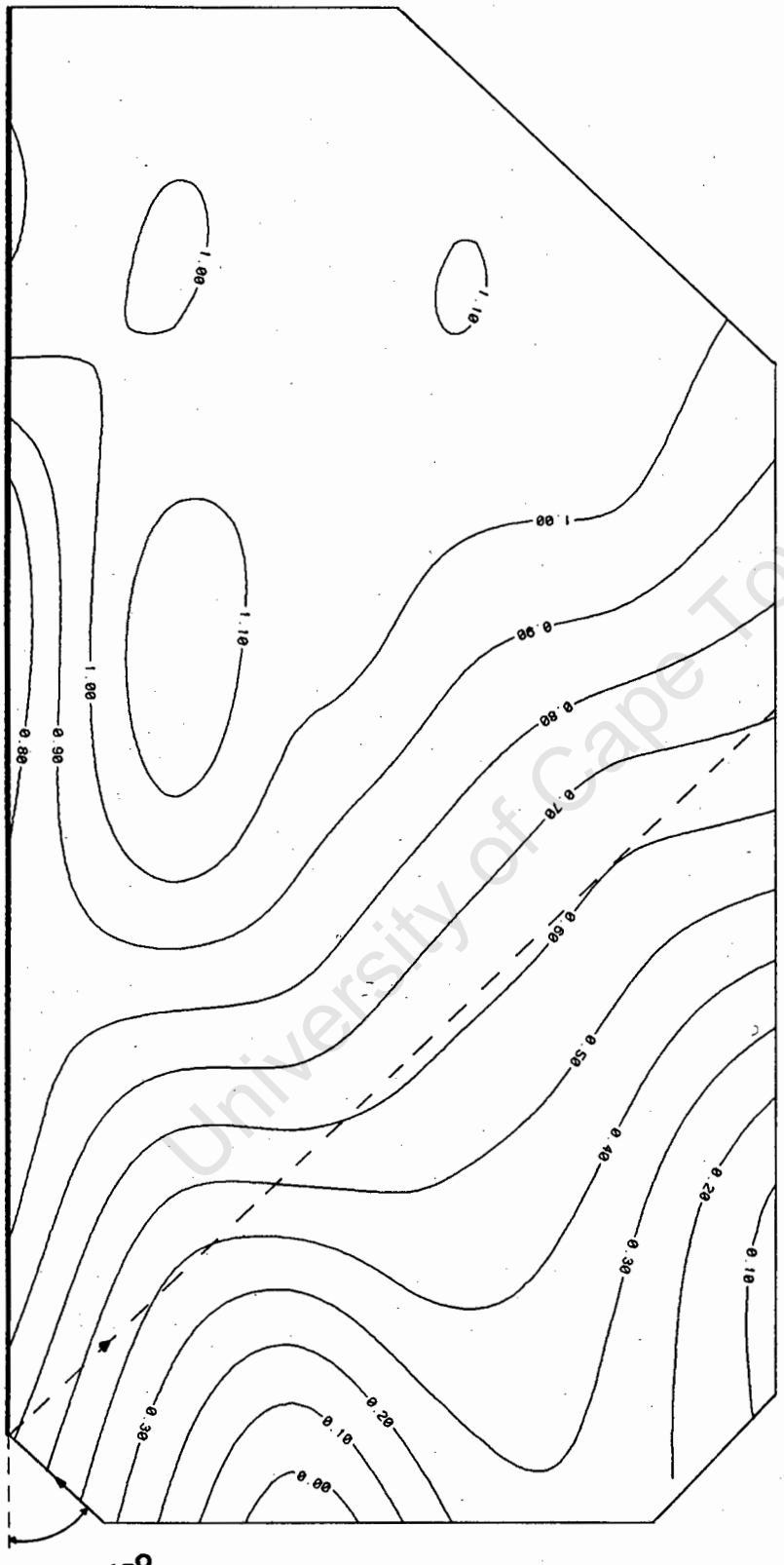

$\theta_o = 47^o$

Scale 1 : 25

University of Cape Town

Fig 7.5 Wave diffraction diagram - 75° wave angle (From Coastal Engineering Research Centre, 1984).

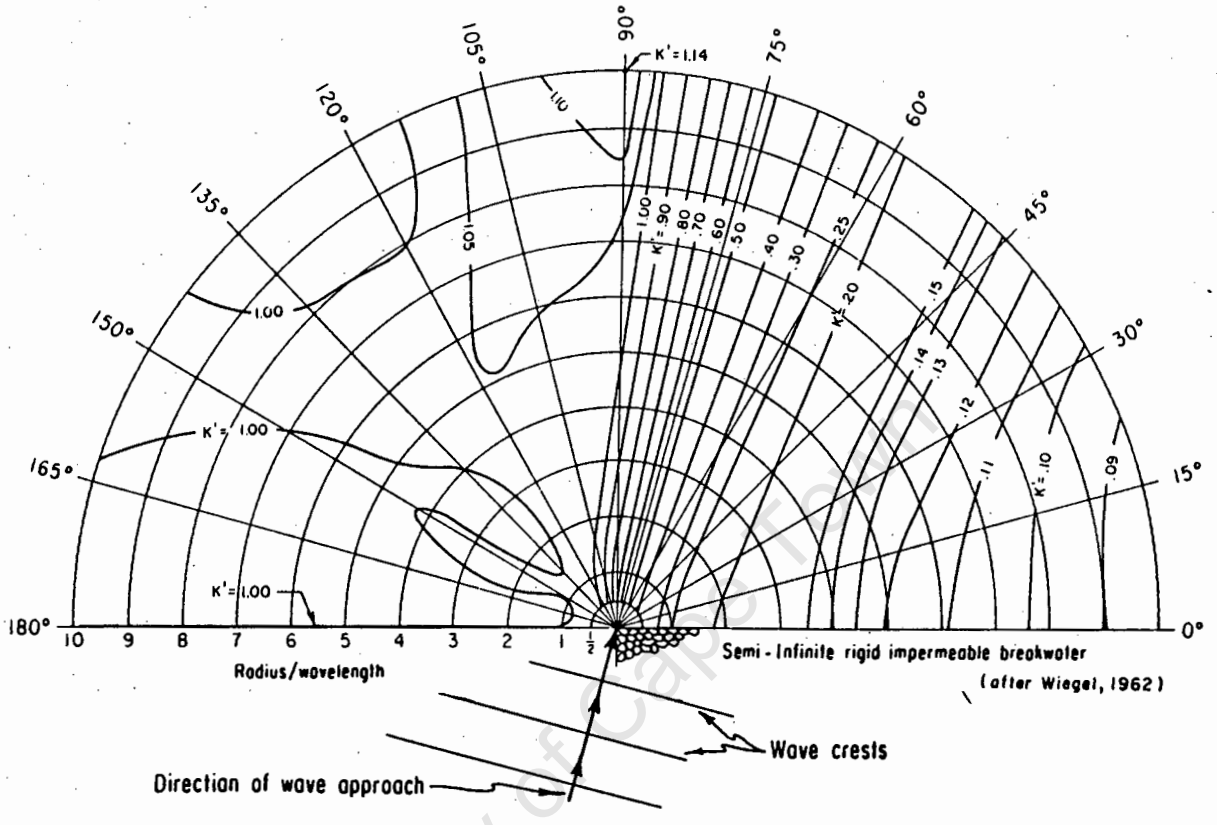

7.3.2 Degree of reflection

It would be realistic to assume that diffraction does occur for the edge of the reflected wave, so as both the diffraction diagrams suggest similar values along the wave orthogonal it would appear that the coefficient of reflection is ≈ 1, The K_r contour plot shows that for where diffraction effects do not occur, $K_r \approx 1$. The negative contour values in the K_r contour plot are attributed to the variation in the incident wave heights.

7.4 Mach wave reflection

Mach wave reflection was investigated for two wave periods T = 0,765 and T = 1,01. The majority of tests were done using T = 0,765 where the effect of change in incidence was investigated. Tests were

Fig 7.6 Contour plot of Mach wave reflection

Stereopair 20, $\theta_o = 34^o$, Mach wave reflection, T = 0,765, H_i = 38,4mm

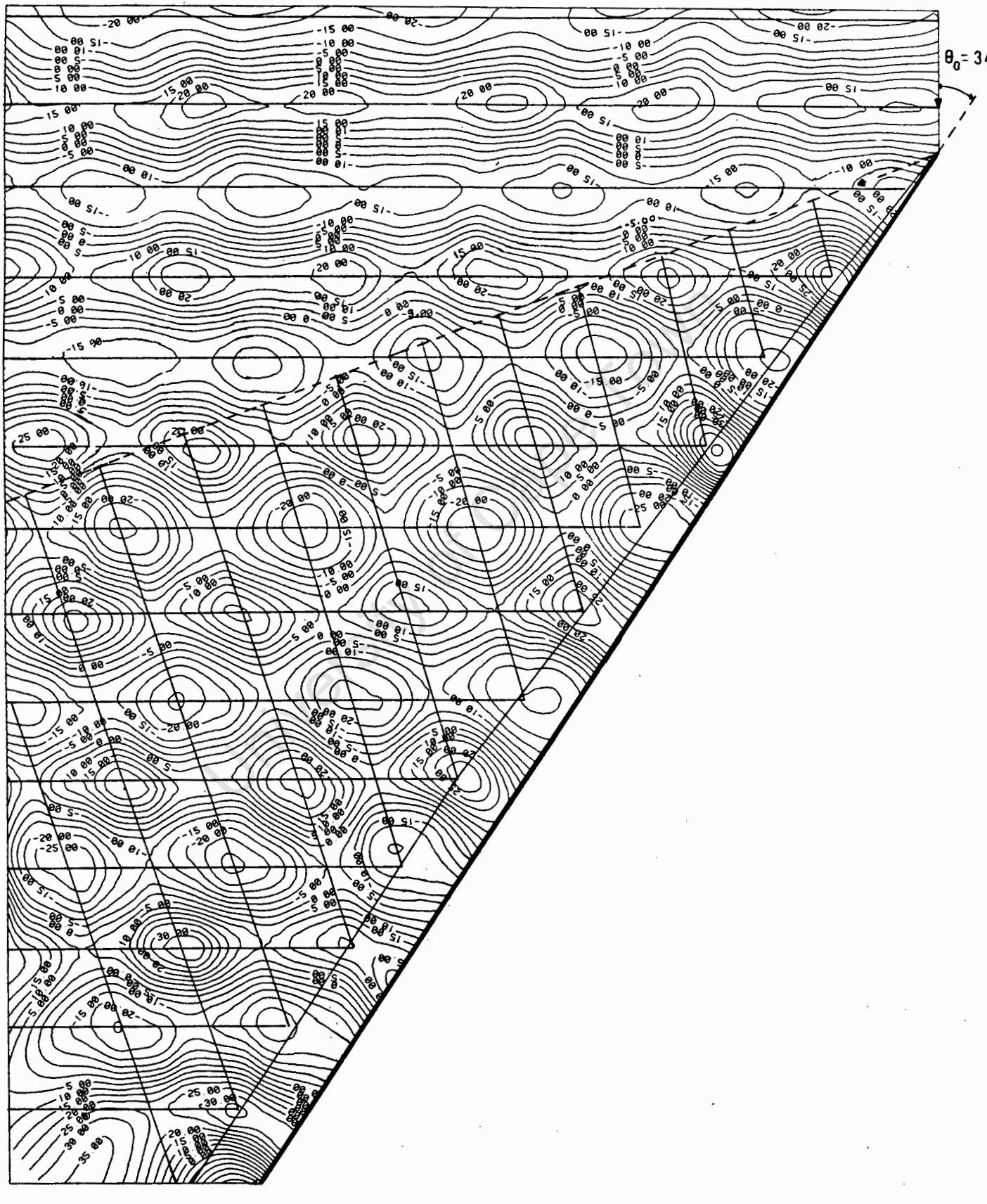

Scale 1 : 25

performed for T = 1,01 with $\theta_o = 34^o$, to investgate the effect of the incident wave height on Mach reflection.

The Mach stem width appears to grow linearly from the start of the wall (see Fig. 7.6), which is consistent with the observations of previous investigators. The angle the Mach stem grows at is α. The Mach stem width is made dimensionless by dividing by the incident wave length. On this basis comparisons could be made between different wave periods.

From the data available it appears that the starting angle for identifiable Mach wave reflection is $\theta_o = 47^o$ (Stereopair 19). In Fig 7.6 it can be seen that the effect of the Mach wave is that the normal oblique reflection pattern starts a finite distance away from the wall. This distance, as defined in Section 7.4.1, is the width of the Mach stem (B). For the section of linear growth of the Mach wave, the incident wave is reflected as if an imaginary reflecting wall was positioned at $(\theta_o + \alpha)^o$. Once the Mach stem has achieved maturity the incident wave reflects from an imaginary wall, parallel to the actual wall, but positioned B away from the actual wall. The incident and reflected wavelengths are similar, and the Mach waves have a wavelength of $L_i/\cos\theta_o$. The angles of incidence and reflection are similar, about the corresponding imaginary walls.

University of Cape Town

7.4.1 Definition of the Mach wave

The Mach stem width (B) has been previously defined by Berger and Kohlhase (1976) as the distance from the reflecting wall to the trough adjacent to the Mach wave (see Section 4.4). From the contour plots of the Mach waves (see fig 7.6) obtained, it was realised that the Mach stem width needed to be redefined. In fig 7.6 the incident and reflected waves have been identified with best fit lines placed through the relevant antinodes. The initial intersection of the incident and reflected lines occurs either at a crest or a trough, and would normally represent the antinode adjacent to the reflecting

wall, intersecting on the boundary of the wall for conventional oblique reflection. It is proposed that the Mach stem width be defined as the distance from the wall to the intersection representing the final antinode before the wall. It is according to this definition that the Mach stem width will be compared in this investigation.

7.4.2 Relationships investigated for Mach wave reflection

There appear to be three factors which affect the resulting Mach wave. The factors identified are

i) angle of incidence

ii) period of the incident wave, or its wavelength

iii) incident wave height.

7.4.2.1 Effect of angle of incidence

To investigate the effects of the angle of incidence, only one set of data is available, stereopairs 21, 25, 26, 27. For these stereopairs the wave period was constant (T = 0,765) and the incident wave height was also kept constant (H_i = 24,8 mm). The data for these stereopairs is presented in table 7.5.

Table 7.5 Data for T = 0,765; H_i = 24,8mm

Stereopair	θ_o	Tan θ_o	α	B	Maximum H_s/H_i
21	34^o	0,675	3^o	0,13 L_i	2,581
25	25^o	0,466	6^o	0,308 L_i	2,419
26	20^o	0,364	$8,5^o$	0,422 L_i	1,774
27	10^o	0,176	$9,5^o$	0,649 L_i	1,472

The only trend that definitely appeared to exist for the data is the linear relationship between the angle of incidence and the Mach stem width. This relationship is described in fig. 7.7, and the line fitted to the data by linear regression obtained a correlation

University of Cape Town

coefficient of -0,999. This function is empirical as the effects occurring due to the incident waveheight and period are unknown. The possibility of the angle of incidence being a tan relationship was investigated, but it does not fit the available data better than the linear relationship. It is possible however that a tan θ_o relationship could be applicable.

Fig 7.7 Mach stem width

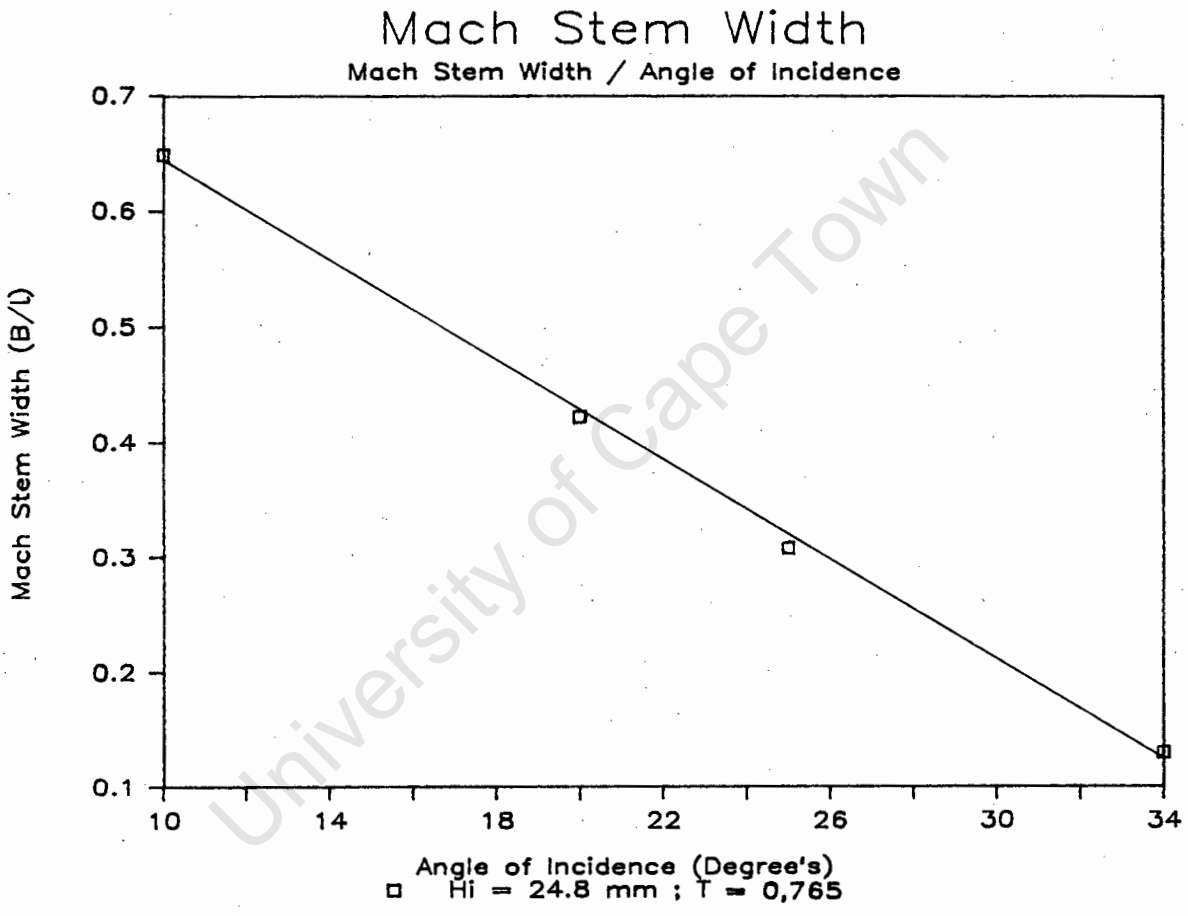

University of Cape Town

The Mach stem grows linearly from the start of the reflecting wall with angle α. The relationship between θ_o and α can be seen in fig 7.8. It appears that a linear relationship could exist for this data, as the line fitted through the data produced a correlation coefficient of -0,961. The stem angle was also plotted against

tan θ_o and a similar coefficient of reflection was obtained as tan is almost linear in this range. More data is required before a decision can be made as to what the exact relationship is.

Fig 7.8 Growth of Mach stem

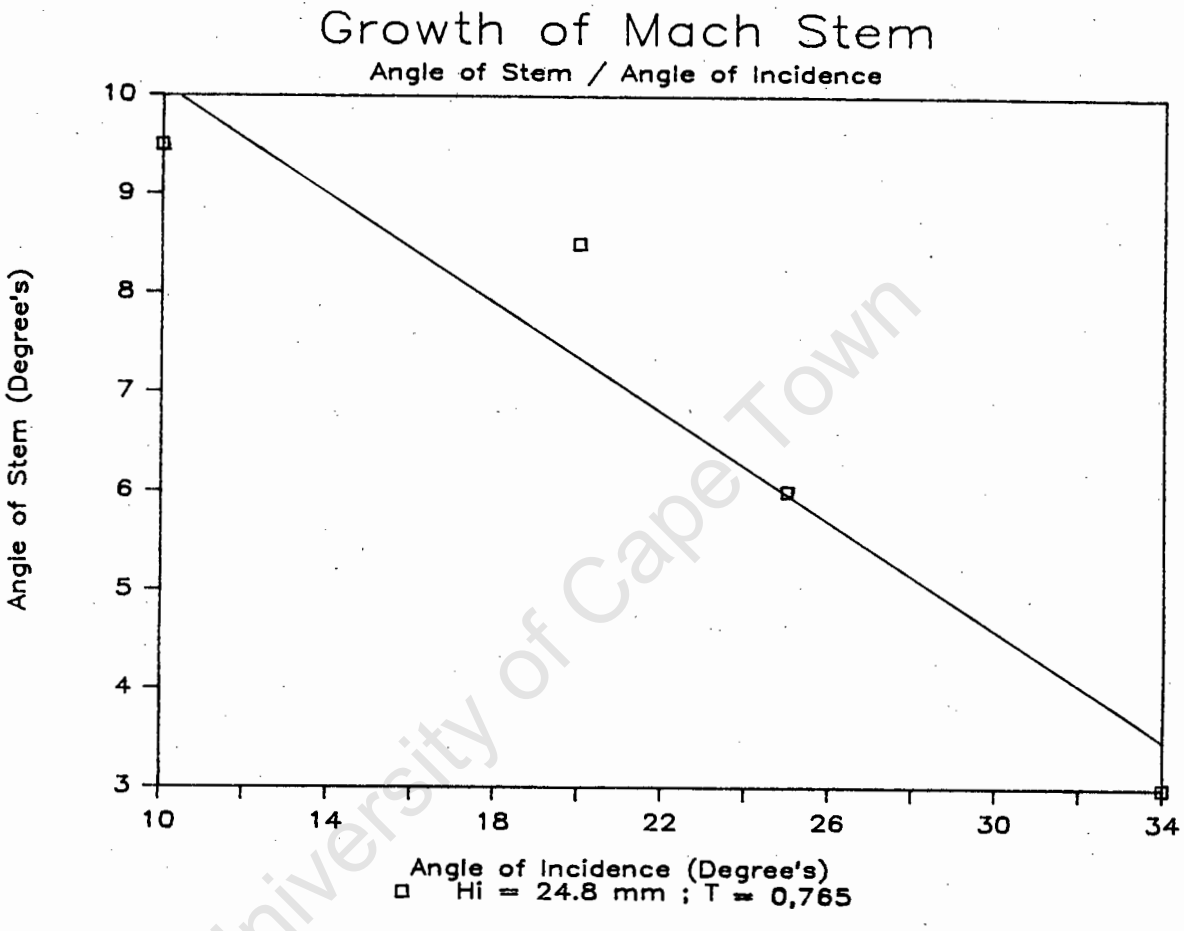

University of Cape Town

Wiegel (1964b) presents data for the α/θ_o relationship for solitary waves for an average of wave heights H_i/d = 0,05 to 0,43. Wiegel obtained a linear relationship for α/θ_o with a gradient that was almost identical to the gradient obtained in this investigation, except that the α intercept was 2^o below the α intercept for this investigation. Wiegel used solitary waves for his investigation and it would appear that Wiegel used the same definition for the edge of the Mach wave as is used in this investigation. The discrepancy in the size of α could be due to the solitary waves, as Wiegel did

observe that solitary waves produce a smaller stem width than periodic waves.

There is a relationship between the maximum H_{ms}/H_i ratio that occurs and its respective angle of incidence. Fig 7.9 shows the increase in H_{ms}/H_i for increasing θ_o, Although the coefficients of reflection for $\theta_o = 10^o$, 20^o may not have reached their maximum values as the length of the reflecting wall may have been too short for the waves to reach maturity. The relationship for this data is not well defined. A linear relationship, which although it fits the available data well, does not predict the probable decrease in the H_{ms}/H_i ratio for increasing angles of incidence as shown by data for different incident waveheights.

Perhaps this tends to 2,6 as for $\theta \to 90°$ as we have previously shown.

Fig. 7.9 Relative height of Mach stem.

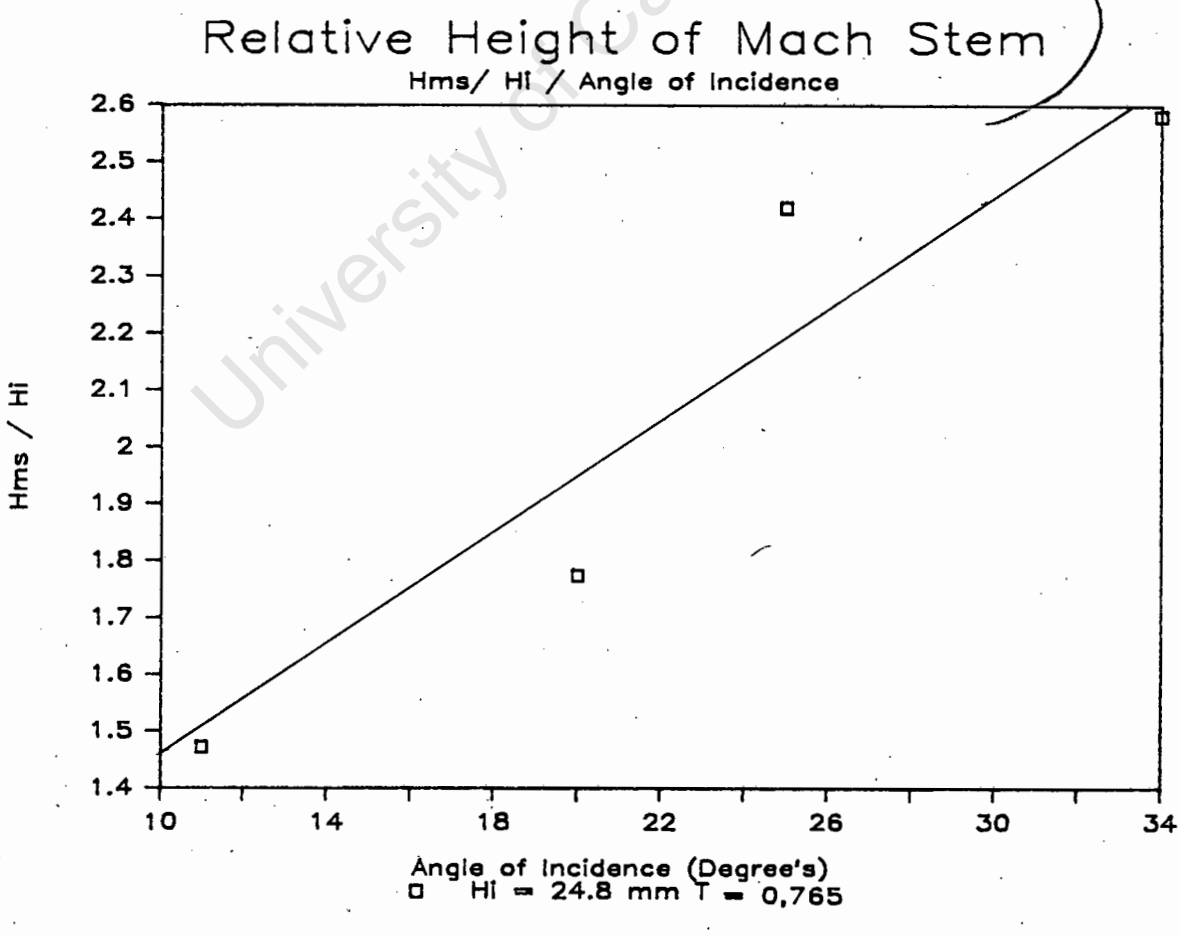

University of Cape Town

7.4.2.2 Effect of varing incident wave height and changes in period

The Mach stem width is affected by the incident wave height, as for as increasing incident wave height the Mach stem becomes wider. An attempt was made to try to establish the relationship between the Mach stem width and the incident wave height for T = 0,765 and T = 1,01 for constant angle of incidence, $\theta_o = 34^o$. The data is summarised in Table 7.6

Table 7.6 Data for $\theta_o = 34^o$

Stereopair	T	H_i	H_i/L	H_s/H_i	B	Comment
20	0,765	38,2	0,050	2,044	$0,325L_i$	Mach wave breaking
21	0,765	24,8	0,032	2,581	$0,130L_i$	
22	1,01	32,7	0,029	2,339	$0,156L_i$	
23	1,01	34,0	0,030	2,882	$0,178L_i$	Mach wave on verge of breaking
24	1,01	39,9	0,036	2,105	$0,183L_i$	Mach wave breaking

The above data is plotted in fig. 7.10, and there does not appear to be any definite relationship. It would appear that the amount of energy available from the incident wave determines the Mach stem width. The effect of the Mach wave breaking on the Mach stem width does not appear to be related for different periods. When the wave starts to break for T = 1,01 there is not a significant increase in the Mach stem width for increase in incident wave height. The opposite relationship exists for T = 0,765. A lot more data is required to define this effect. However for both cases of the Mach stem breaking the incident wave heights are similar (≈ 39 mm) and the H_s/H_i values are similar. This suggests that the wave heights are unstable because of the shallow water relationship. For T = 1,01 the Mach stem would break for a smaller H_i/L ratio than for T = 0,765. If the growth of the Mach stem width is dependent on the incident energy, then when the wave starts to break, any increase in incident

University of Cape Town

energy is dissipated in breaking, so the Mach stem grows very little once breaking starts. In this way the size of the Mach stem for T = 0,765 could have grown somewhat bigger before breaking started than for T = 1,01 before it started to break. This is a possible explanation for the discrepancy in the Mach stem width data.

Fig. 7.10 Mach stem width

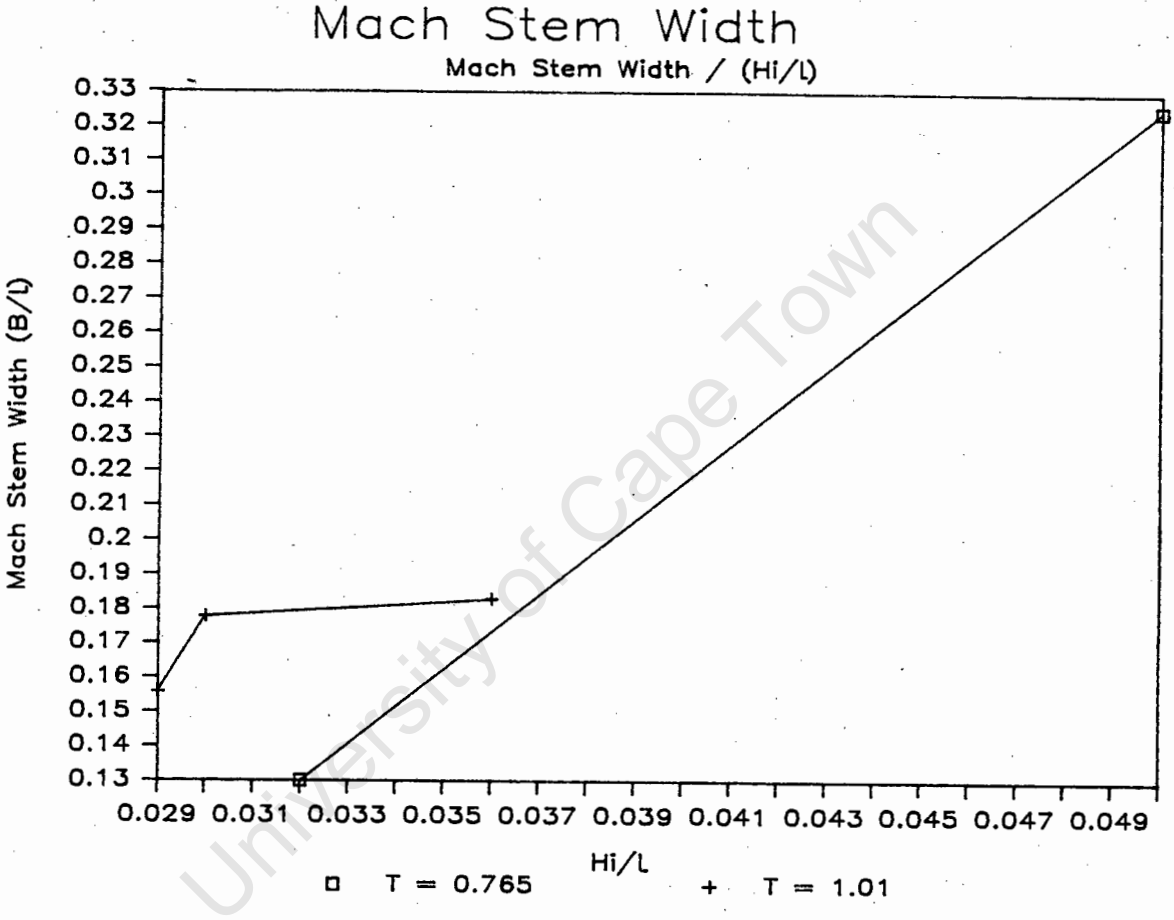

University of Cape Town

7.4.2.3 Coefficient of reflection plots

To investigate any noticeable effects in the reflected wave, coefficient of reflection (K_r) plots were generated (See Appendix B). In the K_r plots the relative height of the Mach wave is also described by K_r values rather than H_{ms}/H_i, so the wave heights can be compared, and contours plotted for the data.

For stereopairs 19,21 where T = 0,765, θ_o = 47, 34° and H_i = 34 mm; 24,8 mm respectively, the Mach stem reaches a peak and then drops off to a trough with an increase in the K_r values next to the trough in the Mach stem. The peak in the Mach stem heights corresponds in both scenarios to the Mach stem reaching its maximum width (B).

7.4.3 Trends in Mach wave development

7.4.3.1 Limiting angle for the mach wave

Previous investigations (Berger, Kohlhase, 1976) suggest that Mach reflection occurs for θ_o less than 45°. In stereopair 19, where T = 0,765 and H_i = 38,4mm, the Mach wave first occurs for θ_o = 47° which is outside the previously established limit. The identification of the Mach wave was only made possible by the technique described in section 7.3, as this wave pattern could very easily be considered to be ordinary oblique reflection by casual inspection. The occurrence of the Mach wave for θ_o = 47° suggests that there does not exist a finite point where the Mach wave does not exist, but that as θ_o tends to 90° the Mach wave tends to zero.

7.4.3.2 Growth of the Mach wave as a function of incident energy

There appears to be a definite relationship between the amount of energy input and the height, the width and the rate of growth of the Mach wave. This incident energy input is affected by the incident waveheight, the incident wave wavelength, and the angle of incidence. From the data presented it is possible that the Mach wave exists for all reflection situations, and could be defined by a relationship which tends to zero for the Mach stem width and angle of growth of the Mach stem, and which tends to 2 for H_{ms}/H_i as θ_o tends to 90°. This relationship could tend to infinity for the Mach stem width and angle of growth and to 1 for H_{ms}/H_i as θ_o tends to 0°.

University of Cape Town

7.4.3.3 Second Mach stem

Berger and Kohlhase (1976) suggest that a second Mach stem exists adjacent to the main Mach wave for $\theta_o < 30^o$. Plate 7.2 shows the phenomenon that was observed during this investigation for $\theta_o = 20^o$. This plate, together with the contour plot (Appendix A; stereopair 26) appear to show that this second Mach wave is actually the resulting reflecting pattern. The angle between the wall and reflected wave orthogonal is small, so the reflected wave which is also small is diffracted and attenuated such that within the limits of the wave basin only one set of defined antinodes is developed next to the Mach stem. Beyond this the reflected wave is so small that it cannot be distinguished from the other imperfections in the incident wave.

Plate 7.2 Mach wave, $\theta_o = 20^o$

University of Cape Town

8. CONCLUSIONS AND RECOMMENDATIONS

8.1 Accuracy of analysis

Photogrammetry is an extremely accurate tool, with a standard deviation for the analysed data of ± 2 mm. The standard deviation for the average heights of the incident waves generated by the wave generator were ± 1 to 3 mm. The standard deviations calculated for the average height of the standing waves were 1 to 5 mm. Unfortunately the error for the oblique wave reflection antinodes is unquantifiable, but could be as large as 15 mm.

It would have been desirable to photograph each wave scenario at least twice, so some idea of the actual magnitude of the deviation of the generated wave could be established. Due to the long period of time required to obtain and analyse a stereopair, it would have been very difficult for any more stereopairs to be taken than were actually taken. The solution to this problem could be to use near real time photogrammetry, once adequately developed, to obtain many sets of data for each wave scenario.

8.2 Standing wave data

The investigation of the standing wave revealed interesting information. The extreme coefficients of reflection (K_r = 1,6) at the reflecting wall was unexpected. Previous investigators had suggested that a K_r = 1,4 could occur at the reflecting wall, but the extreme value of K_r = 1,6 places new emphasis on the importance of the standing wave and the effect it would have for overtopping.

The reduction in the standing wave length compared to the incident wave length for the shallower wave tested was surprising, although it had been suggested by previous investigators. A likely explanation is that there is energy interference between the opposing wave trains, as it would not appear likely that there is a reduction in the wave periods of the two wave trains.

University of Cape Town

8.3 Oblique wave reflection

The oblique wave reflection scenarios behaved as predicted by the wave theory. The angles of incidence and reflection were equal and a reflection coefficient of ≈ 1 was obtained. It was interesting to note that the diffraction pattern occuring for the edge of the reflected wave was similar to that predicted by previously established diffraction diagrams.

8.4 Mach wave reflection

The Mach wave is a complicated relationship, and a lot more data will be required before an adequate knowledge of its characteristics can be established. Two proposed concepts for possible relationships existing for Mach waves are proposed :

i) The Mach wave may exist for all θ_o, but be of negligible stem width for $\theta_o > 50^o$.

ii) The development of the Mach wave is a function of the incident wave energy which depends on the wave height and the period of the incident wave. It is felt that the Mach wave is not a diffraction problem, but an energy problem developing as a function of the non linear properties of the wave.

8.5 Future investigation

This investigation has shown that close range photogrammetry is an excellent technique for investigating water wave surfaces to a high degree of accuracy, and obtaining accurate, comprehensive representations of the water surface. Unfortunately it does not appear possible to use conventional photogrammetrical techniques to perform a comprehensive investigation into wave reflection as an enormous number of man hours would be required.

The author is of the opinion that when near real time photogrammetry systems have developed to sufficient accuracy, the potential exists to complete this wave reflection investigation. It is felt that a large wave basin equipped with a good quality wave generator should be adapted for permanent photogrammetric use. The area of the basin

University of Cape Town

could be covered with pairs of digital cameras synchronised from a single host computer. In this way not only wave reflection, but alternative harbour designs and other wave phenomenon could be investigated to a degree of accuracy and comprehensiveness never before realised. Such a system, although expensive, with adequate software, could revolutionise hydraulic model investigations.

University of Cape Town

BIBLIOGRAPHY

ADAMS, L.P.	1978	The use of Photogrammetry in the Study of the Sea and the Coasts. Proceedings of the 6th Conference of South African Surveyors, Part 1, 1978.
ADAMS, L.P.	1981	X-Ray Stereo Photogrammetry, Locating the Precise Three-Dimensional Position of Image Points. Medical and Biological Engineering Completing, September 1981, pg. 569.
ADAMS, L.P.; POS, J.D.	1981	Model Harbour Waveform Studies by Short Range Photogrammetry. Photogrammetric Record, October 1981, pg. 457.
ATKINSON, K.B.	1980	Developments in Close Range Photogrammetry. Applied Science Publishers 1980.
BERGER, U.; KOHLHASE, S.	1976	Mach Reflection as a Diffraction Problem. Coastal Engineering 1976 Proceedings, Vol. 1, pg. 796.
THE CANADIAN INSTITUTE OF SURVEYING	1986	Proceedings of Symposium "Real Time Photogrammetry - A New Challenge". International Archives of Photogrammetry and Remote Sensing.
COASTAL ENGINEERING RESEARCH CENTRE	1984	Shore Protection Manual, U.S. Government Printing Office, 1984.
FAIG, W.	1972	Photogrammetry and Hydraulic Surfaces. Journal of the Surveying and Mapping Division, Proceedings of the American Society of Civil Engineers, November 1972, pg. 145.
GRUEN, A.W.	1989	Digital Photogrammetric Processing Systems: Current Status and Prospects. Photogrammetric Engineering and Remote Sensing, Vol. 55, No. 5, May 1989, pg. 581.

University of Cape Town

HAMILL, P.A.	1963	Experimental Development of a Perforated Wave Absorber of Simple Construction and Minimum Length. National Research Laboratories, Ottowa Canada, Report No MB-252, May 1963.
HART, C.A.	1943	Air Photography Applied to Surveying. Longmans, Green and Co. Ltd, 1943.
IPPEN, A.T.	1966	Estuary and Coastline Hydrodynamics. McGraw-Hill Book Company, 1966.
JAMIE, A.	1988	Analysis of Wave Reflection at a Vertical Wall Using Close Range Photogrammetry. BSc Thesis, University of Cape Town.
JARLAN, G.E.	1961	A Perforated Vertical Wall Breakwater. The Dock and Harbour Authority, April 1961, pg. 394.
MARESCA, J.W.; SEIBEL, E.	1976	Terrestrial Photogrammetric Measurements of Breaking Waves and Long Shore Currents in the Near Shore Zone. Coastal Engineering 1976 Proceedings, Vol. 1, pg. 681.
MARKS, W.; RONNE, F.C.	1955	Aerial Stereophotography and Ocean Waves. Photogrammetric Engineering 2(1), pg. 107.
NATIONAL SEMI CONDUCTORS	1978	Linear Data Book, pg. 62.
MOFFIT, F.H.	1968	Wave Surface Configuration. Photogrammetric Engineering, Vol. 34, 1968, pg. 179.
moves 1970		
PATERSON, A.J.C.	1986	A Study of Ship Wave Resistance from an Analysis of the Wave Pattern using Close Range Photogrammetry. MSc Thesis, University of Cape Town.
PETZER, J.M.	1987	Analysis of Water Wave Reflection using Photogrammetry, BSc Thesis, University of Cape Town.

University of Cape Town

COEFFICIENT OF REFLECTION CONTOUR PLOT

Stereopair 20, $\theta_o = 34^o$, Mach wave reflection, T = 0,765, H_i = 38,4mm

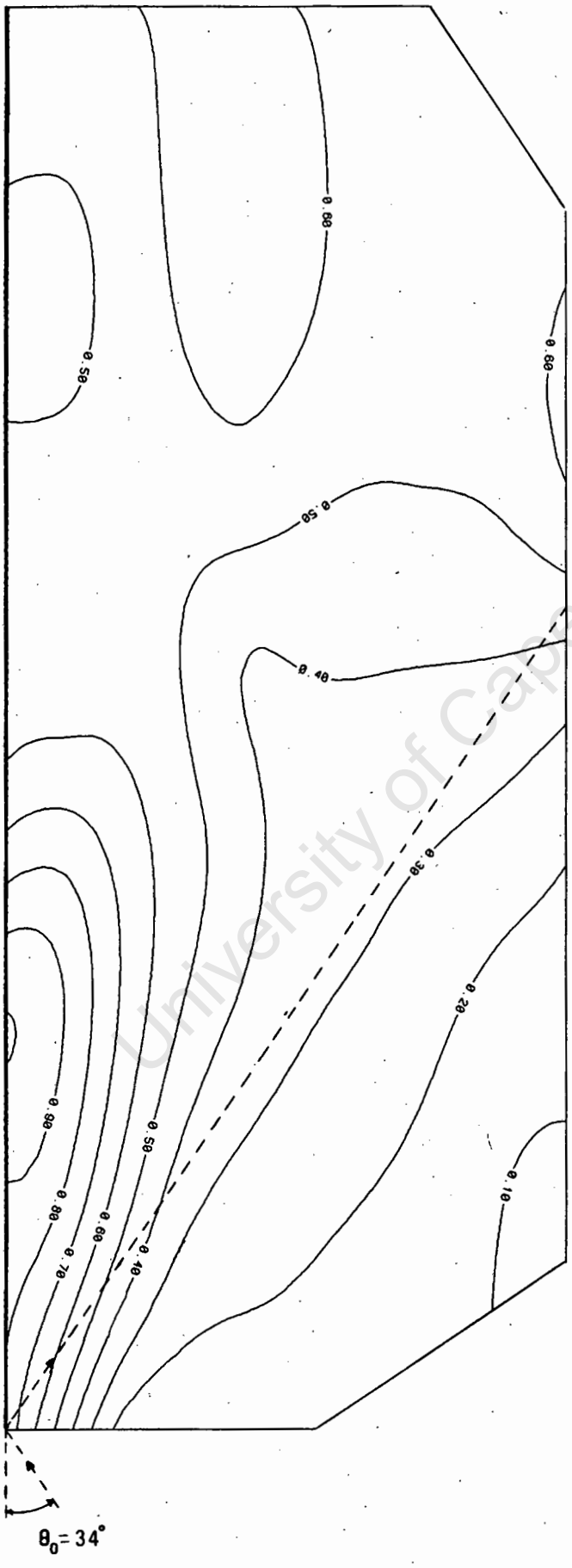

University of Cape Town

Scale 1 : 25

COEFFICIENT OF REFLECTION CONTOUR PLOT

Stereopair 21, $\theta_o = 34^o$, Mach wave reflection, T = 0,765, H_i = 24,8mm

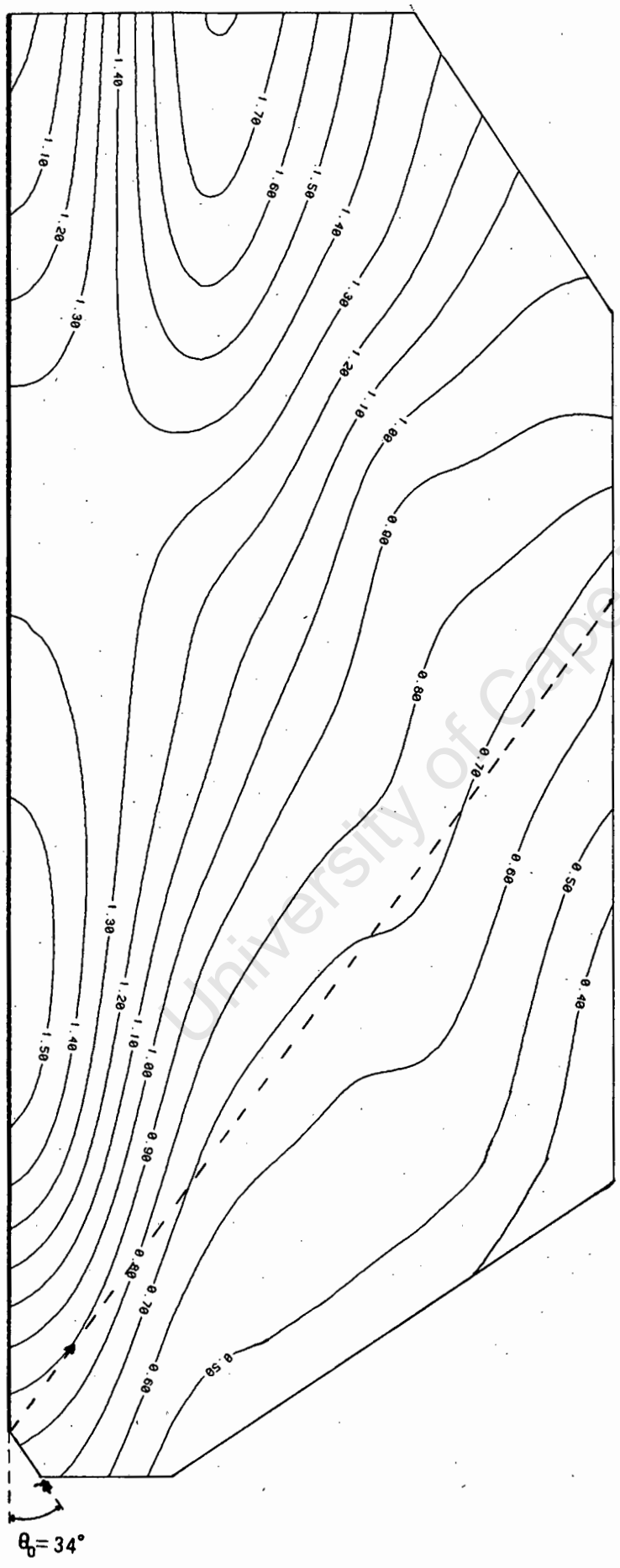

University of Cape Town

Scale 1 : 25

COEFFICIENT OF REFLECTION CONTOUR PLOT

Stereopair 22, $\theta_o = 34^o$, Mach wave reflection, T = 1,01, H_i = 32,7mm

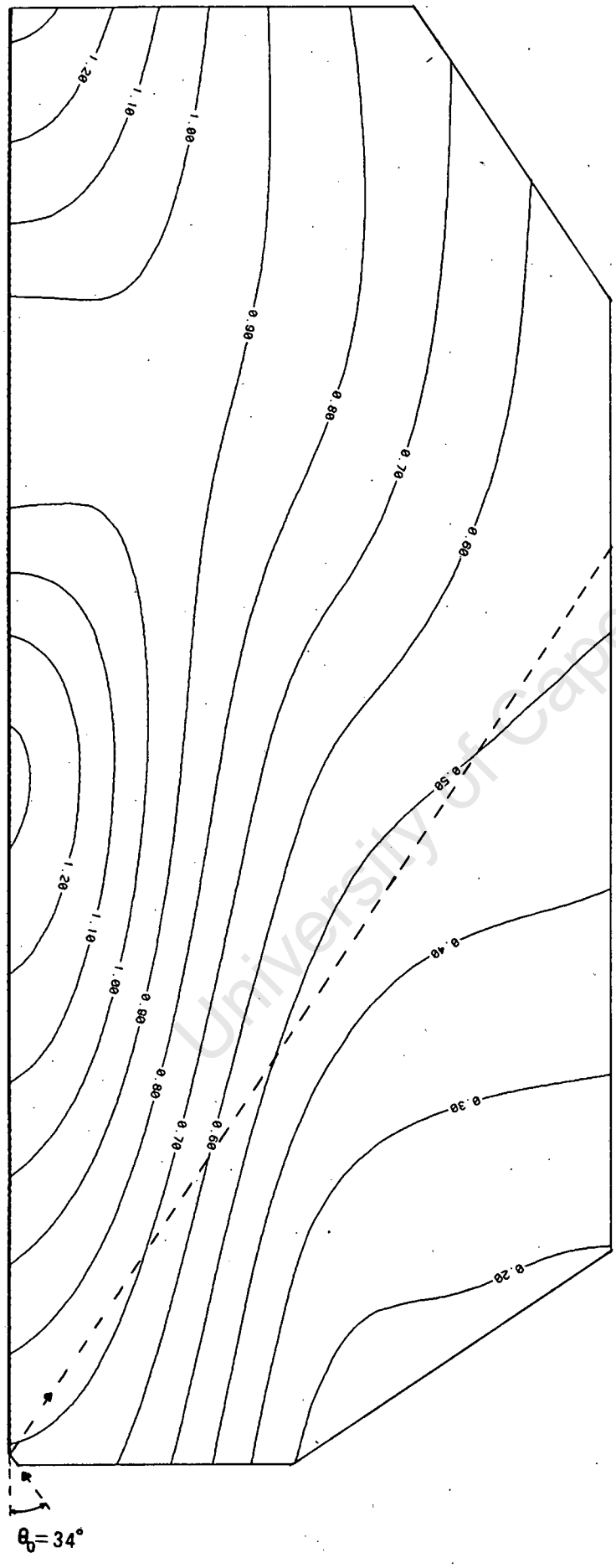

Scale 1 : 25

University of Cape Town

COEFFICIENT OF REFLECTION CONTOUR PLOT

Stereopair 23, $\theta_o = 34^o$, Mach wave reflection, T = 1,01, H_i = 34,0mm

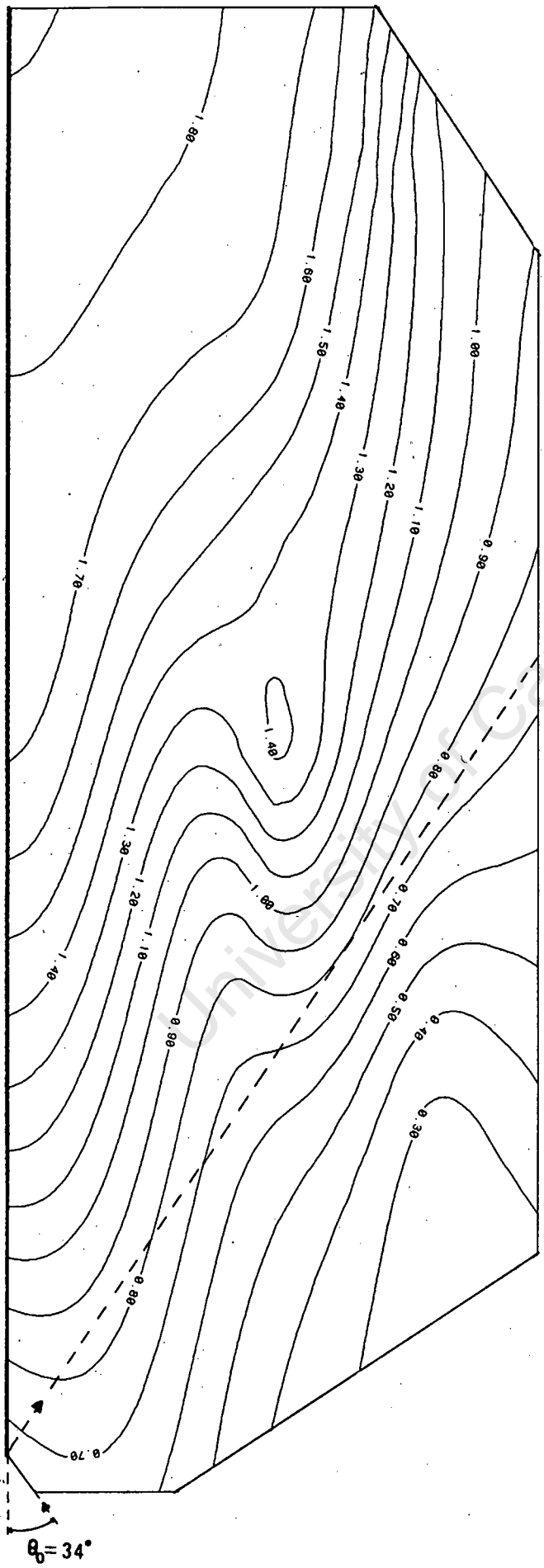

Scale 1 : 25

University of Cape Town

COEFFICIENT OF REFLECTION CONTOUR PLOT

Stereopair 24, $\theta_o = 34^o$, Mach wave reflection, T = 1,01, H_i = 39,9mm

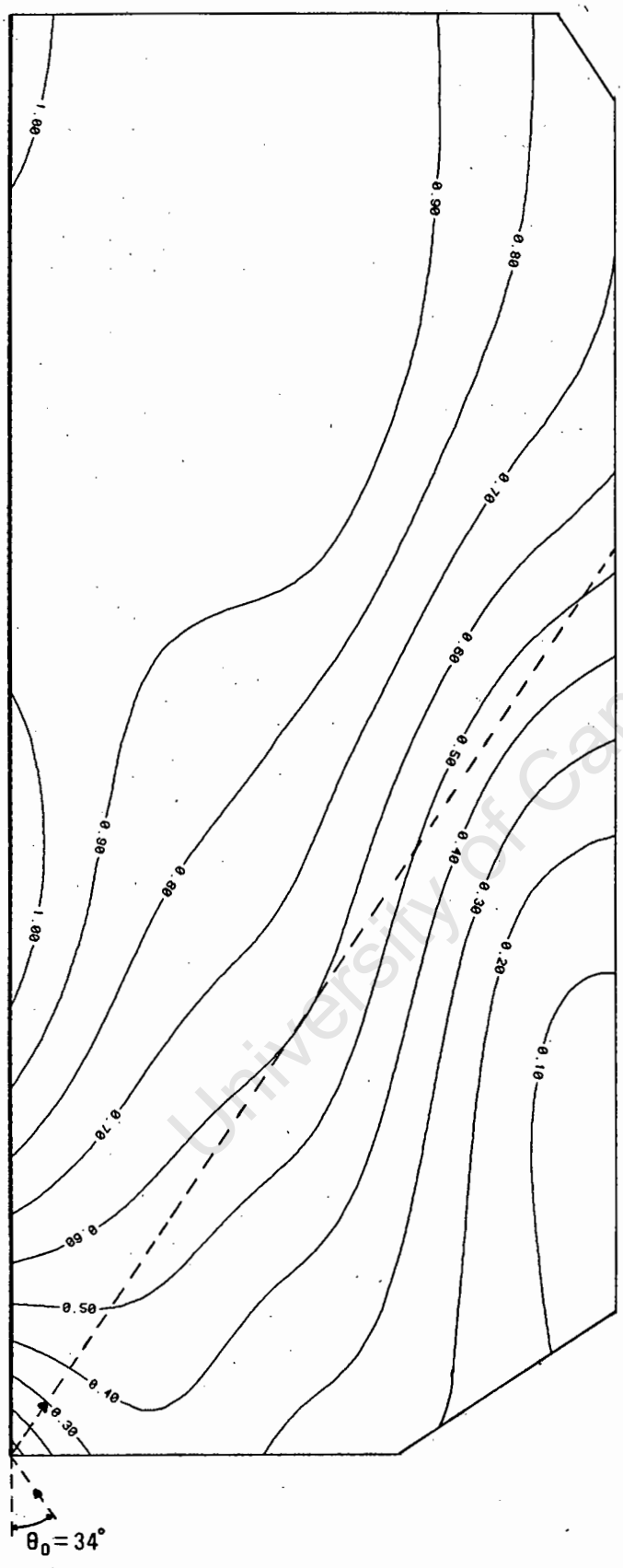

Scale 1 : 25

University of Cape Town

COEFFICIENT OF REFLECTION CONTOUR PLOT

Stereopair 25, $\theta_o = 25^o$, Mach wave reflection, T = 0,765, H_i = 24,8mm

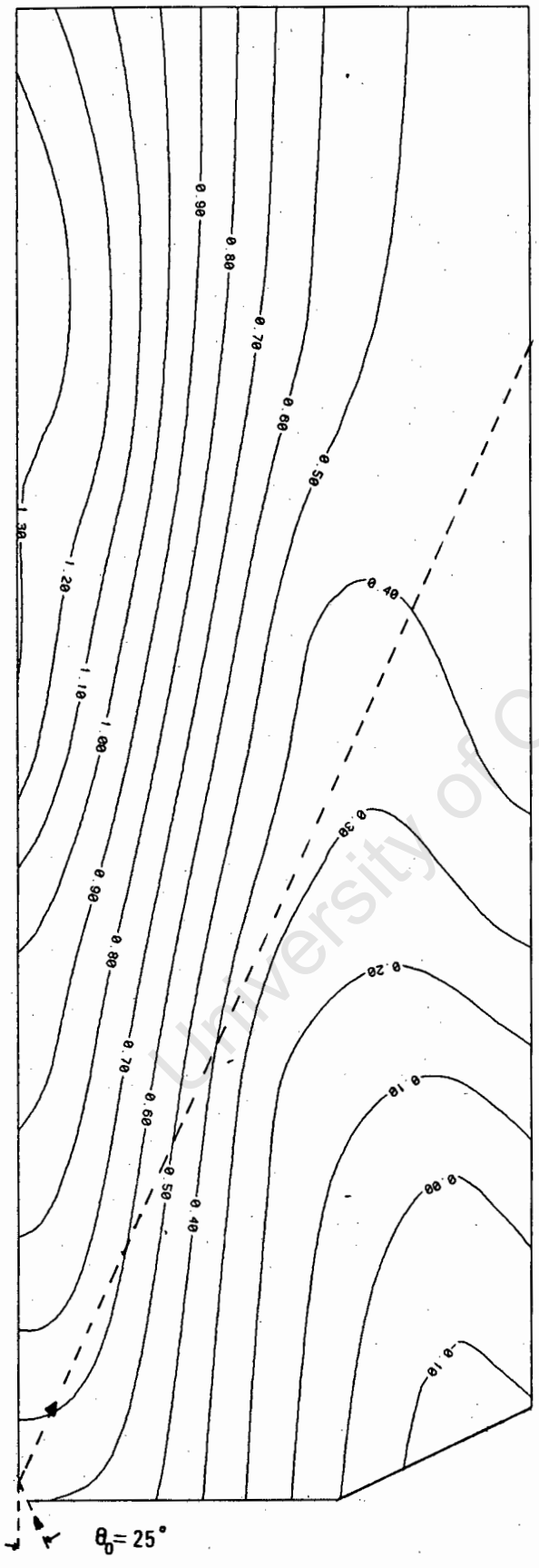

Scale 1 : 25

University of Cape Town

COEFFICIENT OF REFLECTION CONTOUR PLOT

Stereopair 26, $\theta_o = 20^o$, Mach wave reflection, T = 0,765, H_i = 24,8mm

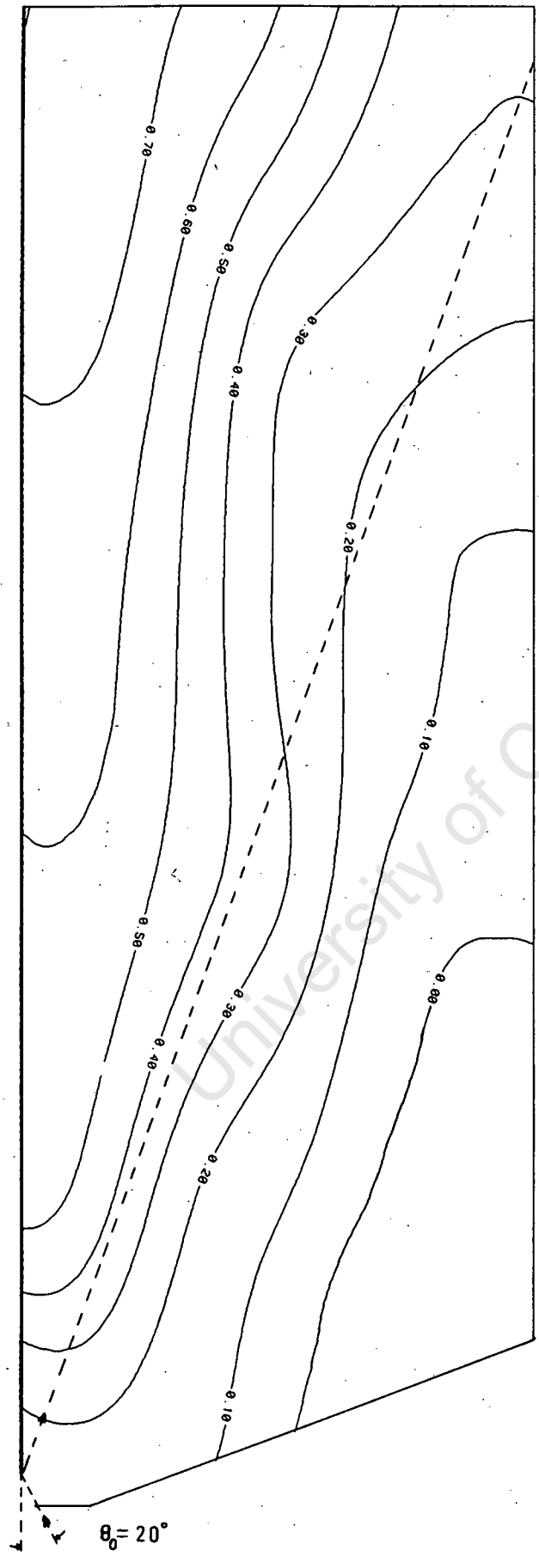

Scale 1 : 25

University of Cape Town

COEFFICIENT OF REFLECTION CONTOUR PLOT

Stereopair 27, $\theta_o = 11^o$, Mach wave reflection, T = 0,765, H_i = 24,8mm

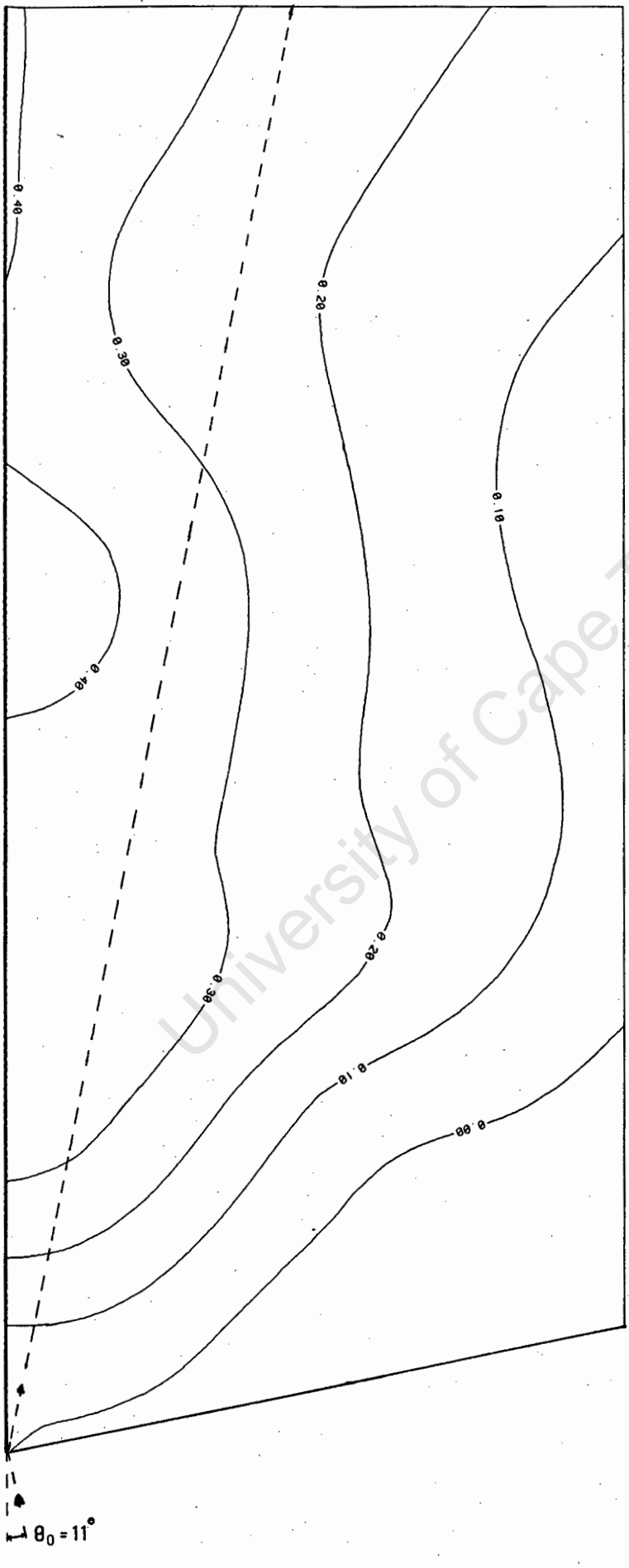

Scale 1 : 25

University of Cape Town

APPENDIX C

Stereopair 28

	T	C	T	C	T	C	T	C	T	C	T	C	T	C
a_{ci}		12,8		12,6		11,8		13,2		13,6		12,3		12,6
a_{ti}	10,8		10,2		11,9		12,3		13,1		12,4		13,1	
Standard deviation	2,7	2,6	1,6	1,2	1,8	1,9	1,6	2,5	1,0	1,5	1,8	2,0	1,3	1,5
H_i	23,6	23,0	22,6	24,5	23,7	24,1	25,5	26,3	26,7	26,0	24,7	25,4	25,7	

Stereopair 29

	C	T	C	T	C	T	C	T	C	T	C	T	C
a_{ci}	23,5*		22,1		20,1		19,6		19,7		18,8		18,6
a_{ti}		18,9*		17,9		19,4		19,1		17,2		18,3	
Standard deviation	2,8	1,6	2,4	1,9	1,4	2,2	2,7	2,1	3,0	1,2	3,3	1,7	2,2
H_i	40,0	38,0	39,5	39,0	38,7	38,8	36,9	36,0	37,1	36,9			

Stereopair 30

	T	C	T	C	T	C	T	C	T	C
a_{ci}		17,4*		19,6		21,8		21,7		23,2
a_{ti}	11,3		12,5		12,9		11,4		10,4	
Standard deviation	2,1	3,3	2,1	2,2	1,4	2,1	1,6	2,4	2,1	1,7
H_i	32,1	32,5	34,7	33,2	33,1	32,1	33,6			

University of Cape Town

Stereopair 31

	T	C	T	C	T	C	T	C	T	C
a_{ci}		23,1*		20,4		20,9		20,8		21,6
a_{ti}	14,6*		15,6*		12,6		13,3		13,3	
Standard deviation	1,3	3,4	1,4	2,8	0,5	2,3	1,3	1,3	2,1	2,0
H_i					33,0	33,5	34,2	34,1	34,1	34,9

Stereopair 32

	T	C	T	C	T	C	T	C	T	C
a_{ci}		25,8*		24,1		24,1		23,4		25,8
a_{ti}	12,9*		18,8*		17,3		15,3		14,6	
Standard deviation	0,5	2,9	2,5	2,1	1,7	1,8	1,6	1,3	1,6	2,2
H_i					41,4	41,4	39,4	38,7	38,0	40,4

Stereopair 33

	C	T	C	T	C	T
a_{ci}	22,3		16,8*		24,1	
a_{ti}		12,7		14,1		13,6
Standard deviation	2,3	0,5	1,1	1,3	1,5	1,6
H_i	35,0			38,2	37,7	

University of Cape Town

APPENDIX D

EXAMINATIONS WRITTEN BY THE AUTHOR TO COMPLETE THE REQUIREMENTS OF THE DEGREE

Course Number		Result	Credit Rating
CIV516F	Coastal Hydraulics	1	5
CIV592F	Project Management in Civil Engineering	3	3
SEA200F	Physical Oceanography	2+	4
CIV525S	Contract Law	2-	3
CIV536S	Coastal Engineering Practice	1	5
CIV593S	Engineering Software Designs	2+	4
CIV500Z	"A study of water wave reflection using Close Range Photogrammetry"		20
			44
	Credit requirements for Degree		40

University of Cape Town

[4 PAGES]

UNIVERSITY OF CAPE TOWN

DEPARTMENT OF CIVIL ENGINEERING

M.Sc. in CIVIL ENGINEERING

CIV 516F : COASTAL HYDRAULICS

UNIVERSITY EXAMINATION : JULY 1988

ALL question may be attempted. TIME: 4 hours +

(OPEN BOOK EXAMINATION)

University of Cape Town

Constants

Sea water density = 1025 kg/m^3

Sea water weight = 10 kN/m^3

QUESTION 1

The standard alignment chart is attached and a new blank line has been inserted at the bottom of the page. This line is to be used for determining values of U_{max} , the maximum horizontal orbital velocity at the water surface, according to the Airy theory. If $U^*_{max} = \frac{U_{max}}{\pi H/T}$ is to be the dimensionless form of the variable on this line, mark off the correct positions of the $\overset{*}{U}_{max}$ values given in the following list.

$\overset{*}{U}_{max}$ = 1,01 2 6
1,10 3
1,40 4

Note that H is the local wave height throughout. Suggest a small change in the line label which would permit the scale to be used for maximum horizontal surface acceleration values. Use the new line to solve the following problem.

A swell of 10 second period with a deep water wave height H_o = 1,59 m approaches a beach with the wave crests parallel to the shore. Plot the value of u_{max} at the water surface for the following selected water depths.

65 m ; 34,4 m ; 15,9 m ; 6,8 m ; 2,86 m .

Use these calculations to estimate the water depth when the U_{max} value first reaches 1,5 m/s and check that the wave has not broken.

QUESTION 2

A sea platform consists of a square concrete slab positioned horizontally on four cylindrical vertical piles, each placed at a corner, the slab side being parallel to the local wave crest. The pile diameter is 1 m, the total pile height above sea bed is 6,4 m, and the slab dimensions are sides of 5 m with a thickness of 200 mm. The local wave characteristics are height 2 m, length 100 m, and period 12 s, the local water depth being 8 m.

(a) Considering the central 1 m high slice of any pile, calculate the horizontal forces per metre due to velocity and acceleration and by plotting these throughout one wave period or otherwise, identify the maximum force and the timing of its occurrence. Check that the velocity and acceleration distributions over the height of the pile are reasonably constant and thus estimate the total force on one pile.

Take C_D = 1,2 and C_M = 2,0 .

University of Cape Town

QUESTION 2 (continued)

(b) Estimate the maximum vertical force on the slab due to wave action.

Take $C_D = 1,0$ and $C_M = 1,8$.

QUESTION 3

In a study of wave penetration into a bay, the 10 m, 9 m and 8 m sea bed contours are approximated by three straight lines with contained angles of 12 degrees as shown on the attached page. An incoming wave orthogonal, 10 second period, impinges on the 10 m contour at an angle of 50 degrees as shown. With the usual approximations obtain by trial the angle at whch the emerging orthogonal cuts the 8 m contour. Take the step lines on the 9,5 m and 8,5 m lines.

[1 diagram attached]

QUESTION 4

A train of waves is approaching a shore line, of regular bed slope 1 in 80, the wave crests being essentially parallel to the shore. Two aerial still photographs are taken 8 seconds apart. On the first photograph, two successive crests are identified as being 247 m apart. A comparison between the two photographs indicates that the trough between the two crests has advanced forward a distance of 153 m. Further, stereo photographs taken at the same time as the first exposure indicate that the wave height in the vicinity of the trough is close to 3 m. Retrace the history of this wave as it came in from deep water, and further trace the progress of the wave as it moves towards the beach, including the following calculations:

(i) the wave length and celerity in deep water ;

(ii) the wave length, celerity and height for water depths at 20 m intervals from deep to the 10 m depth, and at 1 m intervals inshore from this to a depth of 3 m ;

(iii) the depth of water in which the wave breaks, the type of breaker, and the wave height at breaking. Set up and down may be ignored ;

(iv) the energy flow in W/m in two water depths outside the breakers, and one depth in the breaker zone (depths at your choice) and compare.

University of Cape Town

QUESTION 5

(a) A storm at sea generates waves with a period range of 6 to 12 seconds. The resulting swell travels towards a harbour 400 km away. Estimate the time interval between the arrival of the shortest and longest waves, assuming deep water throughout.

(b) A refraction diagram is constructed for a bay, and the spacing between a particular pair of adjacent orthogonals doubles in travelling from deep water to the 10 m depth zone, the wave period being 7 seconds. Estimate the percentage change in wave height occurring between these two zones on the assumption that no breaking waves are present in-between.

(c) In a zero damage design calculation for the armour protection of a rubble mound breakwater, 3 tonne and 5 tonne dolosse are specified for the trunk and head respectively, the slope of the breakwater face being cot α = 2. Estimate the block masses and block heights if tetrapods had been used in the same design. If the design wave height was 3 m, and a storm causes damage of the order 20 - 30 per cent to the tetrapod scheme, estimate the storm wave height (concrete density 2245 kg/m^3).

(d) An incoming swell has crests parallel to a straight beach with a deep water wave height of 2 m. Estimate the horizontal force (per metre along the beach) acting on the beach inside the refraction zone, due to the dynamic action of the waves.

(e) In an area where the sea bed is horizontal, and the water depth is 3 m, a wave has a period of 7 s, a wave length of 38 m, and a wave height of 1,5 m. Estimate the drift velocity at bed level, and indicate the direction. Compare this velocity with the maximum orbital velocity at the same level, and indicate the influence on bed drift of a strong onshore wind.

(f) A coastal model is to be constructed to explore wave action in a sea area 1 km offshore by 2 km along shore. The laboratory area available is 20 m wide and of considerable length. Suggest a linear scale suitable for this and calculate the wave period of the model paddles to duplicate a 12 second wave in nature. Discuss which of the following characteristics are accurately modelled in the laboratory:

(i) wave refraction pattern ;
(ii) wave heights before breaking ;
(iii) wave heights after breaking ;
(iv) settlement of fine sands.

* * * * * * * * *

University of Cape Town

UNIVERSITY OF CAPE TOWN

DEPARTMENT OF CIVIL ENGINEERING

CIV 592F POSTGRADUATE EXAMINATION

PROJECT MANAGEMENT IN CIVIL ENGINEERING

15 JUNE 1988 TOTAL MARK 100

NOTE

* The examination is three (3) hours
* Attempt all questions
* All writing to be in ink or ballpoint pen

1. Refer to Annexure A . Complete and hand in with the answer book.

2. Discuss the functions of a Project Manager. [20]

3. Describe the different types of information required by a Project Manager to plan a project. [20]

4. Discuss the problems which may arise when a Project Manager underestimates the cost of a Contract in his motivation to the Client for acceptance. [10]

5. Indicate , with comment , the cost items which may be affected in a contractor's claim as also the reasons for a claim . [10]

University of Cape Town

Name..... 15 June 1988

ATTEMPT ALL THE FOLLOWING QUESTIONS WITH SHORT PRECISE ANSWERS

TOTAL MARK 40

a) What is the purpose of organising. [1]

.....

.....

b) Give four reasons why organisational charts are useful. [2]

1).....

2).....

3).....

4).....

c) For what reason are people motivated. [1]

.....

.....

d) Name two reasons why a Client would be motivated to undertake a project. [1]

1).....

2).....

e) Time and cost is interrelated but can be in conflict ,is this true or false ? [1]

True / false (circle the correct reply)

d) Indicate which of the following are procedural constraints : [3]

availability of local funding	yes/no
tendering	yes/no
detail design	yes/no
conditions of contract	yes/no
contractural incentives	yes/no
arbitration	yes/no

University of Cape Town

e) Give ten benefits of good planning : [5]

1).....

2).....

3).....

4).....

5).....

6).....

7).....

8).....

9).....

10).....

f) Indicate which of the following can assist with project control . [3]

personal commitment	yes/no
programme coordination	yes/no
review meetings	yes/no
project reports	yes/no
management support	yes/no
communication	yes/no

g) List six project management monitoring actions which should be excercised during construction. [3]

1).....

2).....

3).....

4).....

5).....

6).....

University of Cape Town

h) Indicate four normal reactions to which a person may resort if faced with a risk situation . [2]

1).....

2).....

3).....

4).....

i) Give three types of critical path charts for programming a project . [3]

1).....

2).....

3).....

j) Give eight reasons for providing a client with an estimate for a project . [4]

1).....

2).....

3).....

4).....

5).....

6).....

7).....

8).....

k) What should be considered when compiling a Schedule of Quantities for a project . [3]

1).....

2).....

3).....

4).....

5).....

6).....

University of Cape Town

l) Is the cummulative monthly payments made to a contractor a straight line , if not what shape is it ? [2]

.....

.....

m) Who takes the risk in a fixed priced contract. [1]

.....

n) On which cost elements in a contract are the inflation index values applied. [2]

1).....

2).....

3).....

4).....

o) What is the normal maximum percentage variation of a payment item that can be accepted before a Contractor may request a revision of the pay item rate , and for what reason. [2]

.....

.....

.....

p) What are statutory increases. [1]

.....

University of Cape Town

UNIVERSITY OF CAPE TOWN - JUNE EXAMINATION 1988

OCEANOGRAPHY SEA 200F

TIME: 3 HOURS TOTAL MARKS: 150

Answer ALL questions in SECTION A
Answer ONE question from SECTION B and THREE questions from SECTION C

SECTION A

Answer ALL questions in this section

1. Sketch the oxygen distribution in the deep ocean (4 km deep), at mid-latitude. (2)
2. What variables does the seawater density depend on? (2)
3. Define the "potential temperature". When should this be used in place of the "in situ" temperature? (2)
4. Is the ocean well stratified in the vertical? (2)
5. Give a labelled t,s diagram for the Atlantic ocean at 35^{o} S. (2)
6. Define "sigma-t" and the "standard ocean". (2)
7. Explain how a CTD works and what it measures. (2)
8. What is the "solar constant"? (2)
9. What is Group velocity and how is it related to the phase velocity of "deep water" waves? (2)
10. What is a "tsunami"? (2)
11. Define the terms "geopotential" and "dynamic metre". (2)
12. When does the diurnal inequality of the tide vanish? (2)
13. Sketch and describe the main elements of a Kelvin wave. (2)
14. Describe the terms "amphidromic point", "co-range lines". (2)
15. Give a simple definition of Salinity. (2)

TOTAL (30)

SECTION B

Answer EITHER OF the following questions:

(a) Describe with the aid of suitable diagrams, the characteristics of the major ocean current systems and the major bathymetric features around southern Africa. Include details of current speeds and surface temperatures. (30)

OR

(b) Write an essay on the phenomenon of El Nino - Southern Oscillation (ENSO) in the Pacific Ocean. (30)

University of Cape Town

SECTION C

ANSWER ANY THREE FULL QUESTIONS

(A) Discuss the main elements of the heat budget in the atmosphere and ocean, and give an indication of the relative importance of the terms in the heat budget equation.

Using the concept that a windstress in the y direction causes an Ekman flux or transport in the upper ocean in the x direction, describe how it is possible to set up an anticyclonic gyre in the South Atlantic ocean. (Hint: let y be positive north, and x positive west) (30)

(B) Discuss the method of dynamic sections to obtain the baroclinic, geostrophic velocity structure in the vertical in the Agulhas current. How can these relative velocities be converted into absolute currents?

If the surface slope on the current is 1 m in 100 km, up away from the coast, calculate the barotropic current speed and direction at 30^{o} S. (Use g=10 m s^{-2}, $f=2\Omega\sin(\theta)$, $\Omega = 7.29\ 10^{-5}\ s^{-1}$) (30)

(C) The dispersion of surface wind waves in the ocean is given by

$$\sigma^2 = gk \tanh(kd),$$

where $\sigma = 2\pi f = 2\pi/T$ is the radian frequency and
$k = 2\pi/L$ is the wave number, g = 10 ms^{-2}, d is depth.

Discuss the terms "deep water" and "shallow water" waves, and derive the phase velocities in these cases. What is the "deep water" wavelength of waves with a period of 15 s? What is the phase speed of these waves in 5m deep water?

Given that the approximate average power of the waves off the Cape coast is 40 Kw per metre of wave crest, calculate how many kilometres of wave crest must be harnessed by a wave absorbing device which is 50% efficient at extracting energy from the waves, to equal the power from a Power station producing 2 000 Mega watts. (30)

(D) Write short notes on:
The Phillips-Miles theories of wind wave generation,
South African tides,
Waves entering shoaling water,
Different types of breaking waves,
Fronts and convergences. (30)

University of Cape Town

UNIVERSITY OF CAPE TOWN

DEPARTMENT OF CIVIL ENGINEERING

UNIVERSITY EXAMINATION - NOVEMBER 1988

COURSE CIV 525S - CONTRACT LAW

OPEN BOOK EXAMINATION

Time : 150 Minutes

University of Cape Town

PLEASE ANSWER ALL QUESTIONS, BEARING IN MIND THE NUMBER OF QUESTIONS, IT IS SUGGESTED THAT YOUR ANSWERS BE KEPT AS BRIEF AS POSSIBLE.

TOTAL NUMBER OF MARKS : 100 MARKS

External Examiner 10/11/88

Internal Examiner

External Examiner

106 01 01

QUESTION 1

"It must be conceded that the phraseology of Clause 54 (of the Standard Engineering Contract) is capable of bearing the construction placed upon it by the Court a quo. But in my opinion it is also open to a different interpretation". (Per Van Heerden JA in Melmoth Town Board v Marius Mostert (Pty) Limited 1984 (3) 718 at 728 F).

Comment on the above statement and deal with the powers of the engineer in terms of the said Clause 54.

10 Marks

University of Cape Town

QUESTION 2

You are a director of a construction company.

The construction company applies to an insurance company for the issue of a performance bond and the insurance company requires you to sign a suretyship for the obligations of the construction company in respect of that contract. However, in terms of the suretyship you bind yourself "as surety and co-principal debtor in solidum for the due and faithful performance by the construction company to the insurance company of all and whatsoever obligations undertaken by it on behalf of the construction company in connection with any matter whatsoever".

Shortly afterwards you resign from the construction company, and a year later you receive a letter from the insurance company advising you that in connection with another project carried out by the construction company after you had left its employ, the construction company was indebted to the insurance company, who are now looking to you for payment in terms of the suretyship signed by you.

You are very alarmed because you had not envisaged that you would be liable for obligations which were incurred after you had left the employ of the construction company. You decide to take legal advice.

What are you likely to be told?

10 Marks

University of Cape Town

QUESTION 3

You are a director of a construction company.

In terms of the construction contract, certain work was to be sub-contracted to a sub-contractor nominated by the architect.

The architect obtained a tender for this work from the sub-contractor and instructed your firm to accept the work. You sent an order on your standard printed form which contained on its reverse side printed conditions which included a clause reading as follows :-

"Payment of the amount due in terms of this order will only be effected after we (the main contractor) have received payment from the employer".

The sub-contractor wrote back to you thanking you for the order and the work was carried out.

The employer became insolvent before having paid for all the work.

The sub-contractor calls on you to obtain payment for all the work done by him.

What would you reply?

10 Marks

University of Cape Town

QUESTION 4

You are a director of a construction firm.

You contract with a development company (X Developers (Pty) Limited) to build houses on separate erven which are owned separately by individual owners who are clients of the development company, and with whom the the development company had entered into agreements for the building of these houses.

As the work progressed from time to time, each of the owners paid X Developers (Pty) Limited the amount required from them.

Unfortunately, X Developers (Pty) Limited find fault with your work and advise that they are not prepared to pay you any further sums until you have completed what they regard as the remedial work.

You dispute that in fact any remedial work is necessary, but you are not prepared to continue work until the amount due to you in terms of your contract with X Developers (Pty) Limited has been paid.

The individual owners need their accommodation urgently and decide to contract with another firm to build for them and finish off the work.

You do not want to give up possession of the building sites and the work thereon until you have been paid in full, and the individual owners institute action against your firm for an order claiming possession of the various sites. Your Board asks you for an outline of what your rights are in this matter.

Draw a short memorandum setting out your rights.

10 Marks

University of Cape Town

QUESTION 5

You are a director of a construction company.

It appears that your firm has failed to comply fully with performance of work undertaken in terms of the contract, but you wish to claim for the work which you have done.

You decide to take legal advice on your rights, and the attorney whom you consult says "Ah, this is a B K tooling case", and proceeds to give you certain advice.

On the basis that he knows what he is talking about, write a short memorandum for your managing director setting out what your rights are.

10 Marks

University of Cape Town

QUESTION 6

You are a director of a construction company.

Your firm has entered into a contract to build certain road works, and the contract is in terms of the General Conditions of Contract of 1982 as issued by the South African Institution of Civil Engineers.

Times are difficult - interest rates are rising - and your managing director advises you that it looks like it may be necessary to enter into an arrangement with the company's creditors.

He asks you to prepare a short memorandum for the Board setting out the rights of the employer under your contract, should your company decide to follow this course.

Prepare the memorandum.

10 Marks

University of Cape Town

QUESTION 7

You are a director of a construction company.

In terms of the contract your company has undertaken to pay your employer R10 000,00 a day for every day by which delivery of the completed works is delayed.

Due to internal disputes in the construction company, delivery of the completed works is delayed for a period of 3 months and your company's accountants make provision for the sum of R90 000,00 as being due by your company to the employer.

The managing director asks you to write a short memorandum for the Board setting out whether this is a liability, whether it can be reduced, and whether there would be any defence to a claim.

Write it.

10 Marks

University of Cape Town

QUESTION 8

In what circumstances may an extension of time be granted in terms of the General Conditions of Contract 1982.

10 Marks

University of Cape Town

QUESTION 9

You are a director of a construction company.

It is clear that a dispute is arising between the employer and your company, and the Board intends discussing whether the matter should go to arbitration or litigation.

You are asked to prepare a short memorandum discussing the relative merits of these methods of dispute settlement.

10 Marks

University of Cape Town

QUESTION 10

You are in practise as a consultant engineer.

You are appointed as the engineer in regard to a particular contract entered into in accordance with the General Conditions of Contract 1982.

One of the nominated sub-contractors complains bitterly to you that the main contractor has not paid him for work already done by such sub-contractor, for which you know the employer has already paid the contractor, and the nominated sub-contractor advises you that he is still working under the sub-contract and he would like you to protect him insofar as regards payment in the future.

What could you do?

Would your answer be any different if the sub-contractor was not a nominated sub-contractor?

10 Marks

University of Cape Town

UNIVERSITY OF CAPE TOWN

DEPARTMENT OF CIVIL ENGINEERING

UNIVERSITY EXAMINATION : 29 OCTOBER 1988

CIV 536 - COASTAL ENGINEERING PRACTICE

University of Cape Town

Time Allowed: 3 hours

Answer ALL Questions

There is a potential of 158 marks

SECTION 1 is to be handed in at the end of the first hour - CLOSED BOOK

SECTION 2 is "OPEN BOOK"

Name: .....

QUESTION 1

Briefly explain, in words and by means of annotated sketches, the meaning of the following terms:

1.1 Cope level [2]

1.2 Pendant fender [2]

1.3 Tidal prism [2]

1.4 Seiche [2]

University of Cape Town

1.5 Clinometer [2]

1.6 Show on a sketch plan of Hout Bay where you would expect to observe the effects of wave diffraction and refraction. Clearly indicate the physical cause of each effect and the form of the wave orthogonals and crests. [2]

1.7 Explain, by means of a sketch, the basic physical elements of airborne (single channel) linescan apparatus that could be used for remote sensing of the ground. [2]

1.8 Explain by means of a sketch how a dredger may be positioned using sextant resection. [2]

University of Cape Town

1.9 Explain the principle of subtense ranging using a sextant. Indicate the practical distance limit.
[2]

1.10 Explain by means of a sketch the principle of echo sounding for seabed profiling.
[2]

1.11 Give a sketch of the components and the arrangement that is used for tide recording at Granger Bay.
[2]

1.12 Explain the term "tidal residual". What is the cause of tidal residuals?
(2)

University of Cape Town

1.13 Explain the principle of the "Wave rider" accelerometer buoy. [2]

1.14 Show by means of simple sketches how field measurements of the following may be graphically presented in reports :

wind speed and direction [2]

Radioactive tracers [2]

Beach profiles [2]

1.15(a) Give a typical section of a rubble mound breakwater (annotate). [2]

University of Cape Town

1.15(b) Show the sequence of how this would be constructed in an exposed situation. [2]

1.16 Comment very briefly (<u>with a simple sketch</u>) on the adequacy or inadequacy of the following :

position of the slipway at Granger Bay [2]

boat "access" situation at harbour entrance in Hout Bay [2]

boat "access" situation at Kalk Bay harbour entrance [2]

a boat ramp at 1:6 [2]

University of Cape Town

a boat ramp at 1:15 [2]

1.17 Explain what you would look for in an aerial photograph of the coast to discern the direction of littoral drift. [2]

Total for SECTION 1 = 48 marks.

University of Cape Town

SECTION 2 - OPEN BOOK

2.1 Assuming that you are a Consulting Engineer specialising in coastal matters, reporting to the local authority responsible for the coast, write advisory notes to the responsible Committee on the following :

(a) It is September and the beach has steepened and eroded sufficiently for an adjacent parking area to appear to be in danger of being totally eroded.

Outline your proposed method of investigation, your preliminary advice as to what the Council should instruct you or Contractors to do, what alternatives measures are likely to be appropriate after completing the investigation. Give a staged breakdown of costs with time/construction expense justification. Assume the total beach length is 1 km and that the situation is as occurs at Fish Hoek.

[15]

(b) It is proposed that the harbour at Granger Bay be improved. Write a memorandum to the responsible Committee outlining the problems that occur at present and the approach you would take to improve the situation. Provide an approximate cost for the investigation and the development of a new construction plan. Give a breakdown of the work required. (Give sketch plans as needed).

[15]

(c) Describe the present situation and outline the approach you would take to investigate the cause of the tilt on the breakwater at Hermanus. Indicate two possible alternative causes, and how you would remedy the situation for each case. (In a sketch show the type of construction).

[10]

(d) Briefly explain how you would determine the directions of nett littoral drift and how you would estimate the littoral drift quantity at Hout Bay beach.

[10]

(e) Hout Bay harbour is to be extended to provide for an additional 500 floating berths for small craft. Present a breakwater and mooring layout, and show in plan details of boat ramps, harbour control and other infrastructure requirements that should be considered at a preliminary stage. State all assumptions.

[60]

Total for SECTION 2 = 110 marks

University of Cape Town

University of Cape Town

Department of Civil Engineering

University Examination: 4-November-1988

CIV 593S Engineering Software Design and Development

University of Cape Town

Time: 3 hours

Open Book

Answer All Questions

Total: 110 marks

Internal Examiner: Mr J Vos
External Examiner: Prof GL Murray

1. Software Design

(a) Discuss the five phases of the software development cycle, with specific reference to the inputs and outputs of each phase. (10)

(b) Describe the following concepts as they relate to the quality of software design:

i. *Coupling*

ii. *Cohesiveness*

iii. *Parsimony*

iv. *Predictability*

v. *Scope of effect and Scope of control*

(10)

[20]

2. Structured Programming

(a) Rewrite the following section of code to be more explicit and readable:

```
      parameter (n=3)
      real a(n,n)
      do 1 i = 1,n
      do 1 j = 1,n
1     a(i,j) = (i/j)*(j/i)
```

(5)

(b) Eliminate the GOTO-statements from the following fragment of code:

```
      if (x.lt.y) goto 30
      if (y.lt.z) then
         goto 50
      else
         small = z
         goto 70
      endif
30    if (x.lt.z) then
         goto 60
      else
         small = z
         goto 70
      endif
50    small = y
      goto 70
60    small = x
70    continue
```

University of Cape Town

(7)

(c) Code a lexical function for comparing any two character strings `c1` and `c2` for equality. The function `LEQ(c1,c2)` returns the value `TRUE` if the strings are identical, otherwise it returns the value `FALSE`. Assume the integer function `LENSTR(c)` exists which returns the runtime length of a character string. (8)

[20]

3. Human Factors Guidelines

(a) Discuss how the concept of multilevel design can be applied to screen layouts and error diagnostics in order to improve the terminal interface for users. (6)

(b) Software systems may employ any one of a wide variety of default entry strategies for data entry. Describe the possible asternnatives, as well as their merits and demerits. (7)

(c) Describe some of the guidelines for system message design proposed by Ben Schneiderman. (7)

[20]

4. Modularity and Information Hiding

An interactive finite element preprocessor need to store the information about all nodal points in the finite element mesh of a model. Assume the following information need to be stored for each nodal point:

```
node id, X-coordinate, Y-coordinate
```

The node id for each node is a positive integer value and must be unique, but need not be in sequence. Thus the first three nodes in a mesh could have identifiers 10, 21, and 47. The X,Y-coordinates are real values associated with the node.

Also assume that the total number of nodes is small enough so that they may all be stored in a table in memory rather than on a disk file. The following operations that need to be performed on this table:

(a) Store new nodal point values in the table.

(b) Modify the coordinates of an existing node.

(c) Check whether a node exist or not.

(d) Retrieve the coodinates of a given node.

It is important that the table be organized in such a way to facilitate the fast retrieval of coordinates for a given node, as this operation need to be performed many times over.

Design a module which implements the conceptual model of the nodal point table described above, and its associated operations. Discuss the following aspects of this module:

University of Cape Town

(a) The data structure for storing the nodal points in and the way it is organized.

(b) The algorithms for storing and retrieving nodal point coordinates.

(c) Error conditions that may occur for each operation and how they may be handled.

(d) The names of the routines that implement these operations and their respective interfaces (arguments).

[25]

5. Computer Graphics

(a) Describe the components of a CRT of a colour video monitor and how an image is displayed on it using the shadow-masking technique. (8)

(b) A graphics applications program allows the user the facility to zoom in on the image currently being displayed, by selecting a rectangular area of interest which is then displayed on the screen instead. Write the segment of code which can perform the necessary operations of setting up the required transformations, using the GKS package. Assume the routine `GCHPNT(key,xw,yw)` is available for selecting any point on the image displayed (in world space) by using the cursor keys to move a graphic crosshair on the screen and then pressing any alpha key. (7)

(c) An application program needs to display several polygons, each of which has a varying number of points. Assume that all the points of the polygons are all stored as records in a sequentail file. Each record has the following format:

```
Polygon id, Point id, X-coordinate, Y-coordinate
```

The polygon id and point id are integers and the coordinates are real values. All the points that define a particular polygon are grouped together in the file and have the save polygon id. Write a segment of code that can read this file and display each polygon using the GKS package. Make provision for the fact that a polygon may have a large number of points defining it, which cannot buffered in memory all at the same time. (10)

[25]

Total = [110]

University of Cape Town